NORTHWESTERN UNIVERSITY

Selective Carbonyl Hydroboration via Homogeneous Lanthanide Catalysis

A DISSERTATION

SUBMITTED TO THE GRADUATE SCHOOL

IN PARTIAL FULFILLMENT OF THE REQUIREMENTS

for the degree

DOCTOR OF PHILOSOPHY

Field of Chemistry

By

Christopher Jeffrey Barger

EVANSTON, ILLINOIS

March 2021

ABSTRACT

Selective Carbonyl Hydroboration via Homogeneous Lanthanide Catalysis

Christopher J Barger

The lanthanides, with their limited orbital effects and high oxophilicity, represent a class of catalytic metals highly distinguished from more commonly-utilized transition metals. Homogeneous lanthanide catalysts often afford high catalytic rates and impressive selectivity. However, challenges regarding the synthesis and utilization of highly air- and water-sensitive organo-lanthanide complexes have limited widespread adoption throughout the catalytic and synthetic chemistry communities. The focus of the work presented herein is on the discovery of more accessible methodologies utilizing lanthanide catalysis for the reduction of carbonyl-containing functional groups.

Throughout this work, the ability of commercially-available lanthanide complex $La[N(SiMe_3)_2]_3$ to catalyze the hydroboration of carbonyl groups is explored. First, ketones and aldehydes are shown to be reduced by pinacolborane with catalyst loadings as low as 0.01% and turnover frequencies as high as 40,000 h^{-1}. Second, $La[N(SiMe_3)_2]_3$ is shown to also catalyze the hydroboration of esters with high activity and selectivity over a variety of functional groups. Third, secondary and tertiary amides are cleanly reduced with pinacolborane to their corresponding amines, again using $La[N(SiMe_3)_2]_3$ as a catalyst. Throughout, detailed discussions on the mechanisms of these reactions are presented, supported by robust experimental and computational findings. Notably, it is shown that $La[N(SiMe_3)_2]_3$ does not act as a simple Lewis acid activating the carbonyl for reduction, but rather it catalyzes complex, multi-step reactions involving unusual and highly reactive hemiacetal/hemiaminal intermediates.

ACKNOWLEDGEMENTS

First and foremost, I would like to thank my advisor, Professor Tobin J. Marks for his guidance and mentorship throughout my PhD. His wholehearted commitment to academic research is an inspiration, and I've never met anyone with a greater appreciation of science. Progressor Marks' excitement for research (and ability to recount a story perfectly suited for any occasion) made my time at Northwestern as enjoyable as it was formative. I would also like to thank my thesis committee members, Professors Regan Thomson and Danna Freedman. I count myself truly fortunate to have had a support system that I could always count on for advice.

The mentorship, guidance, and friendship of research professors Tracy Lohr, Max Delferro, and Yanshan Gao was invaluable. Their effective and approachable leadership of the "A-Team" ensured that we were always on track and were never left floundering. Encouraging experimental results were always that much more exciting knowing that they would be there to share them with.

I am very fortunate to count my colleagues in the Marks lab among my closest friends. Working every day with the talented, driven, and passionate members of the Marks lab made my time in the group an incredible experience. Throughout my time in the lab, Vicki Weidner was a true mentor and friend, as were Michael Desanker, Madi Stalzer, Anna Invergo, and Titel Jurca. They were always there to offer guidance and support as I navigated my PhD (and to dance to Ska at my wedding!). And it is hard to imagine my PhD without Miles Tan's unique approach to mentorship. Shanfu Liu, Jiazhen Chen and I started in the Marks group at the same time, grew as scientists and researchers together, and all transitioned to consulting after graduating. I believe our time spent together navigating graduate school and working in the Marks lab instilled in each of us the skills and desire for professional growth that informed our career decisions. Finally, I can't

imagine the final years of my PhD without Rachel Dicken, Jake Rothbaum, and Cole Carter. Getting to work with each of them and see them become incredible scientists was one of the most rewarding aspects of my PhD. Rachel's contribution to the third chapter of this thesis was instrumental to its publication, and Jake's leadership and guidance at recruitment weekend socials and A-Team outings was admirable.

I also would like to acknowledge Jonathan Maendel, Laura Makinen, and Madison Schell for the invaluable support they provide for the department and the sincere devotion they showed to graduate students. Working with them to develop new departmental initiatives and programs was one of the most rewarding and formative aspects of my time at Northwestern, and I credit them with affording myself and many other graduate students with opportunities outside of the academic mainstream and helping us to become well-rounded professionals.

A PhD is a uniquely challenging experience, and it is only with the loving support of my family that I completed it. My wife, Renee, not only gave me the courage to endeavor for a PhD in the first place, but she supported and encouraged me through good times and bad. We moved across the country and started a new life together in Chicago, and we got married shortly thereafter. I will never stop being amazed at her capacity for love, support, and kindness. My parents, Sid and Gaye, raised me to believe that with hard work and determination, anything is possible. Their encouragement and love provided me with the strength and resolve needed to succeed, both in my PhD and thereafter. I was also fortunate to gain two more parents during my PhD, my in-laws Jean-Pierre and Sara Wetli, who, despite me stealing their daughter half way across the country, never failed to provide encouragement and support as if I were their own.

LIST OF ABBREVIATIONS

La^{NTMS} = Tris[*N*,*N*-bis(trimethylsilyl)amide]lanthanum, $La[N(SiMe_3)_2]_3$

Ln^{NTMS} = Tris[*N*,*N*-bis(trimethylsilyl)amide]lanthanide, $Ln[N(SiMe_3)_2]_3$

Ln = any lanthanide

HBpin = Pinacolborane

HBcat = Catecholborane

9-BBN = 9-borabicyclo[3.3.1]nonane

TMS = Trimethylsilane

Cp* = pentamethylcyclopentadienide

DCM = Dichloromethane

THF = Tetrahydrofuran

DMSO = Dimethylsulfoxide

PTFE = Polytetrafluoroethylene

NMR = Nuclear Magnetic Resonance Spectroscopy

ESI-MS = Electrospray Ionization Mass Spectrometry

DFT = Density Functional Theory

LANL2DZ = Los Alamos National Laboratory 2-Double-Z basis set

TDTS = Turnover-Determining Transition State

TDI = Turnover-Determining Intermediate

KIE = Kinetic Isotope Effect

VT = Variable Temperature

TABLE OF CONTENTS

LIST OF TABLES, FIGURES, AND SCHEMES

Chapter 1

Chapter 2

Chapter 3

CHAPTER 1

Rapid, Mild, and Selective Ketone and Aldehyde Hydroboration/Reduction Mediated by a Simple Lanthanide Catalyst

Adapted From:

Weidner, V. L.; Barger, C. J.; Delferro, M.; Lohr, T. L.; Marks, T. J. *ACS Catal*. **2017**, *7*(2), 1244-1247

Abstract

Rapid, clean hydroboration of ketones and aldehydes with HBpin is achieved using the homoleptic rare-earth catalyst La[N(SiMe3)2]3 (La^{NTMS}). The reaction employs low catalyst loadings (0.01–1 mol % LaNTMS), proceeds rapidly (>99% in 5 min) at 25 °C, and is moderately air-tolerant. Additionally, this hydroboration has good functional group compatibility, including halides, nitro groups, and nitriles, and is exclusively carbonyl-selective in the presence of alkenes and alkynes.

Introduction

The reduction of aldehydes and ketones serves as an efficient synthetic route to functionalized alcohols, making this transformation an invaluable tool in fine chemical production and natural product synthesis. Active hydride reagents are used ubiquitously for this transformation, but frequently show poor functional group tolerance (i.e., $LiAlH_4$ reduction of nitro groups, nitriles, amides, etc.) and/or modest reaction rates (i.e., $NaBH_4$ with hindered ketones).[1] Employing a catalyzed system with a less active reductant, such as pinacolborane (HBpin), can greatly enhance both the selectivity and the rate of carbonyl reduction. Unlike catalytic carbonyl hydrosilylation, which has a well-established literature precedent,[2-5] catalytic carbonyl hydroboration remains relatively unexplored, and as such, is currently of great interest.

The catalyst scope for carbonyl hydroboration is rapidly expanding, as detailed in a recent review.[6] Alkaline earth,[7-9] transition metal,[10-17] and main group catalysts[18-22] all mediate this transformation. While most are effective in aldehyde reduction, they typically perform poorly with ketones, requiring high catalyst loadings, long reaction times, or elevated temperatures.

Additionally, many recently reported catalysts require multi-step, air-free syntheses and rigorously dried substrates and solvents. Here we report that inexpensive, commercially available homoleptic $La[N(SiMe_3)_2]_3$ (abbreviated henceforth as La^{NTMS}) catalyzes the rapid, regioselective hydroboration of diverse aldehydes and ketones with HBpin at room temperature.

Organolanthanide catalysts were previously shown to effectively catalyze hydroelementations of olefins, allenes, and acetylenes,[23-29] however their reactivity with carbon-heteroatom multiple bonds remains relatively unexplored. After discovering that $[Cp^*_2LaH]_2$ efficiently catalyzes the hydroboration/dearomatization of pyridines,[30] we sought to investigate hydroborations of other substrates having carbon-heteroatom multiple bonds and to enhance the reaction utility by employing a more synthetically accessible/less air- and water-sensitive catalyst than $[Cp^*_2LaH]_2$. Homoleptic lanthanide amides of the type $Ln[N(SiMe_3)_2]_3$ are commercially available for most lanthanides and are less air- and moisture-sensitive than many other organolanthanides. These complexes ($Ln[N(SiMe_3)_2]_3$) effectively catalyze olefin/allene/alkyne hydroelementation,[24-25,27-29] as well as aldehyde amidation[31] and the Tishchenko reaction,[32-33] but the potentially useful hydroboration of carbonyl-containing substrates has not been investigated.

Results and Discussion

At a loading of 0.01 mol% in benzene, La^{NTMS} catalyzes benzophenone hydroboration with HBpin in up to 99% conversion in less than 5 min at 25 °C by ^1H NMR assay (see Experimental Section for details). This corresponds to a TOF >40,000 h^{-1}, which is among the most rapid pinacolborane-based reductions reported to date.[6,9] Analogous lanthanide amides (Y, Ce, Sm) were also investigated and yielded full conversion with only slightly diminished rates relative to La.[34]

Table 1.1 summarizes the full scope of ketones investigated in this report (see Experimental Section for full product characterization). Electron-rich, aromatic ketones (benzo-phenone, 4-methylbenzophenone, and 4,4'-dimethylbenzo-phenone, Table 1.1 entries 2-4) proceed rapidly at a La^{NTMS} loading of only 0.01 mol%, while aliphatic and less electron-rich ketones require La^{NTMS} loadings of 0.1 mol% for comparable rates. Otherwise, little variation in rate among the various ketones is noted. Note that halogenated substrates are tolerated (Table 1.1 entry 7) and no side-reactions with alkenes or nitro groups are observed (Table 1.1, entries 6 and 10, respectively). Benzalacetone (**6**) undergoes hydroboration selectively at the ketone while preserving the olefin functionality, even at catalyst loadings as high as 5 mol%. This is significant since the low cost and commercial availability of the catalyst make such high loadings practical if required. Rotenone (**11**), a natural product used as a pesticide and insecticide,[35] is likewise only reduced at the ketone, exhibiting >99% selectivity over alkene hydroboration and cyclic ether ring-opening, the latter of which is common for other lanthanide Lewis acids.[36] Note also that La^{NTMS} is not deactivated by the potentially chelating catechol dimethyl ether.

Table 1.1. Scope of ketone hydroboration with La^{NTMS}

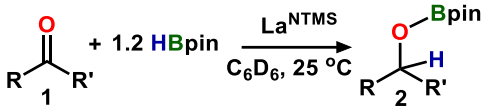

	Substrate (1)	Product (2)	Cat (%)	Time (min)	Yield (%)[a]
1			–	1 week	<1
2			0.01	15	>99
3		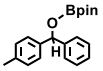	0.01	15	>99
4	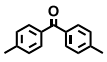	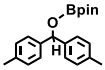	0.01	15	>99
5			0.1	15	>99
6		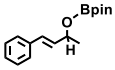	0.1	15	>99
7	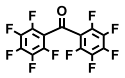	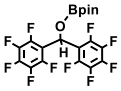	0.1	15	>99
8			0.1	15	>99
9			0.1	15 90	50 98
10		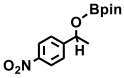	0.1	15	>99
11	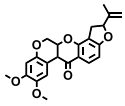	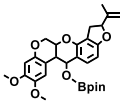	1.0	15	>99

[a]NMR yield. Ketone (0.25mmol) added to 0.5 mL HBpin solution (0.30mmol) and C_6Me_6 internal standard in C_6D_6. La^{NTMS} added from a stock solution of appropriate concentration, and reaction monitored by ^{1}HNMR.

Benzophenone hydroboration serves as the basis for further investigation into the general applicability of this catalytic system, including scalability, ambient atmosphere tolerance, and solvent minimization for "greener" processes. Preparative scale reactions (1 g, repeated 4 times) do not show any obvious loss in reactivity from exposure to ambient atmosphere and no side reactions are observed; after hydrolysis of the product boryl ester, diphenylmethanol is obtained in 86% isolated yield. Note that this reaction was conducted entirely on the bench, foregoing the use of a Schlenk line and using unpurified benzophenone, La^{NTMS}, and benzene, taking no special precautions to exclude air or moisture. Further exploration of the catalyst's tolerance to ambient atmosphere was hindered by the moisture sensitivity of HBpin, which we found to be at least as susceptible to hydrolysis as La^{NTMS}. Other solvents can also be used (e.g., heptane, ether, THF, CH_2Cl_2), and this reaction can be run neat, with HBpin acting as the solvent (safety note: the reaction is exothermic and, without solvent to dissipate evolved heat, should be run in an ice bath). This is highly desirable from a waste-reduction perspective and further demonstrates the robustness of the catalyst. After removing volatiles *in vacuo*, benzophenoxy pinacolborane is obtained in 97% isolated yield.

Aldehydes are also cleanly reduced by this system, showing high selectivity towards C=O reduction over alkenes, alkynes, and nitriles, as well as exhibiting halide tolerance (Table 1.2 entries 6, 4, 8, and 5 resp.). However, reaction rates are generally slower than for ketones, and higher catalyst loadings are required for comparable reaction rates (Table 1.2). This observation is contrary to what has been observed previously, where aldehydes are more reactive than ketones.[6]

Table 1.2. Scope of aldehyde hydroboration with La^{NTMS}.

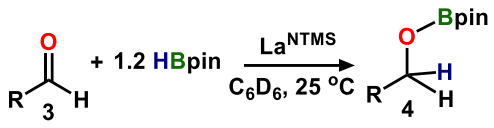

	Substrate (3)	Product (4)	Cat. (%)	Time (min)	Yield (%)[a]
1		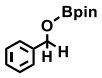	~	60	11%
2		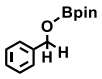	0.1	15 60	50 >99
3		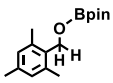	1.0	15	>99
4		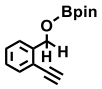	0.1	15	>99
5		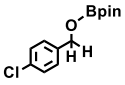	1.0	15	>99
6	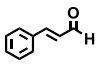	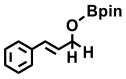	1.0	15	>99
7		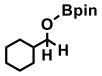	0.1	15	>99
8	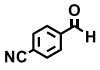	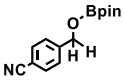	0.1	15	>99
9		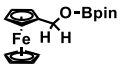	0.1	15	>99
10	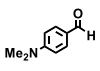	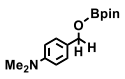	0.1	15	>99

[a.]NMR yield. Aldehyde (0.25mmol) added to 0.5 mL solution of HBpin (0.30 mmol) and C_6Me_6 (0.05mmol) internal standard in C_6D_6. La^{NTMS} added from stock solution of appropriate concentration, and the reaction monitored by ^1H NMR. Isolated alcohol yields of novel boronic esters are reported in the Experimental Section.

The empirical rate law for catalytic ketone hydroboration (eq. 1.1) was determined via ^{1}H NMR monitoring with reference to C_6Me_6 as internal standard (see Experimental Section for details). The most sluggish ketone examined was dicyclohexylketone, which was used for kinetic analysis to enable precise rate monitoring at low conversions (< 20%). Under the present reaction conditions the rate is found to be first-order in [Ketone], [HBpin], and [La^{NTMS}], suggesting all are involved in the turnover-limiting step or in a rapid pre-equilibrium before this step. Activation parameters for the dicyclohexylketone hydroboration are $\Delta H^{\neq} = +17 \pm 1$ kcal/mol and $\Delta S^{\neq} = -15 \pm 2$ e.u. The large $\Delta H^{\neq}$ may reflect unfavorable steric repulsions in the transition state.

$$\text{Rate} = k\,[La^{NTMS}]^1\,[HBpin]^1\,[Ketone]^1 \qquad (1.1)$$

The rate law for catalytic aldehyde hydroboration (eq. 1.2) was determined in a similar manner (see Experimental Section) using cyclohexylcarboxaldehyde due to its structural similarity to dicyclohexylketone. Interestingly, the rate is *zero-order* in [HBpin] and [Aldehyde] under the same conditions, and the activation parameters are markedly different as well ($\Delta H^{\neq} = +12 \pm 2$ kcal/mol and $\Delta S^{\neq} = -33 \pm 7$ e.u.), suggesting distinct mechanistic departure from the ketone hydroboration process. Further mechanistic details are currently under investigation.

$$\text{Rate} = k\,[La^{NTMS}]^1[HBpin]^0[Aldehyde]^0 \qquad (1.2)$$

These surprising ketone vs aldehyde rate and mechanistic differences prompted competition experiments to directly probe hydroboration selectivity. In a reaction of 4-acetyl-benzaldehyde (**11**, Scheme 1.1a) with 1.0 equiv. HBpin at 97% conversion, the aldehyde-only hydroboration

product (**11a**) is obtained in 91% yield (by NMR), with only 6% of the di-hydroborated product (**11b**) and <1% of the ketone-only hydroboration product (**11c**). Subsequent addition of a second equivalent of HBpin gives **11b** in >99% yield by ^{1}H NMR. Similar intramolecular selectivity was reported using a metal-free diazaphospholene catalyst[19] and an aluminum monohydride catalyst.[22] However in those cases ketones are much less reactive than aldehydes in isolated reactions, requiring longer reaction times, higher temperatures, or higher catalyst loadings. In a competition study, where equimolar acetophenone and benzaldehyde are allowed to compete for 1.0 equiv. HBpin (Scheme 1.1b), preference for aldehyde hydroboration is again observed, reaching 91% conversion of benzaldehyde and only 9% conversion of acetophenone. When a second equiv. of HBpin is introduced, both borylated products are obtained in >99% yield. Such selectivity for aldehyde vs ketone hydroboration with pinacolborane is also noteworthy and has only been reported twice before using either $[Ru(p\text{-cymene})Cl_2]_2$[13] or an aluminum monohydride catalyst.[22] Again, these systems exhibit lowered activity with ketones vs aldehydes in independent systems, requiring longer reaction times and/or higher temperatures for ketone reduction. The present system, which displays selectivity that is contrary to what would be expected based on kinetic data, is highly unusual and, to our knowledge, has not been reported previously for pinacolborane-based reductions.

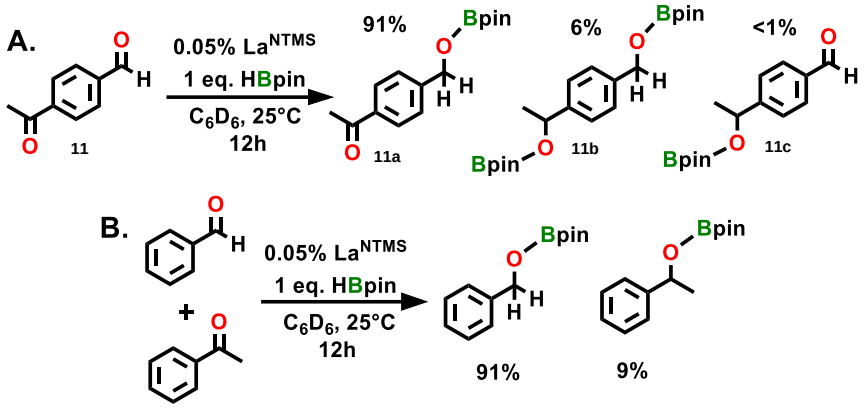

Scheme 1.1. Competitive Aldehyde/Ketone Hydroboration Selectivity Study. **A.** 4-Acetylbenzaldehyde. **B.** Benzaldehyde and acetophenone.

Conclusion

In conclusion, we report the rapid catalytic hydroboration of ketones and aldehydes with HBpin using a simple lanthanum amido catalyst. High selectivity for aldehyde hydroboration over ketones and C-C unsaturation is observed, along with good functional group tolerance for many other groups. Further investigations of scope and mechanism are in progress.

Experimental Section

Materials and Methods. All manipulations of air-sensitive materials were carried out with rigorous exclusion of oxygen and moisture in flame- or oven-dried Schlenk-type glassware on a dual-manifold Schlenk line, interfaced to a high-vacuum line (10^{-6} Torr), or in an argon-filled vacuum atmospheres glovebox with a high capacity recirculator (<1 ppm O_2). Benzene-d6 (Cambridge Isotope Laboratories; 99+ atom % D) was stored over Na/K alloy and vacuum transferred immediately prior to use. $La[N(SiMe_3)_2]_3$ (La^{NTMS})and hexamethylbenzene were purchased from Sigma-Aldrich Co. and sublimed under high-vacuum (10^{-6} Torr). Pinacolborane

("HBpin") was purchased from Sigma-Aldrich Co. and distilled under high-vacuum (10^{-6} Torr). Carbonyl-containing substrates were purchased from Sigma-Aldrich Co. and dried over 3Å molecular sieves and distilled off prior to use (for liquid substrates) or dried under vacuum (for solid substrates). Known boryl esters were characterized by ^{1}H, ^{13}C, and ^{11}B NMR and compared to literature values. Unknown boryl esters were also fully characterized by NMR, and then hydrolyzed by refluxing in 1*M* NaOH/H_2O and MeOH for 1 hour (for dicyclohexyl methanol and phenyl cyclohexyl methanol) or by refluxing with silica gel and H_2O for 3 hours (for perflouorodiphenyl methanol and 2-ethynyl benzyl alcohol). The product was extracted with DCM and the organic layer was dried over $MgSO_4$, and the solvent was removed by rotary evaporation. If necessary, the crude was purified by column chromatography, using 30% THF in hexanes. The resulting alcohol was characterized by ^{1}H and ^{13}C NMR and EI- or ESI-MS.

Physical and Analytical Measurements. NMR spectra were recorded on a Bruker Avance III (500 MHz, ^{1}H ; 125 MHz, ^{13}C), Varian Inova 500 (500 MHz, ^{1}H; 125 MHz, ^{13}C), Agilent DD MR-400 (400 MHz, ^{1}H; 100 MHz, ^{13}C; 128 MHz, ^{11}B), or Agilent DD2 500 (500 MHz, ^{1}H ; 125 MHz, ^{13}C). Chemical shifts (δ) for ^{1}H and ^{13}C are referenced to residual solvent resonances (7.16 and 128.06 ppm, resp., for benzene-d_6). ^{11}B shifts are referenced to an external $BF_3{\cdot}OEt_2$ standard. NMR scale reactions were carried out either in Teflon-sealed J. Young tubes or PTFE septum-sealed tubes. Mass spectra were recorded on a Bruker AmaZon SL LC-MS (ESI, Quadrupole ion trap) or Agilent 5973 GC-MS (EI, Quadrupole ion trap).

Typical NMR-Scale Reaction of HBpin with Solid Ketones and Aldehydes and La^{NTMS} Catalyst. In a glovebox, the aldehyde/ketone (0.25 mmol) was massed in a vial. 500 μL

of a stock solution containing HBpin (0.30 mmol, 1.2 equivalents vs. aldehyde/ketone) and the internal standard hexamethylbenzene (50 μmol) was added to the vial, and the vial was shaken until all solids were dissolved. This solution was added to a J. Young tap NMR tube, and 100 μL of a stock solution containing an appropriate loading of $La[N(SiMe_3)_2]_3$ was added. The tube was capped and shaken, and the reaction was monitored by ^1H NMR.

Typical NMR-Scale Reaction of HBpin with Liquid Ketones and Aldehydes and La^{NTMS} Catalyst. In a glovebox, 100 μL of a stock solution containing an appropriate loading of $La[N(SiMe_3)_2]_3$ was added to a septum-sealed NMR tube. 500 μL of a stock solution containing HBpin (0.30 mmol, 1.2 equivalents vs. aldehyde/ketone) and the internal standard hexamethylbenzene (50 μmol) was added to a septum-sealed vial, and both were brought out of the glovebox. The liquid aldehyde/ketone (0.25 mmol) was injected into the vial with HBpin and standard, the vial was shaken, and the contents were injected into the NMR tube with catalyst, all under N_2. The tube was shaken, and the reaction was monitored by ^1H NMR.

Scale-Up/Air and Moisture Tolerance Test Reaction. Benzophenone (1.0 g, 5.5 mmol) and HBpin (0.96 mL, 6.6 mmol) were dissolved in benzene (5 mL) in a vial outside of a glovebox. To this solution was added La^{NTMS} (34 mg, 0.055 mmol). After stirring for 5 minutes, volatiles were removed in vacuo, and the resulting white powder was taken up in 10 mL of 10% NaOH in MeOH. The mixture was sonicated and refluxed for 1 hour. The product (diphenylmethanol) was extracted in ethyl acetate and purified by column chromatography (1:5 THF:hexanes). Final yield of diphenylmethanol: 0.87g (86%).

Typical NMR-Scale Reaction for Kinetic Monitoring by ^{1}H-NMR Arrays. In a glovebox, 500 μL of a stock solution of aldehyde/ketone and 500 μL of a stock solution containing HBpin and the internal standard, hexamethylbenzene (50 μmol), were mixed in a vial. This solution was then added to a rubber septum-sealed NMR tube, wrapped with parafilm, and removed from the box. At the NMR, the magnet was locked, tuned, and shimmed to the sample, then 100 μL of a stock solution containing an appropriate loading of $La[N(SiMe_3)_2]_3$ was added. The tube was shaken and reinserted into the instrument and scanning was begun. Single (^{1}H NMR) scans were collected at regular intervals. Substrate and/or product concentrations were determined relative to the intensity of the internal standard resonance plotted versus time.

Kinetic Analysis. Kinetic analysis of the NMR-scale reactions described above was carried out by collecting multiple (>15) data points early in the reaction (<20% conversion). Under these conditions, the reaction can be approximated as pseudo-zero-order with respect to the substrate concentrations. The product concentration was measured from the area of the $R_2CHOBpin$ or RCH_2OBpin peak formed in the product standardized to the methyl peak area of the C_6Me_6 internal standard. Data were fit by least-squares analysis ($R^2 > 0.98$) according to eq 1.3, where t is time, [product] is the concentration of product at time t, and m is the rate of reaction.

$$[product] = mt \qquad \text{(Eq. 1.3)}$$

Orders for each reactant were determined from the average rates (≥3 trials) at varying concentrations (Figures 1.1 and 1.2). Ketone/ aldehyde and HBpin concentrations were varied from 25% to 125% (relative to the other reactant) and catalyst concentration was measured at 0.05%, 0.10%, 0.15%, and 0.20% (for dicyclohexylketone) or 0.025%, 0.05%, 0.075%, and 0.1% (for cyclohexylcarboxaldehyde). (Note: in general, ketones react more quickly than aldehydes,

except in the case of dicyclohexylketone). These data were then plotted as ln(rate) vs. ln[ketone].[30] The negative rate of disappearance of ketone is proportional to the concentration of ketone to the order (α) (see eq. 1.4). Therefore, the order is the slope of a plot of ln(rate) vs. ln[ketone] (eq. 1.5).

$$\frac{-d[ketone]}{dt} = k_{obs}[ketone]^{\alpha} \quad \text{(Eq. 1.4)}$$

$$\ln(rate) = lnk_{obs} + \propto \ln [ketone] \quad \text{(Eq. 1.5)}$$

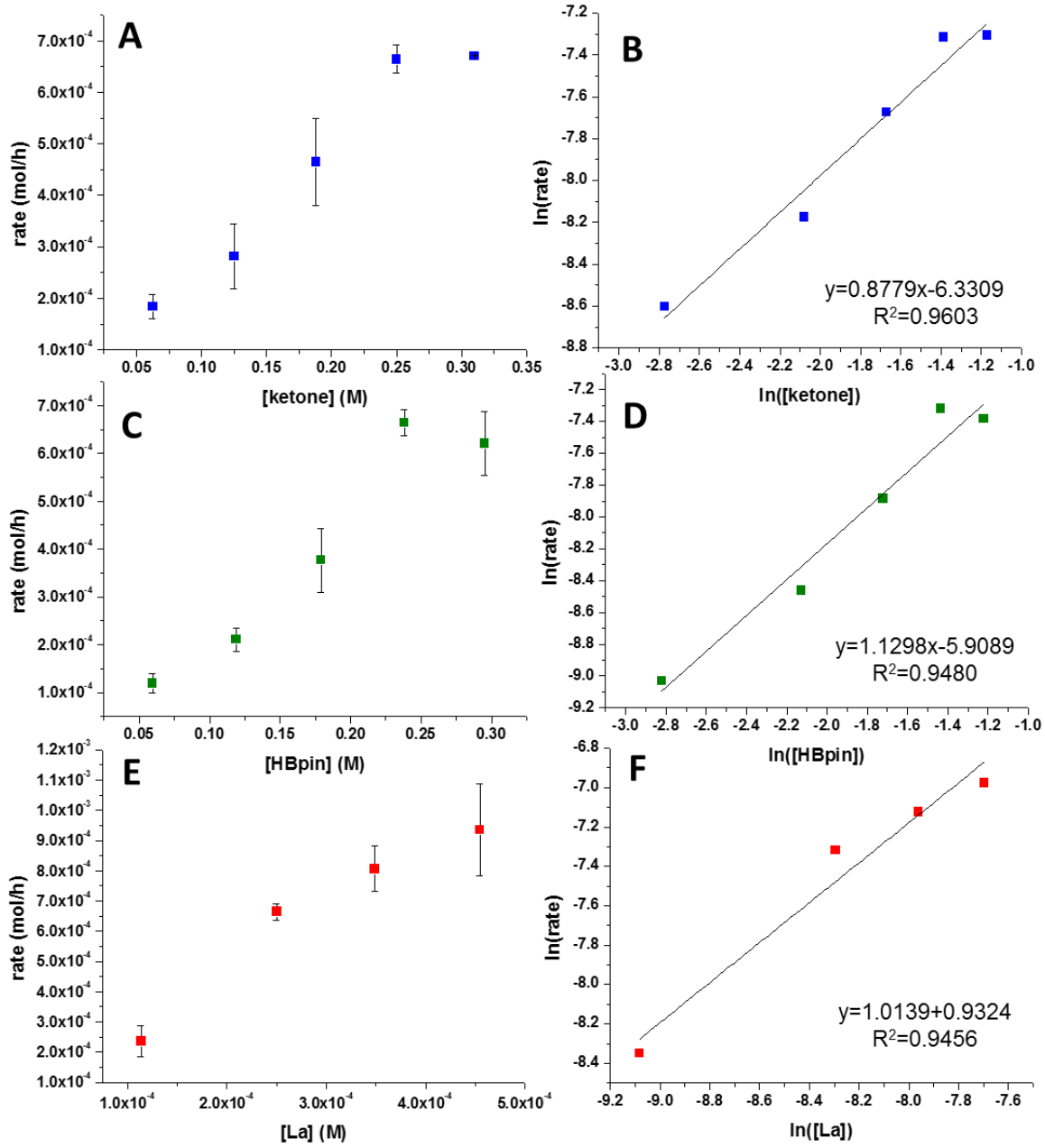

Figure 1.1. (A) Plot of concentration ketone vs. reaction rate (mol/h); (B) Plot for reaction rate law order in [ketone]; (C) Plot of concentration HBpin vs. rate (mol/h); (D) Plot for reaction rate law order in [HBpin]; (E) Plot of concentration **La^{NTMS}** vs. rate (mol/h); (F) Plot for reaction rate law order in **La^{NTMS}**.

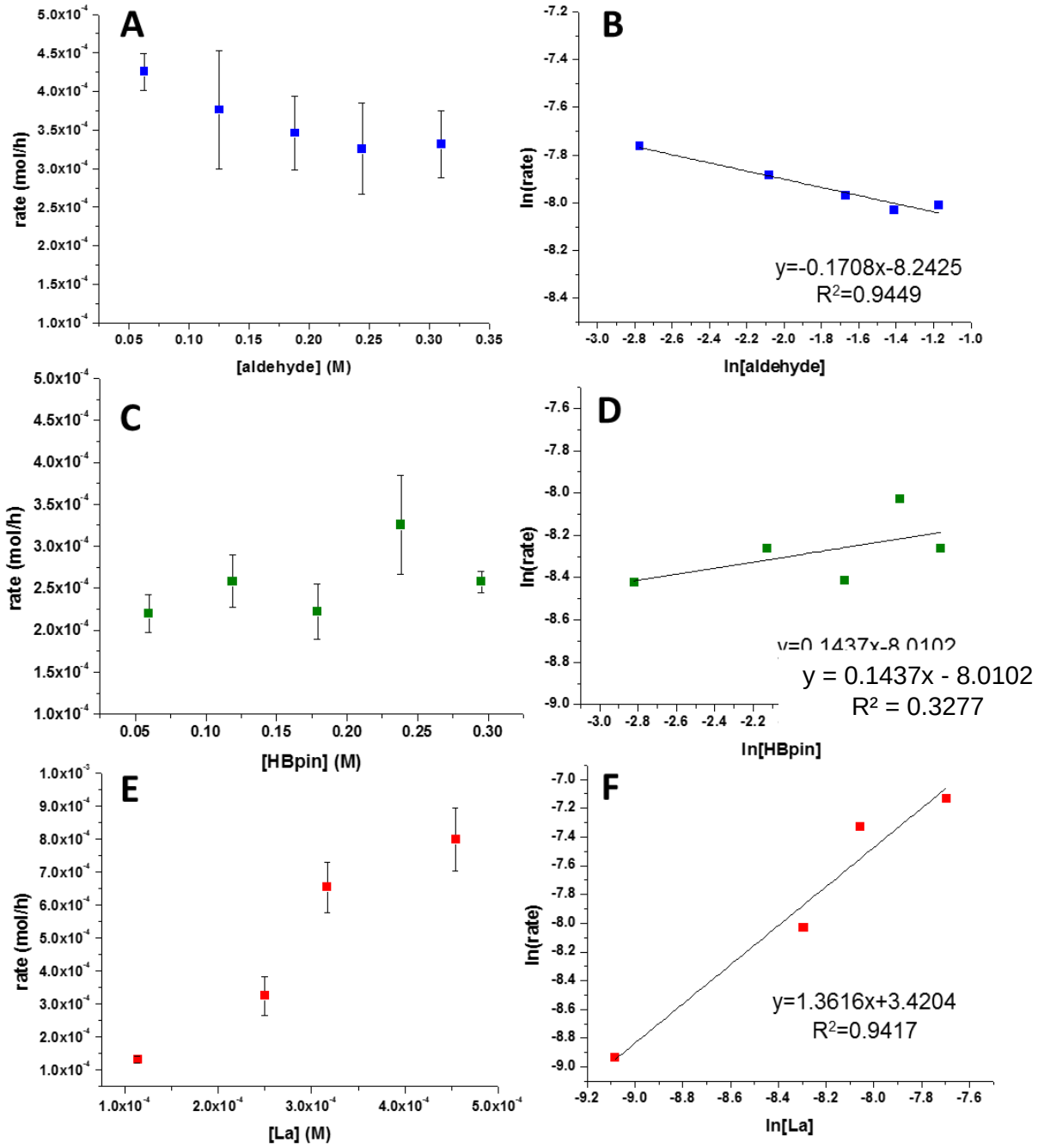

Figure 1.2. (A) Plot of concentration aldehyde vs. reaction rate (mol/h); (B) plot for reaction rate law order in [aldehyde]; (C) Plot of concentration HBpin vs. rate (mol/h); (D) plot for reaction rate law order in [HBpin]; (E) Plot of concentration **La**$^{\mathbf{NTMS}}$ vs. rate (mol/h); (F) plot for reaction rate law order in **La**$^{\mathbf{NTMS}}$.

Temperature Analysis. Data on the rate dependence on temperature was obtained as shown above. A rate at each temperature were determined from the average rates (≥3 trials) at temperatures set on the NMR and measured using a methanol (<25°C) or ethylene glycol (>25°C) standard.

These data were then plotted as 1000/T vs. ln(k/T)[30] (Figure 1.3 and 1.4) from which the enthalpy and entropy of the transition state could be obtained using the Eyring equation (see eq. 1.6). $\Delta H^{\neq}$ is the negative slope times R and $\Delta S^{\neq}$ is the intercept minus the natural log of k_b/h times R.

$$\ln\frac{k}{T} = \frac{\Delta H^{\neq}}{RT}\left[\frac{\Delta S^{\neq}}{R} - \ln\frac{k_b}{h}\right] \qquad \text{(Eq. 1.6)}$$

From a plot of 1000/T vs. ln(k), the activation energy can be obtained using the Arrhenius equation (eq. 1.7). E_a is the negative slope times R.

$$\ln k = -\frac{E_a}{RT} - \ln A \qquad \text{(Eq. 1.7)}$$

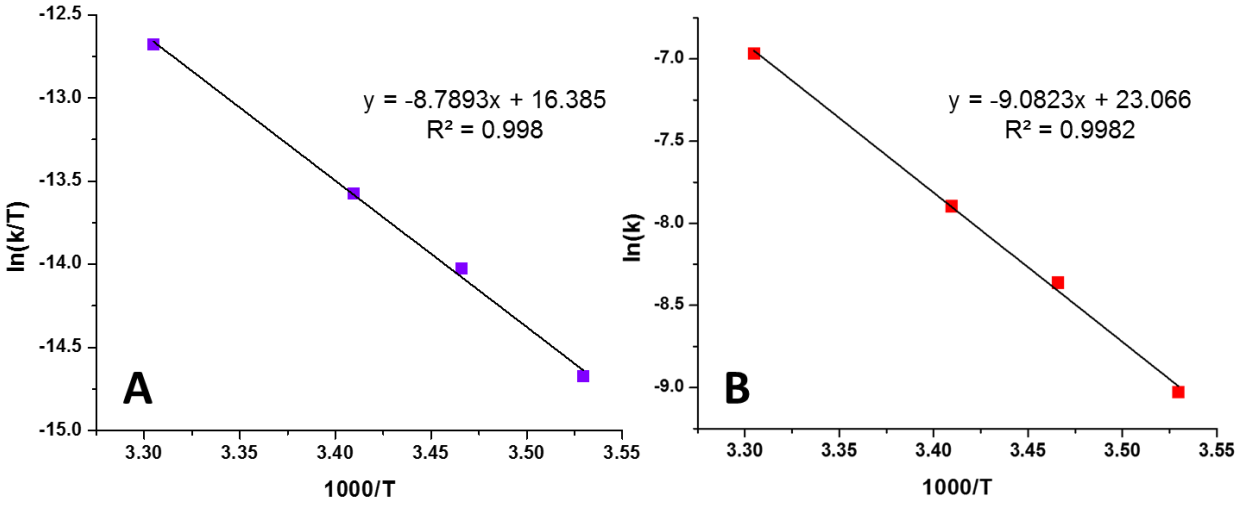

Figure 1.3. (A) Plot of 1000/temperature vs. ln(k/T) for the lanthanum-catalyzed hydroboration of dicyclohexylketone. (B) Plot of 1000/temperature vs. ln (k).

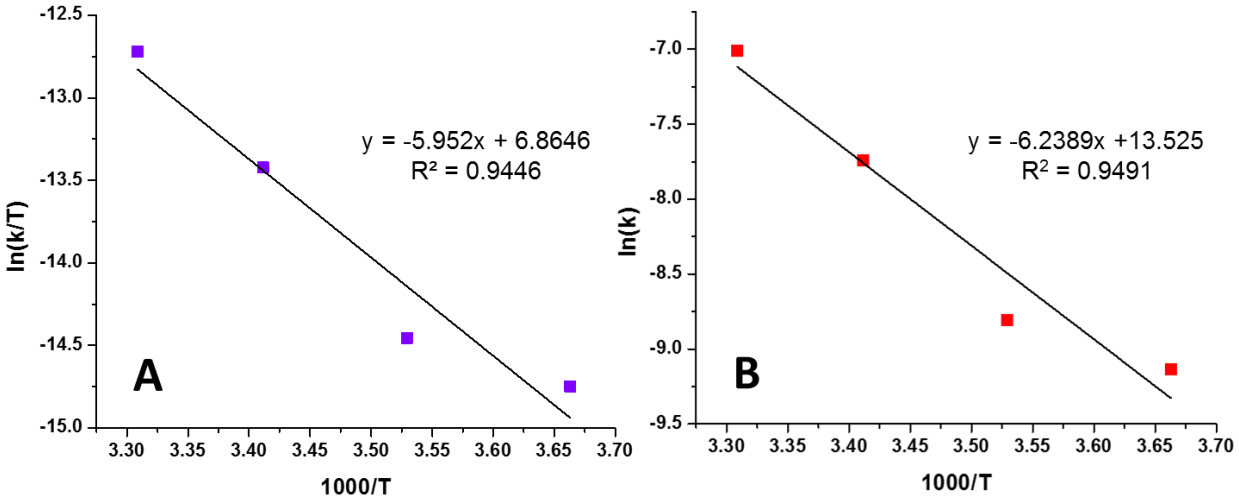

Figure 1.4. (A) Plot of 1000/temperature vs. ln(k/T) for the lanthanum-catalyzed hydroboration of cyclohexylcarboxaldehyde. (B) Plot of 1000/temperature vs. ln (k).

Characterization Data for Ketone/Aldehyde Hydroboration Products

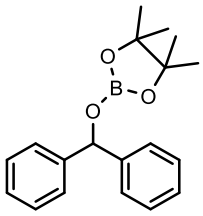

2-(diphenylmethoxy)pinacolborane.

^{1}H, $^{11}B\{^{1}H\}$ and $^{13}C\{^{1}H\}$ spectra are identical to those reported in the literature.[37]

^{1}H NMR (C_6D_6, 500 MHz): 7.45-7.41 (m, 4H), 7.12-7.07 (m, 4H), 7.03-6.98 (tt, 2H, $^{3}J_{HH}$ = 7.4, $^{4}J_{HH}$ = 1.2), 6.41 (s, 1H), 0.98 (s, 12H). **$^{11}B\{^{1}H\}$ NMR (C_6D_6, 128 MHz):** 22.83. **$^{13}C\{^{1}H\}$ NMR (C_6D_6, 125 MHz):** 143.89, 128.57, 127.54, 126.97, 82.85, 78.53, 24.62.

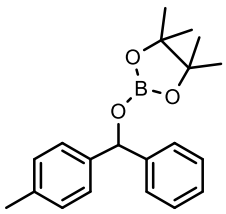

2-(*para*-tolylphenylmethoxy)pinacolborane.

^{1}H, $^{11}B\{^{1}H\}$ and $^{13}C\{^{1}H\}$ spectra are identical to those reported in the literature.[38]

^{1}H NMR (C_6D_6, 500 MHz): 7.46 (d, 2H, $^{3}J_{HH}$= 7.7 Hz), 7.37 (d, 2H, $^{3}J_{HH}$= 7.7 Hz), 7.11 (t, 2H, $^{3}J_{HH}$= 7.5 Hz), 7.01 (t, 1H, 7.5 Hz), 6.93 (d, 2H, $^{3}J_{HH}$= 7.7 Hz), 6.43 (s, 1H), 2.05 (s, 3H), 0.99 (s, 12H). **$^{11}B\{^{1}H\}$ NMR (C_6D_6, 128 MHz):** 22.86. **$^{13}C\{^{1}H\}$ NMR (C_6D_6, 125 MHz):** 144.15, 141.10, 136.93, 129.28, 128.54, 127.46, 127.01, 126.94, 82.80, 78.43, 24.64, 21.06

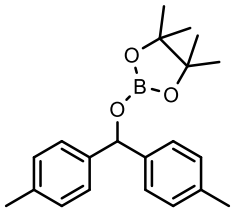

2-(di-*para*-tolylmethoxy)pinacolborane.

^{1}H, $^{11}B\{^{1}H\}$ and $^{13}C\{^{1}H\}$ spectra are identical to those reported in the literature.[39]

^{1}H NMR (C_6D_6, 500 MHz): 7.39 (d, 4H, $^{3}J_{HH}$= 7.7 Hz), 6.94 (d, 4H, $^{3}J_{HH}$= 7.7 Hz), 6.44 (s, 1H), 2.05 (s, 6H), 1.00 (s, 12H). **$^{11}B\{^{1}H\}$ NMR (C_6D_6, 128 MHz):** 22.84. **$^{13}C\{^{1}H\}$ NMR (C_6D_6, 125 MHz):** 141.35, 136.82, 129.24, 126.99, 82.76, 78.33, 24.66, 21.06

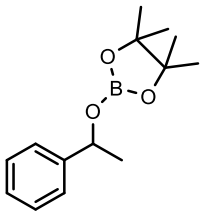

2-(1-phenylethoxy)pinacolborane.

^{1}H, $^{11}B\{^{1}H\}$ and $^{13}C\{^{1}H\}$ spectra are identical to those reported in the literature.[37]

^{1}H NMR (C_6D_6, 500 MHz): 7.37-7.33 (m, 2H), 7.17-7.11 (m, 2H), 7.08-7.02 (tt, ^{1}H, $^{3}J_{HH}$ = 7.4, $^{4}J_{HH}$ = 2.1 Hz), 5.39 (q, 1H, $^{3}J_{HH}$ = 6.4 Hz), 1.45 (d, 3H, $^{3}J_{HH}$ = 6.5 Hz), 1.00 (s, 12H). **$^{11}B\{^{1}H\}$ NMR (C_6D_6, 128 MHz):** 22.52. **$^{13}C\{^{1}H\}$ NMR (C_6D_6, 125 MHz):** 145.39, 128.54, 127.35, 125.70, 82.54, 72.94, 25.79, 24.70, 24.62.

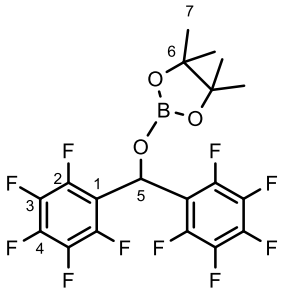

2-(di-perfluorophenylmethoxy)pinacolborane.

^{1}H NMR (C_6D_6, 500 MHz): 6.90 (s, 1H, H-*5*), 1.03 (s, 12H, H-*7*). **^{11}B{^{1}H} NMR (C_6D_6, 128 MHz):** 22.62. **^{13}C{^{1}H} NMR (C_6D_6, 125 MHz):** 145.13 (dm, C-*Ar* , J=253.6 Hz), 141.60 (dt, C-*Ar*, J= 255.4 Hz, J= 13.2 Hz), 137.92 (dt, C-*Ar*, J=250.7 Hz, J=14.1 Hz), 131.78 (s, C-*1*), 84.14 (s, C-*6*), 62.77 (s, C-*5*), 24.45 (s, C-*7*).

Perfluorodiphenylmethanol. 62% isolated yield.

^{1}H NMR (C_6D_6, 500 MHz): 5.94 (d, 1H, H-5, $^{3}J_{HH}$ = 5.8 Hz), 2.20 (d, 1H, O*H*, $^{3}J_{HH}$ = 5.8 Hz). **^{19}F{^{1}H} NMR (C_6D_6, 376 MHz)**: -143.5 - -143.8 (m, 2F), -153.8 (t, 1F, J=22Hz), -161.6 - -162.0 (m, 2F). **^{13}C{^{1}H} NMR (C_6D_6, 125 MHz)**: 144.4 (dm, C-*Ar* , J=253 Hz), 140.9 (dm, C-*Ar*, J= 255 Hz), 137.4 (dm, C-*Ar*, J=251 Hz), 125.5 (s, C-*Ar*), 113.7 (s, *C*-OH). **LC-MS:** $[2M-H]^-$: Calc: 726.9813. Found: 726.9818

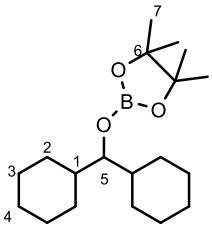

2-(dicyclohexylmethoxy)pinacolborane.

^{1}H NMR (C_6D_6, 500 MHz): 3.78 (t, 1H, H-*5*, $^{3}J_{HH}$ = 6.0 Hz), 1.89-1.82 (m, 2H, H-*1*), 1.75-1.66 (m, 4H, H-*Cy*), 1.64-1.49 (m, 6H, H-*Cy*), 1.29-1.07 (m, 10H, H-*Cy*), 1.10 (s, 12H, H-*7*). **^{11}B{^{1}H} NMR (C_6D_6, 128 MHz):** 22.46. **^{13}C{^{1}H} NMR (C_6D_6, 125 MHz):** 82.79 (C-*6*), 82.14 (C-*5*), 39.66 (C-*1*), 30.19 (C-*Cy*), 27.64 (C-*Cy*), 26.94 (C-*Cy*), 26.82 (C-*Cy*), 26.58 (C-*Cy*), 24.68 (C-*Cy*).

Dicyclohexylmethanol. 92% isolated yield.

^{1}H NMR (C_6D_6, 500 MHz): 2.88 (q, 1H, H-*5*, $^{3}J_{HH}$ = 5.7 Hz), 1.85-1.78 (m, 2H, H-*Cy*), 1.77-1.67 (m, 4H, H-*Cy*), 1.66-1.60 (m, 2H, H-*Cy*), 1.51-1.44 (m, 2H, H-*Cy*), 1.40-1.31 (m, 2H, H-

Cy), 1.25-0.97 (m, 10H, H-*Cy*), 0.81-0.76 (m, 1H, H-O*H*). **^{13}C{^{1}H} NMR (C_6D_6, 125 MHz):** 80.13 (C-*5*), 40.30 (C-*1*), 30.33 (C-*Cy*), 27.69 (C-*Cy*), 27.02 (C-*Cy*), 26.96 (C-*Cy*), 26.65 (C-*Cy*). **GC-MS** $[M\text{-}H_2O]^+$**:** Calc: 178.17; Found: 178.25.

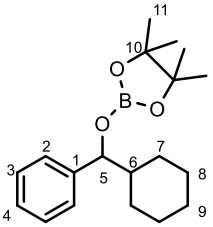

2-(cyclohexylphenylmethoxy)pinacolborane.

^{1}H NMR (C_6D_6, 500 MHz): 7.38-7.33 (m, 2H, H-*2*), 7.20-7.12 (m, 2H, H-*3*), 7.10-7.04 (m, ^{1}H, H-*4*), 5.03 (d, 1H, H-*5*, $^{3}J_{HH}$ = 6.4 Hz), 2.03-1.94 (m, ^{1}H, H-*6*), 1.75-1.45 (m, 6H, H-*Cy*), 1.25-1.05 (m, 4H, H-*Cy*), 1.03 (s, 6H, H-*11*), 0.99 (s, 6H, H-*11*). **^{11}B{^{1}H} NMR (C_6D_6, 128 MHz):** 22.60. **^{13}C{^{1}H} NMR (C_6D_6, 125 MHz):** 143.13 (C-*1*), 128.25 (C-*Ar*), 127.38 (C-*Ar*), 127.05 (C-*Ar*), 82.47 (C-*10*), 81.48 (C-*5*), 45.45 (C-*6*), 29.65 (C-*Cy*), 28.63 (C-*Cy*), 26.78 (C-*Cy*), 26.47 (C-*Cy*), 26.40 (C-*Cy*), 24.64 (C-*Cy*).

Cyclohexyl(phenyl)methanol. 83% isolated yield.

^{1}H NMR (C_6D_6, 500 MHz): 7.22-7.17 (m, 4H, H-*Ar*), 7.12-7.08 (m, 1H, H-*Ar*), 4.10 (dd, 1H, H-*5*, $^{3}J_{HH}$ = 6.8 Hz, $^{4}J_{HH}$ = 3.3 Hz), 2.04-1.98 (m, 1H, H-*6*), 1.72-1.65 (m, 1H, H-*Cy*), 1.61-1.48 (m, 3H, H-*Cy*), 143-1.36 (m, 1H, H-*Cy*), 1.19 (d, 1H, H-*Cy*, $^{3}J_{HH}$ = 3.4 Hz), 1.18-0.98 (m, 4H, H-*Cy*), 0.94-0.85 (m, 1H, H-*Cy*). **^{13}C{^{1}H} NMR (C_6D_6, 125 MHz):** 144.61 (C-*1*), 127.40 (C-*Ar*), 126.99 (C-*Ar*), 79.15 (C-*5*), 45.54 (C-*6*), 29.71 (C-*Cy*), 28.92 (C-*Cy*), 26.86 (C-*Cy*), 26.54 (C-*Cy*), 26.47 (C-*Cy*). **GC-MS** $[M]^+$**:** Calc: 190.14; Found: 190.20.

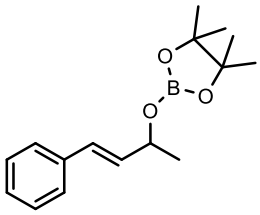

2-(1-cinnamylethoxy)pinacolborane.

^{1}H, $^{11}B\{^{1}H\}$ and $^{13}C\{^{1}H\}$ spectra are identical to those reported in the literature.[37]

^{1}H NMR (C_6D_6, 500 MHz): 7.22-7.17 (m, 2H), 7.12-7.06 (m, 2H), 7.05-6.99 (m, 1H), 6.64 (dd, 1H, $^{3}J_{HH}$ = 16 Hz, $^{4}J_{HH}$ = 0.95 Hz), 6.19 (dd, 1H, $^{3}J_{HH}$ = 16 Hz, $^{3}J_{HH}$ = 5.9 Hz), 4.98 (ddq, 1H, $^{3}J_{HH}$ = 6.2 Hz, $^{3}J_{HH}$ = 6.4 Hz, $^{4}J_{HH}$ = 1.2 Hz), 1.33 (d, 3H, $^{3}J_{HH}$ = 6.4 Hz), 1.06 (d, 12H, $^{3}J_{HH}$ = 2.3 Hz) **^{11}B{^{1}H} NMR (C_6D_6, 128 MHz):** 22.50. **^{13}C{^{1}H} NMR (C_6D_6, 125 MHz):** 137.43, 132.72, 129.49, 128.76, 127.65, 126.88, 82.51, 71.47, 24.95, 24.80, 24.67, 23.43.

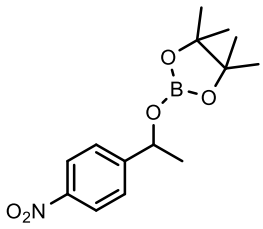

2-(1-(4-nitrophenyl)ethoxy)pinacolborane.

^{1}H, $^{11}B\{^{1}H\}$ and $^{13}C\{^{1}H\}$ spectra are identical to those reported in the literature.[37]

^{1}H NMR (C_6D_6, 500 MHz): 7.80-7.72 (m, 2H), 7.00-6.92 (m, 2H), 5.13 (q, ^{1}H, $^{3}J_{HH}$ = 6.5 Hz), 1.20 (d, 3H, $^{3}J_{HH}$ = 6.5 Hz), 0.94 (s, 12H). **^{11}B{^{1}H} NMR (C_6D_6, 128 MHz):** 22.43. **^{13}C{^{1}H} NMR (C_6D_6, 125 MHz):** 151.82, 147.47, 126.09, 123.64, 82.94, 71.96, 25.33, 24.62.

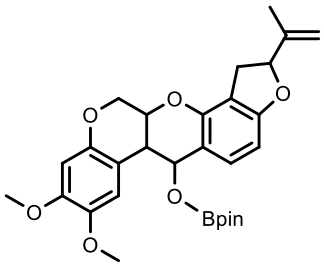

2-(Rotenoxy)pinacolborane.

^{1}H NMR (C_6D_6, 500 MHz): 7.26 (d, 1H, J=8.2 Hz), 6.71 (s, 1H), 6.60 (d, 1H, J=8.2 Hz), 6.51 (s, 1H), 5.48 (d, 1H, J=4.0), 5.08-5.05 (m, 1H), 4.96 (t, 1H, J=8.8 Hz), 4.89 (t, 1H, J=10 Hz), 4.76-4.73 (m, 1H), 4.67-4.61 (m, 1H), 4.17 (ddd, 1H, J=1.2, 4.8, 9.8 Hz), 3.59 (s, 3H), 3.31 (s, 3H), 3.12-3.01 (m, 2H), 2.93-2.85 (m, 1H), 1.58 (s, 3H), 0.95 (s, 6H), 0.92 (s, 6H). **^{11}B{^{1}H} NMR (C_6D_6, 128 MHz):** 22.29. **^{13}C{^{1}H} NMR (C_6D_6, 125 MHz):** 162.60, 150.67, 150.19, 150.12, 144.54, 144.40, 130.38, 114.64, 113.96, 113.20, 111.15, 109.91, 102.88, 101.54, 86.70, 82.67, 70.17, 69.41, 65.45, 56.63, 55.36, 38.03, 32.57, 24.80, 24.31, 17.32. **LC-MS** $[M+Na]^+$ Calc.: 545.232, Found: 545.233

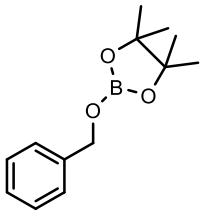

2-(benzyloxy)pinacolborane.

^{1}H, ^{11}B{^{1}H} and ^{13}C{^{1}H} spectra are identical to those reported in the literature.[37]

^{1}H NMR (C_6D_6, 500 MHz): 7.32-7.28 (m, 2H), 7.16-7.10 (m, 2H), 7.08-7.02 (m, 1H), 4.94 (s, 2H), 1.04 (s, 12H). **^{11}B{^{1}H} NMR (C_6D_6, 128 MHz):** 22.79. **^{13}C{^{1}H} NMR (C_6D_6, 125 MHz):** 140.1, 128.59, 127.57, 127.05, 82.75, 66.96, 24.70.

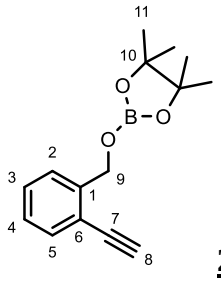

2-(2-ethynylbenzyloxy)pinacolborane.

^{1}H NMR (C_6D_6, 500 MHz): 7.61 (m, 1H), 7.35 (dd, 1H, $^{3}J_{HH}$= 7.7 Hz), 7.04 (dt, 1H, $^{3}J_{HH}$= 7.7 Hz, $^{4}J_{HH}$ = 0.96 Hz), 6.86 (m, 1H), 5.34 (s, 2H) 2.89 (s, 1H), 1.03 (s, 12H). **^{11}B{^{1}H} NMR (C_6D_6, 128 MHz):** 22.76. **^{13}C{^{1}H} NMR (C_6D_6, 125 MHz):** 142.45, 132.67, 129.22, 127.10, 126.24, 119.94, 82.83, 81.11, 65.26, 24.68

2-ethynylbenzyl alcohol. 77% isolated yield.

^{1}H NMR (C_6D_6, 500 MHz): 7.38 (dd, 1H, H-*2*, $^{3}J_{HH}$ = 7.7 Hz, $^{4}J_{HH}$ = 0.9 Hz), 7.32 (d, 1H, H-*5*, $^{3}J_{HH}$ = 7.7 Hz), 7.01 (dt, 1H, H-*3*, $^{3}J_{HH}$ = 7.7 Hz, $^{4}J_{HH}$ = 1.1 Hz), 6.85 (t, 1H, H-*4*, $^{3}J_{HH}$ = 7.7 Hz), 4.67 (s, 2H, H-*9*), 2.85 (s, 1H, H-*8*), 1.42 (br s, 1H, O*H*). **^{13}C{^{1}H} NMR (C_6D_6, 125 MHz):** 144.34 (C-*1*), 132.82 (C-*Ar*), 129.23 (C-*Ar*), 127.15 (C-*Ar*), 127.00 (C-*Ar*), 120.22 (C-*6*), 82.37 (C-*9*), 81.53 (C-*7*), 63.43 (C-*8*). **GC-MS** $[M]^{+}$**:** Calc: 132.06; Found: 132.10.

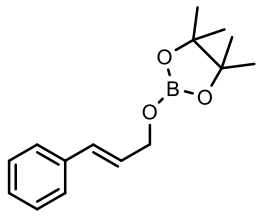

2-(cinnamylmethoxy)pinacolborane.

^{1}H, ^{11}B{^{1}H} and ^{13}C{^{1}H} spectra are identical to those reported in the literature.[40]

^{1}H NMR (C_6D_6, 500 MHz): 7.22-7.16 (m, 2H), 7.13-7.07 (m, 2H), 7.06-7.00 (m, 1H), 6.62 (dt, 1H, $^{3}J_{HH}$ = 15.9 Hz, $^{4}J_{HH}$ = 1.7 Hz), 6.19 (dt, 1H, $^{3}J_{HH}$ = 15.9 Hz, $^{3}J_{HH}$ = 5.3 Hz), 4.55 (dd, 2H, $^{3}J_{HH}$ = 5.3 Hz, $^{4}J_{HH}$ = 1.7 Hz), 1.08 (s, 12H). **^{11}B{^{1}H} NMR (C_6D_6, 128 MHz):** 22.70. **^{13}C{^{1}H} NMR (C_6D_6, 125 MHz):** 137.36, 130.91, 128.76, 127.69, 127.52, 126.85, 82.70, 65.54, 24.74.

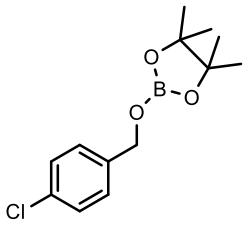

2-(4-chlorobenzyloxy)pinacolborane.

^{1}H, $^{11}B\{^{1}H\}$ and $^{13}C\{^{1}H\}$ spectra are identical to those reported in the literature.[37]

^{1}H NMR (C_6D_6, 500 MHz): 7.09-7.04 (m, 2H), 7.02-6.96 (m, 2H), 4.76 (s, 2H), 1.03 (s, 12H). **$^{11}B\{^{1}H\}$ NMR (C_6D_6, 128 MHz):** 22.64. **$^{13}C\{^{1}H\}$ NMR (C_6D_6, 125 MHz):** 138.46, 133.35, 128.71, 128.40, 82.87, 66.09, 24.69.

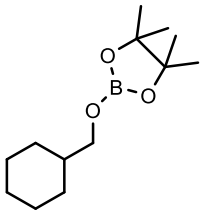

2-(cyclohexylmethoxy)pinacolborane.

^{1}H, $^{11}B\{^{1}H\}$ and $^{13}C\{^{1}H\}$ spectra are identical to those reported in the literature.[37]

^{1}H NMR (C_6D_6, 500 MHz): 3.76 (d, 2H, $^{3}J_{HH}$ = 64 Hz), 1.75-1.67 (m, 2H), 1.65-1.57 (m, 2H), 1.56-1.45 (m, 2H), 1.18-1.04 (m, 3H), 1.07 (s, 12H), 0.97-0.84 (m, 2H). **$^{11}B\{^{1}H\}$ NMR (C_6D_6, 128 MHz):** 22.29. **$^{13}C\{^{1}H\}$ NMR (C_6D_6, 125 MHz):** 82.37, 70.60, 39.86, 29.74, 26.90, 26.18, 24.77.

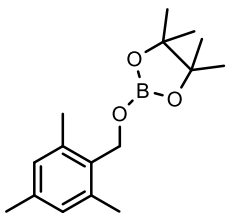

2-(mesitylmethoxy)pinacolborane.

^{1}H, ^{11}B{^{1}H} and ^{13}C{^{1}H} spectra are identical to those reported in the literature.[41]

^{1}H NMR (C_6D_6, 500 MHz): 6.73 (s, 2H), 5.03 (s, 2H), 2.37 (s, 6H), 2.12 (s, 3H), 1.04 (s, 12H). **^{11}B{^{1}H} NMR (C_6D_6, 128 MHz):** 22.58. **^{13}C{^{1}H} NMR (C_6D_6, 125 MHz):** 137.78, 137.39, 132.98, 129.35, 82.53, 61.53, 24.70, 21.07, 14.64.

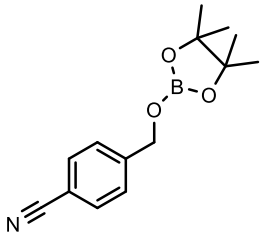

2-(4-cyanobenzyloxy)pinacolborane.

^{1}H, ^{11}B{^{1}H} and ^{13}C{^{1}H} spectra are identical to those reported in the literature.[39]

^{1}H NMR (C_6D_6, 500 MHz): 7.03-6.99 (m, 2H), 6.92-6.87 (m, 2H), 4.667 (s, 2H), 1.04 (s, 12H). **^{11}B{^{1}H} NMR (C_6D_6, 128 MHz):** 22.66. **^{13}C{^{1}H} NMR (C_6D_6, 125 MHz):** 144.57, 132.10, 126.78, 118.85, 111.61, 83.10, 65.84, 24.67.

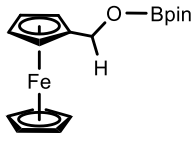

2-(ferrocenylmethoxy)pinacolborane.

^{1}H, ^{11}B{^{1}H} and ^{13}C{^{1}H} spectra are identical to those reported in the literature.[37]

^{1}H NMR (C_6D_6, 500 MHz): 4.75 (s, 2H), 4.21 (dd, 2H, $^{3}J_{HH}$ = 1.9 Hz, $^{4}J_{HH}$ = 1.9 Hz), 3.98 (s, 5H), 3.95 (dd, 2H, $^{3}J_{HH}$ = 1.9 Hz, $^{4}J_{HH}$ = 1.9 Hz), 1.07 (s, 12H). **^{11}B{^{1}H} NMR (C_6D_6, 128 MHz):** 22.67. **^{13}C{^{1}H} NMR (C_6D_6, 125 MHz):** 86.08, 82.61, 69.02, 68.80, 68.52, 63.44, 24.82.

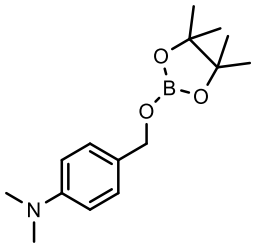

2-(4-N,N-dimethylaminobenzyloxy)pinacolborane

^{1}H, $^{11}B\{^{1}H\}$ and $^{13}C\{^{1}H\}$ spectra are identical to those reported in the literature.[39]

^{1}H NMR (C_6D_6, 500 MHz): 7.36-7.32 (m, 2H), 6.60-6.53 (m, 2H), 5.00 (s, 2H), 2.50 (s, 6H), 1.07 (s, 12H). **$^{11}B\{^{1}H\}$ NMR (C_6D_6, 128 MHz):** 22.80. **$^{13}C\{^{1}H\}$ NMR (C_6D_6, 125 MHz):** 150.16, 128.57, 112.42, 82.15, 66.85, 39.92, 24.39.

CHAPTER 2

$La[N(SiMe_3)_2]_3$ – Catalyzed Ester Reductions with Pinacolborane. Scope and Mechanism of Ester Cleavage

Adapted From:

Barger, C. J.; Motta, A.; Weidner, V. L.; Lohr, T. L.; Marks, T. J.; *ACS Catal*. **2019**, *9*(10), 9015-9024

Abstract

Tris[N,N-bis(trimethylsilyl)amido]lanthanum (La^{NTMS}) is an efficient, highly active, and selective homogeneous catalyst for ester reduction with pinacolborane (HBpin). Alkyl and aryl esters are cleaved to the corresponding alkoxy- and aryloxy-boronic esters which can then be straightforwardly hydrolyzed to alcohols. Ester reduction is achieved with 1 mol% catalyst loading at 25-60°C, and most substrates are quantitatively reduced in 1 hour. Nitro, halide, and amino functional groups are well-tolerated, and ester reduction is completely chemoselective over potentially competing intra- or intermolecular alkene or alkyne hydroboration. Kinetic studies, isotopic labeling, and DFT calculations with energetic span analysis argue that ester reduction proceeds through a rate-determining hydride transfer step that is ligand-centered (hydride is transferred directly from bound HBpin to bound ester) and not through a metal hydride-based intermediate that is often observed in organolanthanide catalysis. The active catalyst is proposed to be a La-hemiacetal, $[(Me_3Si)_2N]_2$La-OCHR(OR)[HBpin], generated *in situ* from La^{NTMS} via hydroboronolysis of a single La-$N(SiMe_3)_2$ bond. These results add to the growing compendium of selective oxygenate transformations that La^{NTMS} is competent to catalyze, further underscoring the value and versatility of homoleptic lanthanide complexes in homogeneous catalytic organic synthesis.

Introduction

The selective reduction of esters is a topic of great interest to both the academic and industrial synthetic chemistry communities.[1] In addition to being an important transformation in the synthesis of fine chemicals and pharmaceuticals,[2] ester linkages are ubiquitous in lignocellulosic biomass and plant-based oils, valuable renewable sources of fuels and chemical feedstocks, and their selective reduction is of great importance.[3] Unlike ketones and aldehydes, esters are generally inert towards mild reductants as typified by $NaBH_4$ and instead require more aggressive reductants such as BH_3 and $LiAlH_4$, reagents which can pose significant handling risks and often suffer from poor selectivity in the presence of other reducible functionalities.[4] Catalytic hydrogenation has been explored extensively as a more atom-efficient and selective route to ester reduction, however the high pressures and temperatures required to achieve satisfactory conversions, typically in excess of 5 bar and 100°C, pose significant safety concerns, and require capital-intensive equipment.[5] The need for safer and more convenient ester reduction methodologies has generated great interest in recent years in catalytic hydrosilylation, leading to a wealth of reports detailing the selective reduction of esters and other carbonyl groups at ambient pressures and moderate temperatures (typically < 100°C).[6] Conversely, reports of efficient, selective ester hydroboration are sparse,[7] a surprising observation considering that silanes and boranes often behave similarly in other hydrofunctionalization processes,[1a, 6b, 8] and that hydroboration is well-developed in the context of ketone/aldehyde reduction.[7c, 9]

Encouraged by recent results from this laboratory on lanthanide triflate-catalyzed ester C_{alkoxy}-O bond tandem hydrogenolysis processes, we turned our focus to kinetically labile and electrophilic

lanthanide complexes with alternative reducing agents to affect C_{acyl}-O bond reduction, specifically hydroboronolysis (Figure 2.1A).[10] Tris[N,N-bis(trimethylsilyl)amido]lanthanide complexes ($Ln[N(SiMe_3)_2]_3$, abbreviated here as Ln^{NTMS}, Figure 2.1B) are commercially available for many lanthanides, or they can be readily synthesized/purified, rendering them accessible and of great utility to the synthetic methods community.[11] As such, they are frequently employed as precursors to more elaborate lanthanide organometallics[12] and as homogeneous catalysts, particularly for alkene/alkyne hydrofunctionalization.[13] Recently, we reported that La^{NTMS} displays remarkable catalytic activity for ketone and aldehyde hydroboration with HBpin (Figure 2.1B), with turnover frequencies as high as 40,000 h^{-1} at 25°C.[9l] With this in mind, we sought to explore the catalytic hydroboration activity of La^{NTMS} with more complex, less readily-reduced oxygenates. While this investigation was in progress, Patnaik and Sadow reported that the homoleptic lanthanide tris-hydrocarbyl $La[C(SiHMe_2)_3]_3$ is highly active for the hydroboration of epoxides and esters, raising the intriguing question of whether commercially available lanthanide amides such as La^{NTMS} might be viable ester hydroboration catalysts, and if so, with what scope and reaction mechanism.[7a]

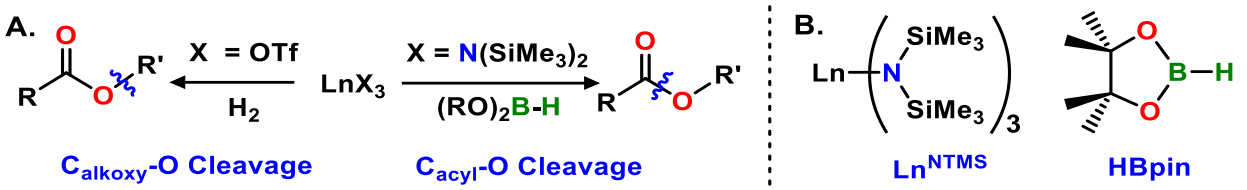

Figure 2.1. A. Comparison of ester C_{alkoxy}-O bond cleavage/hydrogenolysis, previously reported for lanthanide (Ln) triflates),[10] and Ln-catalyzed C_{acyl}-O bond cleavage/hydroboronolysis pathways (this work). OTf^- = $CF_3SO_3^-$. **B**. Structures of tris[N,N-bis(trimethylsilyl)amido]lanthanide complexes (Ln^{NTMS}) where Ln = any lanthanide, and pinacolborane (HBpin).

Here we report that La^{NTMS} effectively mediates the cleavage of a wide variety of alkyl and aryl esters to the corresponding alkoxyboranes. This system, which utilizes a commercially available catalyst, mild reaction conditions, and easily-handled HBpin, represents a significant advance over traditional ester reduction methods. We discuss the scope and mechanism of this transformation through combined experiment and DFT-level theory, which is, to the best of our knowledge, the first attempt to do so in the field of catalytic ester hydroboration. It will be seen that the reaction, which is selective over nitro functionalities as well as alkene and alkyne reductions, proceeds through a La-hemiacetal active catalyst/resting state with a very unusual ligand-centered hydride transfer step.

Results

Ester catalytic reduction scope. Optimal conditions for ester cleavage (Table 2.1) are achieved with 1 mol % of La^{NTMS} catalyst and a slight excess of HBpin (2.2 equiv vs. ester). Table 2.1 shows

the full scope of esters investigated. Other Ln^{NTMS} complexes (Ln = Ce, Sm, Yb, and Y) were also screened with phenyl benzoate reduction as the model reaction. These catalysts are found to have similar, though slightly diminished reduction rates relative to La^{NTMS}. This, combined with the relative ease with which NMR spectra of metal-organics containing diamagnetic La^{3+} can be analyzed, led us to pursue further studies with La^{NTMS} exclusively. Catecholborane ("HBcat") and 9-borabicyclo[3.3.1]nonane ("9-BBN") were also explored as alternative reductants to HBpin (also using phenyl benzoate reduction as a model reaction). HBcat produces negligible product (<5%) after 20 hours at 25°C, while 9-BBN affords 46% conversion under the same conditions. These are both significantly poorer performing than HBpin (97% yield after 16 hours at 25°C; Table 2.1).

As can be seen in Table 2.1, all esters are reduced near-quantitatively at 25°C under the conditions described above, although several require heating at 60°C for more convenient reaction times (≤ 5 h). Importantly, side-reactions with nitro groups or conjugated alkenes are not observed (Table 2.1, entries 16 and 11, respectively), and intermolecular competition experiments indicate that the esters are preferentially reduced with complete exclusion of added 1-octene or 1-octyne (Scheme 2.1). Given the high activity observed for La^{NTMS}-catalyzed ketone and aldehyde hydroboration,[9l] selectivity for ester reduction over these more reactive functional groups would not be expected. Predictably, reduction of *tert*-butyl acetoacetate occurs only at the ketone, and the ester functionality remains intact, even after 16 hours at 25°C. Preparative-scale (2.5 mmol) reduction of ethyl acetate (entry 2) gives a 94% isolated yield of EtOBpin under conditions identical to those used in the NMR scale reaction.

Table 2.1. Scope of La^{NTMS}-catalyzed ester reduction/cleavage with pinacolborane[a]

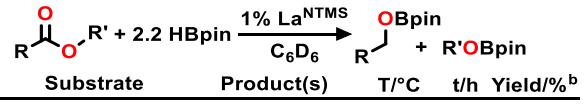

#	Substrate	Product(s)	T/°C	t/h	Yield/%[b]
1	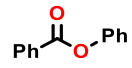	$PhCH_2OBpin$ + PhOBpin	25 60	16 5	97 99
2	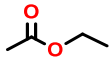	2 EtOBpin	25	0.25	>99
3	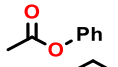	PhOBpin + EtOBpin	25 60	5 1	>99 >99
4	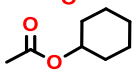	CyOBpin + EtOBpin	25	1	>99
5	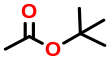	^{t}BuOBpin + EtOBpin	25 60	16 1	>99 >99
6	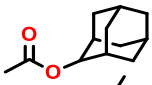	AdmOBpin + EtOBpin	25	1	>99
7[c]	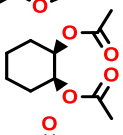	$Cy(OBpin)_2$ + 2EtOBpin	25 60	48 1	98 >99
8	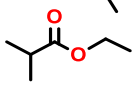	^{i}BuOBpin + EtOBpin	25	0.25	>99
9	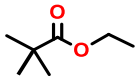	$(CH_3)_3CCH_2OBpin$ + EtOBpin	25	0.5	>99
10	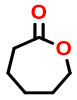	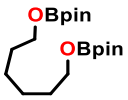	25	0.25	>99
11[d]	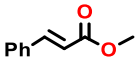	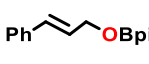	25 60	16 3	>99 >99
12[d]	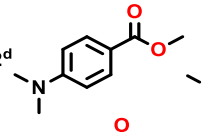	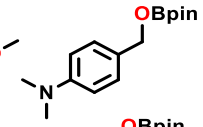	25	16	98
13[d]	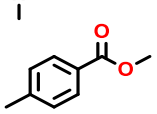	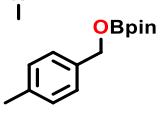	25	1.5	93
14[d]	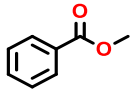	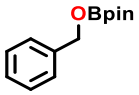	25	1.5	>99
15[d]	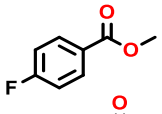	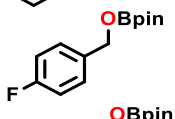	25	1.5	>99
16[d]	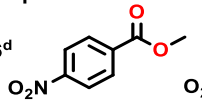	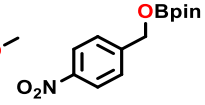	25	0.25	>99

[a] Reaction conditions: Ester (0.25 mmol) and HBpin (0.55 mmol, 2.2 equiv) in C_6D_6 (500 μL), and La^{NTMS} (2.5 μmol). [b] Yields of RCH_2OBpin products calculated by integration of product ^1H NMR signals vs hexamethylbenzene internal standard. [c] 4.4 equiv. HBpin. [d] Product + MeOBpin

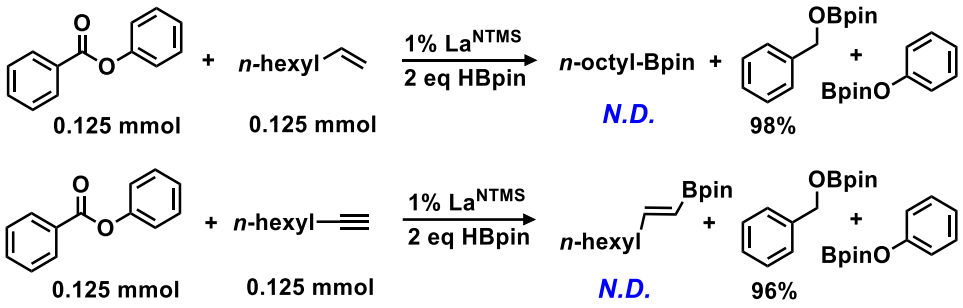

Scheme 2.1. Competition experiments illustrating the selective reduction of phenyl benzoate in the presence of 1-octene (top) and 1-octyne (bottom). ***N.D.*** = not detected. Conditions: 1.00 mL C_6D_6, 60°C, 5h.

While all ester substrates are efficiently reduced at 60°C, steric impediments at the alkoxy-position (R' in Table 2.1) significantly depress rates at 25°C, with *tert*-butyl acetate (Table 2.1, entry 5) requiring 16 h to reach completion, vs. 1 h for cyclohexyl- and 2-adamantyl acetate (entries 4 and 6, respectively) and only 10 min for ethyl acetate (entry 2). Interestingly, steric impediments at the acyl position (R in Table 2.1) have very little effect on the rate of reduction, with ethyl acetate ethyl isobutyrate, and ethyl pivalate (entries 2, 8, and 9, respectively) all required ≤ 30 min at 25°C to reach completion. The presence of a phenyl group in the R' position (entries 1 and 3) likewise depresses the rate, suggesting the charge density on the alkoxy oxygen is an important factor in determining the overall conversion rate, possibly implicating La-O coordination in the turnover-limiting step (*vide infra*). Note also that ε-caprolactone (Table 2.1, entry 10) is reduced quantitatively to the ring-opened bis-borane at 25°C in ~15 min, with no evidence of potentially competing polymerization. This is surprising since the analogous Sm^{NTMS} and Y^{NTMS} complexes are reported to be highly active catalysts for caprolactone ring-opening polymerization.[14] Indeed, when ε-caprolactone is added to a La^{NTMS} solution in benzene without HBpin present, rapid

polymerization ensues, as evidenced by solidification of the reaction mixture. Interestingly, subsequent addition of HBpin to the polycaprolactone results in rapid de-polymerization and conversion to a non-viscous liquid that is NMR spectroscopically identical to the product of entry 10 in Table 2.1.

Experimental kinetic studies. To probe the mechanism of the present ester cleavage process, the rate law for catalytic phenyl benzoate reduction was determined by a combination of initial rates analysis at various catalyst concentrations (for the order in La^{NTMS} concentration) and by monitoring substrate consumption under pseudo-first order conditions. The reaction rate is observed to have a first-order dependence on La^{NTMS} concentration, whereas ester and HBpin concentration variations over a broad range have no detectable effect on the rate (eq. 2.1). Activation parameters calculated for the reduction of phenyl benzoate over the temperature range of 15-35°C reveal a relatively

$$\text{Rate} = k[La^{NTMS}]^1[\text{Ester}]^0[\text{HBpin}]^0 \qquad (2.1)$$

low apparent activation enthalpy ($\Delta H^{\ddagger} = 8.2 \pm 0.3$ kcal/mol) and a very large, negative activation entropy ($\Delta S^{\ddagger} = -53.1 \pm 0.9$ e.u.). To gauge the impact of electron density at the carbonyl carbon on the rate of reaction, a Hammett plot (Figure 2.2) was constructed using a series of *para*-substituted methyl benzoates (Table 2.1 entries 12-16). A significant increase in turnover is observed for substrates with electron-withdrawing substituents at the R position, as indicated by a positive value (1.11) for the parameter ρ. Additional mechanistic details were obtained from

isotopic labeling studies. Replacing HBpin with DBpin in the reduction of methyl 4-(*N,N*-dimethylamino)benzoate eliminates both methylene protons in the product ^{1}H NMR spectra, indicating both hydride equivalents are delivered to the carbonyl carbon (Figure 2.3). Comparing these reaction rates yields a kinetic isotope effect (KIE) of 1.49.

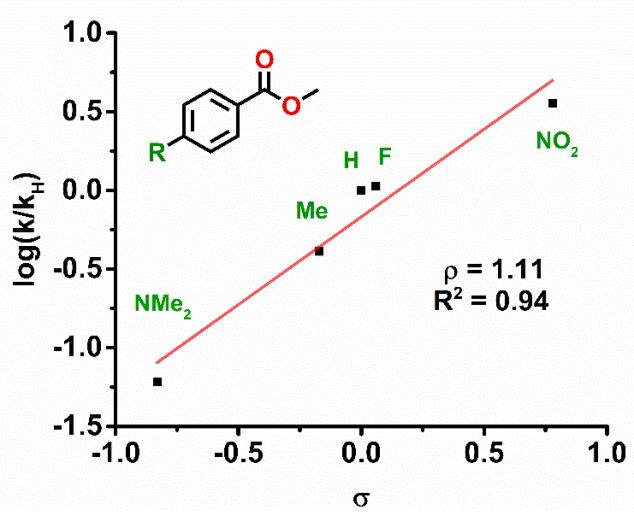

Figure 2.2. Hammett plot generated for the La^{NTMS}-catalyzed reduction of *para*-substituted methyl benzoates with HBpin.

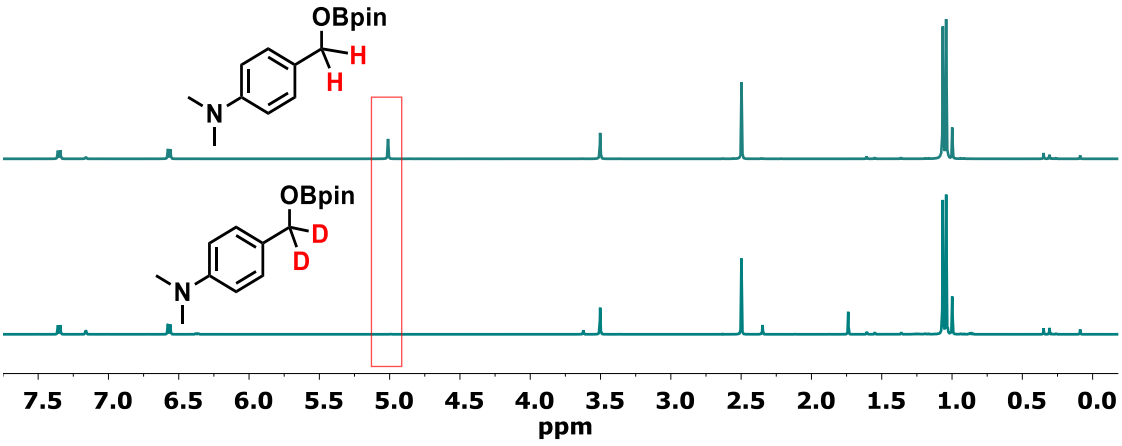

Figure 2.3. ^{1}H NMR spectra of the La^{NTMS}-catalyzed reduction of methyl 4-(dimethylamino)benzoate with 2 equiv of HBpin (top) and DBpin (bottom). The absence of a signal in the ~δ 5.0 ppm region (outlined in red) for reduction with DBpin shows that both ^{1}H NMR-silent deuteride equivalents are delivered to the carbonyl carbon of the substrate.

***In Situ* Stoichiometric ^{1}H, ^{13}C and ^{11}B NMR Spectroscopic Studies.** The pathway(s) and species involved in the present ester hydroboration process were probed *in situ* by examining the reactivity of La^{NTMS} with stoichiometric amounts of ester and/or HBpin at room temperature. No reaction is observed between La^{NTMS} and phenyl benzoate only, however the ^{1}H NMR signals of both species shift slightly, suggesting that ester reversibly coordinates to Lewis acidic La^{NTMS}.[15] In contrast, La^{NTMS} and HBpin undergo reaction, as evidenced by the appearance of several new signals in the ^{1}H, ^{13}C and, ^{11}B NMR spectra. In the ^{1}H NMR, singlets at δ 0.37 and 1.03 ppm (integrating as 18 and 12 H, respectively) are attributable to the known compound pinB-N(SiMe$_3$)$_2$.[16] Singlets at δ 1.37 and 1.56 ppm, both integrating to 6 H, as well as a quartet in the ^{11}B NMR at -6.3 ppm, are indicative of a reaction pathway involving ring-opening of a pinacolborane ring to give the off-cycle borate complex shown below (A_{OC}, Scheme 2.2A). A similar complex was reported, by this laboratory, to be an off-cycle product of lanthanocene-catalyzed pyridine dearomatization with

pinacolborane (Scheme 2.2B) and characterized by x-ray diffraction.[17] Notably, in the present system, the La-O bond integrity is maintained, as evidenced by a greater downfield shift in the adjacent C(C*H*$_3$)$_2$ protons (1.56 ppm),[18] whereas with pyridine hydroboration, this bond is broken and replaced by an intact Bpin moiety (adjacent C(C*H*$_3$)$_2$ protons appear at 1.30 ppm; Scheme 2.2B). When ester is added to complex A_{OC}, or when stoichiometric ester and HBpin are added simultaneously to La^{NTMS}, the ^{11}B NMR signal at -6.3 ppm disappears and a triplet at 47.4 ppm grows in, indicating a hydride is transferred from the R-BH_3^- group, yielding R-BH_2 and a partially reduced ester (B_{OC}, Scheme 2.2A). Subsequent addition of excess substrates does not result in turnover, indicating this is, in fact, an off-cycle pathway that likely results in deactivation. We propose that the true active catalyst (*vide infra*) is not detectable by NMR, likely due to the availability of the above deactivation pathway at low substrate concentrations relative to catalyst concentration (such as those employed in the above spectroscopic studies). Attempts to more fully characterize these off-cycle products were unsuccessful due to their decomposition into intractable, white solids over the course of 2 hours at room temperature. However, DFT analysis argues that these products are energetically accessible in the conditions employed above and their formation is highly exergonic.

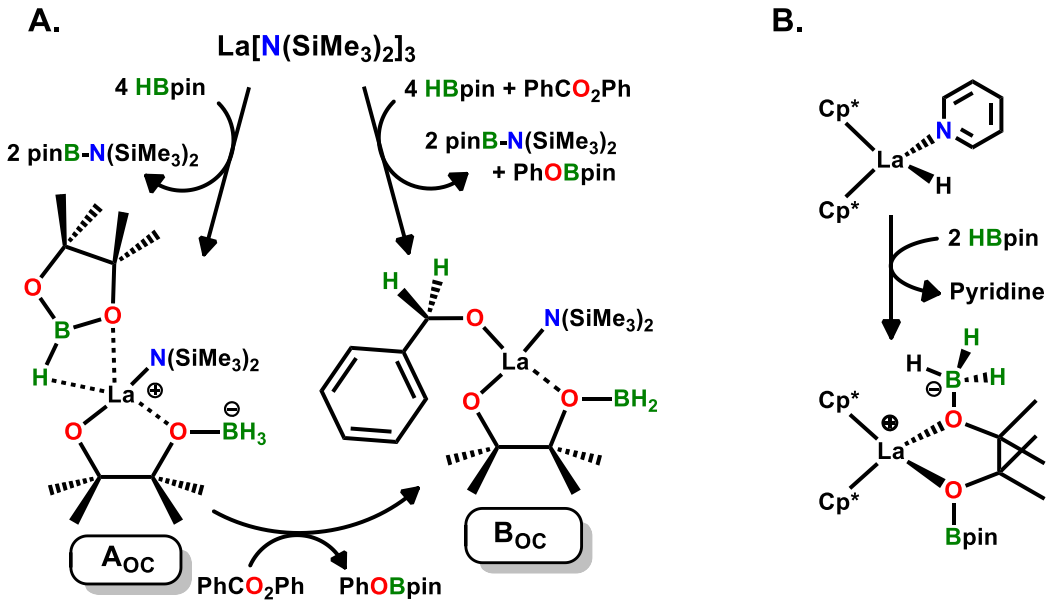

Scheme 2.2. **A**. Catalyst off-cycle products observed in NMR studies of stoichiometric substrate and La^{NTMS}. **B**. Structure of a product similar to A_{OC} isolated from an organolanthanide-catalyzed pyridine dearomatization/hydroboration process.[17] Cp* = η^5-pentamethylcyclopentadienyl

DFT Mechanistic Analysis. To more fully understand the mechanism of La^{NTMS}-catalyzed ester reduction with pinacolborane, DFT modeling of the catalyst activation process, catalytic cycle, and potential off-cycle pathways was performed using methyl benzoate as a model ester. Figure 2.4 shows the computed catalyst activation process. The La^{NTMS} pre-catalyst is activated for ester reduction first by HBpin-mediated cleavage of a La-N$(SiMe_3)_2$ bond (**TS_{act}-1**), forming complex **Iact-2**. Direct hydride transfer from the coordinated $[(SiMe_3)_2NB(H)pin]^-$ molecule of **Iact-2** to a coordinated ester molecule (**TS_{act}-2**) then affords lanthanide-hemiacetal species **I_{act}-3** and pinB-N$(SiMe_3)_2$ as a byproduct. Subsequent coordination of a second HBpin molecule leads to the active catalyst. The entire process is exergonic (-44.9 kcal/mol) and has an energy barrier of only 9.9 kcal/mol associated with the scission of the La-N bond in **TS_{act}-1**. The possibility of a

$[(Me_3Si)_2N]_2La$-H active catalyst was also explored due to the ubiquity of proposed L_2Ln-H species as both active catalysts and intermediates in the organolanthanide literature,[17, 19] however the energy required to form such a species in the present system (> 30kcal/mol) appears to be unlikely.

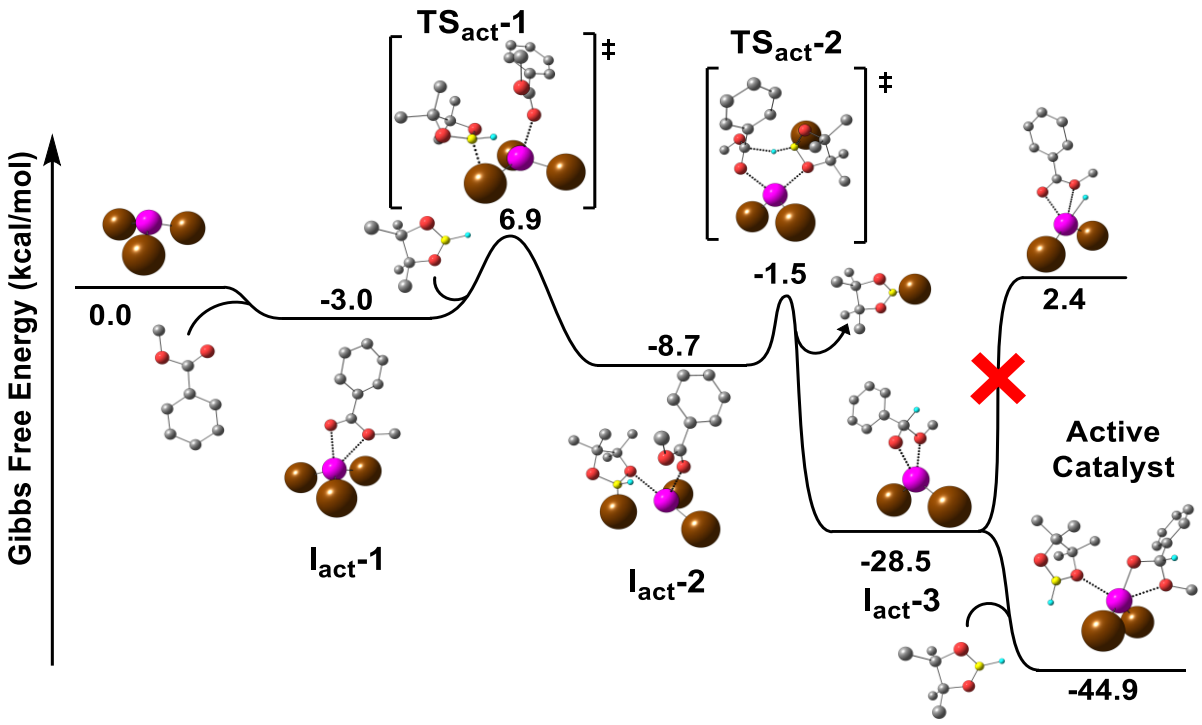

Figure 2.4. Gibbs free energy profile (kcal/mol) of the La^{NTMS} pre-catalyst activation process using methyl benzoate as a model ester substrate. The occurrence of a La-centered hydride (via the step denoted by a red "X") is energetically implausible. La = violet, C = grey, H = cyan, B = yellow, and $N[SiMe_3]_2$ = brown.

The proposed catalytic cycle consists of three principal steps (Figure 2.5): 1) Lewis acidic boron (of the coordinated HBpin molecule) attack on the hemiacetal oxygen of the active catalyst **A** (**TS1**), leading to formation of a new B-O bond and dissociation of the La-$O_{hemiacetal}$ bond. This step, which produces a La-coordinated hemiacetal-pinacolborate species, proceeds with a computed barrier of 3.1 kcal/mol, and the subsequent coordination of a second ester molecule leads to an overall stabilization (-12.4 kcal/mol) and generates complex **B**. 2) Transfer of the ester methoxy group to the coordinated HBpin, followed by a rapid hydride transfer from $[HB(OMe)(pin)]^-$ to the La-hydroborate complex (**TS2**), forms the first reduction product, MeOBpin. The product of this step (complex **C**) is highly stabilized by the coordination of both ester and HBpin molecules, leading to an overall stabilization of -46.0 kcal/mol. 3) Intramolecular hydride transfer from complex **C** to the coordinated ester (**TS3**) leads to formation and subsequent release of the second reduction product, $PhCH_2OBpin$, restoring the active catalyst **A**. In the transition state structure, HBpin loses its coordination with the La metal center and interacts weakly with the carbonyl oxygen of the coordinated ester. This step is exergonic (-7.1 kcal/mol) and represents the rate-determining step with an energy barrier of 14.7 kcal/mol.

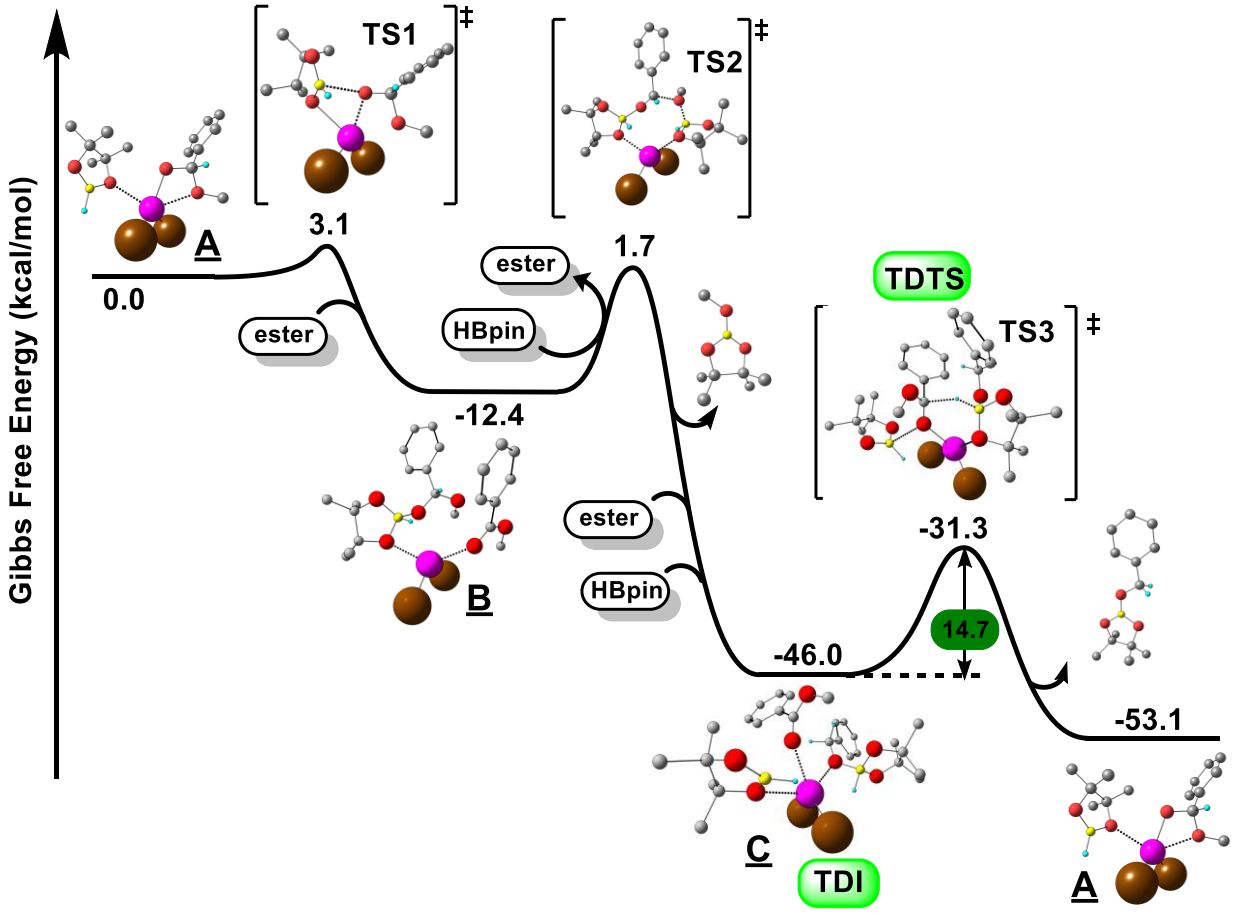

Figure 2.5. Gibbs free energy profile (kcal/mol) for the catalytic cleavage of methyl benzoate via hydroboration. The active catalyst is derived from La^{NTMS} (Figure 2.4); TDI = turnover-determining intermediate, TDTS = turnover-determining transition state. La = violet, C = grey, H = cyan, B = yellow, and $N[SiMe_3]_2$ = brown.

Discussion

Figure 2.6 presents a plausible scenario that accounts for the experimental mechanistic observations and DFT calculations discussed above. Note that negligible reaction is observed in stoichiometric mixtures of La^{NTMS} and phenyl benzoate, providing evidence that La^{NTMS} must be activated with HBpin to initiate the catalytic reduction cycle. According to the DFT and NMR results described above, activation of the ester-coordinated precatalyst with HBpin, followed by coordination of additional HBpin, generates the lanthanide-hemiacetal active catalyst **A** and known pinB-N$(SiMe_3)_2$ as a by-product. Just as in the stoichiometric studies described above, the TMS methyl protons of the aminoborane are also observed in the *in situ* ^{1}H NMR spectra of catalytic reactions (the Bpin methyl protons are obscured by substrate/product signals).[16] This resonance integrates in an approximate 1:2 ratio to the La^{NTMS} methyl protons (at δ 0.28 ppm), arguing mono-activation of the pre-catalyst does in fact occur. Furthermore, Sadow and co-workers recently proposed a similar hemiacetal-based catalytic intermediate, [La]-OCHR(OR), for La[C$(SiHMe_2)_3]_3$-catalyzed ester hydroboration based on detailed kinetic studies.[7a] The similarities between these homoleptic lanthanide complexes, both in terms of structure and reactivity, suggest similar species would be active for ester hydroboration. Additionally, the involvement of both ester *and* HBpin in catalyst activation is supported in the present work by the off-cycle reaction observed when HBpin is allowed to react with La^{NTMS} in the absence of ester (*vide supra*). This suggests that without a substantial excess of ester (relative to La^{NTMS}) to accept the hydride from La-coordinated HBpin and generate **A**, an unstable La-hydride/borate species is formed, opening the pinacolate ring of HBpin and deactivating the La center.[17]

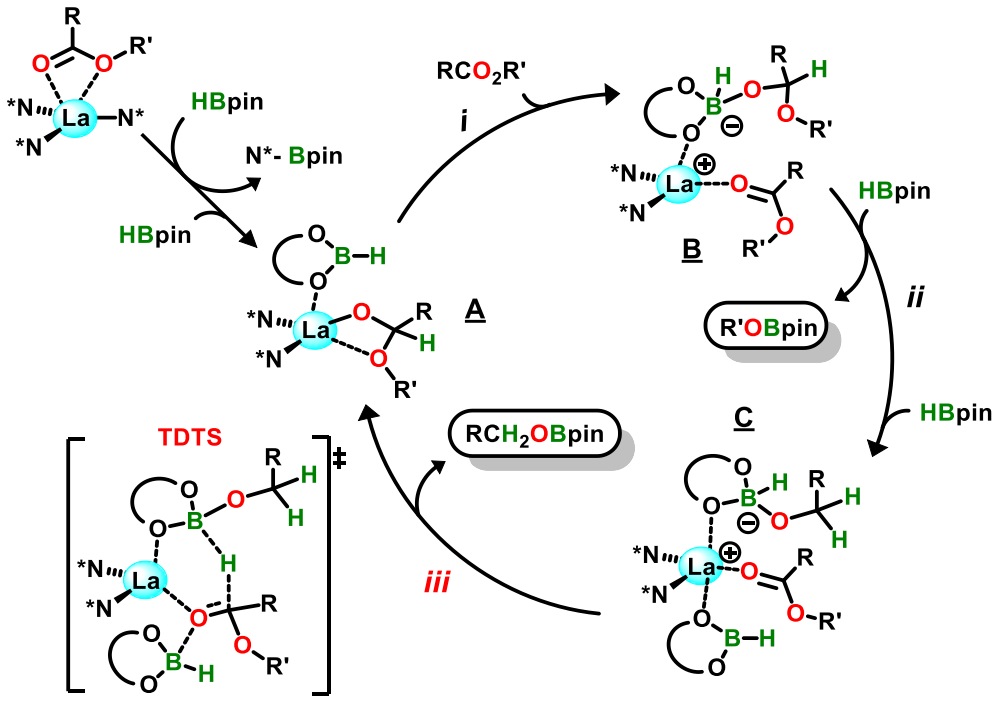

Figure 2.6. Catalyst activation and catalytic cycle for La^{NTMS}-catalyzed ester hydroboration. N* = $N(SiMe_3)_2$. Step ***iii*** is proposed to be turnover limiting, and the DFT-computed turnover-determining transition state (TDTS) is shown.

Activated by the oxophilic La center, HBpin promotes La-$O_{hemiacetal}$ bond dissociation and B-$O_{hemiacetal}$ bond formation (Figure 2.6, step *i*), producing a transient complex that is spontaneously stabilized by coordination of a new ester molecule, yielding intermediate **B**. This sterically congested species then rearranges intramolecularly, yielding R'OBpin. Subsequent, barrierless coordination of HBpin affords stabilized complex **C** (step *ii*). Finally, intramolecular hydride transfer from the boron atom of the hydroborate-La complex to the coordinated ester (step ***iii***) restores the active catalyst **A** for subsequent catalytic cycles. Assignment of this step as turnover-limiting is supported by several experimental observations. The experimentally derived activation

parameters, consisting of a small, positive $\Delta H^{\ddagger}$ and large, negative $\Delta S^{\ddagger}$, suggest the transition state is highly organized and sterically congested, and the overall first-order reaction rate requires that the turnover-limiting step is intramolecular.[20] Notably, the activation parameters reported for this system ($\Delta H^{\ddagger}$ = 8.2 kcal/mol, $\Delta S^{\ddagger}$ = -53.1 e.u.) are very similar to those reported previously for aldehyde hydroboration with B-alkyl-9-BBN ($\Delta H^{\ddagger}$ = 9.1 - 9.8 kcal/mol, $\Delta S^{\ddagger}$ = -43 - -49 e.u.).[21] The transition state proposed for this reaction is also quite similar to the one proposed above, as it proceeds through a sterically congested and conformationally constrained transition state and involves intramolecular hydride transfer to the carbonyl.

The zero order reaction rate law found experimentally for HBpin and ester concentrations is supported by the DFT calculations (Figure 2.5), which find that neither HBpin nor ester enters the catalytic cycle between the turnover-determining intermediate (TDI, **C**) and the turnover-determining transition state (TDTS, **TS3**).[22] The high degree of steric congestion in the transition state would lead to depressed rates for sterically encumbered substrates, which is observed experimentally. A small, positive Hammett ρ value (ρ = 1.11, Figure 2.2) indicates that the transition state is stabilized by withdrawal of electron density from the carbonyl carbon, but to a much lesser extent than is observed for typical base-catalyzed ester cleavages (ρ =1.9-2.5).[23] This supports the present assignment that the turnover-limiting step involves nucleophilic hydride attack on a carbonyl bond that has been activated, in this case by simultaneous C=O coordination to both HBpin and La, priming the acyl carbon for nucleophilic attack and diminishing ρ.

While the present KIE of 1.49 for ester reduction with DBpin is small for a primary KIE, it is much larger than typical values for secondary isotope effects, [20] supporting an assignment of B-H scission in the turnover-limiting step. While the lack of previously reported KIEs for HBpin-based

ester reduction prevents direct comparison, analogous reductions of N-heteroarenes,[24] ketones,[25] and nitriles[26] proceed with somewhat higher KIEs, ranging from 2.3-2.8. However, Hartwig and co-workers report a similarly small KIE (1.62) for the addition of catecholborane, via σ-bond metathesis, to a Ru-alkyl, indicating KIEs this small are not without precedent for B-H bond scission.[27] In this system, it is likely that slight O→B interaction in the TDTS likely weakens the B-H bond prior to scission, contributing to the lower KIE than might be expected for such a reaction. The terminal location of the borane derived hydrogens is also telling. As noted above, the deuterium-labelling experiment shows that both hydride equivalents are delivered to the carbonyl carbon, effectively ruling out the possibility of a reverse-Tishchenko-based mechanism (Scheme 2.3). Such a mechanism warrants consideration since the Tishchenko reaction (coupling of aldehydes to form esters) is catalyzed by Ln^{NTMS} complexes,[28] and a similar mechanism was proposed previously for Mg-catalyzed ester hydroboration.[7d] Note also that a Tishchenko-like pre-equilibrium could not account for substrates lacking an α-H in the R' position (i.e., Table 2.1, entries 1, 3, and 5) since the aldehyde C=O bond cannot form at a fully substituted carbon center.

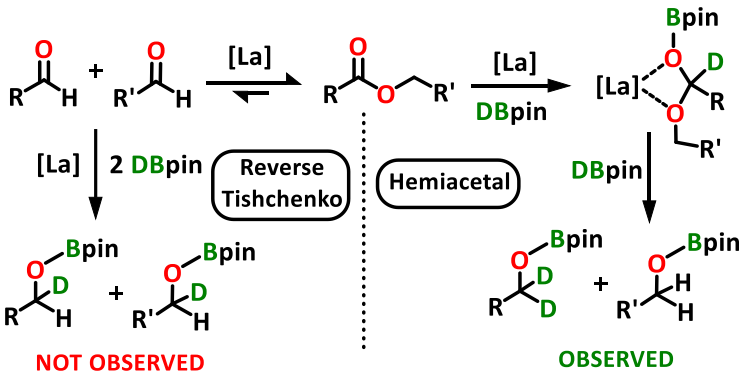

Scheme 2.3. Isotopic labelling differentiation of the hemiacetal-based ester hydroboration mechanism proposed here and the reverse-Tishchenko type mechanism proposed for Mg-catalyzed ester hydroboration.[7d]

Conclusions

The scope and mechanism of La^{NTMS}-catalyzed, pinacolborane-based reduction of a diverse series of esters is investigated experimentally and by DFT computation. The catalyst shows complete selectivity for ester reduction over competing nitro groups, alkenes, and alkynes, even at temperatures as high as 60°C. Experimental and computation-based mechanistic studies indicate that the active catalyst is generated from the La^{NTMS} pre-catalyst by HBpin-mediated La-N bond scission, generating a La-hemiacetal species that is active for ester reduction. The presence of ester in the catalyst activation process likely inhibits the formation of a L_2La-H species, which could explain the selectivity of this catalyst over alkene and alkyne hydroboration, reactions which have previously been proposed to proceed through a L_2La-H active catalyst.[13k, 19e] The turnover-limiting step is proposed to involve intramolecular, concerted hydride transfer/C-O bond cleavage, leading to an overall first-order rate law, rate = $[La^{NTMS}]^1[ester]^0[HBpin]^0$. This report further demonstrates the important role that lanthanide catalysis can play in experimental chemical synthesis, and it represents the first attempt at a combined experimental-theoretical approach to discerning HBpin-mediated ester reduction. By combining a mild reductant like HBpin with the highly active and readily accessible catalyst La^{NTMS}, a safer, more selective, and convenient route to ester reduction has been realized.

Experimental Section

Materials and Methods. All manipulations of air-sensitive materials were carried out with rigorous exclusion of O_2 and moisture in flame- or oven-dried Schlenk-type glassware on a dual-manifold Schlenk line or in an argon-filled glovebox with a high capacity recirculator (<0.5 ppm O_2). Benzene-d_6 (Cambridge Isotope Laboratories; 99+ atom % D) was stored over Na/K alloy and vacuum transferred prior to use. La[N(SiMe$_3$)$_2$]$_3$ (La^{NTMS}) and hexamethylbenzene were purchased from Sigma-Aldrich Co. and sublimed under high-vacuum (10^{-6} Torr). Pinacolborane ("HBpin") was purchased from Sigma-Aldrich Co. and distilled under high-vacuum (10^{-6} Torr) to remove trace boronic acid impurities and stored at -35°C in a glovebox.[17] Ester substrates were purchased from Sigma-Aldrich Co. and dried over 3Å molecular sieves (liquid esters) or under vacuum overnight (solid esters). The products of ester cleavage (alkoxy boryl esters) were characterized by ^{1}H, ^{13}C, and ^{11}B NMR. NMR spectra were recorded on a Bruker Avance III (500 MHz, ^{1}H; 125 MHz, ^{13}C), Varian Inova 500 (500 MHz, ^{1}H; 125 MHz, ^{13}C), Agilent DD MR-400 (400 MHz, ^{1}H; 100 MHz, ^{13}C; 128 MHz, ^{11}B), or Agilent DD2 500 (500 MHz, ^{1}H; 125 MHz, ^{13}C). Chemical shifts (δ) for ^{1}H and ^{13}C are referenced to residual solvent resonances (7.16 and 128.06 ppm, resp., for benzene-d_6). ^{11}B shifts are referenced to an external $BF_3 \cdot OEt_2$ standard. NMR scale reactions were carried out either in Teflon-sealed J. Young tubes or rubber septum-sealed tubes.

General Procedure for NMR-scale, LaNTMS-catalyzed ester reductions with HBpin.

For solid esters: In the glovebox, the ester substrate (0.25 mmol) and HBpin (0.55 mmol) were dissolved in benzene-d_6 (total volume 1.0 mL). This solution was then injected into a vial containing La^{NTMS} (2.5 μmol) and shaken to dissolve the catalyst. The reaction mixture was next transferred to a J. Young capped NMR tube and removed from the glovebox, and the ensuing reaction was monitored by ^{1}H NMR.

For liquid esters: In a glovebox, La^{NTMS} (2.5 μmol) was placed in a rubber septum-sealed NMR tube, and the cap was wrapped with Parafilm. HBpin (0.55 mmol) and benzene-d_6 were next added to a septum-sealed vial, and the cap was wrapped with electrical tape. Outside the glovebox, the liquid ester (0.25 mmol) was then injected into the vial with HBpin and internal standard, the vial was shaken, and the contents were injected into the NMR tube containing the catalyst, all under N_2. The tube was shaken to dissolve the catalyst, and the ensuing reaction was monitored by ^{1}H NMR.

Typical NMR-Scale Reaction for Kinetic Monitoring by ^{1}H-NMR Arrays. In a glovebox, ester, HBpin, and the internal standard were mixed in a vial and dissolved in C_6D_6 (V_{total}=1 mL). This solution was then added to a rubber septum-sealed NMR tube, wrapped with film, and removed from the box. At the NMR, the magnet was locked, tuned, and shimmed to the sample, then a stock solution containing an appropriate loading of $La[N(SiMe_3)_2]_3$ (also prepared in a glovebox) was injected into the tube. The tube was shaken and reinserted into the instrument and the experiment was started. Single ^{1}H NMR scans were collected at regular intervals. Substrate and/or product concentrations were determined relative to the intensity of the internal standard resonance and plotted versus time.

Kinetic Analysis. Kinetic analysis of the NMR-scale reactions described above was carried out by collecting multiple (>15) data points early in the reaction (<20% conversion). Under these conditions, the reaction can be approximated as pseudo-zero-order with respect to the substrate concentrations. The product concentration was measured from the area of the RC*H*$_2$OBpin product peaks relative to a C_6Me_6 internal standard. Data were fit by least-squares analysis ($R^2 > 0.98$) according to eq. 2.2, where t is time, [product] is the concentration of product at time t, and m is the rate of reaction.

$$[product] = mt \tag{2.2}$$

Orders for HBpin and ester (phenyl benzoate) were determined by running the reaction under pseudo-first-order conditions (10-fold excess of non-measured reactant). The order of the reactant not in excess was determined from the linearity of plots of [A] vs. time (zeroth order), ln[A] vs. time (first order), and $[A]^{-1}$ vs. time (second order).[34]

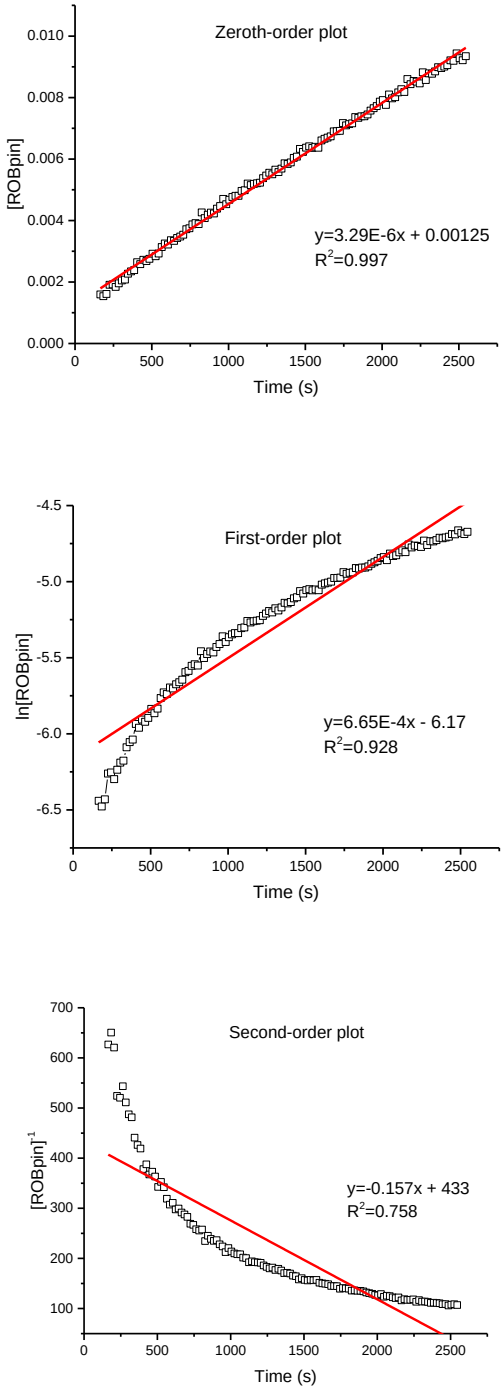

Figure 2.7. Pseudo-first order plots for reaction order in HBpin for ester reduction (10-fold excess of ester). Only the zeroth-order plot ([ROBpin] vs. time) is linear. Reaction conditions: 0.125 μmol La^{NTMS}, 1.25 mmol phenyl benzoate, 0.125 mmol HBpin, 0.0330 mmol C_6Me_6, C_6D_6 (total volume 1.00 mL).

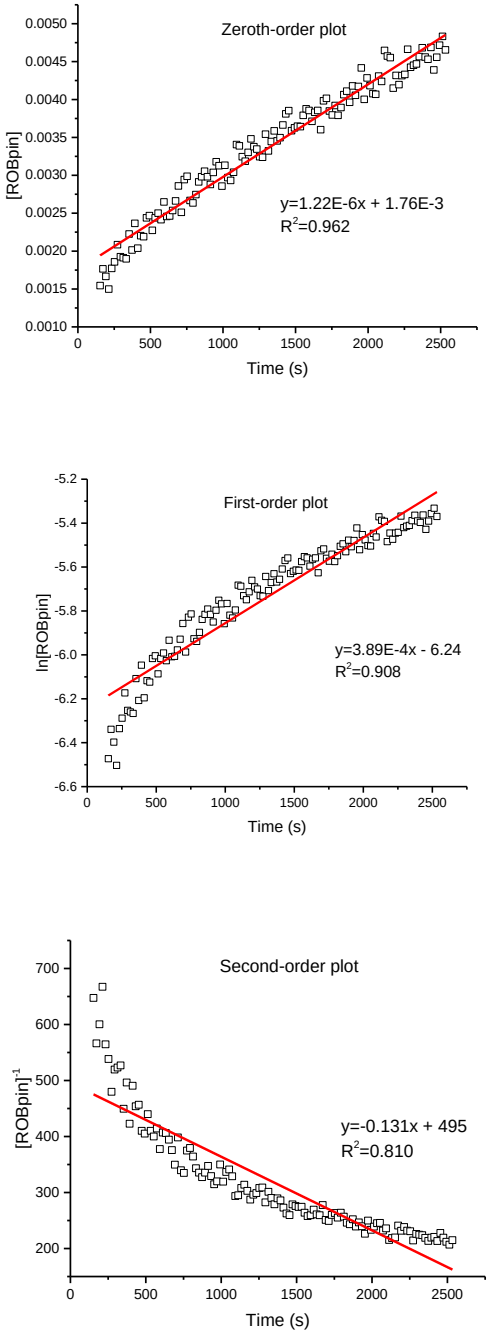

Figure 2.8. Pseudo-first order plots for reaction order in phenyl benzoate (10-fold excess of HBpin). Only the zeroth-order plot ([ROBpin] vs. time) is linear. Reaction conditions: 0.125 μmol La^{NTMS}, 0.125 mmol phenyl benzoate, 1.25 mmol HBpin, 0.0330 mmol C_6Me_6, C_6D_6 (total volume 1.00 mL).

The order for La^{NTMS} was determined from the rates of reduction at 5 different catalyst loadings (0.1-0.5%). The rates were measured as the slope of the line for [Product] vs. time at conversion < 20%. These rates were then plotted as ln(rate) vs. ln[La^{NTMS}]. The negative rate of disappearance of La^{NTMS} is proportional to the concentration of La^{NTMS} to the order (α) (see eq. 2.3). Therefore, the order is the slope of a plot of ln(rate) vs. ln[La^{NTMS}] (eq. 2.4).[17]

$$\frac{-d[LaNTMS]}{dt} = k_{obs}[LaNTMS]^{\alpha} \tag{2.3}$$

$$\ln(rate) = lnk_{obs} + \propto \ln [LaNTMS] \tag{2.4}$$

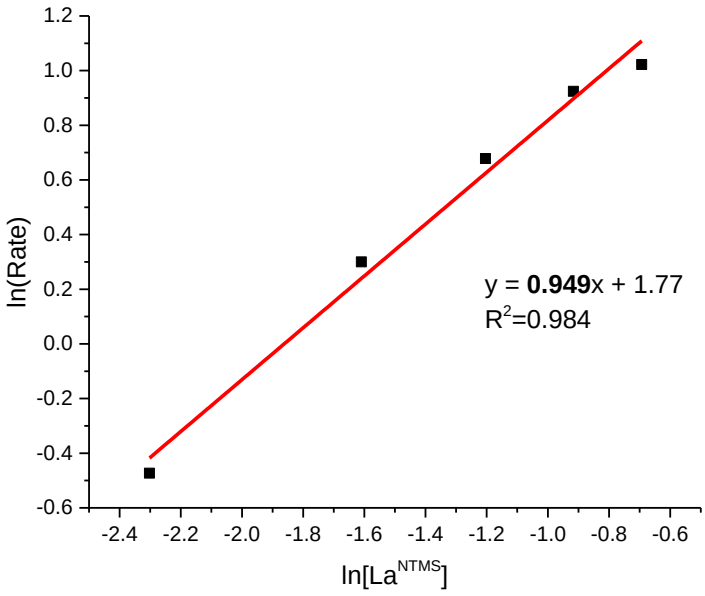

Figure 2.9. Ln vs. ln rate plot for the determination of the reaction order in [La^{NTMS}] for ester reduction.

DBpin Synthesis. This synthesis was adapted from literature procedures.[29] BD_3•SMe_2 (Cambridge Isotope Laboratories, 8.5 mmol, 10 *M*) was diluted with 10 mL DCM in an addition funnel under N_2. This solution was next added dropwise over 30 min to a 0°C solution of pinacol (8.5 mmol, 1.0 g) in 20 mL DCM. After addition was complete, the solution was brought to room temperature and stirred until bubbling was no longer observed (1 h). The DBpin was purified by distillation (0°C at 10 mmHg). ^{1}H NMR (400 MHz, C_6D_6): 1.00 (s, 12H, DB*pin*) ^{11}B NMR (128 MHz, C_6D_6): 28.37 (t, $^2J_{DB}$=22.8 Hz).

Kinetic Isotope Effect Determination. Rate studies were carried out with HBpin and DBpin under the same ^{1}H NMR kinetic monitoring conditions outlined above - 0.125 mmol ester, 0.275 mmol HBpin, 0.0330 mmol C_6Me_6, C_6D_6 (total volume 1.00 mL), using methyl 4-(dimethylamino)benzoate as a representative substrate.

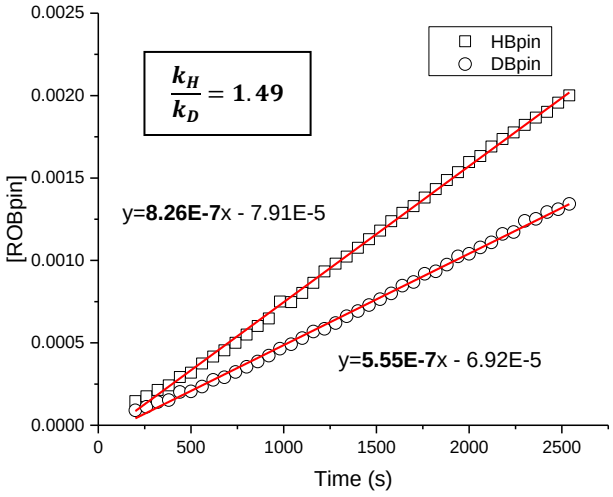

Figure 2.10. Plot for the determination of the kinetic isotope effect for ester reduction using HBpin and DBpin.

Temperature Analysis. Temperature-dependent rate data were obtained *via* arrayed NMR scans as described above. Temperatures were set on the NMR instrument using an external temperature controller and calibrated using ethylene glycol (>25°C) or methanol (<25°C) standards. Rates at each temperature were determined from the average of three trials.

These data were then plotted as 1000/T vs. ln(k/T) from which the enthalpy and entropy of the transition state could be obtained using the Eyring equation (see eq. 2.5). $\Delta H^{\neq}$ is the negative slope times R and $\Delta S^{\neq}$ is the intercept minus the natural log of k_b/h times R.

$$\ln \frac{k}{T} = \frac{\Delta H^{\neq}}{RT} \left[\frac{\Delta S^{\neq}}{R} - \ln \frac{k_b}{h} \right] \tag{2.5}$$

From a plot of 1000/T vs. ln(k), the activation energy can be obtained using the Arrhenius equation (eq. 2.6). E_a is the negative slope times R.

$$\ln k = -\frac{E_a}{RT} - \ln A \tag{2.6}$$

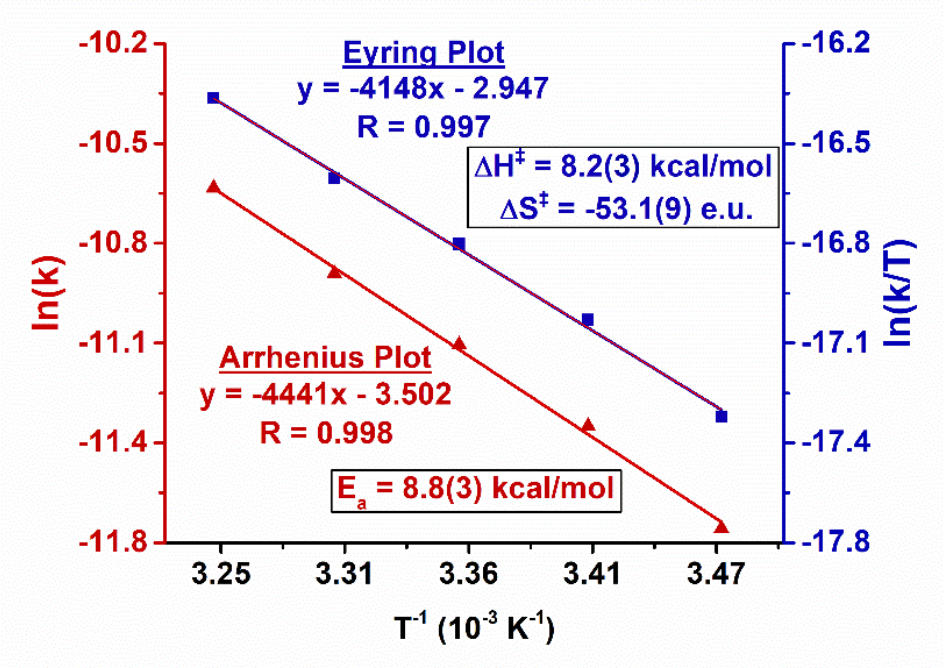

Figure 2.11. Eyring (blue) and Arrhenius (red) plots for the reduction of phenyl benzoate.

Hammett Analysis. Rates were determined by ^{1}H NMR (*vide supra*) for a series of *para*-substituted methyl benzoates (NO_2, F, H, Me, NMe_2). The rates of reduction for each substrate were plotted according to the Hammett equation (eq. 2.7), so that the slope of the line gives rho (ρ), which indicates the sensitivity of the reaction to the electron density at the carbonyl carbon of the substrate.[35]

$$log\frac{k}{k_H} = \sigma\rho \tag{2.7}$$

Competition Studies. To gauge the selectivity of La^{NTMS} for ester hydroboration over olefin hydroboration, intermolecular competition experiments were performed using 1-octene and 1-

octyne (representative ^{1}H NMR spectrum below). Phenyl benzoate (0.125 mmol), 1-octene/1-octyne (0.125 mmol), and HBpin (0.275 mmol) were dissolved in C_6D_6 in a J. Young capped NMR tube. La^{NTMS} (1.25 μmol) was added and the tube was shaken. After 5 hours at 60°C, complete conversion of the phenyl benzoate was observed, with no concomitant reduction of olefin.

To test the selectivity of La^{NTMS}-catalyzed ester reduction over more easily reduced ketones, the reduction of *tert*-butyl acetoacetate was examined. *Tert*-butyl acetoacetate (0.25 mmol) and HBpin (0.80 mmol, 3.2 equiv.) were dissolved in 0.500 mL C_6D_6. This solution was added to La^{NTMS} (0.0025 mmol) in 0.100 mL C_6D_6 in a J. Young capped NMR tube. The reaction was monitored by ^{1}H NMR. Complete reduction of the ketone moiety was observed after 30 minutes, and no reduction of the ester group was observed, even after heating the solution at 60°C for 5 hours.

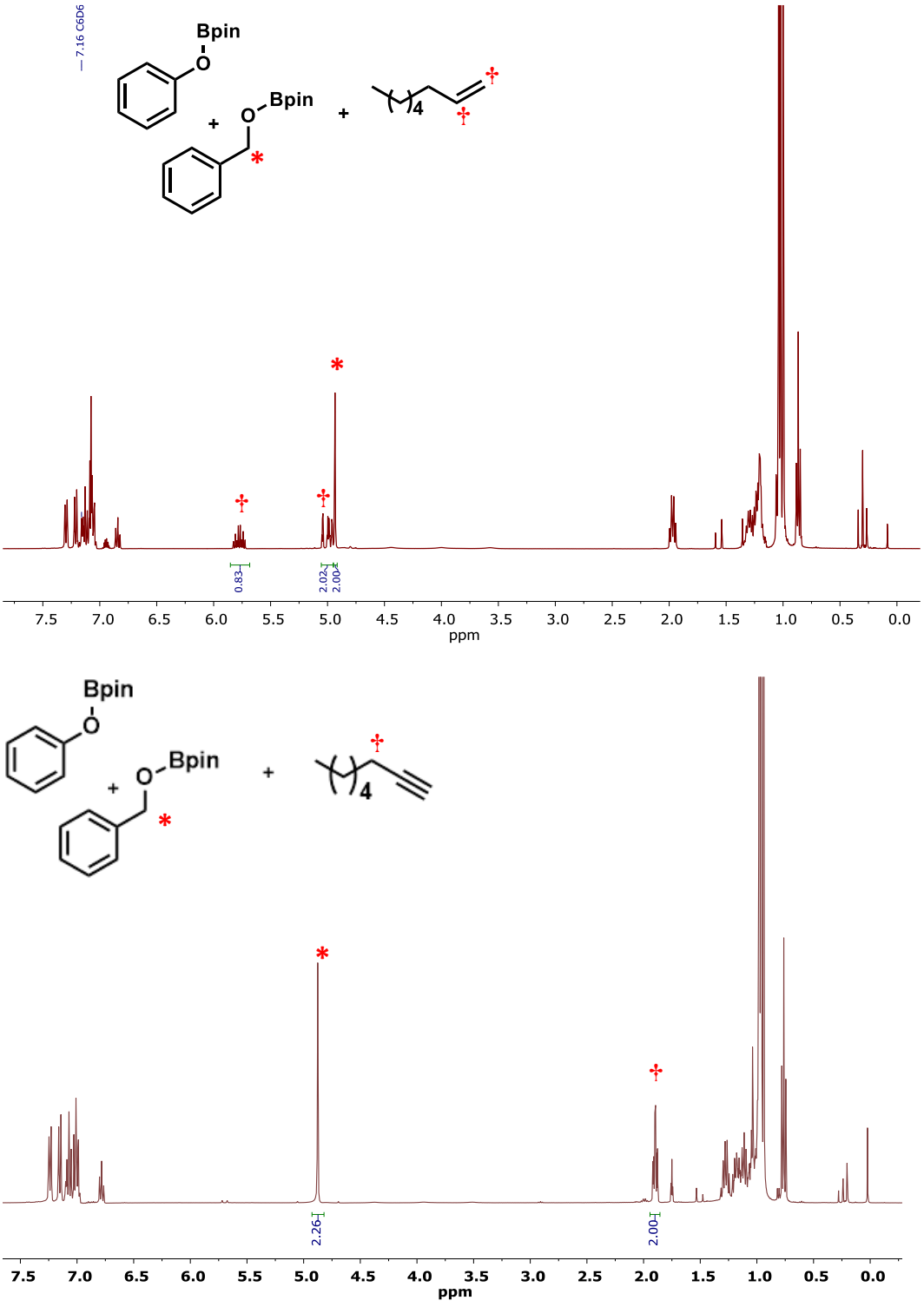

Figure 2.12. ^{1}H NMR spectra showing the selective reduction of phenyl benzoate in the presence of 1-octene (top) and 1-octyne (bottom).

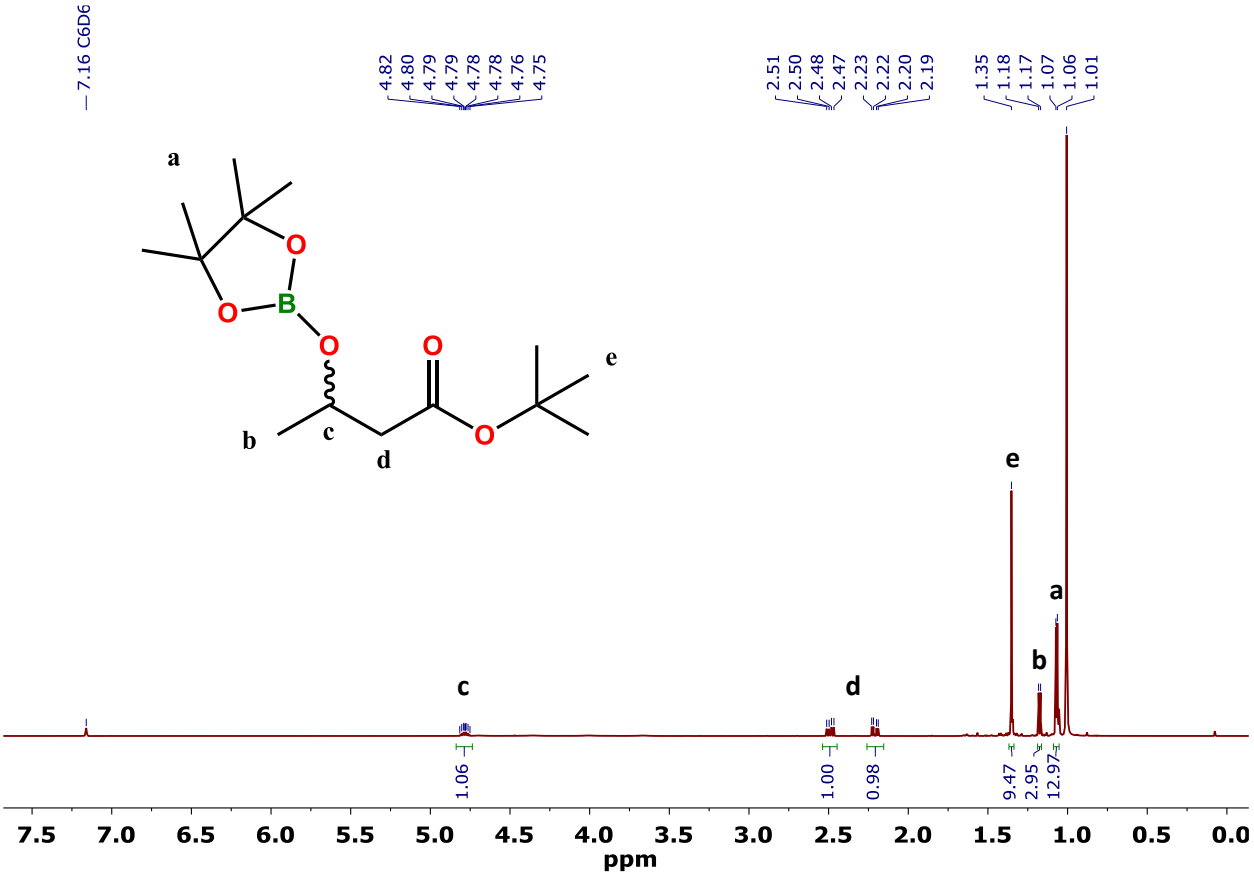

Figure 2.13. ^{1}H NMR spectrum of the reduction of *tert*-butyl acetoacetate. Spectrum shows complete conversion to the partially reduced species $CH_3CH(OBpin)COO^tBu$.

Stoichiometric Studies. Attempts to experimentally characterize the catalyst activation process were carried out by monitoring stoichiometric mixtures of La^{NTMS} and substrates HBpin and phenyl benzoate via ^{1}H and ^{11}B NMR. However, only the proposed off-cycle/deactivation products described above are observed (Scheme 2.2). When various mixtures of La^{NTMS} and HBpin are examined (0.5-6 equiv HBpin), the spectrum below is obtained with varying degrees of conversion of La^{NTMS}. Full conversion is observed at 4 equiv HBpin, which matches what would be expected given the proposed deactivation pathway. However, additional, uncharacterized decomposition products are observed at such high HBpin ratios, and therefore 1:3 La^{NTMS}:HBpin mixtures were studied further (Figures 2.14-2.16). Addition of phenyl benzoate (1 equiv vs La^{NTMS}) to either a pre-mixed solution of La^{NTMS} and HBpin, or simultaneous mixing of all reagents, leads to the partial reduction of the ester, as evidenced by a new peak at 4.76 ppm in the ^{1}H NMR (Figure 2.17), the disappearance of the RBH_3^- quartet at -6.42ppm and the appearance of a triplet (RBH_2) at 47.20 ppm in the ^{11}B NMR (Figure 2.18).

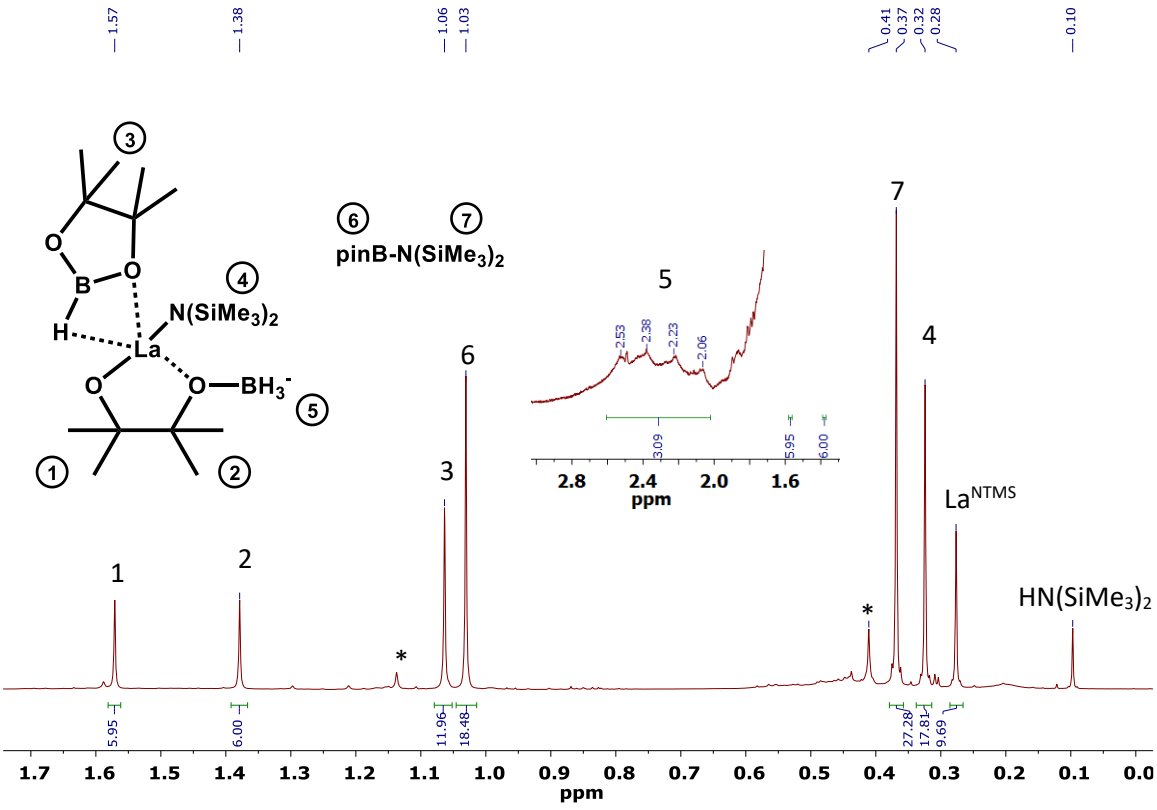

Figure 2.14. ^{1}H NMR spectra of catalyst deactivation product (A_{Deact}, Scheme 2.2) obtained from 1:3 mixture of La^{NTMS} and HBpin in benzene-d_6. Top: Full spectrum. Bottom: Expanded portion with relevant peaks labeled. * = unidentified side product.

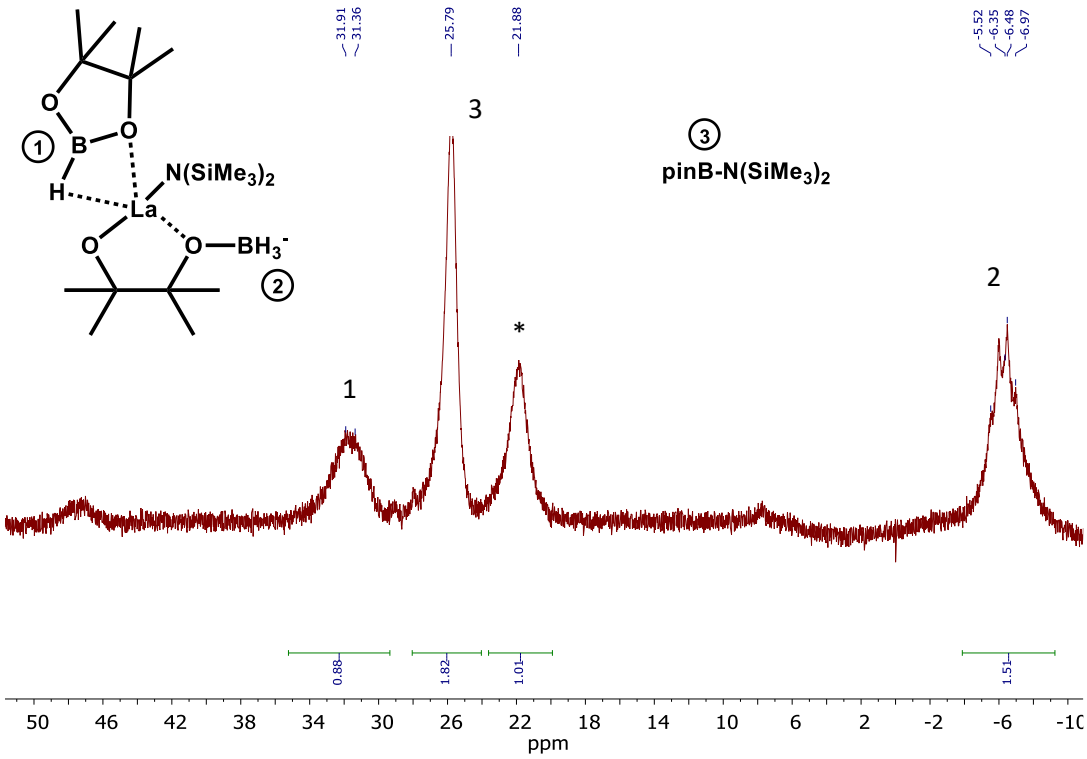

Figure 2.15. ^{11}B NMR spectrum of catalyst deactivation product (A_{Deact}, Scheme 2.2) obtained from 1:3 mixture of La^{NTMS} and HBpin in benzene-d_6. * = Unidentified side product, possibly weakly and reversibly coordinated pinB-N$(SiMe_3)_2$ or B_2pin_3. Peak at 31.6 ppm is a broad doublet, likely due to coordination of the B-H to the metal center or exchange with RBH_3^-. The downfield shift is similar to previously reported coordinated boranes.[36]

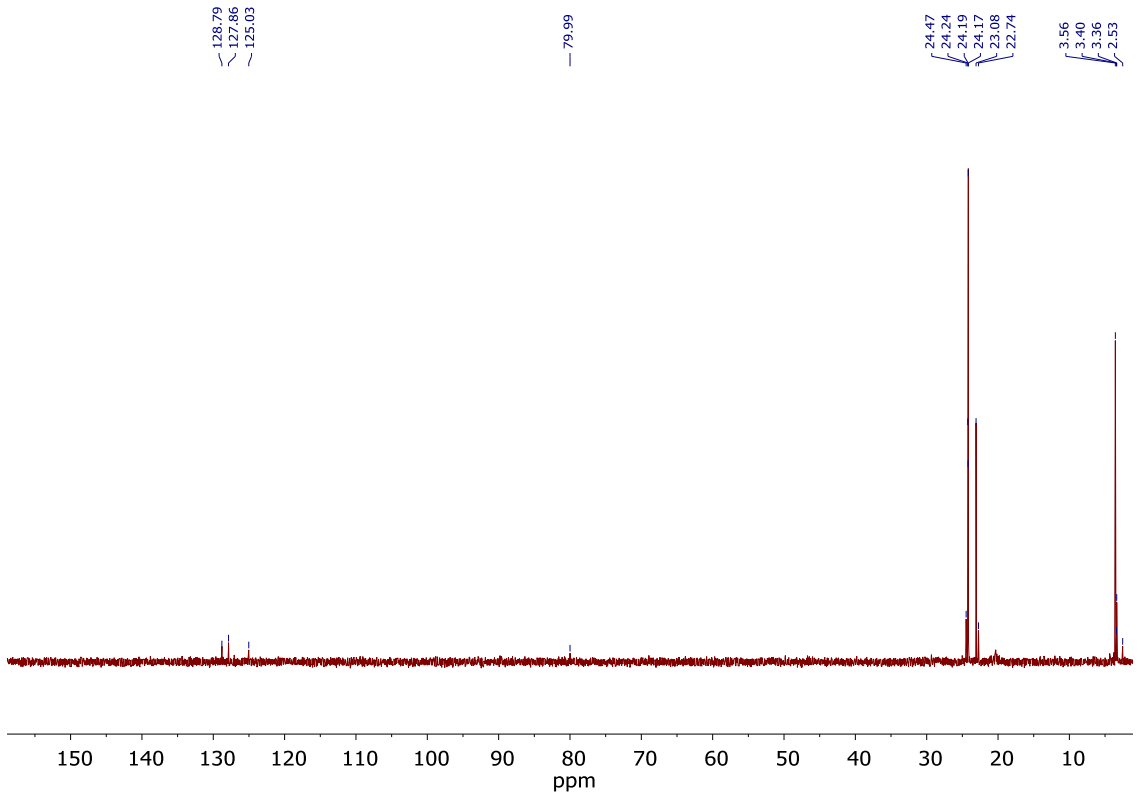

Figure 2.16. ^{13}C NMR spectrum of catalyst deactivation product (A_{Deact}, Scheme 2.2) obtained from 1:3 mixture of La^{NTMS} and HBpin in benzene-d_6.

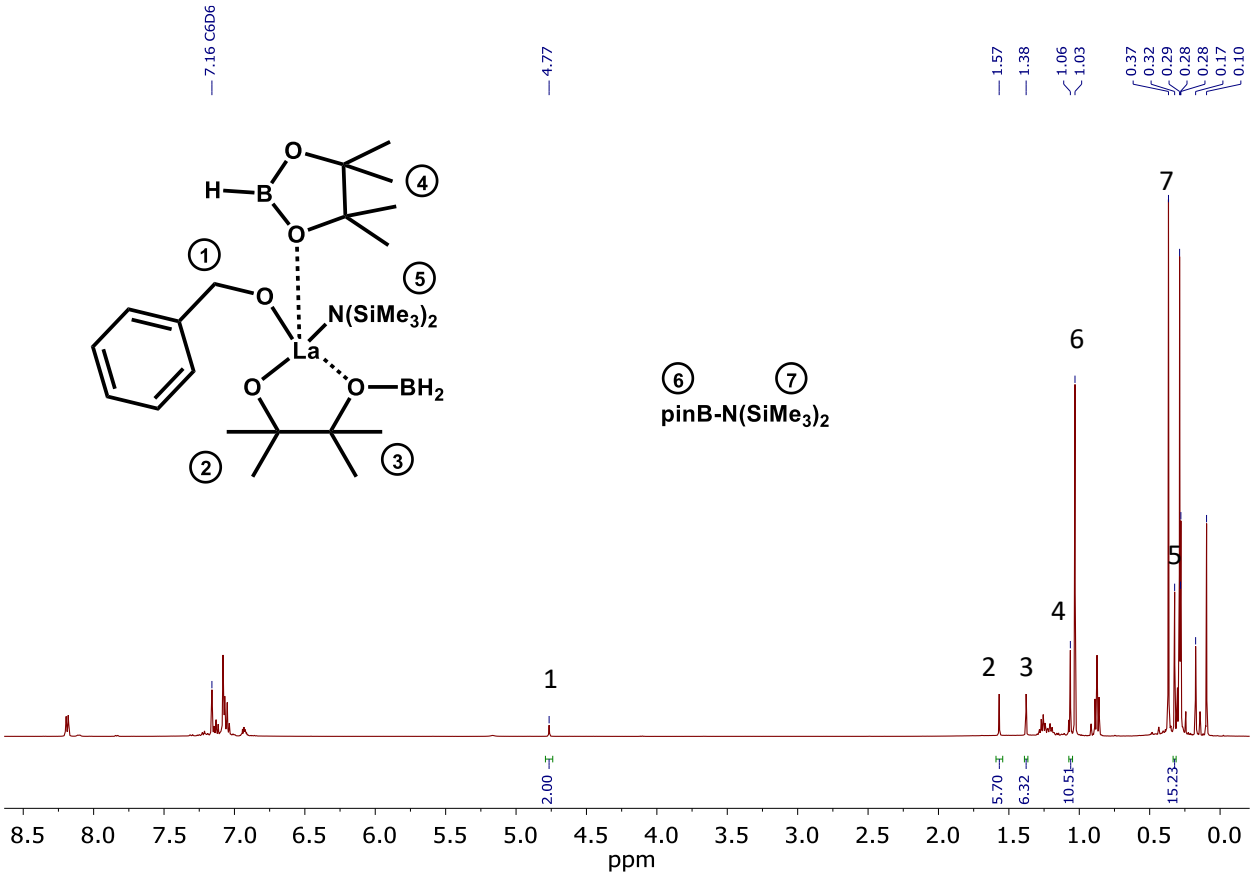

Figure 2.17. ^{1}H NMR spectrum of catalyst deactivation product (B_{Deact}, Scheme 2.2) obtained from 1:3:1 mixture of La^{NTMS} : HBpin : Phenyl Benzoate in benzene-d_6.

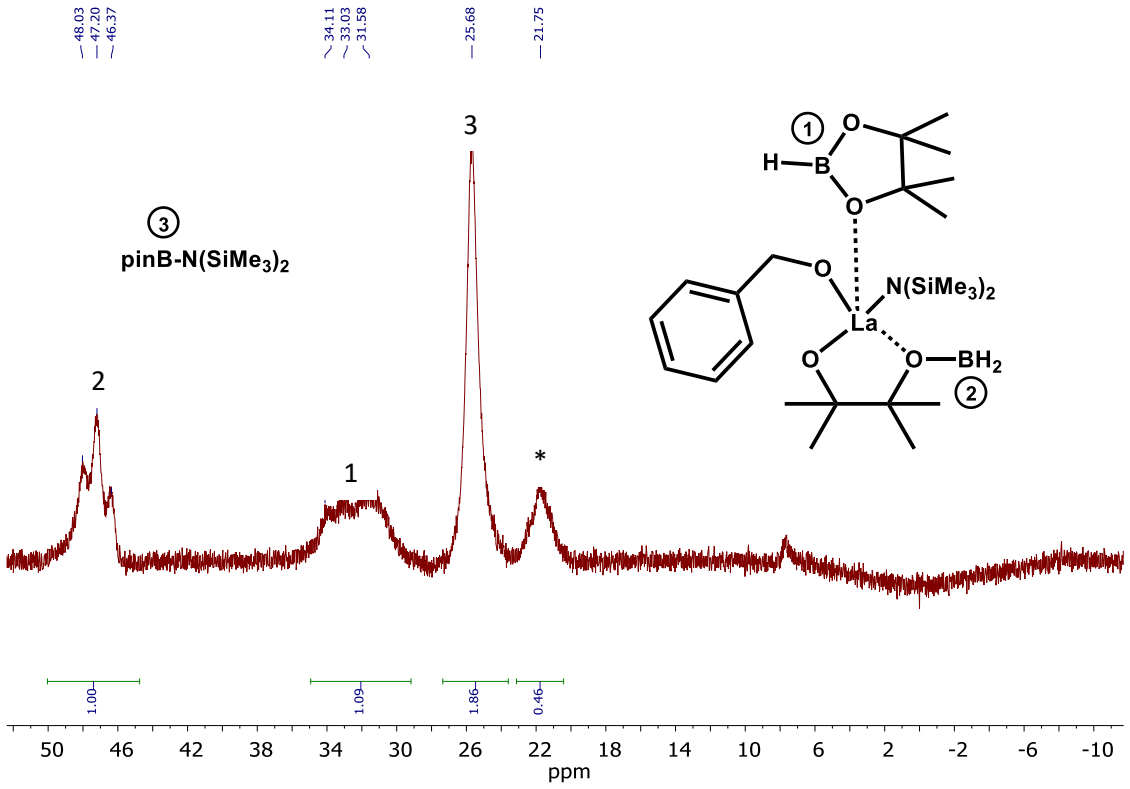

Figure 2.18. ^{11}B NMR spectrum of catalyst deactivation product (B_{Deact}, Scheme 2.2) obtained from 1:3:1 mixture of La^{NTMS} : HBpin : Phenyl Benzoate in benzene-d_6. * = Unidentified side product, possibly weakly and reversibly coordinated pinB-$N(SiMe_3)_2$ or B_2pin_3.

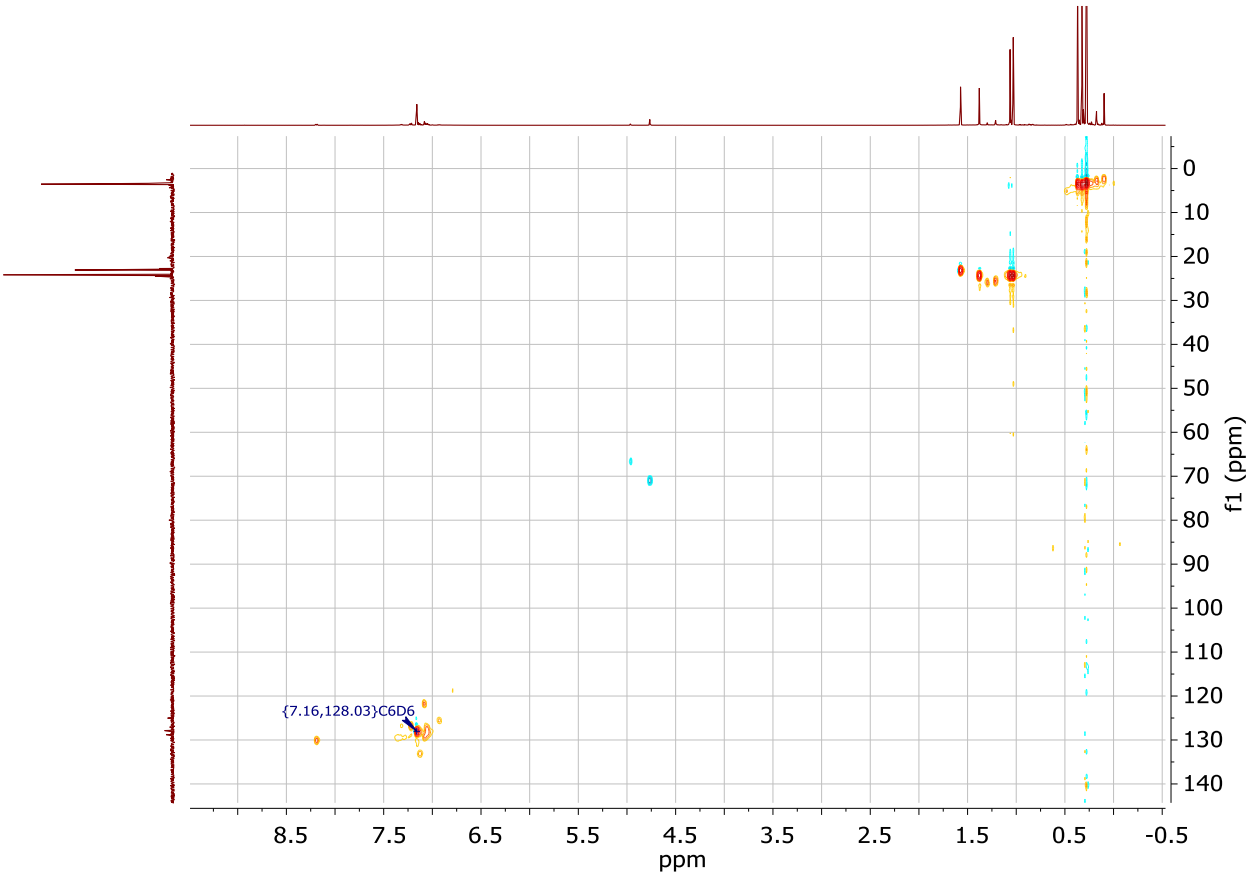

Figure 2.19. ^{1}H-^{13}C HSQC DEPT NMR spectrum of catalyst deactivation product (B_{Deact}, Scheme 2.2) obtained from 1:3:1 mixture of La^{NTMS} : HBpin : Phenyl Benzoate in benzene-d_6.

Computational Details. Geometry optimizations of all reactants, products, intermediates, and transition states were carried out along the entire catalytic cycle. Calculations were performed adopting the M06 hybrid meta-GGA functional. The effective core potential of Hay and Wadt[30], (LANL2DZ) and the relative basis set were used for the La and Si atoms. The standard all-electron 6-31G** basis[31] was used for all the remaining atoms. Molecular geometry optimization of stationary points was carried out without symmetry constraints and used analytical gradient techniques. The transition states were searched with the "distinguished reaction coordinate procedure" along the emerging bonds. Step *i* of Figure 2.4 was monitored along the emerging C–O bond, whereas the subsequent bond formation/breaking step induced by the approach of a second HBpin molecule (step *ii*) was monitored along the breaking C–O bond. Finally, the hydride transfer of step *iii* and the catalyst activation step were monitored along the emerging C-H bond. Methyl benzoate was adopted as substrate model. Frequency analysis was performed to obtain thermochemical information about the reaction pathways at 298 K using the harmonic approximation. The difference in translational and rotational Gibbs free energy when moving from gas to solvent are accounted for by adding an energy contribution of 8RT to each species as detailed in the literature.[32] Moreover, the effect of concentration on moving from 1 atm to 1 *M* is accounted for by adding an energy contribution of 1.89 kcal/mol ($RTln(P_{1M}/P_{1atm})$) to each species. All calculations were performed using the G16 code[33] on Linux cluster systems.

DFT Examination of Catalyst Decomposition Pathway. DFT calculations were performed to better understand the decomposition path of the La^{NTMS} precatalyst induced by HBpin without ester (Figure 2.20). The decomposition path involves four main steps. The coordination of the first

HBpin leads to the formation of the pinBH-$N(SiMe_3)_2^-$ borate species (**I_{deact}-1**, -7.0 kcal/mol). The second step is promoted by the approach of a second HBpin leading to hydride transfer from the pinBH-$N(SiMe_3)_2^-$ species to the coordinated HBpin, producing a new H_2Bpin^- species and releasing the pinB-$N(SiMe_3)_2$ molecule. This intermediate is stabilized by the coordination of a third HBpin (**I_{deact}-2,** -28.5 kcal/mol). The third step is analogue to the first one involving the formation of a new pinBH-$N(SiMe_3)_2^-$ borate species (**I_{deact}-3,** -29.4 kcal/mol). The last step involves the opening of the H_2Bpin^- species and the subsequent hydride transfer from pinBH-$N(SiMe_3)_2^-$ to the opened H_2Bpin^- leading to the final product. A second pinB-$N(SiMe_3)_2$ molecule is released and a new HBpin coordinates and stabilizes the final product (-34.5 kcal/mol). This last step is the rate determining step with a Gibbs free energy barrier of 14.9 kcal/mol.

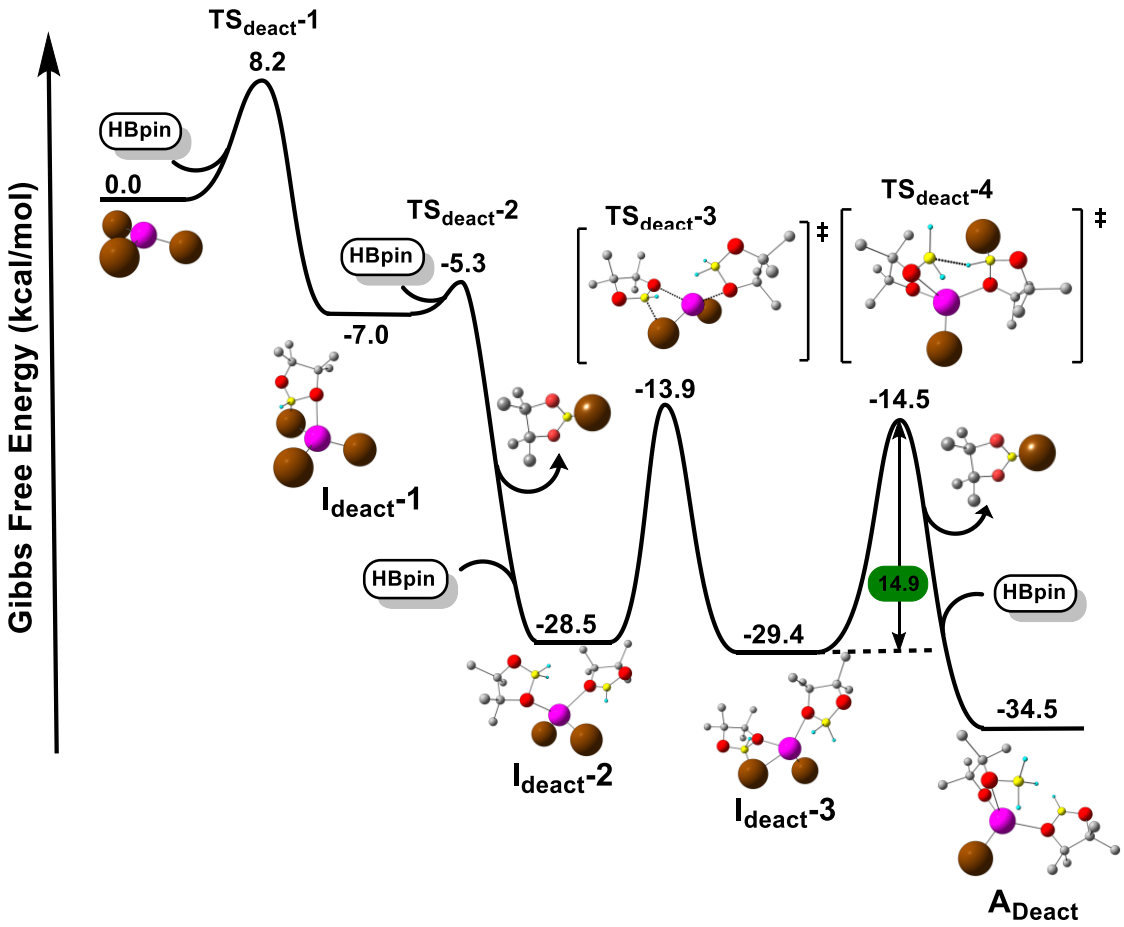

Figure 2.20. Energy profile associated with the decomposition pathway of La^{NTMS} precatalyst induced by HBpin.

The reaction of HBpin with La^{NTMS} can also induce the deactivation of the catalyst during the ester hydroboration process starting from the intermediate **C** (Figure 2.21). In this case the releasing of the $PhCH_2OBpin$ product occurs by the hydride exchange from the hydridoborate-La complex to the coordinated HBpin instead of to the coordinated ester. The subsequent exchange of the ester substrate with the HBpin molecule leads to the intermediates $\mathbf{I_{deact}}$**-2** and $\mathbf{I_{deact}}$**-3** as previously described. However, in presence of ester the subsequent releasing of the pinB-$N(SiMe_3)_2$ is followed by the coordination of a new ester molecule instead of the HBpin leading to the $\mathbf{I_{deact}}$**-4** (ΔG = -46.1 kcal/mol). A barrierless and slightly endergonic proton transfer from the ring-opened $pinBH_3^-$ to the ester molecule leads to $\mathbf{I_{deact}}$**-5** (ΔG = -42.7 kcal/mol). The coordination of an additional HBpin molecule promotes a barrierless transfer of the ester methoxy group to the coordinated HBpin ($\mathbf{I_{deact}}$**-6**, ΔG = -64.0 kcal/mol). Finally, hydride transfer from the $[HB(OMe)(pin)]^-$ to the La-hydridoborate complex occurs with an energy barrier of 8.2 kcal/mol. The MeOBpin product is released, leading to the final deactivated species (ΔG = -71.3 kcal/mol). The overall energy barrier is computed to be 23.8 kcal/mol with **I2** as the TDI and $\mathbf{TS_{deact}}$**-3** as the TDTS.

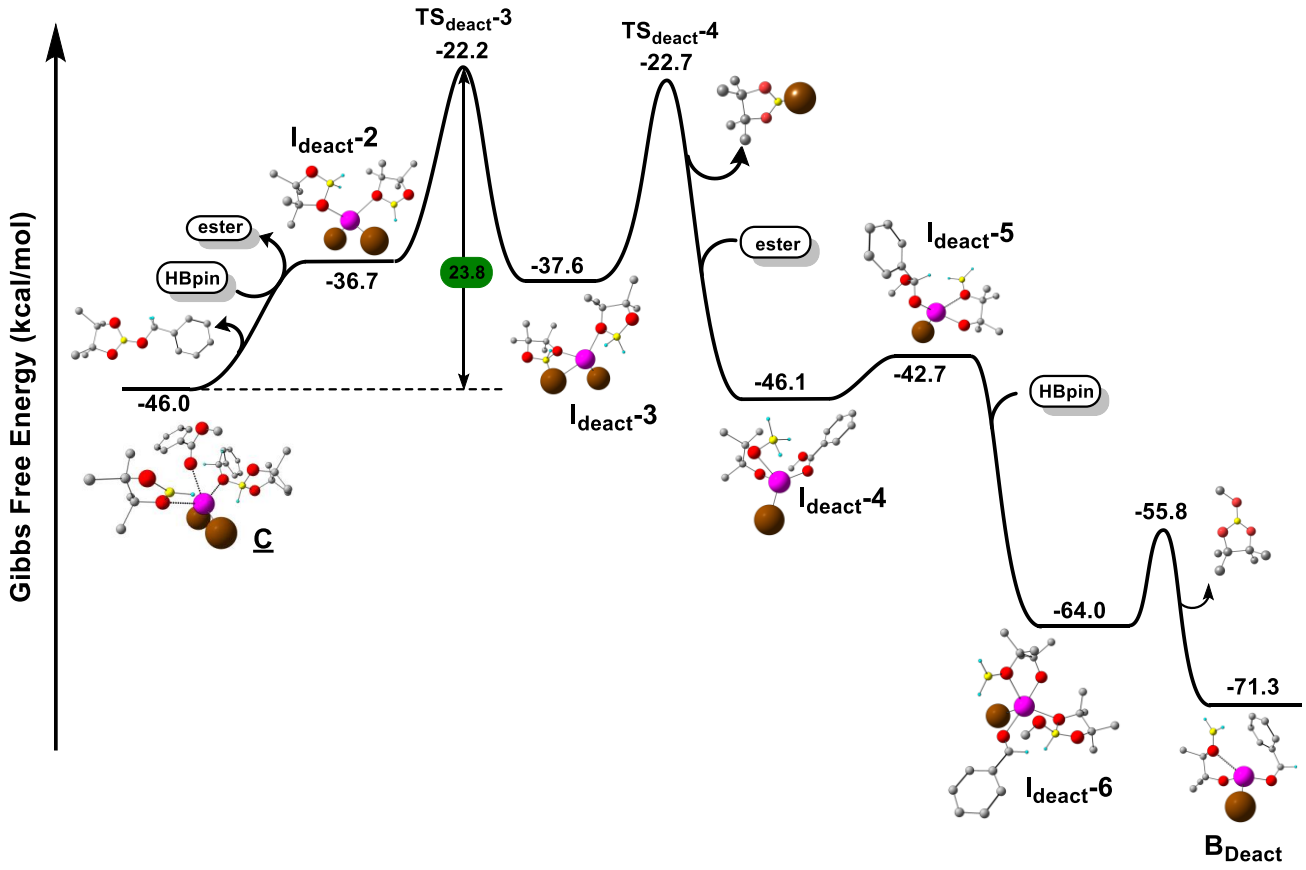

Figure 2.21. Energy profile associated to the decomposition path of La^{NTMS} active catalyst along the ester hydroboration process.

Product Characterization. Characterization data for the products of ester reduction are given below. Previously reported products were characterized by ^{1}H, $^{11}B\{^{1}H\}$, and $^{13}C\{^{1}H\}$ NMR. Previously unreported products were run at a preparative scale (1 mmol ester). The boryl ester was characterized by ^{1}H, $^{11}B\{^{1}H\}$, and $^{13}C\{^{1}H\}$ NMR, then hydrolyzed according to established procedures.[9l] The corresponding alcohol was then characterized by ^{1}H and $^{13}C\{^{1}H\}$ NMR.

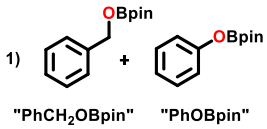

NMR spectra are identical to those reported in the literature.[9l, 37]

^{1}H NMR (400 MHz, C_6D_6): 1.03 (s, 12H, PhCH$_2$OB*pin*), 1.04 (s, 12H, PhOB*pin*), 4.92 (s, 2H, PhC*H*$_2$OBpin), 6.82-6.87 (m, 1H, *Ph*OBpin), 7.03-7.10 (m, 3H, *Ph*OBpin/*Ph*CH$_2$OBpin), 7.11-7.15 (m, 2H, *Ph*CH$_2$OBpin), 7.17-7.21 (m, 2H, *Ph*OBpin), 7.26-7.30 (m, 2H, *Ph*CH$_2$OBpin). **$^{11}B\{^{1}H\}$ NMR (128 MHz, C_6D_6)**: 22.1 (PhO*B*pin), 22.4 (PhCH$_2$O*B*pin). **$^{13}C\{^{1}H\}$ NMR (125 MHz, C_6D_6):** 24.6 (PhOB*pin*), 24.7 (PhCH$_2$OB*pin*), 66.9 (Ph*C*H$_2$OBpin), 82.8 (PhCH$_2$OB*pin*), 83.3 (PhOB*pin*), 120.1 (*Ph*OBpin), 123.3 (*Ph*OBpin), 127.0 (*Ph*CH$_2$OBpin), 127.6 (*Ph*CH$_2$OBpin), 128.6 (*Ph*CH$_2$OBpin), 129.6 (*Ph*OBpin), 140.0 (*Ph*CH$_2$OBpin), 154.4 (*Ph*OBpin).

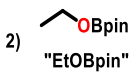

NMR spectra are identical to those reported in the literature.[7d]

^{1}H NMR (400 MHz, C_6D_6): 1.05 (s, 12H, EtOB*pin*), 1.09 (t, $^{3}J_{HH}$ = 7.0 Hz, 3H, C*H*$_3$CH$_2$OBpin), 3.87 (q, $^{3}J_{HH}$ = 7.0 Hz, 2H, CH$_3$C*H*$_2$OBpin). **^{11}B{^{1}H} NMR (128 MHz, C_6D_6)**: 22.4 (EtO*B*pin). **^{13}C{^{1}H} NMR (125 MHz, C_6D_6):** 17.5 (*C*H$_3$CH$_2$OBpin), 24.8 (EtOB*pin*), 60.7 (CH$_3$*C*H$_2$OBpin), 82.4 (EtOB*pin*).

3) 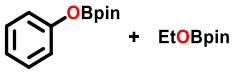

NMR spectra are identical to those reported in the literature.[7d, 37]

^{1}H NMR (400 MHz, C_6D_6): 1.03 (s, 12H, EtOB*pin*), 1.05 (s, 12H, PhOB*pin*), 1.10 (t, $^{3}J_{HH}$ = 7.1 Hz, 3H, C*H*$_3$CH$_2$OBpin), 3.89 (q, $^{3}J_{HH}$ = 7.1 Hz, 2H, CH$_3$C*H*$_2$OBpin) 6.82-6.87 (m, 1H, *Ph*OBpin), 7.03-7.10 (m, 2H, *Ph*OBpin), 7.19-7.23 (m, 2H, *Ph*OBpin). **^{11}B{^{1}H} NMR (128 MHz, C_6D_6)**: 22.1 (PhO*B*pin), 22.4 (EtO*B*pin). **^{13}C{^{1}H} NMR (125 MHz, C_6D_6):** 17.5 (*C*H$_3$CH$_2$OBpin), 24.6 (PhOB*pin*), 24.8 (EtOB*pin*), 60.7 (CH$_3$*C*H$_2$OBpin), 82.4 (EtOB*pin*), 83.3 (PhOB*pin*), 120.1 (*Ph*OBpin), 123.3 (*Ph*OBpin), 129.6 (*Ph*OBpin), 154.4 (*Ph*OBpin).

4) 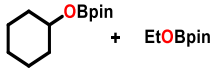

NMR spectra are identical to those reported in the literature.[7d, 25]

^{1}H NMR (400 MHz, C_6D_6): 1.05 (s, 12H, EtOB*pin*), 1.07 (s, 12H, CyOB*pin*), 1.09 (t, $^{3}J_{HH}$ = 7.0 Hz, 3H, C*H*$_3$CH$_2$OBpin), 1.10-1.18 (m, 3H, *Cy*OBpin), 1.24-1.34 (m, 1H, *Cy*OBpin), 1.38-1.50 (m, 2H, *Cy*OBpin), 1.55-1.65 (m, 2H, *Cy*OBpin), 1.81-1.91 (m, 2H, *Cy*OBpin), 3.87 (q, $^{3}J_{HH}$ = 7.0 Hz, 2H, CH$_3$C*H*$_2$OBpin), 4.12-4.21 (m, 1H, *Cy*OBpin). **^{11}B{^{1}H} NMR (128 MHz, C_6D_6)**: 22.4 (CyO*B*pin/EtO*B*pin). **^{13}C{^{1}H} NMR (125 MHz, C_6D_6):** 17.5 (*C*H$_3$CH$_2$OBpin), 24.1 (*Cy*OBpin),

24.8 (CyOB*pin*/EtOB*pin*), 25.8 (*Cy*OBpin), 34.8 (*Cy*OBpin), 60.7 (CH_3CH_2OBpin), 72.7 (*Cy*OBpin), 82.2 (CyOB*pin*), 82.4 (EtOB*pin*).

5) 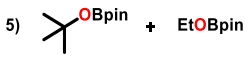 + EtOBpin

NMR spectra are identical to those reported in the literature.[7d, 37]

^{1}H NMR (400 MHz, C_6D_6): 1.05 (s, 12H, EtOB*pin*), 1.06 (s, 12H, ^{t}BuOB*pin*), 1.09 (t, $^{3}J_{HH}$ = 7.0 Hz, 3H, C*H*$_3$CH$_2$OBpin), 1.34 (s, 9H, (C*H*$_3$)$_3$CH$_3$OBpin), 3.87 (q, $^{3}J_{HH}$ = 7.0 Hz, 2H, CH$_3$C*H*$_2$OBpin). **^{11}B{^{1}H} NMR (128 MHz, C_6D_6)**: 21.5 (^{t}BuO*B*pin), 22.4 (EtO*B*pin). **^{13}C{^{1}H} NMR (125 MHz, C_6D_6):** 17.5 (*C*H$_3$CH$_2$OBpin), 24.7 (^{t}BuOB*pin*), 24.8 (EtOB*pin*), 30.3 ((*C*H$_3$)$_3$CH$_3$OBpin), 60.7 (CH$_3$*C*H$_2$OBpin), 73.5 ((CH$_3$)$_3$*C*H$_3$OBpin), 81.8 (^{t}BuOB*pin*), 82.4 (EtOB*pin*).

6)  + EtOBpin

NMR spectra are identical to those reported in the literature.[7d, 25]

^{1}H NMR (400 MHz, C_6D_6): 1.05 (s, 12H, EtOB*pin*), 1.07 (s, 12H, AdmOB*pin*), 1.09 (t, $^{3}J_{HH}$ = 7.0 Hz, 3H, C*H*$_3$CH$_2$OBpin), 1.39-1.46 (m, 2H, *Adm*OBpin), 1.53-1.64 (m, 5H, *Adm*OBpin), 1.66-1.74 (m, 3H, *Adm*OBpin), 2.00-2.05 (m, 2H, *Adm*OBpin), 3.87 (q, $^{3}J_{HH}$ = 7.0 Hz, 2H, CH$_3$C*H*$_2$OBpin), 4.39-4.44 (m, 1H, *Adm*OBpin). **^{11}B{^{1}H} NMR (128 MHz, C_6D_6)**: 22.4 (AdmO*B*pin/EtO*B*pin). **^{13}C{^{1}H} NMR (125 MHz, C_6D_6):** 17.5 (*C*H$_3$CH$_2$OBpin), 24.8 (AdmOB*pin*/EtOB*pin*), 27.5 (*Adm*OBpin), 28.0 (*Adm*OBpin), 31.6 (*Adm*OBpin), 34.6 (*Adm*OBpin), 36.7 (*Adm*OBpin), 37.9 (*Adm*OBpin), 60.7 (CH$_3$*C*H$_2$OBpin), 77.1 (*Adm*OBpin), 82.2 (*Adm*OBpin), 82.4 (EtOB*pin*).

7) 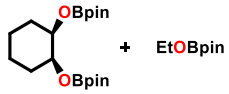 + EtOBpin

NMR spectra of EtOBpin are identical to those reported in the literature.[7d] Cy(OBpin)$_2$ had not been reported previously, and as such, was characterized per the above procedure. The NMR spectra of the alcohol are identical to those reported in the literature.[38]

^{1}H NMR (400 MHz, C$_6$D$_6$): 1.01-1.06 (m, 2H, *Cy*(OBpin)$_2$), 1.05 (s, 12H, EtOB*pin*), 1.09 (t, $^3J_{HH}$ = 7.0 Hz, 3H, C*H*$_3$CH$_2$OBpin), 1.11 (s, 12H, Cy(OB*pin*)$_2$), 1.14 (2, 12H, Cy(OB*pin*)$_2$), 1.32-1.43 (m, 2H, *Cy*(OBpin)$_2$), 1.50-1.60 (m, 2H, *Cy*(OBpin)$_2$), 1.81-1.91 (m, 2H, *Cy*(OBpin)$_2$), 3.87 (q, $^3J_{HH}$ = 7.0 Hz, 2H, CH$_3$C*H*$_2$OBpin). 4.30-4.38 (m, 2H, *Cy*(OBpin)$_2$). **^{11}B{^{1}H} NMR (128 MHz, C$_6$D$_6$)**: 22.4 (*Cy*(O*B*pin)$_2$/EtO*B*pin). **^{13}C{^{1}H} NMR (125 MHz, C$_6$D$_6$):** 17.5 (*C*H$_3$CH$_2$OBpin), 21.9 (*Cy*(OBpin)$_2$), 24.7 (Cy(OB*pin*)$_2$), 24.8 (EtOB*pin*), 24.9 (*Cy*(OBpin)$_2$), 29.8 (*Cy*(OBpin)$_2$), 60.7 (CH$_3$*C*H$_2$OBpin), 73.5 (*Cy*(OBpin)$_2$), 82.3 (Cy(OB*pin*)$_2$), 82.4 (EtOB*pin*).

***cis*-Cy(OH)$_2$** (white powder in 85% yield)- **^{1}H NMR (400MHz, CDCl$_3$):** 1.26-1.34 (m, 2H), 1.72-1.81 (m, 6H), 2.18 (br s, 2H), 3.75-3.77 (m, 2H). **^{13}C{^{1}H} NMR (125 MHz, CDCl$_3$):** 21.5, 30.0, 70.5

8) 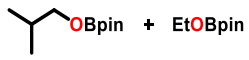 + EtOBpin

NMR spectra are identical to those reported in the literature.[7d, 39]

^{1}H NMR (400 MHz, C$_6$D$_6$): 0.83 (d, $^3J_{HH}$ = 6.7 Hz, 6H, (C*H*$_3$)$_2$CHCH$_2$OBpin), 1.05 (s, 12H, EtOB*pin*), 1.06 (s, 12H, ^{i}BuOB*pin*) 1.09 (t, $^3J_{HH}$ = 7.0 Hz, 3H, C*H*$_3$CH$_2$OBpin), 1.77 (nonet, $^3J_{HH}$ = 6.7 Hz, 1H, (CH$_3$)$_2$C*H*CH$_2$OBpin), 3.68 (d, $^3J_{HH}$ = 6.5, 2H, (CH$_3$)$_2$CHC*H*$_2$OBpin), 3.87 (q, $^3J_{HH}$

= 7.0 Hz, 2H, CH_3CH_2OBpin). **$^{11}B\{^1H\}$ NMR (128 MHz, C_6D_6)**: 22.4 (EtO*B*pin/^{i}BuO*B*pin). **$^{13}C\{^1H\}$ NMR (125 MHz, C_6D_6):** 17.5 (CH_3CH_2OBpin), 19.0 ($(CH_3)_2CHCH_2OBpin$), 24.8 (EtOB*pin*/^{i}BuOB*pin*), 30.3 ($(CH_3)_2CHCH_2OBpin$), 60.7 (CH_3CH_2OBpin), 71.5 ($(CH_3)_2CHCH_2OBpin$), 82.4 (EtOB*pin*/^{i}BuOB*pin*).

9) 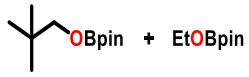

NMR spectra are identical to those reported in the literature.[40]

^1H NMR (400 MHz, C_6D_6): 0.88 (s, 9H, $(CH_3)_3CCH_2OBpin$), 1.05 (s, 12H, EtOB*pin*), 1.07 (s, 12H, $(CH_3)_3CCH_2OB$*pin*) 1.09 (t, $^3J_{HH}$ = 7.0 Hz, 3H, CH_3CH_2OBpin), 3.61 (s, 2H, $(CH_3)_3CCH_2OBpin$), 3.87 (q, $^3J_{HH}$ = 7.0 Hz, 2H, CH_3CH_2OBpin). **$^{11}B\{^1H\}$ NMR (128 MHz, C_6D_6)**: 22.4 (EtO*B*pin/$(CH_3)_3CCH_2O$*B*pin). **$^{13}C\{^1H\}$ NMR (125 MHz, C_6D_6):** 17.5 (CH_3CH_2OBpin), 24.8 (EtOB*pin*/$(CH_3)_3CCH_2OB$*pin*), 26.2 ($(CH_3)_3CCH_2OBpin$), 32.5 ($(CH_3)_3CCH_2OBpin$), 60.7 (CH_3CH_2OBpin), 75.1 ($(CH_3)_3CCH_2OBpin$), 82.4 (EtOB*pin*/$(CH_3)_3CCH_2OB$*pin*).

10) 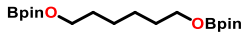

pinBO$(CH_2)_6$OBpin had not been reported previously and was characterized per the above procedure. The NMR spectra of the alcohol are identical to those reported in the literature.[41]

^1H NMR (400 MHz, C_6D_6): 1.07 (s, 24H, *pin*BO$(CH_2)_6$OB*pin*), 1.18-1.24 (m, 4H, pinBO$CH_2CH_2CH_2CH_2CH_2CH_2$OBpin), 1.40-1.49 (m, 4H, pinBO$CH_2CH_2CH_2CH_2CH_2$-

CH_2OBpin), 3.85 (t, $^3J_{HH}$ = 6.6 Hz, 4H, pinBOC*H*$_2$$CH_2CH_2CH_2CH_2C$*H*$_2$OBpin). **^{11}B{^{1}H} NMR (128 MHz, C_6D_6)**: 22.5 (pin*B*O$(CH_2)_6$O*B*pin). **^{13}C{^{1}H} NMR (125 MHz, C_6D_6):** 24.8 (*pin*BO$(CH_2)_6$OB*pin*), 25.7 (pinBO(*C*H_2)$_6$OBpin), 32.0 (pinBO(*C*H_2)$_6$OBpin), 65.0 (pinBO(*C*H_2)$_6$OBpin), 82.4 (*pin*BO$(CH_2)_6$OB*pin*).

HO$(CH_2)_6$OH (white powder in 92% yield) – **^{1}H NMR (400 MHz, $CDCl_3$)**: 1.19-1.27 (m, 4H), 1.28-1.49 (m, 4H), 3.27-3.46 (m, 4H), 4.11 (br s, 2H). **^{13}C{^{1}H} NMR (125 MHz, $CDCl_3$):** 25.4, 32.6, 62.6.

11) 

NMR spectra are identical to those reported in the literature.[9l, 42]

^{1}H NMR (400 MHz, C_6D_6): 1.03 (s, 12H, PhCH=CHCH$_2$OB*pin*), 1.06 (s, 12H, MeOB*pin*), 3.48 (s, 3H, *Me*OBpin), 4.51 (dd, $^4J_{HH}$ = 1.4 Hz, $^3J_{HH}$ = 5.3 Hz, 2H, PhCH=CHC*H*$_2$OBpin), 6.16 (dt, $^3J_{HH}$ = 5.3 Hz, $^3J_{HH}$ = 15.9 Hz, 1H, PhCH=C*H*CH$_2$OBpin), 6.55-6.61 (m, 1H, PhC*H*=CHCH$_2$OBpin), 6.98-7.03 (m, 1H, *Ph*CH=CHCH$_2$OBpin), 7.05-7.10 (m, 2H, *Ph*CH=CHCH$_2$OBpin), 7.15-7.19 (m, 2H, *Ph*CH=CHCH$_2$OBpin). **^{11}B{^{1}H} NMR (128 MHz, C_6D_6)**: 22.6 (PhCH=CHCH$_2$O*B*pin/MeO*B*pin). **^{13}C{^{1}H} NMR (125 MHz, C_6D_6):** 24.8 (PhCH=CHCH$_2$OB*pin*/MeOB*pin*), 52.4 (*Me*OBpin), 65.5 (PhCH=CH*C*H$_2$OBpin), 82.5 (MeOB*pin*), 82.7 (PhCH=CHCH$_2$OB*pin*), 126.8 (PhCH=*C*HCH$_2$OBpin), 127.5 (Ph*C*H=CHCH$_2$OBpin), 127.7 (*Ph*CH=CHCH$_2$OBpin), 128.8 (*Ph*CH=CHCH$_2$OBpin), 130.9 (*Ph*CH=CHCH$_2$OBpin), 137.3 (*Ph*CH=CHCH$_2$OBpin).

12) 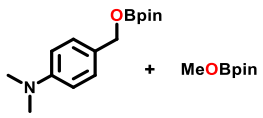

NMR spectra are identical to those reported in the literature.[25, 42]

^{1}H NMR (400 MHz, C_6D_6): 1.04 (s, 12H, Me_2NPhCH_2OBpin), 1.06 (s, 12H, MeOB*pin*), 2.51 (s, 6H, *Me*$_2$NPhCH2OBpin), 3.49 (s, 3H, *Me*OBpin), 4.98 (s, 2H, Me_2NPhCH_2OBpin), 6.53-6.59 (m, 2H, Me_2NPhCH_2OBpin), 7.29-7.35 (m, 2H, Me_2NPhCH_2OBpin). **^{11}B{^{1}H} NMR (128 MHz, C_6D_6)**: 22.6 (Me_2NPhCH_2OBpin/MeOBpin). **^{13}C{^{1}H} NMR (125 MHz, C_6D_6):** 24.7 (MeOB*pin*), 24.8 (Me_2NPhCH_2OBpin), 40.3 (*Me*$_2$NPhCH$_2$OBpin), 52.4 (*Me*OBpin), 67.2 (Me_2NPhCH_2OBpin), 82.5 (Me_2NPhCH_2OBpin/MeOB*pin*), 112.8 (Me_2NPhCH_2OBpin), 128.0 (Me_2NPhCH_2OBpin), 129.0 (Me_2NPhCH_2OBpin), 150.6 (Me_2NPhCH_2OBpin).

13) 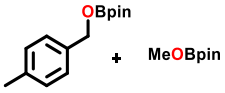

NMR spectra are identical to those reported in the literature.[7d, 42]

^{1}H NMR (400 MHz, C_6D_6): 1.04 (s, 12H, $MePhCH_2OBpin$), 1.05 (s, 12H, MeOB*pin*), 2.09 (s, 3H, *Me*PhCH2OBpin), 3.49 (s, 3H, *Me*OBpin), 4.94 (s, 2H, $MePhCH_2OBpin$), 6.96 (d, $^{3}J_{HH}$ = 7.9 Hz, 2H, $MePhCH_2OBpin$), 7.24 (d, $^{3}J_{HH}$ = 7.9 Hz, 2H, $MePhCH_2OBpin$). **^{11}B{^{1}H} NMR (128 MHz, C_6D_6)**: 22.6 ($MePhCH_2OBpin$/MeOBpin). **^{13}C{^{1}H} NMR (125 MHz, C_6D_6):** 21.1 (*Me*PhCH$_2$OBpin), 24.7 (MeOB*pin*), 24.8 ($MePhCH_2OBpin$), 52.4 (*Me*OBpin), 66.9 (MePh*C*H$_2$OBpin), 82.5 (MeOB*pin*), 82.7 ($MePhCH_2OBpin$), 127.2 (Me*Ph*CH$_2$OBpin), 129.3 (Me*Ph*CH$_2$OBpin), 137.0 (Me*Ph*CH$_2$OBpin), 137.2 (Me*Ph*CH$_2$OBpin).

14) 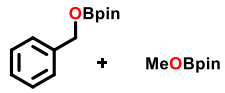

NMR spectra are identical to those reported in the literature.[37, 42]

^{1}H NMR (400 MHz, C_6D_6): 1.04 (s, 12H, PhCH$_2$OB*pin*), 1.05 (s, 12H, MeOB*pin*), 3.49 (s, 3H, *Me*OBpin), 4.93 (s, 2H, PhC*H*$_2$OBpin), 7.02-7.08 (m, 1H, *Ph*CH$_2$OBpin), 7.10-7.16 (m, 2H, *Ph*CH$_2$OBpin), 7.27-7.33 (m, 2H, *Ph*CH$_2$OBpin). **^{11}B{^{1}H} NMR (128 MHz, C_6D_6)**: 22.6 (PhCH$_2$O*B*pin/MeO*B*pin). **^{13}C{^{1}H} NMR (125 MHz, C_6D_6):** 24.7 (MeOB*pin*), 24.8 (PhCH$_2$OB*pin*), 52.4 (*Me*OBpin), 66.9 (Ph*C*H$_2$OBpin), 82.5 (MeOB*pin*), 82.7 (PhCH$_2$OB*pin*), 127.0 (*Ph*CH$_2$OBpin), 127.6 (*Ph*CH$_2$OBpin), 128.6 (*Ph*CH$_2$OBpin), 140.0 (*Ph*CH$_2$OBpin).

15) 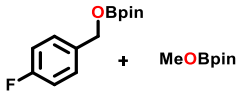

NMR spectra are identical to those reported in the literature.[42, 43]

^{1}H NMR (400 MHz, C_6D_6): 1.04 (s, 12H, FPhCH$_2$OB*pin*), 1.05 (s, 12H, MeOB*pin*), 3.49 (s, 3H, *Me*OBpin), 4.79 (s, 2H, FPhC*H*$_2$OBpin), 6.73-6.81 (m, 2H, F*Ph*CH$_2$OBpin), 7.05-7.11 (m, 2H, F*Ph*CH$_2$OBpin). **^{11}B{^{1}H} NMR (128 MHz, C_6D_6)**: 22.6 (FPhCH$_2$O*B*pin/MeO*B*pin). **^{13}C{^{1}H} NMR (125 MHz, C_6D_6):** 24.69 (FPhCH$_2$OB*pin*), 24.74 (MeOB*pin*), 52.4 (*Me*OBpin), 66.2 (FPh*C*H$_2$OBpin), 82.6 (MeOB*pin*), 82.8 (FPhCH$_2$OB*pin*), 115.3 (d, $^{2}J_{CF}$ = 21.5 Hz, F*Ph*CH$_2$OBpin), 135.8 (F*Ph*CH$_2$OBpin), 161.7 (F*Ph*CH$_2$OBpin), 163.6 (F*Ph*CH$_2$OBpin).

16) 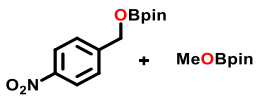

NMR spectra are identical to those reported in the literature.[7d, 42]

^{1}H NMR (400 MHz, C_6D_6): 1.04 (s, 12H, NO$_2$PhCH$_2$OB*pin*), 1.06 (s, 12H, MeOB*pin*), 3.49 (s, 3H, *Me*OBpin), 4.70 (s, 2H, NO$_2$PhC*H*$_2$OBpin), 6.96 (d, $^{3}J_{HH}$ = 8.6 Hz, 2H, NO$_2$*Ph*CH$_2$OBpin), 7.82 (d, $^{3}J_{HH}$ = 8.6 Hz, 2H, NO$_2$*Ph*CH$_2$OBpin). **^{11}B{^{1}H} NMR (128 MHz, C_6D_6)**: 22.6 (NO$_2$PhCH$_2$O*B*pin/MeO*B*pin). **^{13}C{^{1}H} NMR (125 MHz, C_6D_6):** 24.67 (NO$_2$PhCH$_2$OB*pin*),

24.74 (MeOB*pin*), 52.4 (*Me*OBpin), 65.6 (NO_2PhCH_2OBpin), 82.6 (MeOB*pin*), 83.2 (NO_2PhCH_2OBpin), 123.6 (NO_2PhCH_2OBpin), 125.8 (NO_2PhCH_2OBpin), 146.7 (NO_2PhCH_2OBpin), 147.6 (NO_2PhCH_2OBpin).

CHAPTER 3

$La[N(SiMe_3)_2]_3$-Catalyzed Deoxygenative Reduction of Amides with Pinacolborane. Scope and Mechanism

Adapted From:

Barger, C. J.; Dicken, R. D.; Weidner, V. L.; Motta, A.; Lohr, T. L.; Marks, T. J.; *J. Am. Chem. Soc*. **2020**, *142*(17), 8019-8028

Abstract

Tris[N,N-bis(trimethylsilyl)amide]lanthanum (La^{NTMS}) is an efficient and selective homogeneous catalyst for the deoxygenative reduction of tertiary and secondary amides with pinacolborane (HBpin) at mild temperatures (25–60 °C). The reaction, which yields amines and $O(Bpin)_2$, tolerates nitro, halide, and amino functional groups well, and this amide reduction is completely selective, with the exclusion of both competing inter- and intramolecular alkene/alkyne hydroboration. Kinetic studies indicate that amide reduction obeys an unusual mixed-order rate law which is proposed to originate from saturation of the catalyst complex with HBpin. Kinetic and thermodynamic studies, isotopic labeling, and DFT calculations using energetic span analysis suggest the role of a $[(Me_3Si)_2N]_2La\text{-}OCHR(NR'_2)[HBpin]$ active catalyst, and hydride transfer is proposed to be ligand-centered. These results add to the growing list of transformations that commercially available La^{NTMS} is competent to catalyze, further underscoring the value and versatility of lanthanide complexes in homogeneous catalysis.

Introduction

The deoxygenative reduction of amides to amines is an important transformation in academic, pharmaceutical, and industrial synthetic chemistry (Figure 3.1A).[1-5] The natural prevalence and synthetic accessibility of amides makes them valuable precursors to amines, but the inertness of the resonance-stabilized amide C═O bond generally necessitates the use of harsh reductants such as $LiAlH_4$, BH_3, and pressurized H_2.[6-9] These reagents present significant safety concerns and often suffer from poor functional group tolerance, particularly with nitro groups and alkenes/alkynes. As such, novel methods enabling the safe, selective, and efficient reduction of amides would be valuable additions to the synthetic chemist's toolkit.[10] Significant progress has been made in this area, with much of the focus directed toward catalytic hydrosilylation.[11-13] Interestingly, amide reduction via catalytic hydroboration (with mild, easily handled boranes such as HBpin, Figure 3.1B) is largely unexplored, especially with lanthanide catalysts,[14-17] despite extensive precedent for the use of boranes as reductants for ketones and aldehydes,[14,18-26] as well as the intense recent interest in the more-challenging reduction of esters via hydroboration.[14,27-31] Recently, we reported that the homoleptic lanthanide amide $La[N(SiMe_3)_2]_3$ (La^{NTMS}, Figure 3.1B) displays extremely high catalytic activity for a variety of carbonyl reductions using HBpin, with 25–60 °C turnover frequencies as high as 40,000 h^{-1} for ketones and aldehydes and 400 h^{-1} for esters.[31,32] With these results in mind, we sought to explore the La^{NTMS}-catalyzed hydroboration of more challenging amides.

Tris[*N*,*N*-bis(trimethylsilyl)amido]lanthanide complexes ($Ln[N(SiMe_3)_2]_3$, abbreviated here as Ln^{NTMS}) are encountered frequently in the lanthanide catalysis literature, both as precursors to

more complex lanthanide organometallics[33-43] and as homogeneous catalysts, particularly for hydro-functionalization/reduction of alkenes and alkynes.[44-56] These complexes are commercially available for many lanthanides, or can be readily synthesized and purified, rendering them highly accessible and of great interest to the synthetic methods community.[57-59] A report from the Marks laboratory showed that it is possible to carry out the catalytic *synthesis* of amides with Ln^{NTMS},[60] but the La^{NTMS}-catalyzed *reduction* of amides had not yet been investigated. Given this, and the proven ability of La^{NTMS} to catalyze carbonyl hydroboration, La^{NTMS}-catalyzed amide hydroboration was an intriguing target.

Here we report that La^{NTMS} effectively mediates the deoxygenative reduction of a variety of alkyl and aryl amides to the corresponding amines. This system, which utilizes a commercially available catalyst, mild reaction conditions, and easily handled HBpin, constitutes a significant advance over traditional amide reduction methods, and is the first report of a borane-based amide reduction catalyzed by a lanthanide complex. We discuss here the scope of this transformation, as well as a proposed mechanism informed by a combined experimental-theoretical investigation.

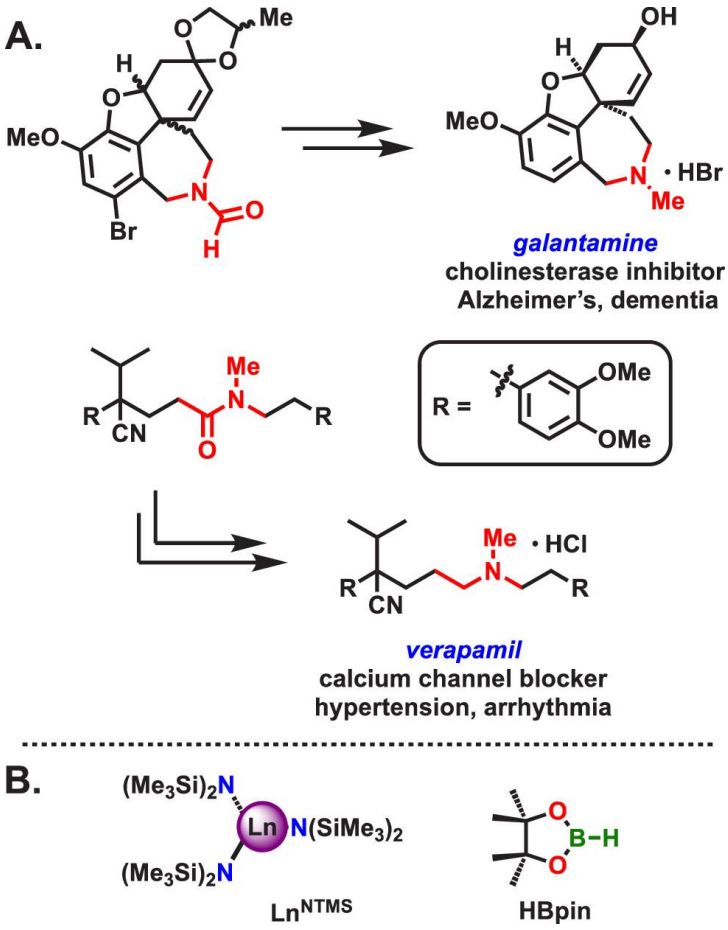

Figure 3.1. **A**. Examples of selective deoxygenative amide reductions practiced at scale.[1] **B**. Structures of tris[*N*,*N*-bis(trimethylsilyl)amido]lanthanide complexes (Ln^{NTMS}), where Ln = any lanthanide, and pinacolborane (HBpin).

Results and Discussion

Hydroboration Scope. Amide reduction is found to occur via deoxygenation to yield the corresponding amine and bis(pinacolboryl)oxide (pinB-O-Bpin, ^{1}H NMR: δ 1.00 ppm, ^{11}B NMR: δ 21.7 ppm in C_6D_6) as a co-product (Table 3.1), analogous to that reported for other borane- and silane-based reductions.[13,15,61] Near quantitative conversion of amide to amine is observed for each of the substrates examined (Table 3.1) at a catalyst loading of 5 mol%, and acidic workup of preparative reactions (0.5 g scale) affords the amine hydrochloride product in good yields without the need for column chromatography (see Experimental Section below). Although only 2 equiv of HBpin (relative to amide) is formally required by stoichiometry for complete amide reduction, 5 equiv was typically found necessary to achieve full conversion over the time and temperature range selected. This is likely attributable to reversible formation of transient amide–borane and amine–borane adducts which, once formed, would effectively reduce the amount of active HBpin available in solution. Considering the DFT-derived geometries in the proposed catalytic cycle, bulky HBpin-amide or HBpin-amine adducts would be expected to approach the catalyst complex and participate in amide reduction with greater difficulty. Such effects were previously observed in similar reductions, and other catalytic systems require HBpin to be held in even greater excess.[15] Tertiary amides are reduced cleanly at 25 °C, although sterically encumbered amides and lactams (Table 3.1, entry 7) require elevated temperature (60 °C) for rapid reduction. Formamides (R = H) generally react more rapidly than amides (R ≠ H; e.g., Table 3.1, entry 1 vs 2). Similarly, steric encumbrance at the R′ and R″ positions depresses the turnover rate (e.g., Table 3.1, entry 1 vs 5). Even with HBpin in excess, the reduction of amides is completely chemoselective over the hydroboration of alkenes and alkynes in intermolecular competition

experiments (Scheme 3.1). Likewise, no intramolecular alkene hydroboration products are observed during the reduction of *N*-allyl-*N*-methylbenzamide (Table 3.1, entry 8). In addition to La^{NTMS}, the catalytic activity of commercially available Sm^{NTMS} and Y^{NTMS} was also investigated for the reduction of *N*,*N*-dimethylbenzamide (Table 3.1, entry 4). While the reaction proceeds similarly in all three cases, the observed rate of reduction, not unexpectedly, diminishes as the ionic radius of the central metal decreases (i.e., La > Sm > Y).

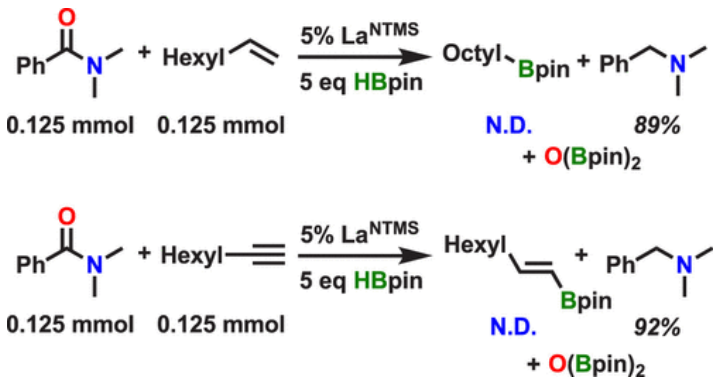

Scheme 3.1. Selective Reduction of *N*,*N*-Dimethylbenzamide in the Presence of 1-Octene (Top) and 1-Octyne (Bottom) (Yields calculated via ^{1}H NMR of crude reaction mixtures. N.D. = not detected. Conditions: 1.00 mL of C_6D_6, 60 °C, 2 h.)

Table 3.1. Scope of La^{NTMS}-Catalyzed Amide Reduction with Pinacolborane[a]

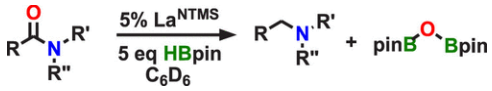

#	Substrate	Product	T/°C	t/h	Yield[b]
1			25	1	97
2			25	6.5	94
3			25	1	99
4	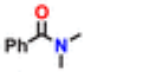		25 25[c] 25[d] 60	17 25 36 2	>99 >99 >99 >99
5			25 60	96 24	>99 >99
6			25 60	20 0.5	>99 >99
7[e]			25 60	72 24	>99 >99
8	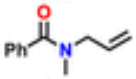	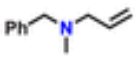	25 60	14 1	>99 >99
9			25 60	72 24	<1 70
10	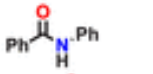		25 60	72 48	<1 90
11	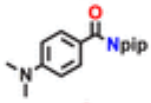	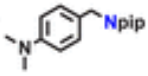	25 60	1 2	9 95
12	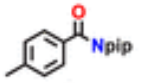	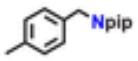	25 60	1 2	18 >99
13	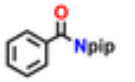	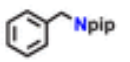	25 60	1 2	28 99
14	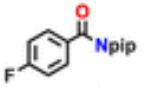	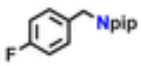	25 60	1 1	38 97
15	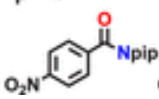	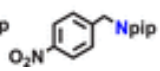	25 60	1 1	68 >99

[a] Reaction conditions: La^{NTMS} (12.5 μmol), amide (0.25 mmol), and HBpin (1.25 mmol, 5 equiv) in C_6D_6 (1 mL total volume). [b] % yields of amine products calculated by integration vs a hexamethylbenzene internal standard. [c] Sm^{NTMS}. [d] Y^{NTMS}. [e] 10 equiv of HBpin.

Secondary amides proved somewhat more challenging, requiring both elevated temperatures and longer reaction times to reach satisfactory yields (Table 3.1, entries 9 and 10). This is likely attributable to the rapid conversion of La^{NTMS} to a lanthanide tris-amidate species *in situ*, possibly hindering formation of the active catalyst for amide reduction (Scheme 3.2). Such a reactivity pattern has been reported previously[62] and is supported by the presence of free $HN(SiMe_3)_2$ in the ^1H NMR spectrum of the secondary amide reaction mixture. In an attempt to fully characterize these tris-amidate complexes, the stoichiometric reaction of La^{NTMS} and benzanilide (1:3) was conducted. Upon mixing, the ^1H NMR spectrum shows the complete conversion of the La^{NTMS} signal (δ 0.29 ppm, C_6D_6) to a new signal corresponding to $HN(Si\mathit{Me}_3)_2$ (δ 0.10 ppm, C_6D_6). Additionally, upon complexation, the aromatic proton signals belonging to benzanilide become quite broad when compared to the ^1H NMR spectrum of the secondary amide alone (Figures 3.15 and 3.16). Variable-temperature (VT) NMR studies were next performed in toluene-d_8 due to the superior temperature profile enabled by toluene vs benzene. However, the aromatic proton signals of the La-benzanilide tris-amidate species do not sharpen or coalesce with increasing temperature (up to 100 °C in toluene-d_8). Furthermore, integrations of these spectra provide minimal information. However, *in situ* studies conducted by adding amide and HBpin to the aforementioned 1:3 mixture of La^{NTMS} and benzanilide (i.e., forming the lanthanide tris-amidate species *in situ*) suggest this species is a less active but nevertheless competent amide reduction catalyst (Figure 3.17). Our attempts to isolate these tris-amidate complexes were unsuccessful. Reduction does not occur with the two primary amides tested (acetamide and benzamide), and instead an intractable, off-white precipitate is formed. While ligand insertion into carbon–heteroatom double bonds has been observed previously with

similar rare earth silylamide complexes,[63] DFT studies indicate that, in this system, a ligand insertion pathway is energetically unfavorable (see Experimental Section). Furthermore, spectroscopic studies reveal that upon addition of benzamide to La^{NTMS}, $HN(SiMe_3)_2$ is produced instantaneously with precipitation of a catalytically inactive La-amide species. Characterization of this marginally soluble species by ^1H and ^{29}Si NMR spectroscopy suggests that it is a La-hemiaminalate complex, e.g., $[(Me_3Si)_2N]_2La\{\eta^2\text{-}OC(NH)Ph\}$ (monomeric or oligomeric; see Experimental Section).[64] Formation of this marginally soluble complex likely precludes the HBpin coordination necessary for efficient reduction to take place.

Scheme 3.2. Observed Reaction of La^{NTMS} with Secondary Amides

Kinetics and Mechanism. To probe the mechanism of this reaction, the rate law for catalytic *N*,*N*-dimethylbenzamide reduction was determined by a combination of initial rates analysis at various catalyst concentrations (for the order in La^{NTMS} concentration) and by monitoring substrate consumption under pseudo-first-order conditions (see Experimental Section for details). Amide reduction is found to proceed with a first-order dependence on the La^{NTMS} concentration and zero-order dependence on the amide concentration. The order in HBpin was not amenable to determination under pseudo-zero-order conditions (10 equiv of amide), as evidenced by a non-

linear correlation for zeroth-, first-, and second-order plots (see Experimental Section). Initial rates analysis reveals that at low HBpin concentrations ([HBpin] < 1.67 *M*, 5–7 equiv vs amide), the rate has a first-order dependence on HBpin concentration; however, a transition occurs when [HBpin] ≥ 1.67 *M* (≥8 equiv vs amide), and the order in HBpin becomes 0. This mixed-order system (eq 3.1) is reminiscent of Michalis–Menten kinetics, wherein the turnover-limiting step in

$$\text{Rate} = k[\text{La}^{\text{NTMS}}]^1[\text{Amide}]^0[\text{HBpin}]^{1/0} \qquad \text{(Eq. 3.1)}$$

the catalytic cycle depends on an equilibrium involving a substrate–catalyst complex.[65] While this regime is not frequently encountered outside of enzyme catalysis,[66] there are a few notable examples where saturation kinetics are observed in hydroelementation reactions.[30,67-69] The presence of an equilibrium between a La complex and HBpin in or immediately preceding the turnover-limiting step could explain the unusual rate behavior observed above. However, a non-equilibrium process, such as the availability of two different turnover-determining transition states, the relative energies of which depend on [HBpin], could also explain this rate law. As such, activation parameters for the reduction of *N*,*N*-dimethylbenzamide were determined at both low [HBpin] (5 equiv of HBpin vs amide) and high [HBpin] (10 equiv of HBpin vs amide) conditions over a temperature range of 30–70 °C. Both low and high [HBpin] conditions yield very similar activation parameters consisting of relatively small and positive enthalpies ($\Delta H^{\ddagger}$ = 10.3 and 11.3 kcal/mol, respectively) and extremely large and negative entropies ($\Delta S^{\ddagger}$ = −49.7 and −46.4 e.u., respectively). These data support assignment of a transition state that is highly organized, sterically congested, and associative, and they strongly suggest the same rate-determining step is operative in low and high [HBpin] reactions, indicating the mixed-order rate law is most likely due to

saturation of the catalyst complex with HBpin at ~8 equiv of HBpin vs amide (i.e., the reaction becomes pseudo-first-order at this point; *vide infra* for a closer examination with DFT techniques).

To gauge the impact of electron density at the carbonyl carbon on the rate of amide reduction, a Hammett plot (Figure 3.2) was created using a series of *para*-substituted benzoyl piperidines. A slight increase in activity is observed for substrates with electron-withdrawing substituents at the R position, as indicated by a small, positive value for the Hammett parameter ρ of 0.56. Additional mechanistic details were obtained from isotopic labeling studies. Replacing HBpin with DBpin (see Experimental Section for details) leads to complete disappearance of the RC*H*$_2$NR′R″ ^{1}H NMR resonance when DBpin is the reductant. Rate studies with DBpin and HBpin yield a kinetic isotope effect (KIE) of 1.50 for reduction of *N*,*N*-dimethylbenzamide.

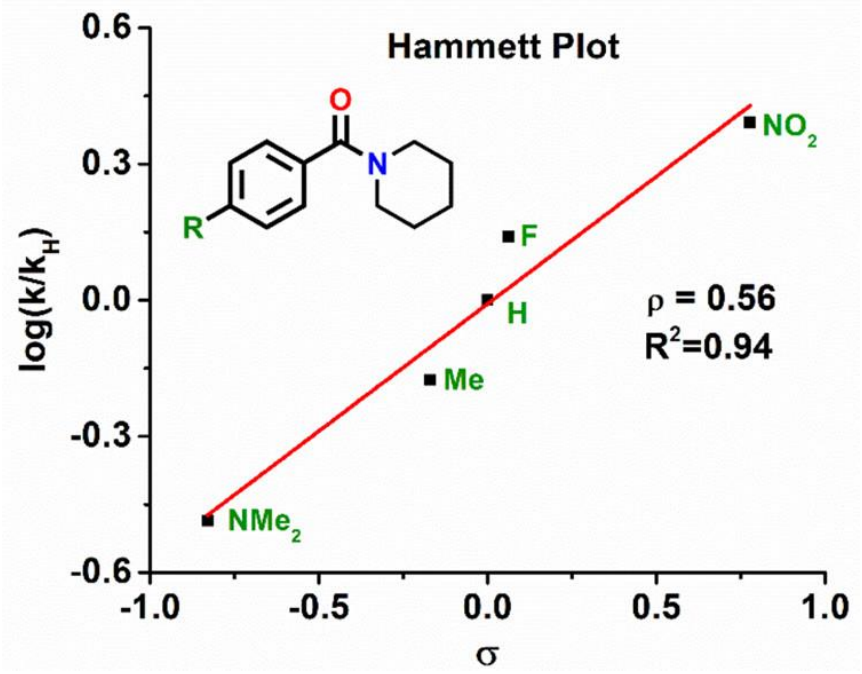

Figure 3.2. Hammett plot generated from the reduction of para-substituted *N*-benzoylpiperidines with HBpin. Rates determined via integration of product ^{1}H NMR signals relative to a hexamethylbenzene internal standard.

Computational Mechanistic Analysis. Informed by the above kinetic and thermodynamic data, DFT modeling was next employed to better understand the mechanism of La^{NTMS}-catalyzed amide hydroboration. In order to accurately model the behavior of the central metal, various computational approaches were taken, using a number of different basis sets including LANL2DZ, LANL2DZ+pol,[70] and Def2-SVP.[71] However, the addition of such polarization functions affords negligible changes in the stabilization energies of the key intermediates and transition states along the proposed reaction coordinate (see Experimental Section). Therefore, as in our previous work detailing a similar reduction of esters,[31] the LANL2DZ basis set was ultimately used to model the

lanthanum atom in this transformation. It will be seen that the active catalyst for this transformation is found to be the lanthanum hemiaminal species [$(Me_3Si)_2N]_2$La-OCHR(NR′$_2$)-[HBpin] (Figure 3.3, **B**), a species which bears a striking resemblance to the active catalyst this laboratory found recently for La^{NTMS}-catalyzed ester hydroboration.[31] While the transient nature of this complex (*vide infra*) precludes its NMR spectroscopic observation *in situ*, the formation of this species is supported by the appearance of 1.0 equiv (relative to La^{NTMS}) of pinB-N$(SiMe_3)_2$ in the ^{1}H NMR spectra of catalytic reactions (at δ 1.03 and δ 0.37 ppm),[72] indicating that the hydroboronolysis of a single −N$(SiMe_3)_2$ precatalyst ligand occurs. The formation of pinB-N$(SiMe_3)_2$ could also be indicative of a metal–hydride active catalyst (e.g., [$(Me_3Si)_2N]_2$La-H]), (**A**, Figure 3.3) however the energy required to form such a species (+20.5 kcal/mol vs −21.2 kcal/mol barrierless for structure **B**) makes its presence in the catalytic cycle highly unlikely (see Figure 3.5). Moreover, no spectroscopic evidence indicating the presence of a La–H species is observed. Attempts to isolate complex **B** were unsuccessful due to the formation of an off-cycle product containing ring-opened pinacolborane (see Experimental Section for characterization details) that predominates at the low substrate concentrations required for stoichiometric studies. This is identical to the deactivation product observed for La^{NTMS}-catalyzed ester hydroboration and is analogous to that found in lanthanocene-catalyzed pyridine dearomatization (Figure 3.4).[31,73] In an attempt to further investigate the proposed catalyst activation process shown in Figure 3.3, NMR-monitored stoichiometric experiments were conducted. Species **I-$_{act}$-1** was obtained from a 1:1 mixture of La^{NTMS} and *N*,*N*-dimethylbenzamide. Full conversion of the La[N(Si*Me*$_3)_2]_3$ proton signal at δ 0.29 ppm (C_6D_6) to a new signal at δ 0.41 ppm (C_6D_6) indicates the formation of what is presumed to be **I-$_{act}$-1** (Figures 3.33 and 3.34). Regarding species **I-$_{act}$-**

2 and **I-$_{act}$-3**, we attempted to isolate and characterize these intermediates by adding 1 equiv of HBpin to a 1:1 mixture of La^{NTMS} and *N*,*N*-dimethylbenzamide (**I-$_{act}$-1**), however, the resulting spectra revealed a complex mixture of products and obvious decomposition. The ratios of La^{NTMS}, amide, and HBpin were also varied but these too yielded mixtures of products. Additionally, adding 1 equiv of amide to a solution of a precoordinated HBpin-La^{NTMS} complex was carried out, but attempts to isolate or unambiguously characterize **I-$_{act}$-2** or **I-$_{act}$-3** were ultimately unsuccessful.

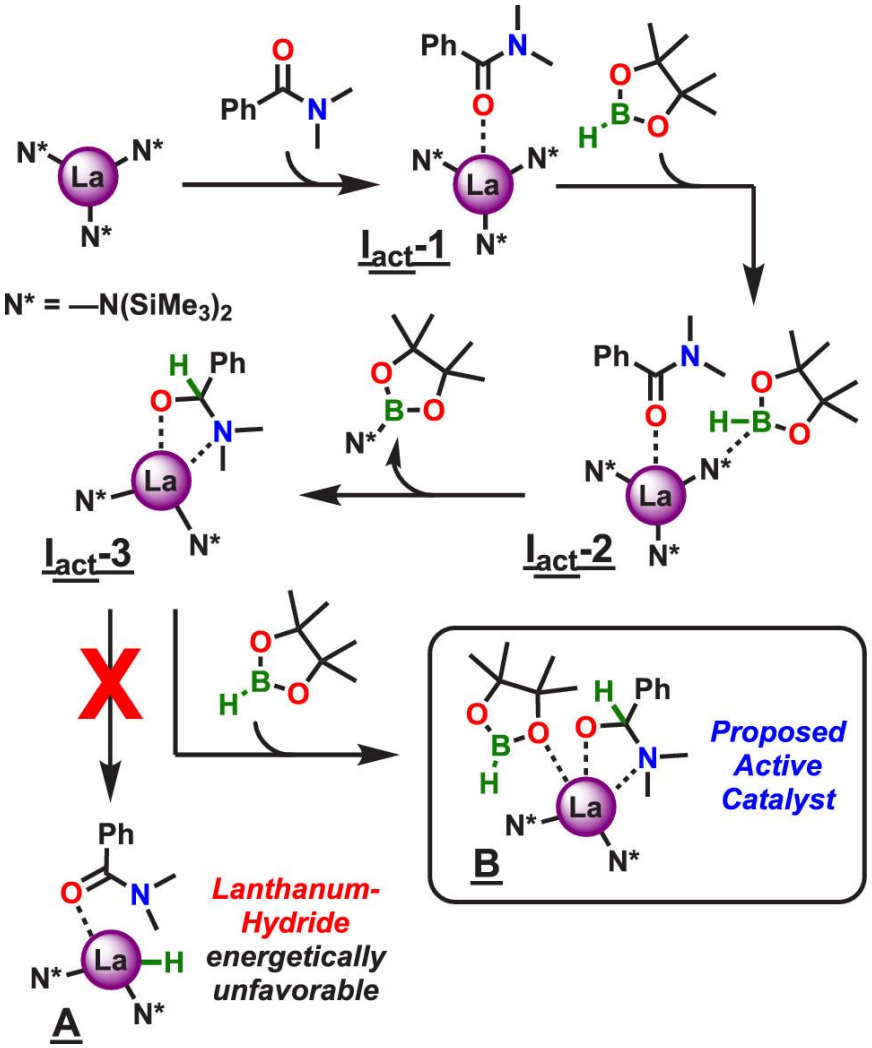

Figure 3.3. Proposed catalyst activation process for the hydroboration/reduction of amides catalyzed by La^{NTMS}.

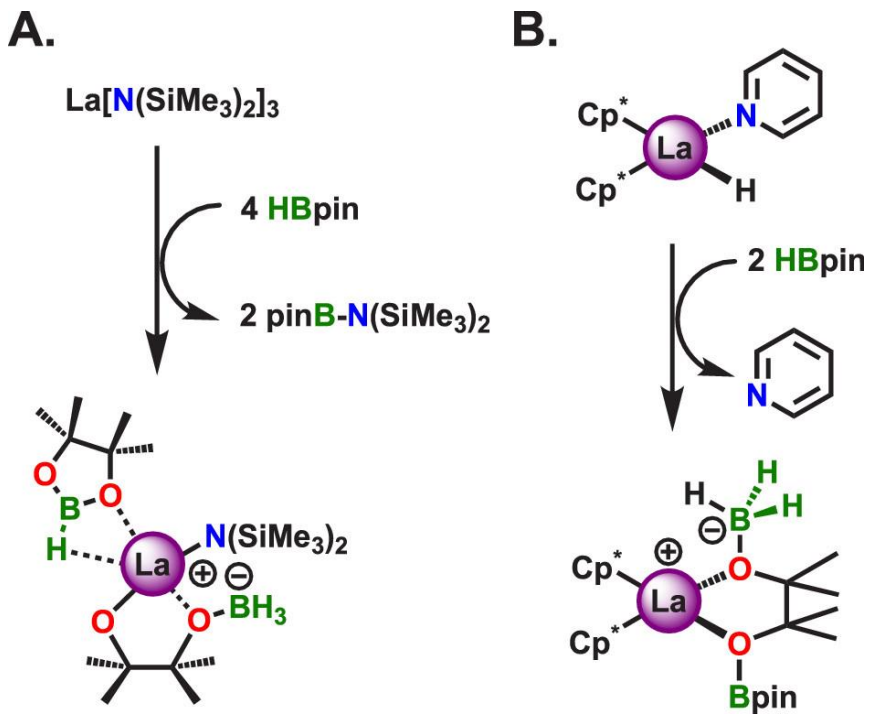

Figure 3.4. **A**. Off-cycle product observed in stoichiometric studies of both amide and ester hydroboration catalyzed by La^{NTMS}.[31] **B**. Comparable deactivation product reported for $[Cp^*_2LaH]_2$-catalyzed pyridine dearomatization; Cp* = η^5-pentamethylcyclopentadienyl and characterized by single-crystal X-ray diffraction.[69]

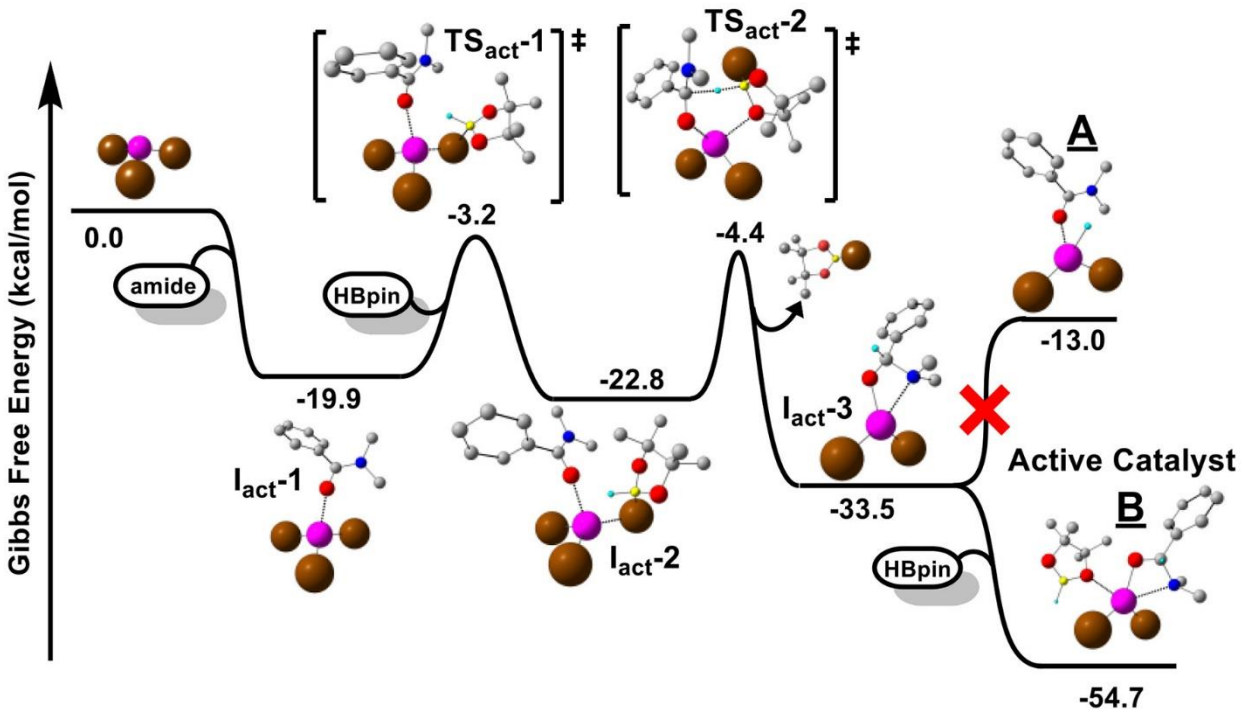

Figure 3.5. DFT-computed Gibbs free energy profile of the catalyst activation process for the subsequent hydroboration/reduction of amides catalyzed by La^{NTMS}.

The proposed mechanistic pathway consists of four major steps (Figure 3.6). First, coordination of an additional amide molecule and approach of the Lewis acidic boron center of the coordinated HBpin molecule toward the hemiaminal oxygen of active catalyst **B**, leads to the formation of a new B–O bond and dissociation of the La–O bond. This step, which yields a La-coordinated pinacolborate species, proceeds spontaneously, providing an overall stabilization energy of 19.4 kcal/mol and producing **C** as a relative minimum in the energetic profile (Figure 3.7). Next, a HBpin molecule approaches the catalyst complex. Hydride transfer from the La-coordinated hemiaminal-hydroborate species to the coordinated HBpin forms La-coordinated $[H_2Bpin]^-$, a species often proposed to facilitate hydride transfer in HBpin-mediated reductions.[29,30,74-77] With reorganization, and the approach and subsequent coordination of an additional amide substrate after **TS1**, the complex then forms species **D** with a stabilization energy of 18.4 kcal/mol. A significant portion of this stabilization energy coming from amide coordination alone (Figure 3.7). Third, C–O bond scission of the hemiaminal–borane species **D** results in a transient carbocationic species and La-bound −OBpin (**TS2**). The carbocationic species is subsequently reduced by $[H_2Bpin]^-$ to yield free amine. This step proceeds with a 4.0 kcal/mol barrier and is highly exergonic (−41.3 kcal/mol) forming species **E**. Next, a second HBpin molecule approaches the catalyst complex forming complex $\mathbf{E_{HBpin}}$. Even though this step is slightly exoenthalpic (ΔH = −3.2 kcal/mol), the entropy gain related to the association process shifts up the energy value along the Gibbs free energy profile (ΔG = 4.7 kcal/mol). Finally, hydride transfer from the activated HBpin of $\mathbf{E_{HBpin}}$ to the coordinated amide substrate acquired in the second step allows for the formation of the pinB-O-Bpin co-product and restoration of the active catalyst **B**. It is worth noting that because the reaction described requires an excess of HBpin, it is plausible that an equilibrium

exists between catalyst–amide and catalyst–HBpin coordination. For this reason, it is likely that other intermediates which are not shown in Figure 3.7 do exist within the proposed catalytic cycle. DFT calculation also supports this notion (Figure 3.25). However, the proposed catalytic cycle includes only the most stable intermediates and transition states, as these species are the largest contributors to the thermodynamic and kinetic behavior experimentally observed. In the transition state structure (**TS3**), HBpin interacts weakly with the carbonyl oxygen of the coordinated amide. This step is isoergonic and proceeds with an energy barrier of 20.3 kcal/mol. The above energetic profile shows that species **E** can be assigned as the turnover-determining intermediate (TDI) and **TS3** can be assigned as the turnover-determining transition state (TDTS). The computed parameters, $\Delta H^{\ddagger}$ = 10.9 kcal/mol and $\Delta S^{\ddagger} \approx -35$ e.u., agree well with the experimental findings. Moreover, the formation of the $\mathbf{E}_{\mathbf{HBpin}}$ complex convincingly explains the shift from first to zero-order [HBpin] experimentally observed by increasing the HBpin concentration (Figure 3.11).

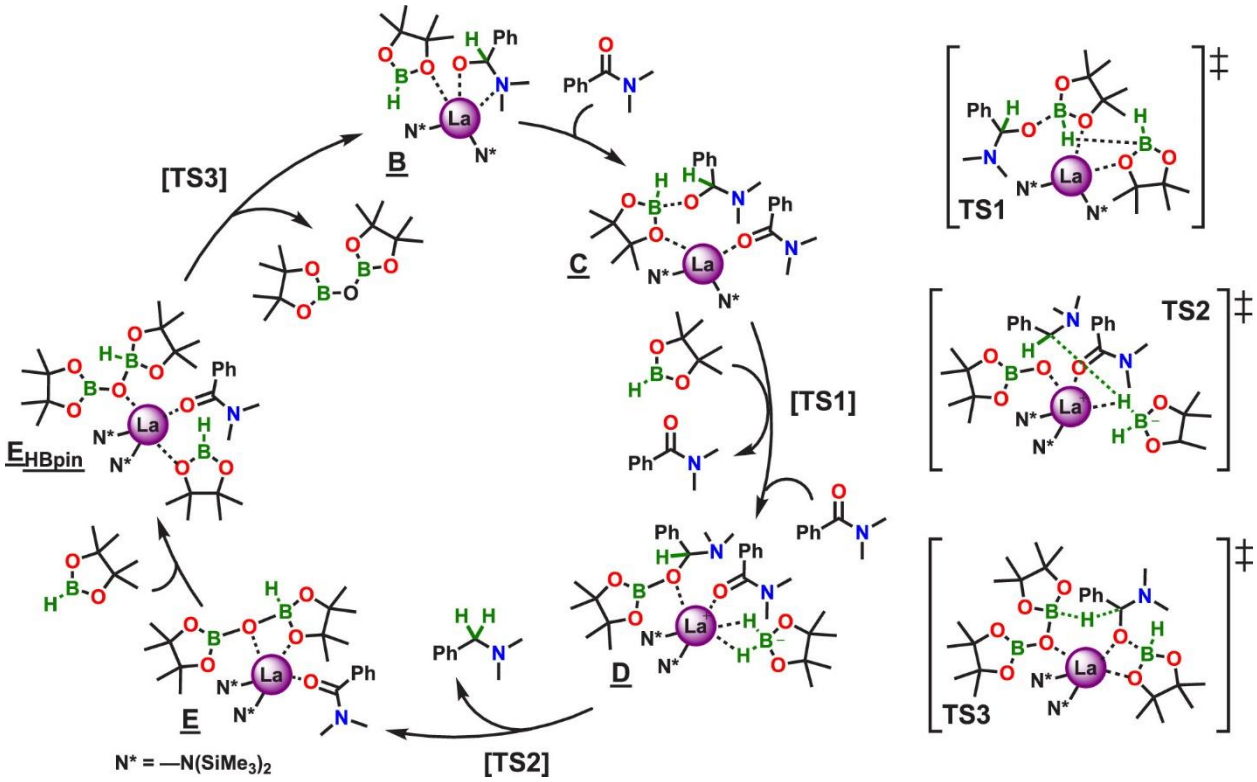

Figure 3.6. Proposed DFT-computed catalytic cycle and transition states for the catalytic hydroboration/reduction of *N,N*-dimethylbenzamide catalyzed by La^{NTMS}.

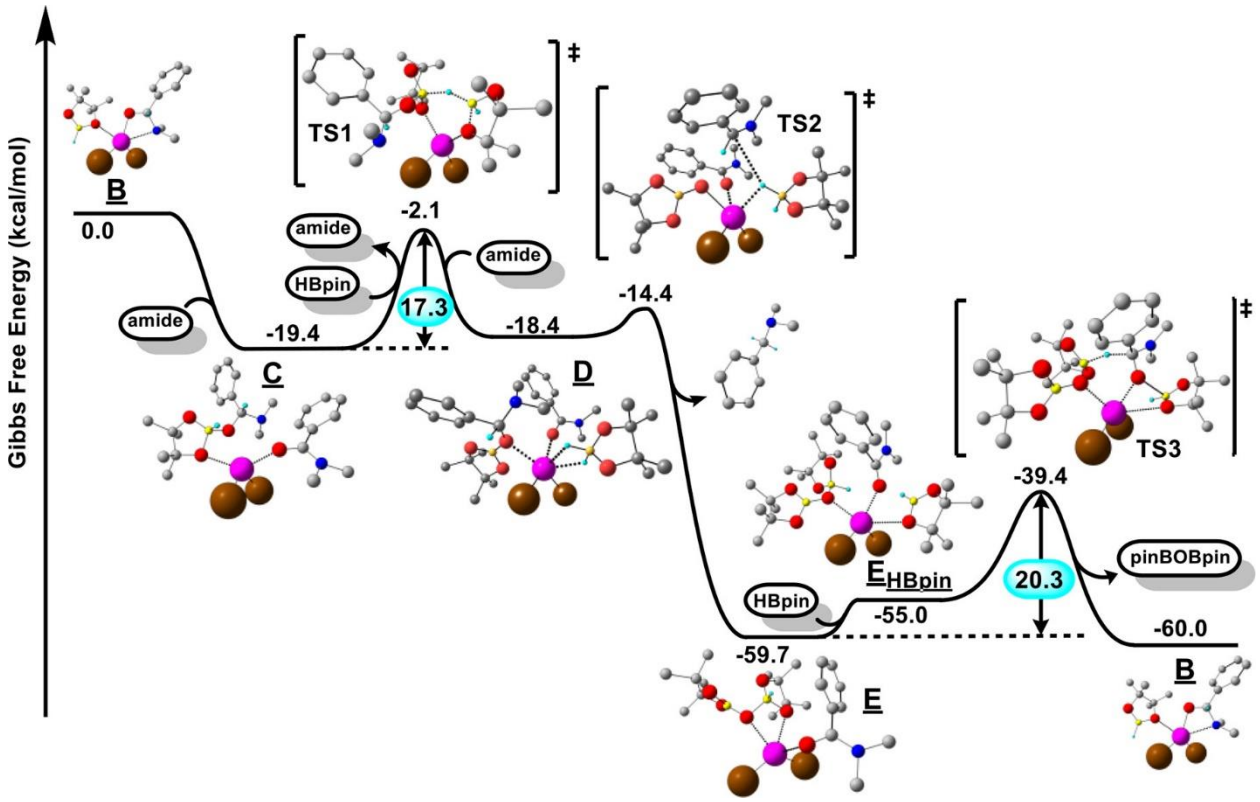

Figure 3.7. DFT-computed Gibbs free energy profile/catalytic cycle for the hydroboration/ reduction of *N*,*N*-dimethylbenzamide catalyzed by La^{NTMS}.

A first-order dependence on [HBpin] is expected, as HBpin enters the catalytic cycle between the **TDI** and **TDTS**, in agreement with the low [HBpin] rate law determined experimentally, Rate = $k[La]^1[Amide]^0[HBpin]^1$ (*vide supra*). However, the observation that a high HBpin concentration can induce saturation of the catalyst complex with HBpin (effectively eliminating $\underline{\mathbf{E}}_{\mathbf{HBpin}}$ from the energetic profile) likely underlies the first-to-zero-order transition observed for [HBpin] in the rate law.

In addition to the activation parameters discussed above, other experimental observations point to **E** and **TS3** as the TDI and TDTS, respectively. Steric encumbrance on the amide substrate strongly depresses the reaction rates at 25 °C, which is to be expected for an associative, crowded transition state such as **TS3**. A small, positive Hammett ρ value (ρ = 0.56, Figure 3.2) indicates that the transition state is stabilized by withdrawal of electron density from the carbonyl carbon, but to a much lesser extent than is observed for typical base-catalyzed ester cleavages (ρ = 1.9–2.5).[19] This supports the present assignment that the turnover-limiting step involves nucleophilic hydride attack on a carbonyl bond that has been activated, in this case by simultaneous C═O coordination to both HBpin and La, priming the acyl carbon for nucleophilic attack and diminishing ρ. Similar results were recently found for the analogous ester hydroboration process.[31] Finally, the observed HBpin/DBpin KIE of 1.50 indicates that a bond to an HBpin-derived hydride is broken or formed during the rate-determining step.[78] No other KIEs have been reported for amide hydroboration, making direct comparison impossible, but this value is significantly smaller than KIEs found for several comparable reactions.[79-82] However, this laboratory recently reported a nearly identical KIE (1.49) for ester hydroboration.[31] Notably, in the TDTS of both systems, the B–H bond of a coordinated hemiaminal-/hemiacetal-hydroborate is broken, and a new C–H bond is formed.

Conclusions

The scope and mechanism of La^{NTMS}-catalyzed, pinacolborane-based deoxygenative reduction of a diverse group of variously substituted amides are reported. The catalyst shows complete selectivity for amide reduction over nitro groups, alkenes, and alkynes, even at

temperatures as high as 60 °C and catalyst loadings of 5 mol%. A combined experimental/theoretical analysis of the mechanism of this reaction reveals an unusual catalytic cycle involving ligand-centered hydride transfer. This gives rise to a rate law that is mixed-order with respect to HBpin: Rate = k[La]^1[Amide]^0[HBpin]^1 at low [HBpin] and Rate = k[La]^1[Amide]^0[HBpin]^0 at high [HBpin]. This represents the first time a lanthanide catalyst has been employed for the pinacolborane-based reduction of amides, and it is the first attempt at a computationally aided analysis of the mechanism of amide hydroboration. By combining a mild reductant such as HBpin with a highly active and readily accessible catalyst like La^{NTMS}, a safer, more selective, and convenient route to amide reduction has been realized, highlighting the important role lanthanide catalysis can play in experimental chemical synthesis.

Experimental Section

Materials and Methods. All manipulations of air-sensitive materials were carried out with rigorous exclusion of oxygen and moisture in flame- or oven-dried Schlenk-type glassware on a dual-manifold Schlenk line or in an argon-filled glovebox with a high capacity recirculator (<1 ppm O_2). Benzene-d_6 (Cambridge Isotope Laboratories; 99+ atom % D) was stored over Na/K alloy and vacuum transferred prior to use. La[N(SiMe$_3$)$_2$]$_3$ (La^{NTMS})* and hexamethylbenzene were purchased from Sigma-Aldrich Co. and sublimed under high-vacuum (10^{-6} Torr). Pinacolborane ("HBpin") was purchased from Sigma-Aldrich Co. and distilled under high-vacuum (10^{-6} Torr) to remove trace boronic acid impurities. Amide substrates were purchased from Sigma-Aldrich Co. and used as received or prepared according to established procedures. The products of amide deoxygenation were isolated as the amine hydrochlorides and then characterized by ^{1}H-NMR and

^{13}C-NMR, unless otherwise noted. The La^{NTMS} precatalyst can also be used as received without further purification.

Physical and Analytical Measurements. NMR spectra were recorded on a Bruker Avance III (500 MHz, ^{1}H; 125 MHz, ^{13}C; 125 MHz, ^{29}Si), Varian Inova 500 (500 MHz, ^{1}H; 125 MHz, ^{13}C), Agilent DD MR-400 (400 MHz, ^{1}H; 100 MHz, ^{13}C; 128 MHz, ^{11}B;), or Agilent DD2 500 (500 MHz, ^{1}H; 125 MHz, ^{13}C). Chemical shifts (δ) for ^{1}H are referenced to residual solvent resonances (δ 7.16 for benzene-d_6; 4.79 ppm for D_2O). ^{13}C shifts are referenced to residual solvent resonances (δ 128.06 ppm for benzene-d_6) or external $SiMe_4$ standard. ^{11}B shifts are referenced to an external $BF_3{\cdot}OEt_2$ standard. ^{29}Si shifts are referenced to an external $SiMe_4$ standard. NMR scale reactions were carried out either in Teflon-sealed J. Young tubes or rubber septum-sealed tubes (*vide infra*).
Typical NMR-scale reaction involving solid amides. In a glovebox, the amide (0.25 mmol), internal standard hexamethylbenzene (50 μmol), and HBpin (1.25 mmol) were dissolved in benzene-d_6 (total volume 1.0 mL). This solution as injected into a vial containing La^{NTMS} (12.5 μmol), shaken to dissolve the catalyst. The reaction mixture was transferred to a J. Young capped NMR tube, and the reaction was monitored by ^{1}H-NMR spectroscopy.

Typical NMR-scale reaction involving liquid amides. In a glovebox, La^{NTMS} (12.5 μmol) was placed in a septum-sealed NMR tube, and the cap was wrapped in film. Internal standard (50 μmol), HBpin (1.25 mmol) and benzene-d_6 were added to a septum-sealed vial. Outside the glovebox (to prevent amine poisoning of the glovebox circulation catalyst), the liquid amide (0.25 mmol) was injected into the vial with HBpin and internal standard, the vial was shaken, and the

contents were injected into the NMR tube containing the catalyst, all under N_2. The tube was shaken to dissolve the catalyst, and the reaction was monitored by ^{1}H-NMR spectroscopy.

Scale-Up/ Isolation of Amine Hydrochlorides. In a glovebox, La^{NTMS} (0.125mmol) was weighed into a 25 mL round bottom and dissolved in 5 mL benzene. HBpin (12.5 mmol) and amide (2.5 mmol) were dissolved in 5 mL benzene, and the solution was injected into the stirred catalyst solution at 25 °C or 60 °C. Low boiling amines (trimethylamine, *N,N*-dimethylethylamine, *N*-methylpyrrolidine, *N*-methylethylamine,) were isolated by evaporation. Nitrogen was bubbled into a solution containing the reaction mixture. A cannula needle was used to bubble the volatile amine product into a 1M HCl/methanol solution cooled to 0 ºC (Figure 3.8). The methanol was then removed by rotary evaporation, and the remaining solid was washed with pentanes. Amines with boiling points similar to HBpin (*N*-methylpiperidine and *N,N*-diisopropylmethylamine) were first isolated by distillation under vacuum. To the distillate, 1M HCl/methanol was added, precipitating a solid that was subsequently collected and washed with pentanes. The remaining high-boiling or solid amines were isolated by first removing HBpin under vacuum, re-dissolving the amine in benzene, and filtering the solution through a basic alumina plug to remove trace HBpin, pinB-O-Bpin, and the catalyst. A 1M HCl/methanol solution was then added, precipitating a solid that was collected and washed with ether or pentanes.

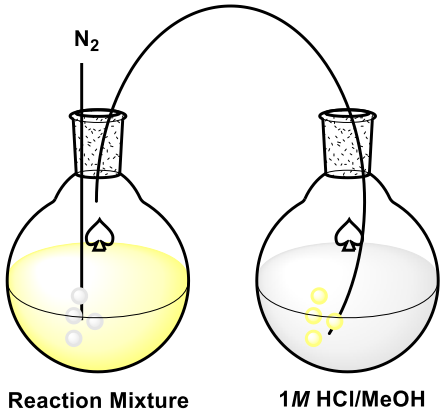

Figure 3.8. Schematic of reaction apparatus to trap volatile amine products from large-scale amide reductions.

Typical NMR-Scale Reaction for Kinetic Monitoring by ^{1}H-NMR Arrays. In a glovebox, amide, HBpin, and the internal standard were mixed in a vial and dissolved in C_6D_6 (V_{total} =1.0 mL). This solution was then added to a rubber septum-sealed NMR tube, wrapped with film, and removed from the box. At the NMR, the magnet was locked, tuned, and shimmed to the sample, then a stock solution containing an appropriate loading of La[N(SiMe$_3$)$_2$]$_3$ was injected into the tube. The tube was shaken and reinserted into the instrument and the experiment was started. Single (^{1}H-NMR) scans were collected at regular intervals. Substrate and/or product concentrations were determined relative to the intensity of the internal standard resonance and plotted versus time.

Kinetic Analysis. Kinetic analysis of the NMR-scale reactions described above was carried out by collecting multiple (>15) data points early in the reaction (<20% conversion). Under these conditions, the reaction can be approximated as pseudo-zero-order with respect to the substrate concentrations. The product concentration was measured from the area of the RC*H*$_2$NR'R" product

peaks relative to the C_6Me_6 internal standard. Data were fit by least-squares analysis ($R^2 > 0.98$) according to eq. 3.2, where "t" is time, "[product]" is the concentration of product at time t, and "m" is the rate of reaction.

$$[product] = mt \tag{3.2}$$

Reaction orders for HBpin and *N,N*-dimethylbenzamide were determined by running reaction under pseudo-first-order conditions (10-fold excess of non-measured reactant). The order of the reactant not in excess was determined from the linearity of plots of [A] vs. time (zeroth order), ln[A] vs. time (first order), and $[A]^{-1}$ vs. time (second order).[83] As discussed in the paper, the order in HBpin for amide reduction was not amenable to determination under pseudo-first order conditions (Figure 3.10) and instead had to be determined by initial rates analysis (Figure 3.11).

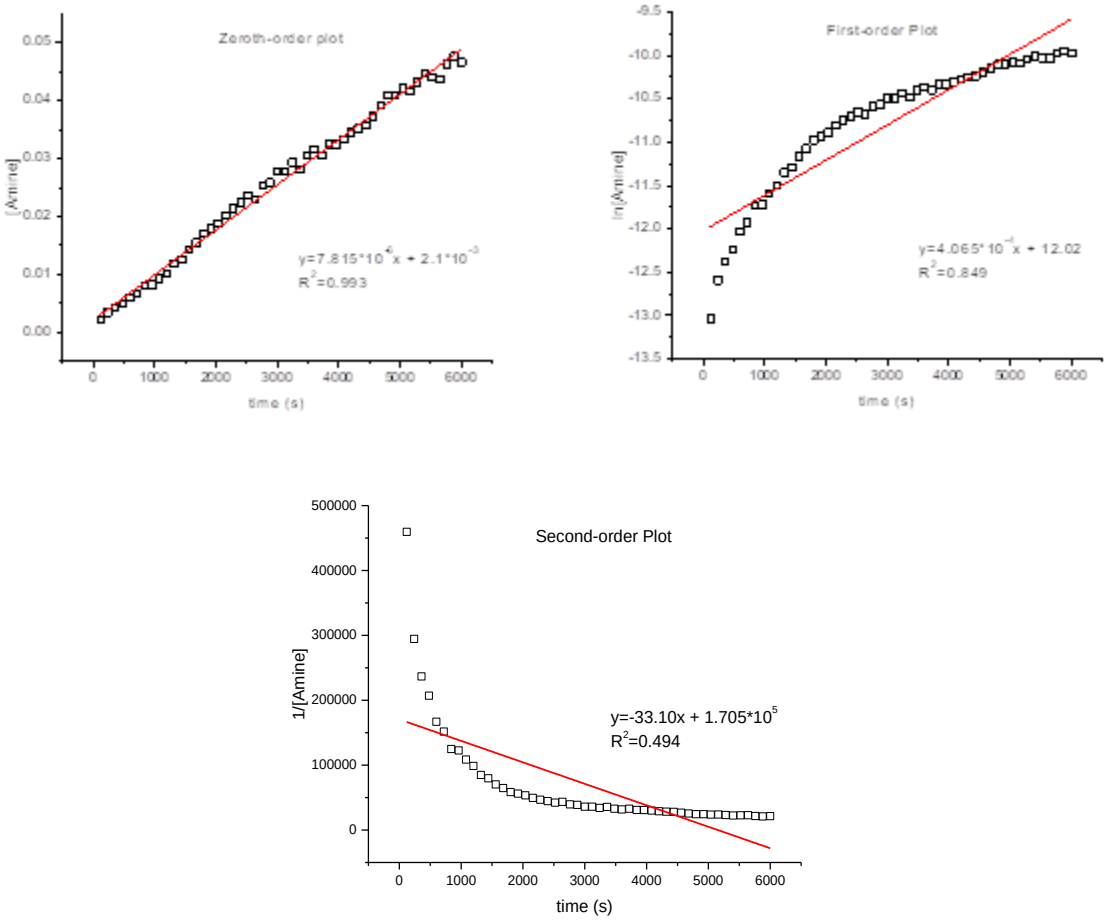

Figure 3.9. Pseudo-first order plots for reaction order in *N*,*N*-dimethylbenzamide (HBpin in 10-fold excess). The zeroth-order plot ([Amine] vs. time, top-left) is linear, while the other two plots are not. Reaction conditions: 6.25 μmol La^{NTMS}, 0.125 mmol *N*,*N*-dimethylbenzamide, 1.25 mmol HBpin, 0.0330 mmol C_6Me_6, C_6D_6 (total volume 1.00 mL).

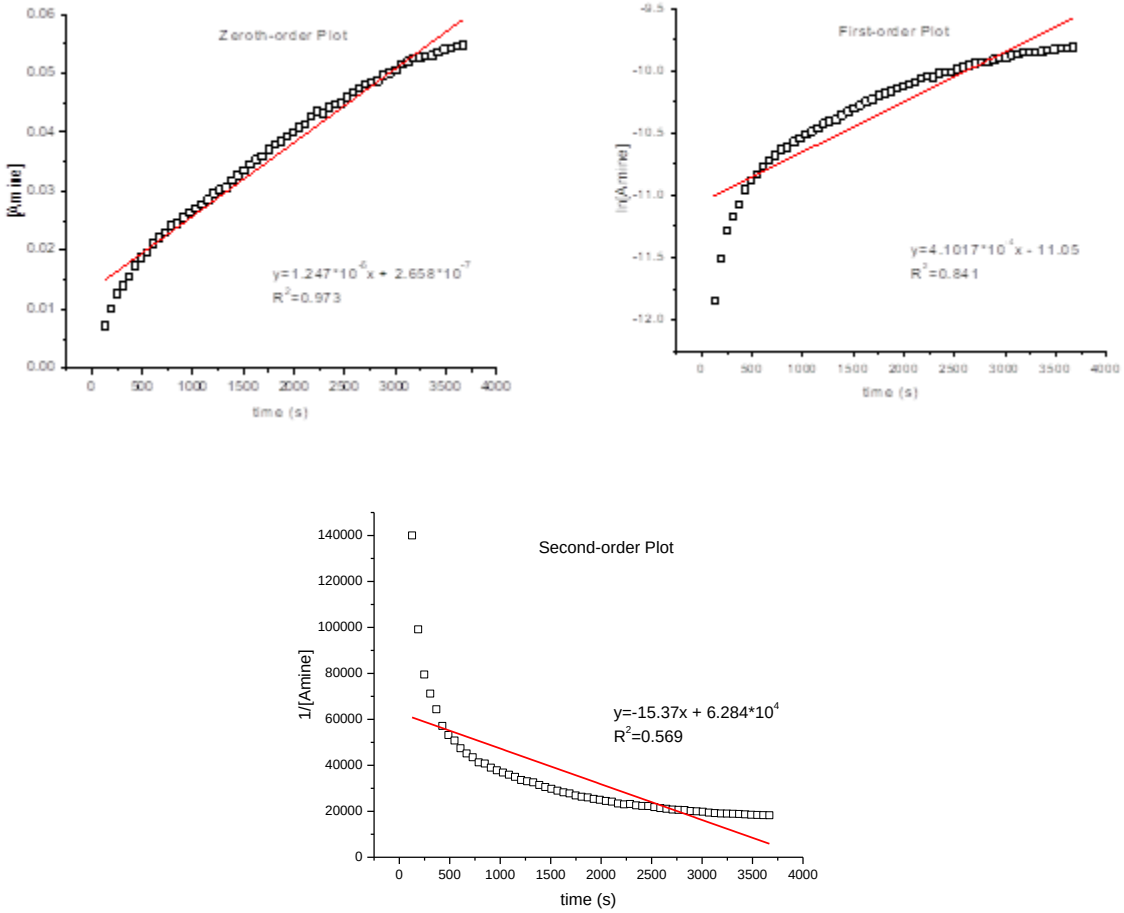

Figure 3.10. Pseudo-first order plots for reaction order in HBpin for amide reduction (10-fold excess of amide). None of the plots are linear, indicating HBpin consumption is likely mixed-order for amide reduction. Reaction conditions: 6.25 μmol La^{NTMS}, 1.25 mmol *N,N*-dimethylbenzamide, 0.125 mmol HBpin, 0.0330 mmol C_6Me_6, C_6D_6 (total volume 1.00 mL).

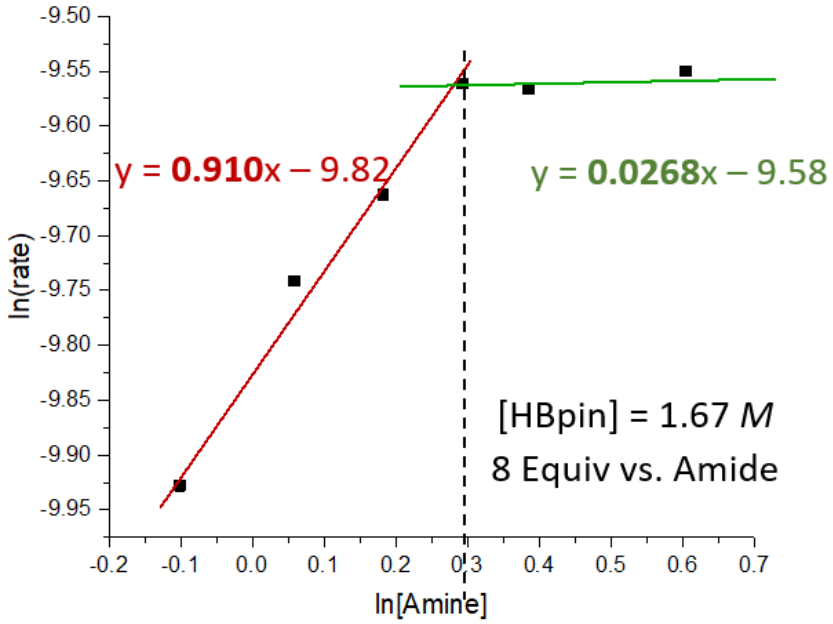

Figure 3.11. Ln vs. ln plot for the determination of reaction order of HBpin in amide reduction. A mixed order system is observed, wherein at [HBpin] < 1.67 *M*, the order in HBpin = 1 (slope = 0.910 ≈ 1, *vide infra* for derivation and explanation). At [HBpin] ≥ 1.67 *M*, the order in HBpin = 0 (slope = 0.0268 ≈ 0).

The order for La^{NTMS} was determined from the rates of reduction of *N,N*-dimethylbenzamide at 5 different catalyst loadings (0.5-2.5%). The rates were measured as the slope of the line for [Product] vs. time at conversion < 20%. These rates were then plotted as ln(rate) vs. ln[La^{NTMS}]. The negative rate of disappearance of La^{NTMS} is proportional to the concentration of La^{NTMS} to the order (α) (see eq. 3.3). Therefore, the order is the slope of a plot of ln(rate) vs. ln[amide] (eq. 3.4).[84]

$$\frac{-d[LaNTMS]}{dt} = k_{obs}[LaNTMS]^{\alpha} \tag{3.3}$$

$$\ln(rate) = lnk_{obs} + \propto \ln [LaNTMS] \tag{3.4}$$

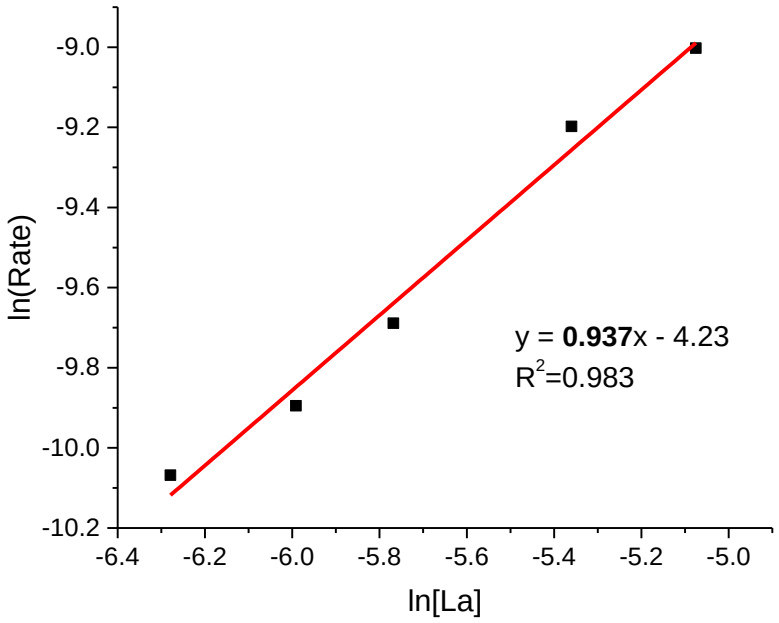

Figure 3.12. Ln vs. ln plot for the determination of the reaction order of La^{NTMS} for reduction of *N,N*-dimethylbenzamide.

Isotopic Labeling Studies. DBpin was synthesized according to literature procedures.[85] BD_3•SMe_2 (Cambridge Isotope Laboratories, 8.5 mmol, 10 *M*) was diluted in 10 mL DCM in an addition funnel under N_2. This solution was added dropwise over 30 min to a 0 °C solution of pinacol (8.5 mmol, 1.0 g) in 20 mL DCM. After addition was complete, the solution was brought to room temperature and stirred until bubbling was no longer observed (1 h). DBpin was purified by distillation (0°C at 10 mmHg). **^{1}H-NMR (400 MHz, C_6D_6)**: 1.00 (s, 12H, DB*pin*) **^{11}B{^{1}H-NMR (128 MHz, C_6D_6)**: 28.37 (t, $^2J_{DB}$=22.8 Hz, D*B*pin).

Rate studies were carried out with HBpin and DBpin under the same ^{1}H NMR kinetic monitoring conditions outlined above using *N,N*-dimethylbenzamide (Figure 3.13).

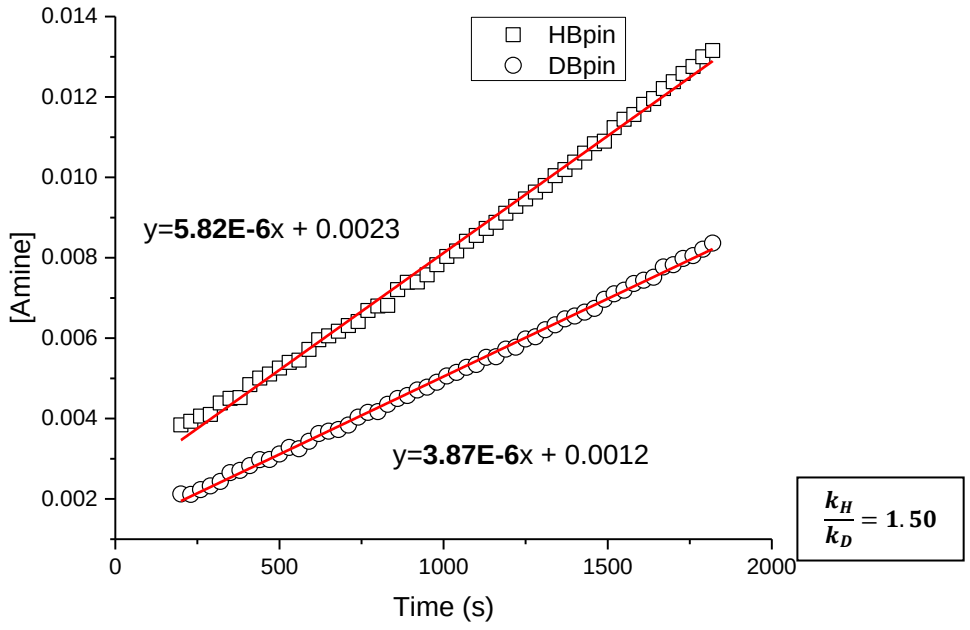

Figure 3.13. Plots for the determination of the kinetic isotope effect for reduction of *N,N*-dimethylbenzamide using HBpin and DBpin.

Variable-Temperature Kinetic Analysis. Temperature-dependent rate data were obtained *via* arrayed NMR scans as described above. Temperatures were set on the NMR instrument using an external temperature controller and calibrated using ethylene glycol (>25 °C) or methanol (<25 °C) standards. Rates at each temperature were determined from the average of three trials. These data were then plotted as 1000/T vs. ln(k/T) from which the enthalpy and entropy of the transition state could be obtained using the Eyring equation (see eq. 3.5). $\Delta H^{\neq}$ is the negative slope times R and $\Delta S^{\neq}$ is the intercept minus the natural log of k_b/h times R.

$$\ln\frac{k}{T} = \frac{\Delta H^{\neq}}{RT}\left[\frac{\Delta S^{\neq}}{R} - \ln\frac{k_b}{h}\right] \tag{3.5}$$

From a plot of 1000/T vs. ln(k), the activation energy can be obtained using the Arrhenius equation (eq. 3.6). E_a is the negative slope times R.

$$\ln k = -\frac{E_a}{RT} - \ln A \tag{3.6}$$

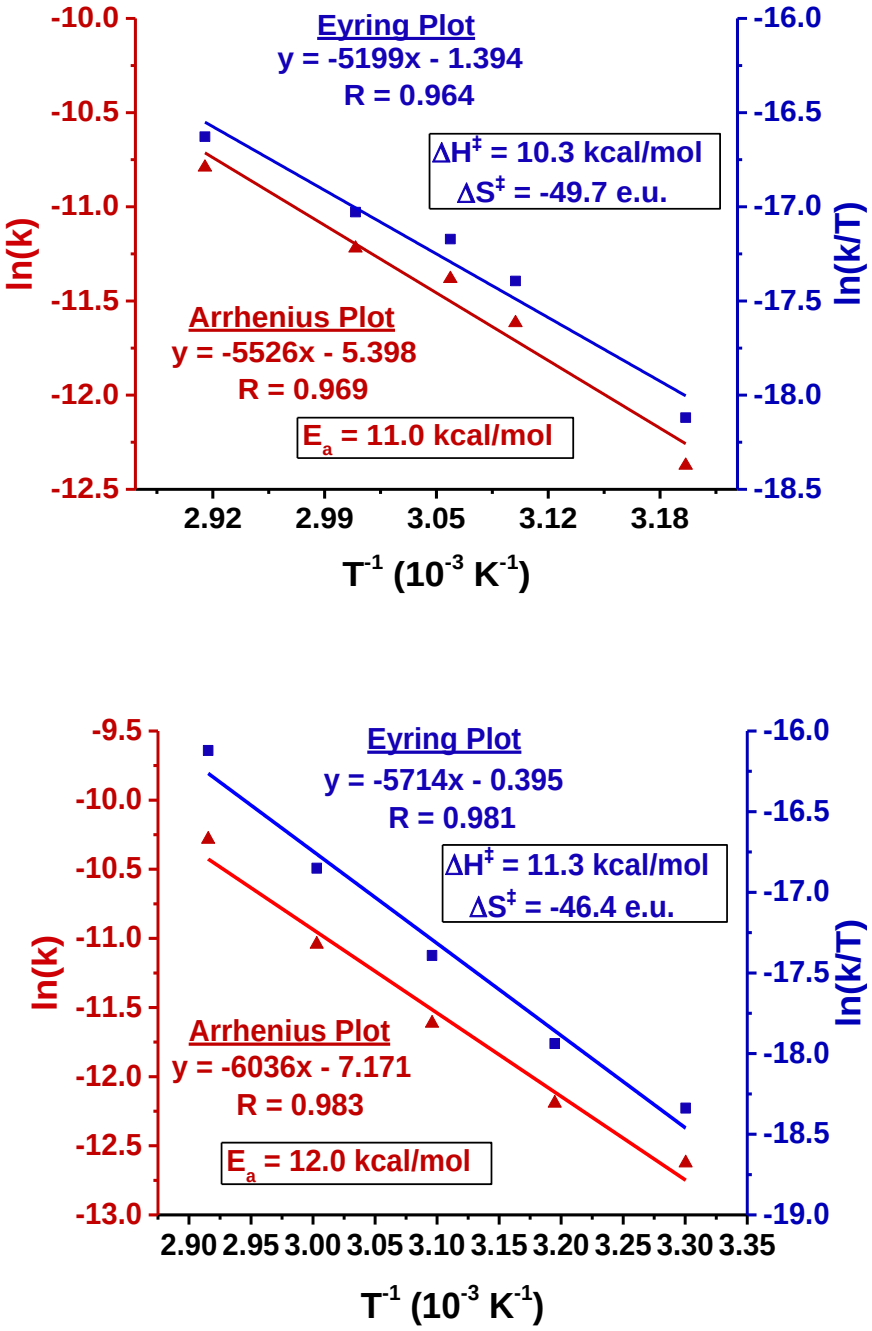

Figure 3.14. Eyring (blue) and Arrhenius (red) plots for the reduction of *N,N*-dimethylbenzamide at low [HBpin] (5 equiv, top) and high [HBpin] (10 equiv, bottom).

Hammett Analysis. A series of *para*-substituted N-benzoyl piperidines was synthesized from the corresponding benzaldehydes and piperidine according to literature procedures (^{1}H- and ^{13}C-NMR spectra were identical to those previously reported).[86] Rates were determined by ^{1}H-NMR spectroscopy (*vide supra*). The rates of reduction for each substrate were plotted according to the Hammett equation (eq. 3.7), so that the slope of the line gives rho (ρ), which indicates the sensitivity of the reaction to the electron density at the carbonyl carbon of the substrate.[87]

$$log\frac{k}{k_H} = \sigma\rho \tag{3.7}$$

Competition Studies. To gauge the selectivity of La^{NTMS} for amide hydroboration over olefin/alkyne hydroboration, intermolecular competition experiments were performed using 1-octene and 1-octyne. *N*,*N*-dimethylbenzamide (0.125 mmol), 1-octene/1-octyne (0.125 mmol), and HBpin (0.625 mmol) were dissolved in C_6D_6 in a J. Young capped NMR tube. La^{NTMS} (6.25 μmol) was added and the tube was shaken. After 2 h at 60 °C, complete conversion of the *N*,*N*-dimethylbenzamide was observed, with no concomitant reduction of olefin.

Secondary Amide Reduction. To determine the active catalyst for secondary amide reduction, La^{NTMS} (2.08 μmol) and benzanilide (6.25 μmol, 3 equiv.) were dissolved in C_6D_6 in a J. Young capped NMR tube. After 15 min at 25 °C, no La^{NTMS} was observed in the ^{1}H-NMR spectrum (ligand methyl signals appear at 0.30 ppm), and only free $HN(SiMe_3)_2$ (0.10 ppm) was present, indicating complete conversion of the precatalyst to a lanthanide tris-amidate species had occurred. Introducing additional benzanilide (0.125 mmol) and HBpin (0.625 mmol) to this in situ generated catalyst results in ~90% conversion of the amide.

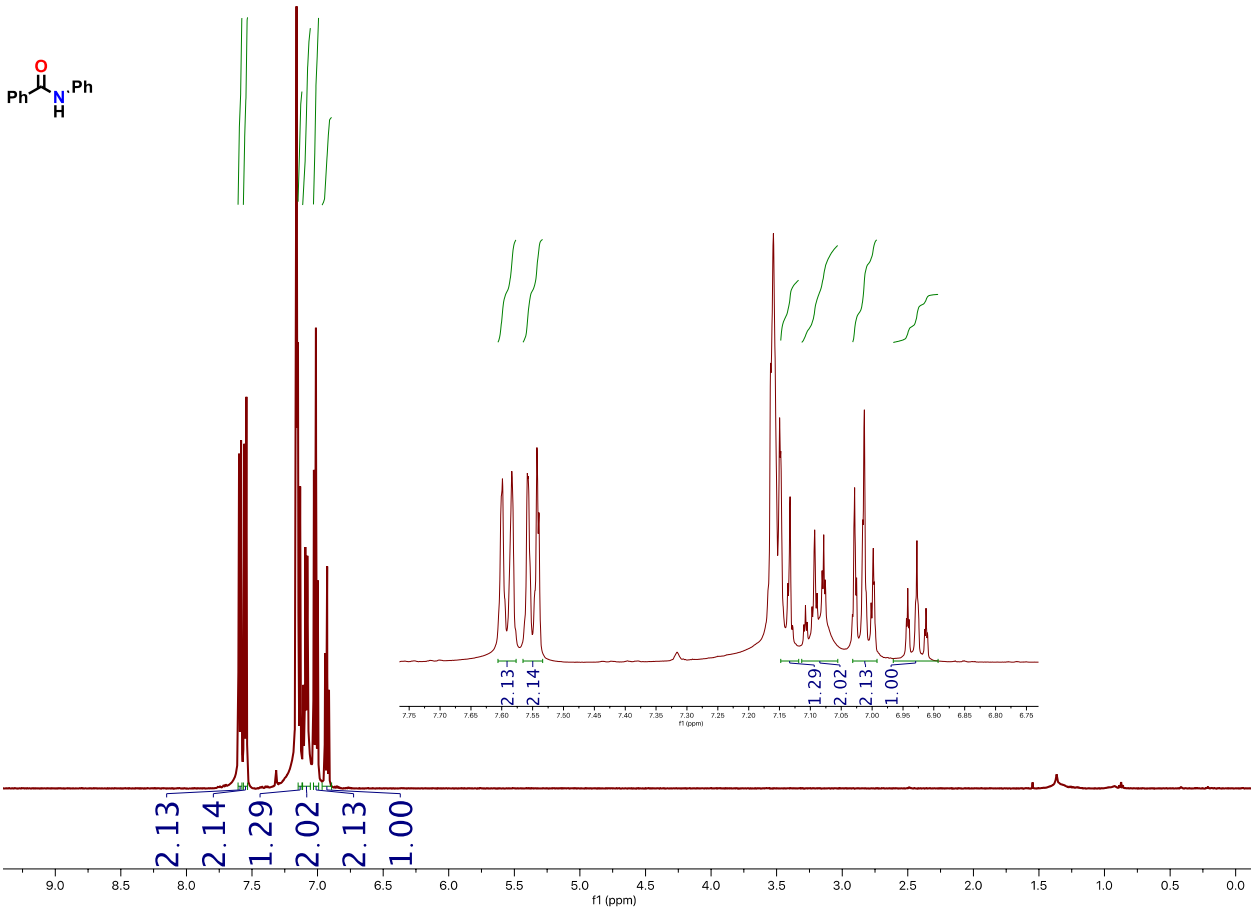

Figure 3.15. ^{1}H-NMR (500 MHz) spectrum of benzanilide in benzene-d_6.

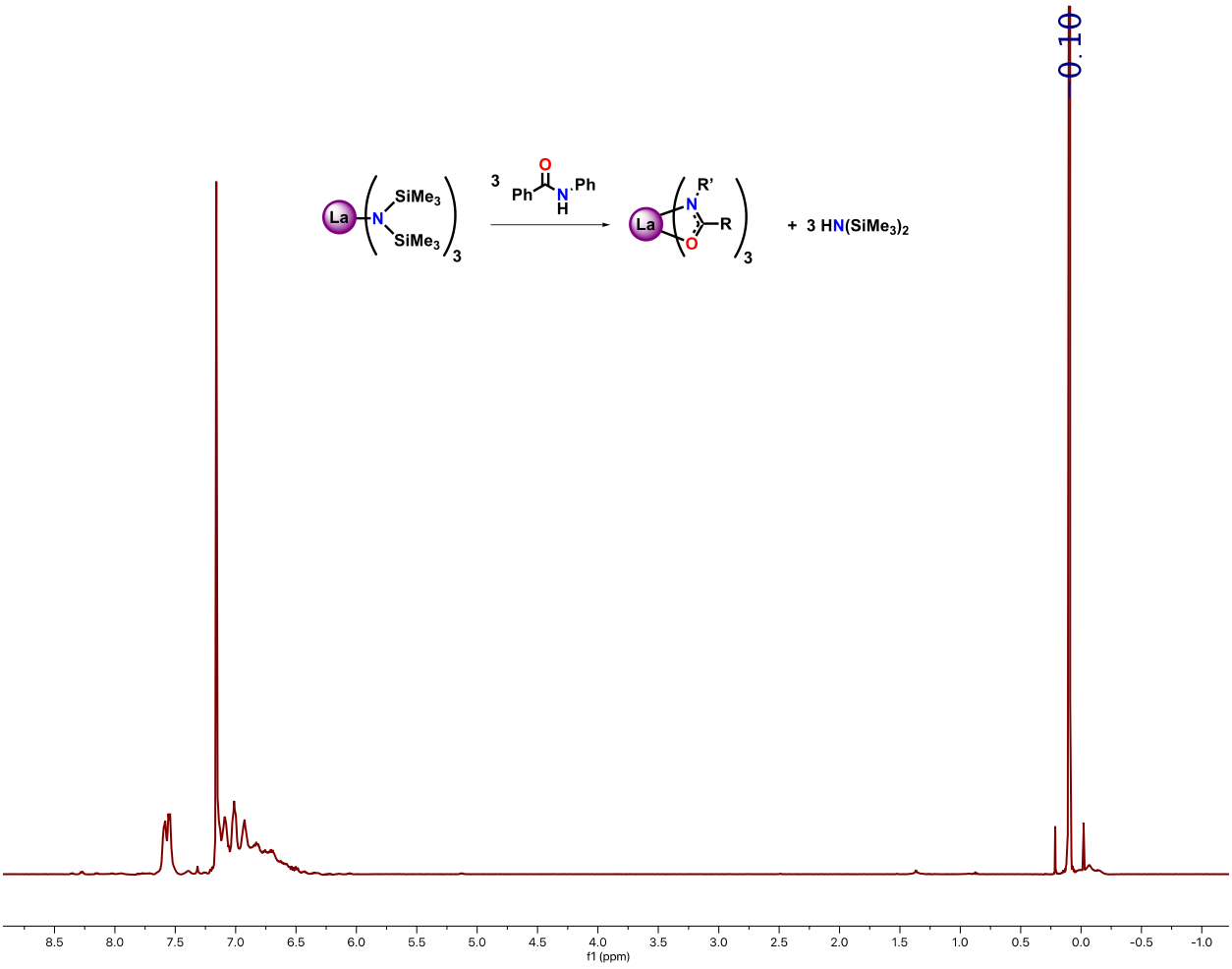

Figure 3.16. ^{1}H-NMR (500 MHz) spectrum of *in situ* formed lanthanum tris-amidate catalyst obtained from benzanilide and La^{NTMS} (3:1 molar ratio) in benzene-d_6.

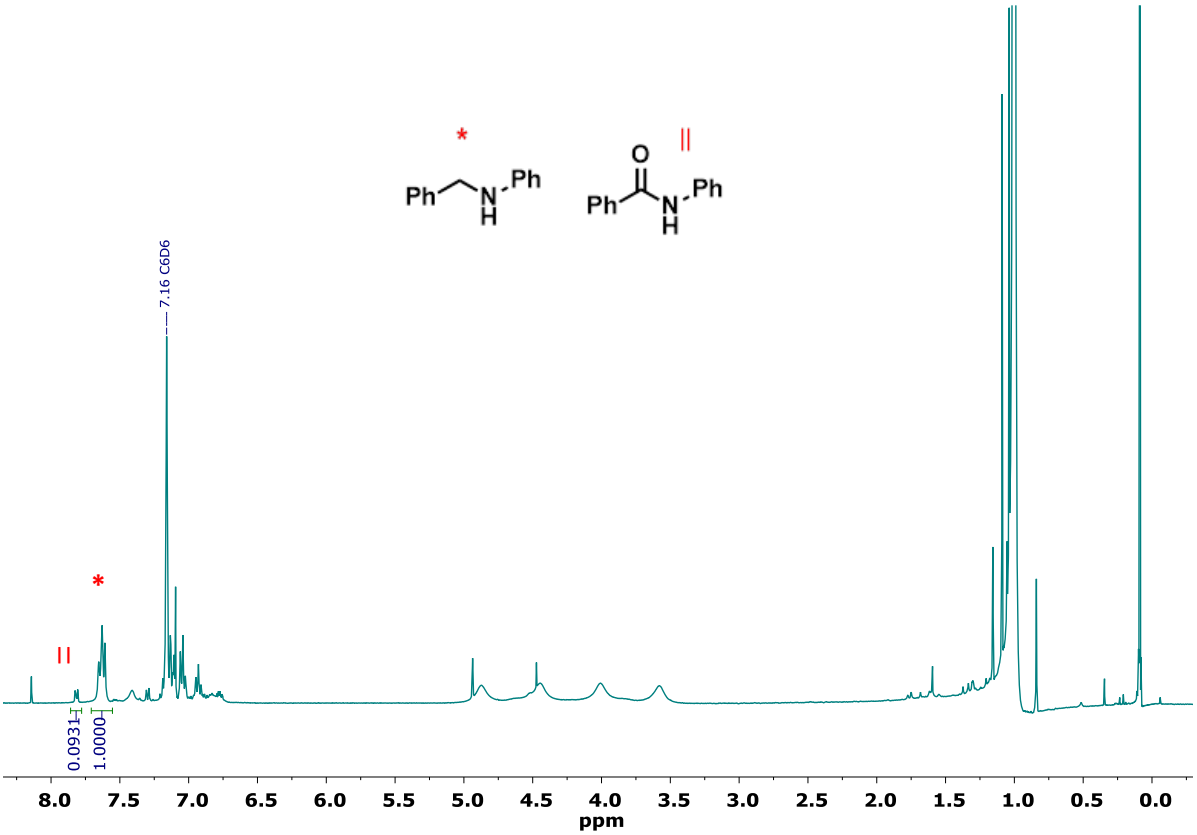

Figure 3.17. ^{1}H-NMR (500 MHz) spectrum of the reduction of benzanilide with HBpin using an *in situ* formed lanthanum tris-amidate catalyst.

Primary Amide Reduction. Reduction does not occur with the two primary amides tested (acetamide and benzamide), and instead an intractable, off-white precipitate is observed. To determine the identity of the precipitate formed during primary amide reduction, first La^{NTMS} (50 μmol) and benzamide (50 μmol, 1 equiv.) were dissolved in C_6D_6 in a J. Young capped NMR tube at rt in an inert atmosphere glovebox. A white precipitate was immediately formed and allowed to settle to the bottom of the NMR tube. The solvent was decanted and the J. Young capped NMR tube containing the white precipitate was sealed, removed from the glovebox, and dried on a high vacuum line. After drying, the NMR tube was again sealed and taken into the glovebox where the precipitate was dissolved in THF to give a pale yellow solution. A sealed capillary containing d_6-DMSO was added in to provide a solvent lock. NMR spectroscopic experiments were then performed (Figures 3.19, 3.20). After all data were collected, the NMR tube containing the precipitate dissolved in THF was opened under strong flow of argon and 1 drop of D_2O was added in order to confirm ligand identities by hydrolyzing/quenching the metal complex. The tube was gently inverted to obtain a homogeneous solution before additional NMR experiments were performed, again using a d_6-DMSO solvent lock (Figures 3.21, 3.22). The spectroscopic experiments support the identity of the precipitate to be the unsymmetrical La-hemiaminalate complex $[(Me_3Si)_2N]_2La\{\eta^2\text{-}OC(NH)Ph\}$ which is not catalytically active under the reaction conditions described. Based on the low solubility of this complex, it is plausible that it may exist as an oligomeric species, having bridging hemiaminalate ligands. There is no spectroscopic evidence of a ligand insertion reaction between the La^{NTMS} precatalyst and the primary amide (i.e. $-N(SiMe_3)_2$ insertion into the amide C=O bond).

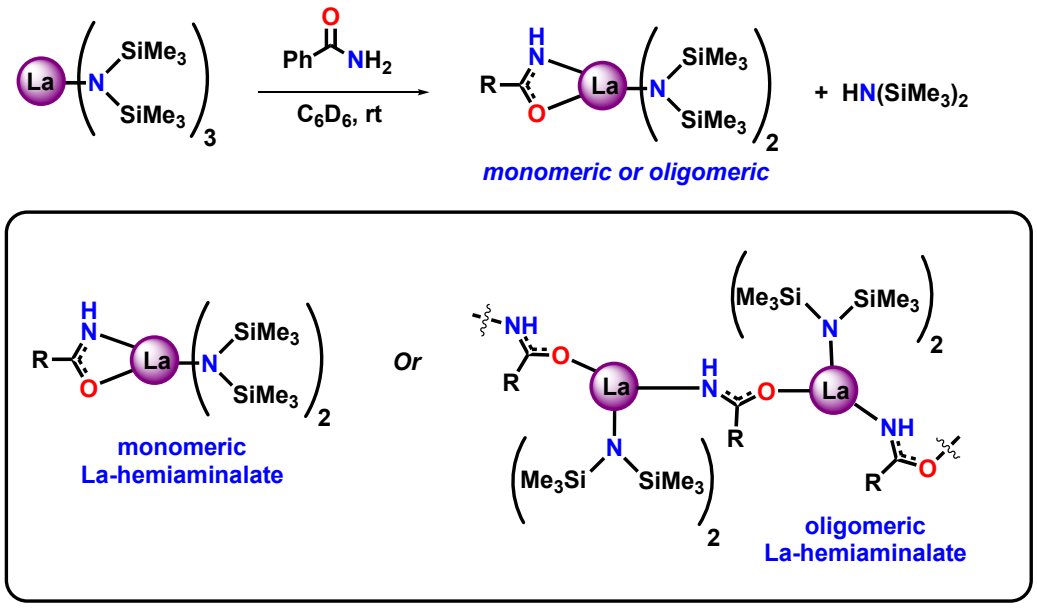

Figure 3.18. Proposed monomeric or oligomeric La-hemiaminalate complex $[(Me_3Si)_2N]_2La\{\eta^2\text{-}OC(NH)Ph\}$ obtained from the reaction of La^{NTMS} with the primary amide benzamide.

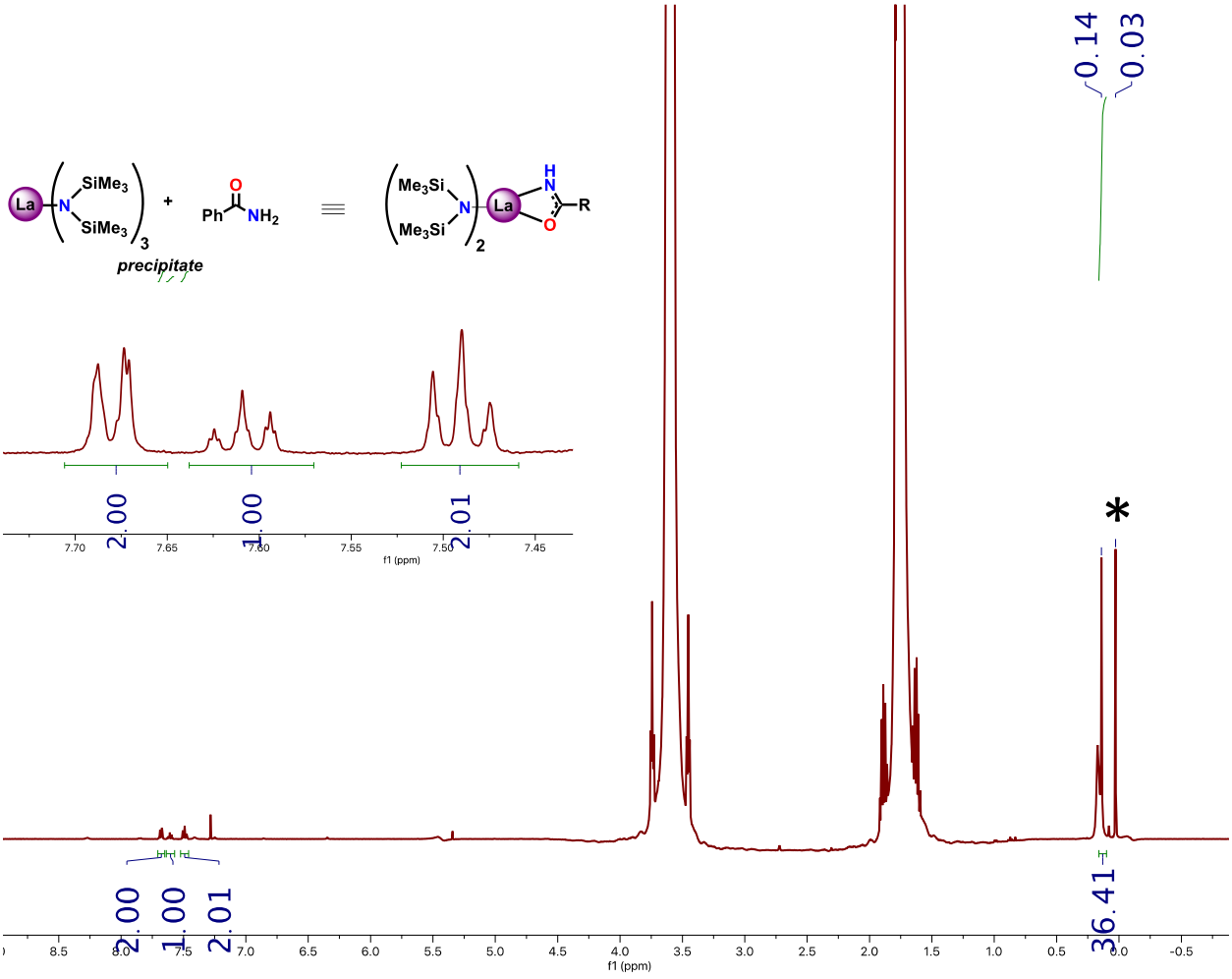

Figure 3.19. ^{1}H-NMR (500 MHz) spectrum of a proposed La-hemiaminalate complex $[(Me_3Si)_2N]_2La\{\eta^2\text{-}OC(NH)Ph\}$ obtained as a precipitate from the reaction of benzamide and La^{NTMS} (1:1 molar ratio) in benzene-d_6. Spectrum obtained from a solution of precipitate in THF with a sealed capillary containing d_6-DMSO. * = $HN(SiMe_3)_2$

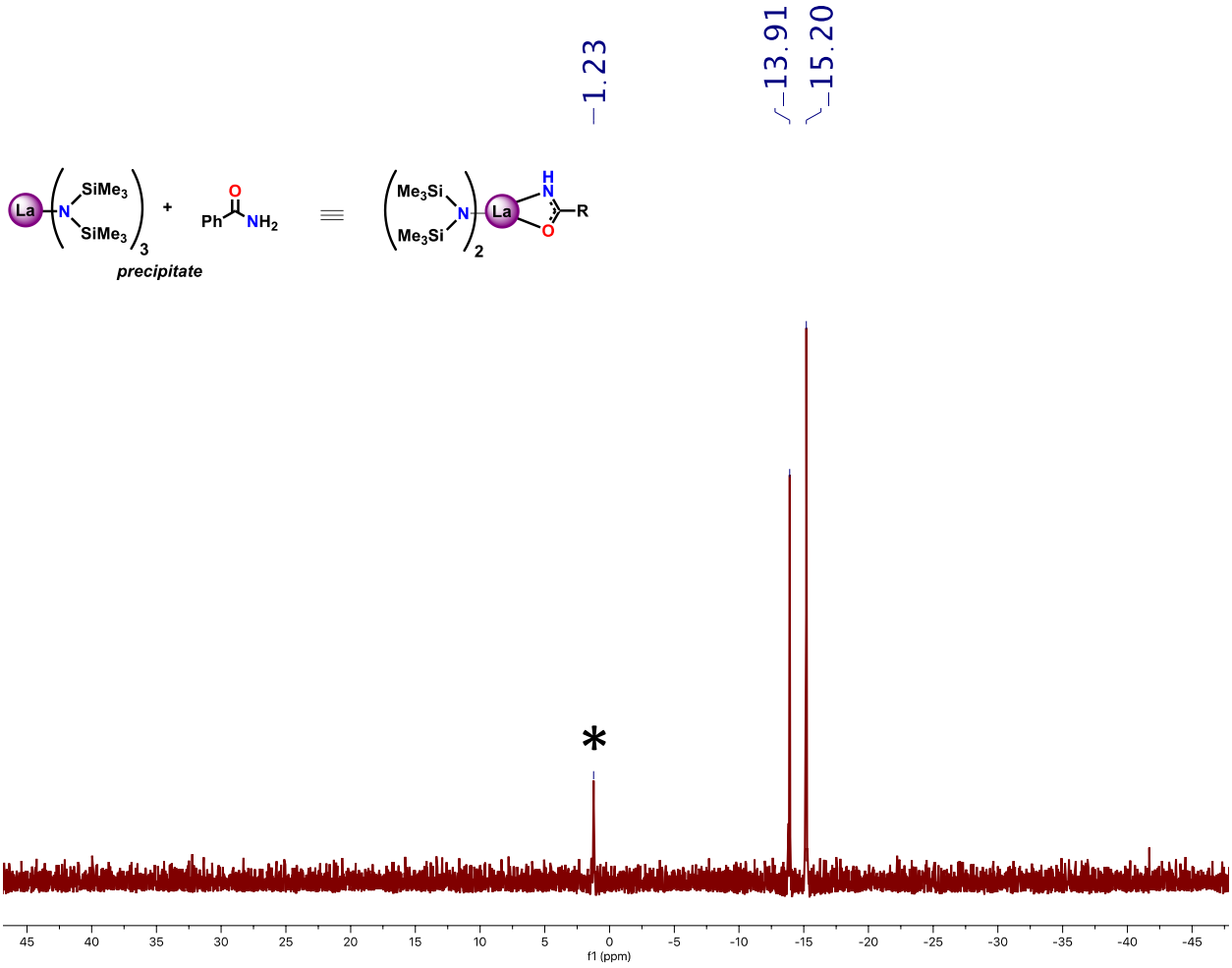

Figure 3.20. ^{29}Si-NMR (125 MHz) spectrum of a proposed La-hemiaminalate complex $[(Me_3Si)_2N]_2La\{\eta^2\text{-}OC(NH)Ph\}$ obtained as a precipitate from the reaction of benzamide and La^{NTMS} (1:1 molar ratio) in benzene-d_6. Spectrum obtained from a solution of precipitate in THF with a sealed capillary containing d_6-DMSO. * = $HN(SiMe_3)_2$

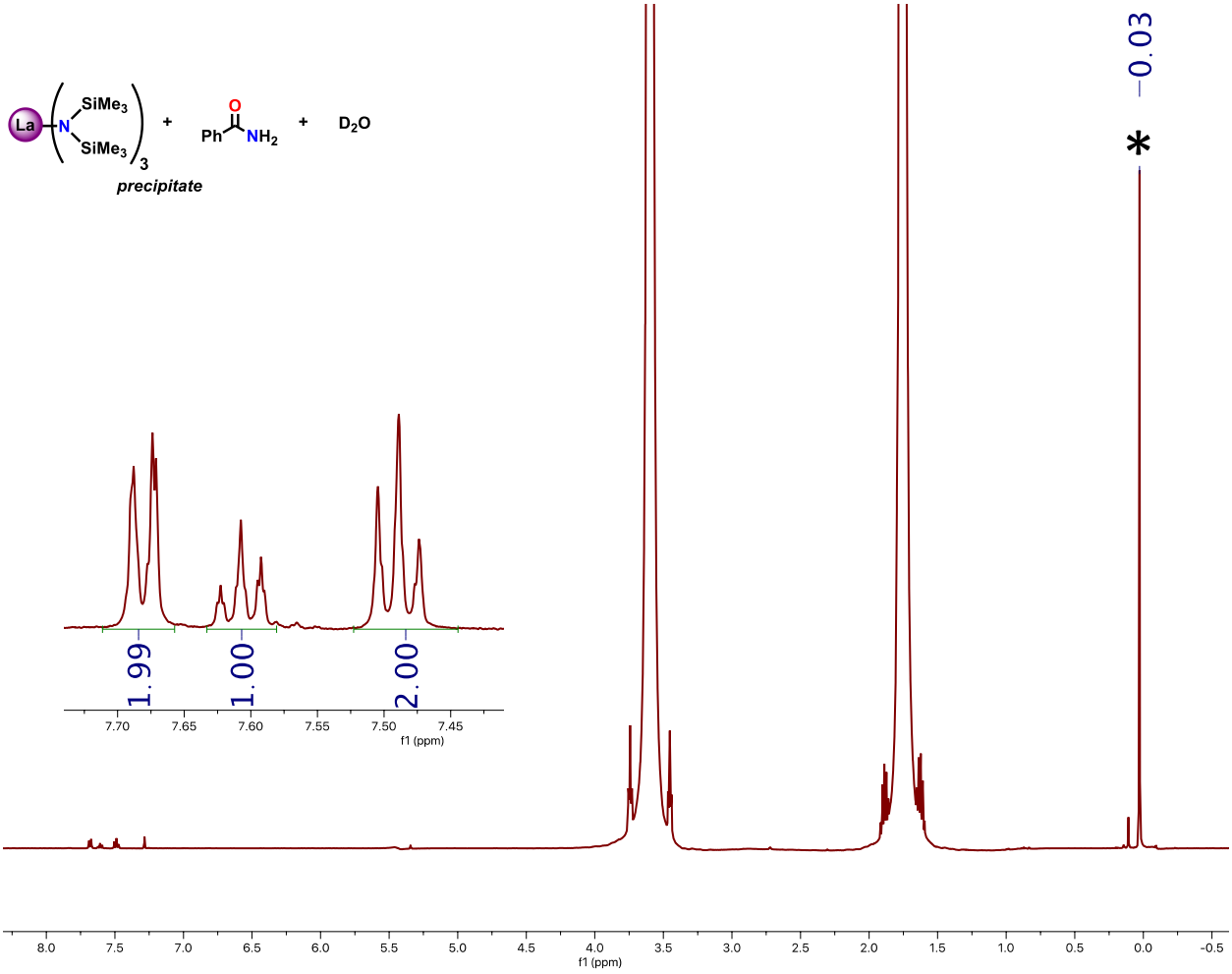

Figure 3.21. ^{1}H-NMR (500 MHz) spectrum of the D_2O-*quenched* proposed La-hemiaminalate complex $[(Me_3Si)_2N]_2La\{\eta^2\text{-}OC(NH)Ph\}$ obtained as a precipitate from the reaction of benzamide and La^{NTMS} (1:1 molar ratio) in benzene-d_6. Spectrum obtained from a solution of precipitate in THF with a sealed capillary containing d_6-DMSO. * = $HN(SiMe_3)_2$

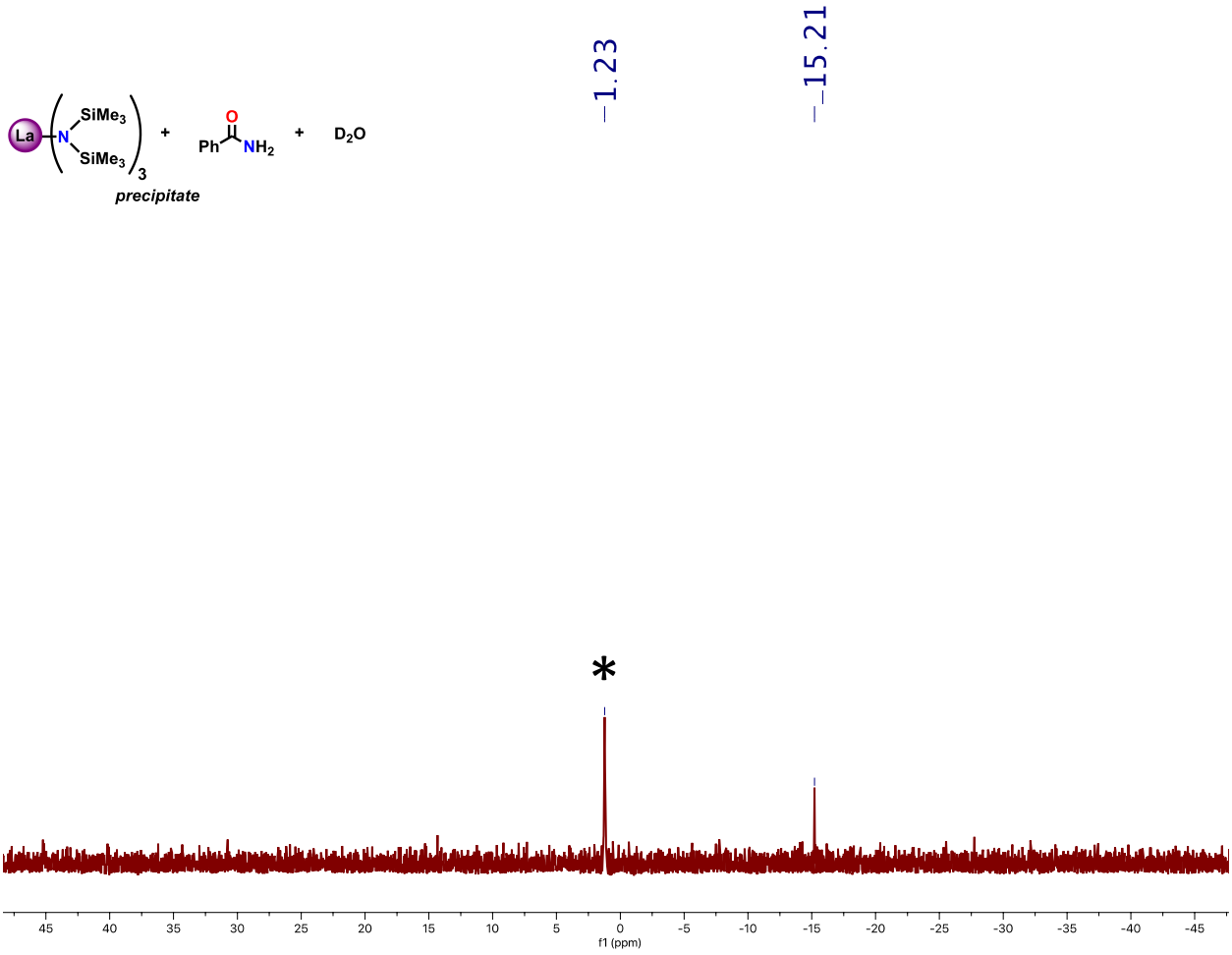

Figure 3.22. ^{29}Si-NMR (125 MHz) spectrum of the D_2O-*quenched* proposed La-hemiaminalate complex $[(Me_3Si)_2N]_2La\{\eta^2\text{-}OC(NH)Ph\}$ obtained as a precipitate from the reaction of benzamide and La^{NTMS} (1:1 molar ratio) in benzene-d_6. Spectrum obtained from a solution of precipitate in THF with a sealed capillary containing d_6-DMSO. * = $HN(SiMe_3)_2$

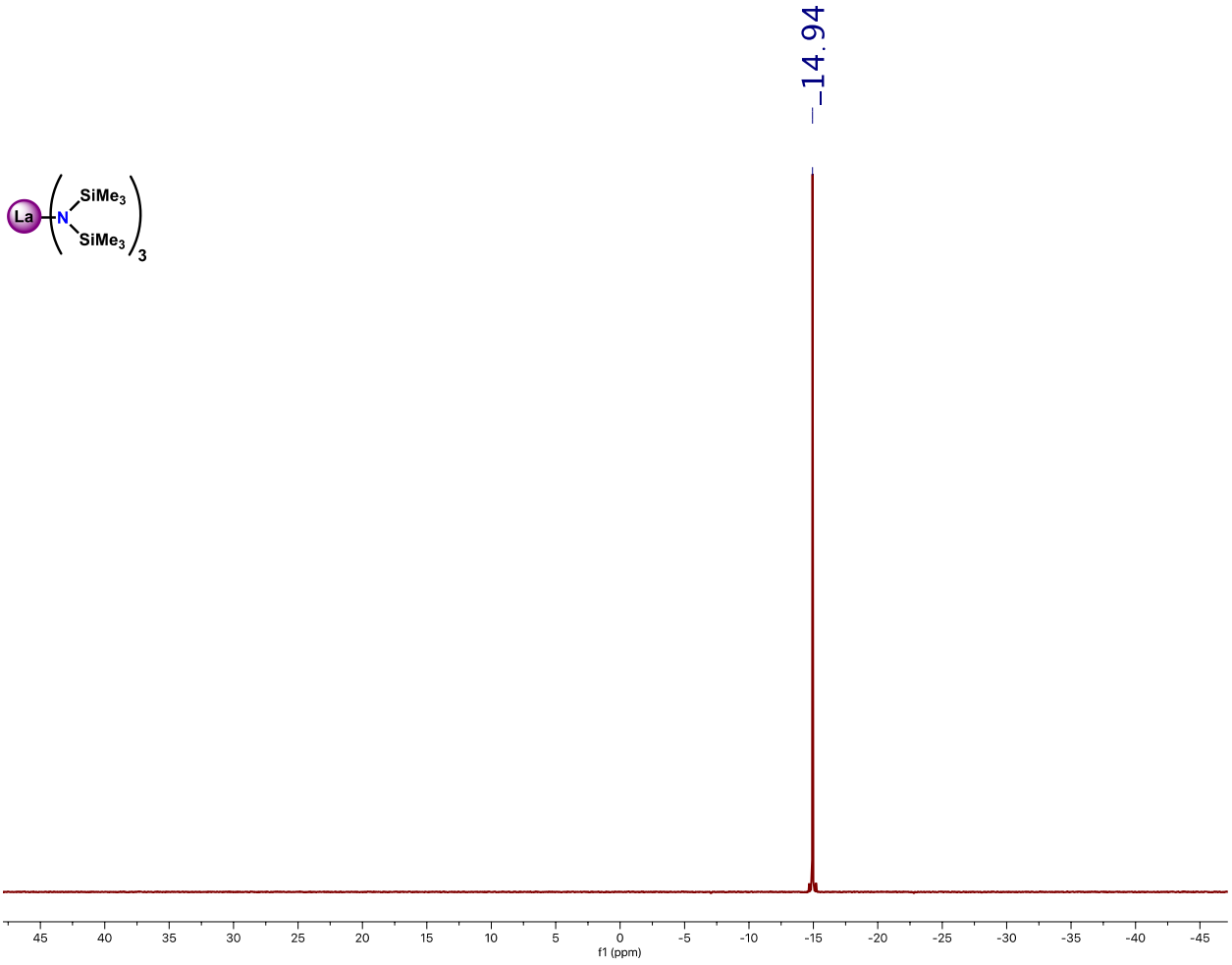

Figure 3.23. ^{29}Si-NMR (125 MHz) spectrum of La^{NTMS} precatalyst in benzene-d_6 included for reference. (For ^{1}H-NMR spectrum of La^{NTMS} precatalyst in benzene-d_6, see Figure 3.29).

DFT Examination of Primary Amide Reduction. DFT calculations were performed to assess the feasibility of a ligand insertion reaction between the La^{NTMS} precatalyst and the primary amide benzamide (i.e., La-$N(SiMe_3)_2$ insertion into the amide C=O bond) (Figure 3.24). The insertion of the La-silylamide group (-$N(SiMe_3)_2$) into the primary amide C=O bond and subsequent silyl migration to yield a La-siloxide complex was modeled. First, the approach of the primary amide produces a stabilization of 17.4 kcal/mol due to an interaction between the carbonyl group of the amide and the La metal center. However, the insertion of the La-silylamide (La-$N(SiMe_3)_2$) into the primary amide C=O bond is very endoergonic (+22.8 kcal/mol) with an energy barrier of +32.6 kcal/mol. Finally, the silyl migration and formation of a La-siloxide complex is exoergonic (-0.6 kcal/mol with an energy barrier of +21.2 kcal/mol). Thus, the overall reaction is slightly endoergonic (+4.8 kcal/mol) with an energy barrier of +44.0 kcal/mol.

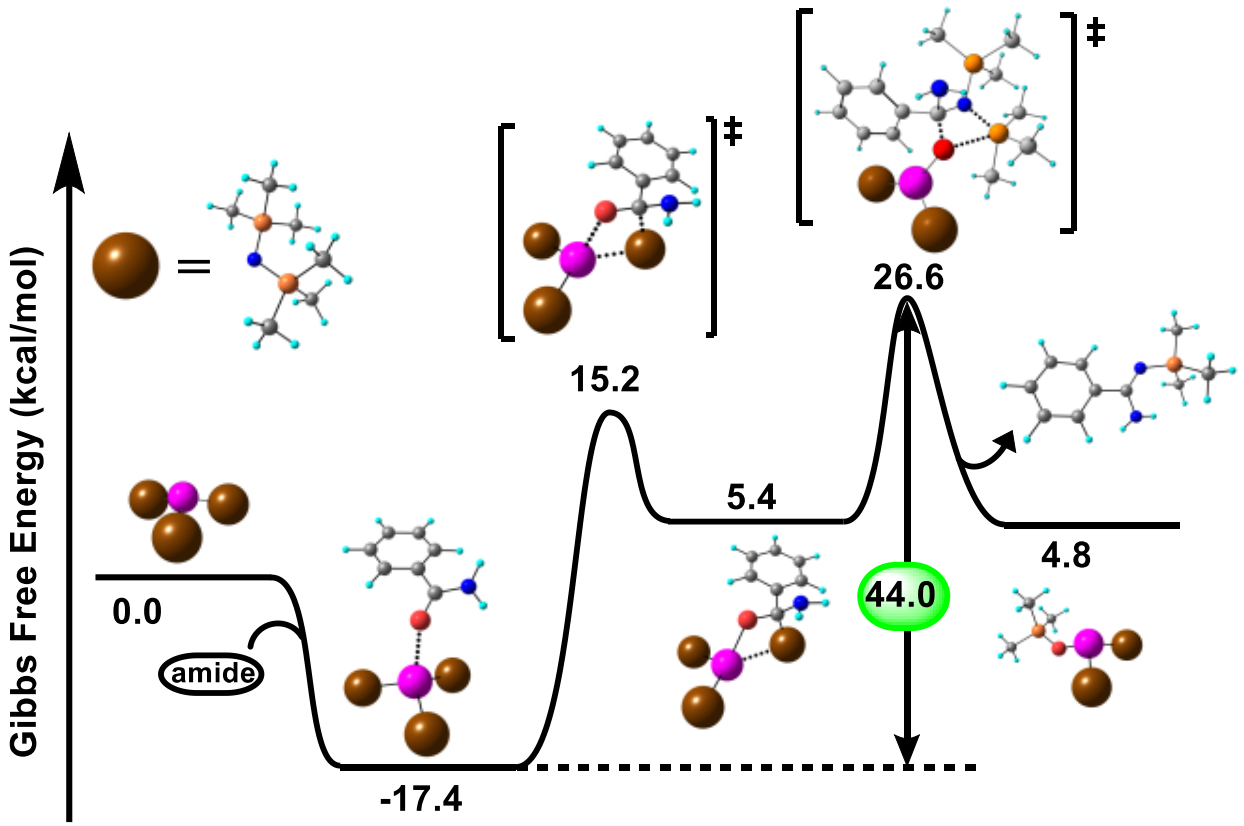

Figure 3.24. Gibbs free energy profile for a La-silylamide group (La-N(SiMe$_3$)$_2$) insertion of the La^{NTMS} precatalyst into the benzamide C=O bond and subsequent silyl migration to yield a La-siloxide complex.

Computational Details. Geometry optimizations of all reactants, products, intermediates, and transition states were carried out along the entire catalytic cycle. Calculations were performed adopting the M06 hybrid meta-GGA functional. The effective core potential of Hay and Wadt,[88,89] (LANL2DZ) and the relative basis set were used for the La and Si atoms. The standard all-electron 6-31G** basis[90] was used for all the remaining atoms. Molecular geometry optimization of stationary points was carried out without symmetry constraints and used analytical gradient

techniques. The transition states were searched with the "distinguished reaction coordinate procedure" along the emerging bonds. *N,N*-dimethylbenzamide was adopted as substrate model. Frequency analysis was performed to obtain thermochemical information about the reaction pathways at 298 K using the harmonic approximation. The difference in translational and rotational entropy when moving from gas to solvent are accounted for by adding an energy contribution of 8RT to the Gibbs free energy of each species as detailed in the literature.[91] Moreover, the effect of concentration on moving from 1 atm to 1 *M* is accounted for by adding an energy contribution of 1.89 kcal/mol ($RTln(P_{1M}/P_{1atm})$) to each species. All calculations were performed using the G16 code[92] on a Linux cluster system.

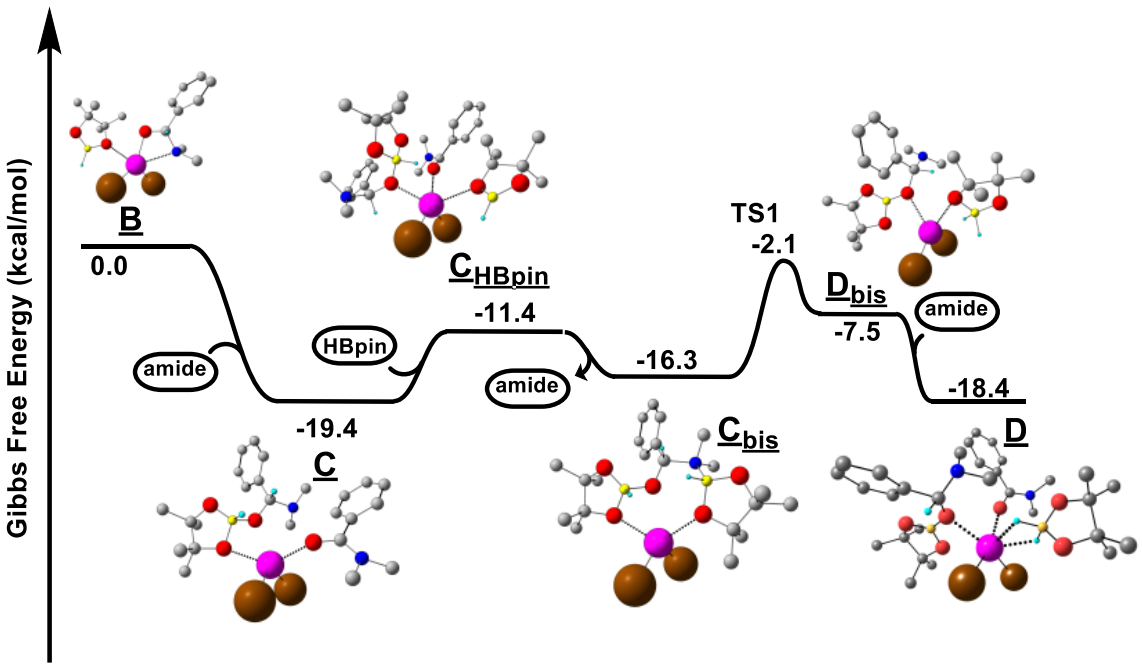

Figure 3.25. Gibbs free energy profile/catalytic cycle for the hydroboration/reduction of amides catalyzed by La^{NTMS}, and conversion of active catalyst **B** to species **D**.

Stoichiometry Reactivity Studies. Catalyst activation intermediate **I-$_{act}$-1** was obtained from a 1:1 mixture of the La^{NTMS} precatalyst and *N*,*N*-dimethylbenzamide. This intermediate was characterized using ^{1}H- and ^{13}C- NMR spectroscopy (Figures 3.26-3.32). Attempts to experimentally characterize additional catalyst activation intermediates were carried out by monitoring stoichiometric mixtures of La^{NTMS} and substrates HBpin and *N*,*N*-dimethylbenzamide via ^{1}H- and ^{11}B-NMR. However, only the proposed off-cycle/deactivation product described in the main text is observed. When various mixtures of La^{NTMS} and HBpin are examined (0.5-6 equiv HBpin), the spectrum below is obtained with varying degrees of conversion of La^{NTMS}. Full conversion is observed at 4 equiv HBpin, which matches what would be expected given the proposed deactivation pathway. However, additional, uncharacterized decomposition products are observed at such high HBpin ratios, and therefore 1:3 La^{NTMS}:HBpin mixtures were studied further (Figures 3.33-3.34). A solution of La^{NTMS}, HBpin and *N*,*N*-dimethylbenzamide (1:3:1) yields incomplete reduction of the amide, as evidenced by the appearance of O(Bpin)$_2$ and amine, but primarily the off-cycle product described below.

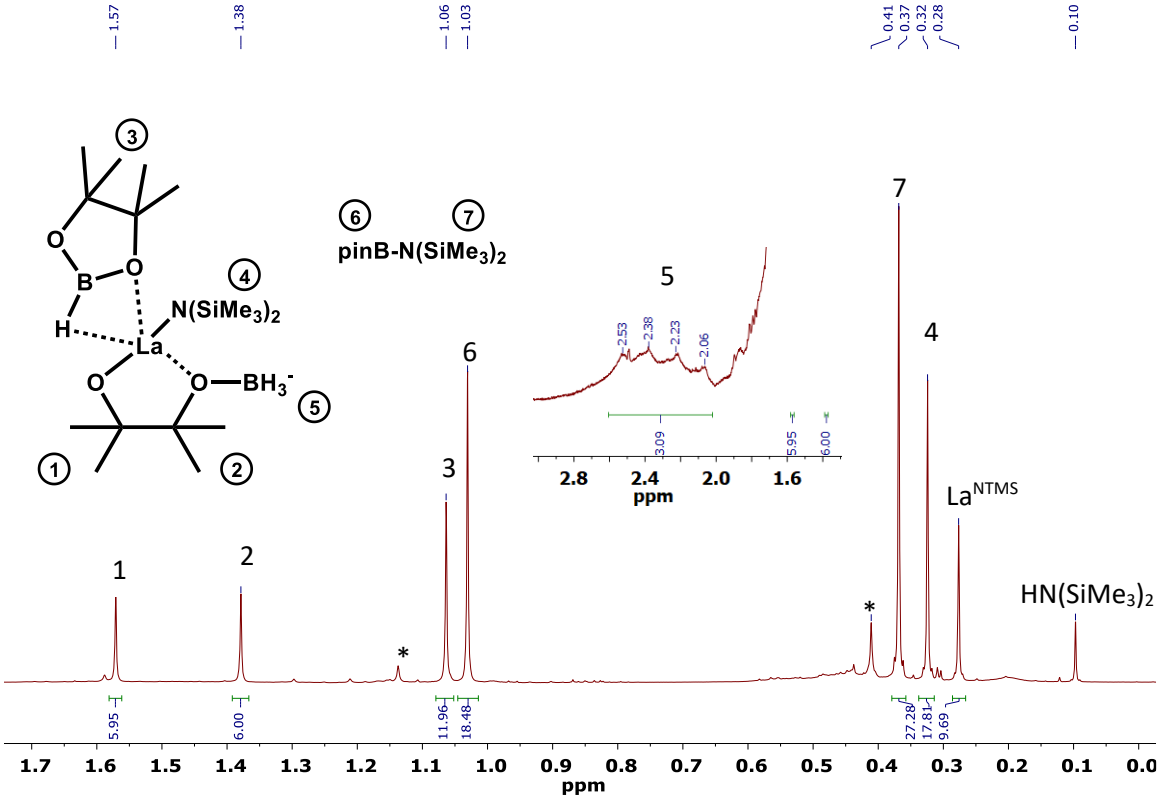

Figure 3.26. ^{1}H-NMR (500 MHz) spectrum of the catalyst deactivation product (Figure 3.4A) obtained from 1:3 mixture of La^{NTMS} and HBpin in benzene-d_6.

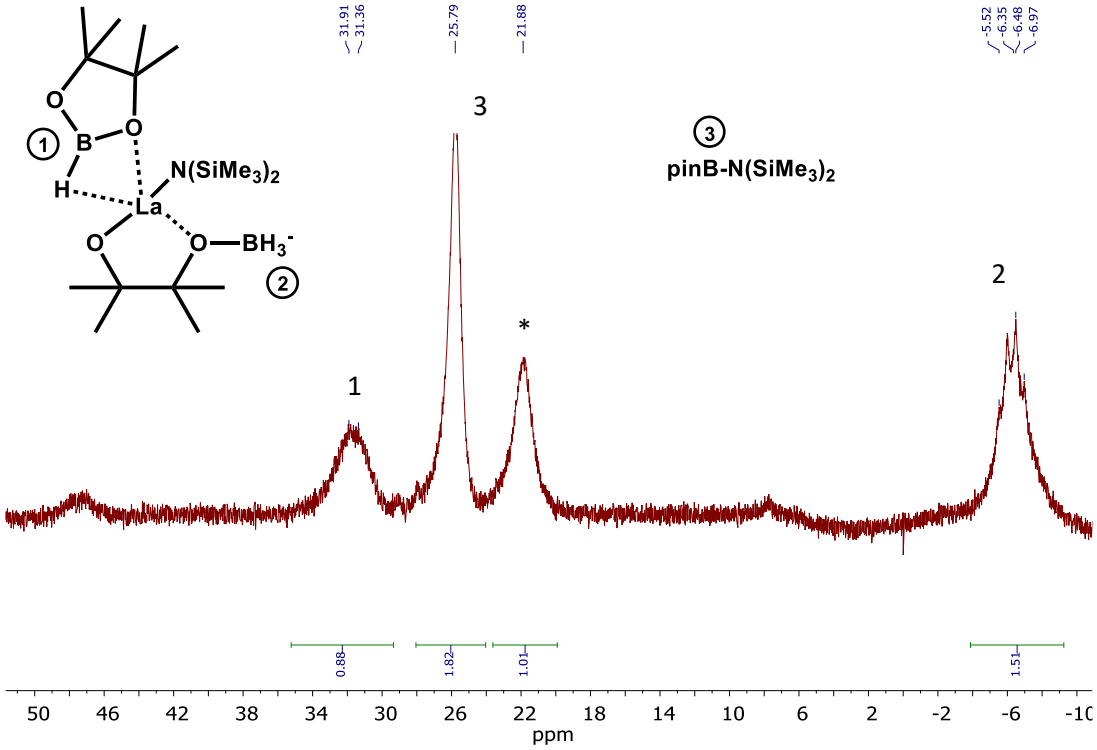

Figure 3.27. ^{11}B-NMR (128 MHz) spectrum of the catalyst deactivation product (Figure 3.4A) obtained from 1:3 mixture of La^{NTMS} and HBpin in benzene-d_6. * = Unidentified side product, possibly weakly and reversibly coordinated pinB-N$(SiMe_3)_2$ or B_2pin_3. The peak at δ 31.6 ppm is a broad doublet, likely due to coordination of the B-H to the metal center or exchange with RBH_3^-. The downfield shift is similar to previously reported coordinated boranes.[93]

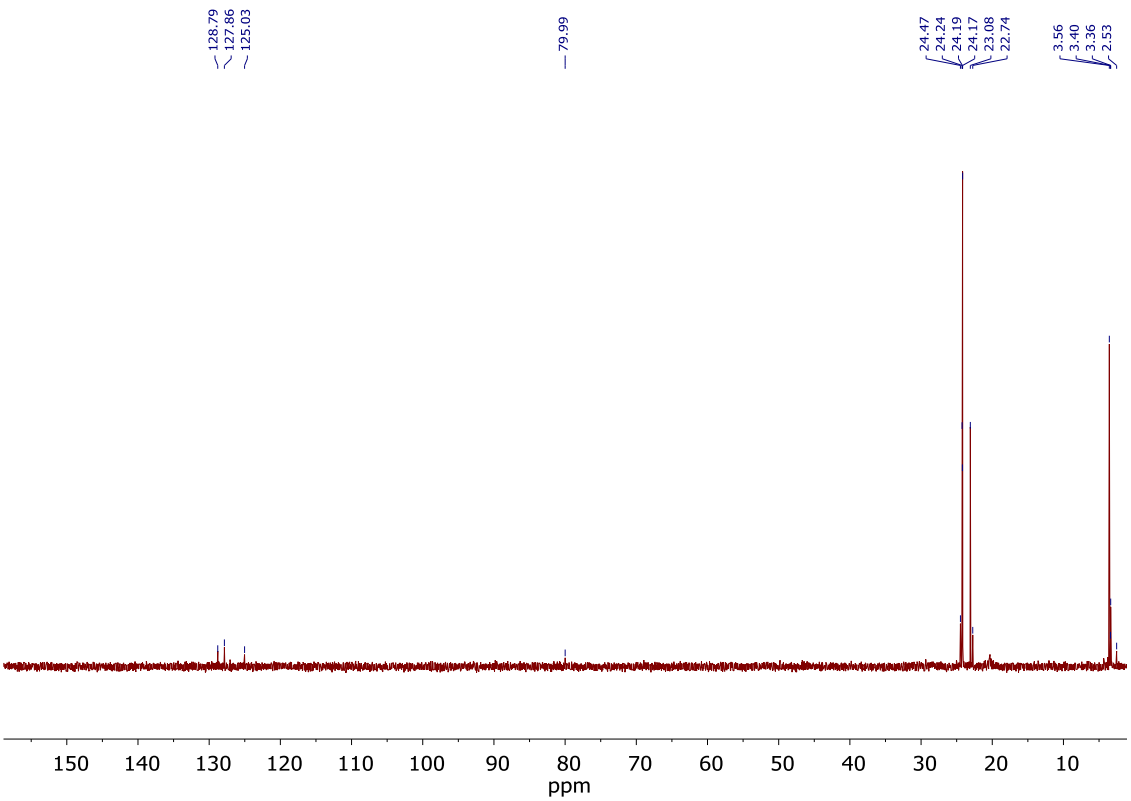

Figure 3.28. ^{13}C-NMR (125 MHz) spectrum of the catalyst deactivation product (Figure 3.4A) obtained from 1:3 mixture of La^{NTMS} and HBpin in benzene-d_6.

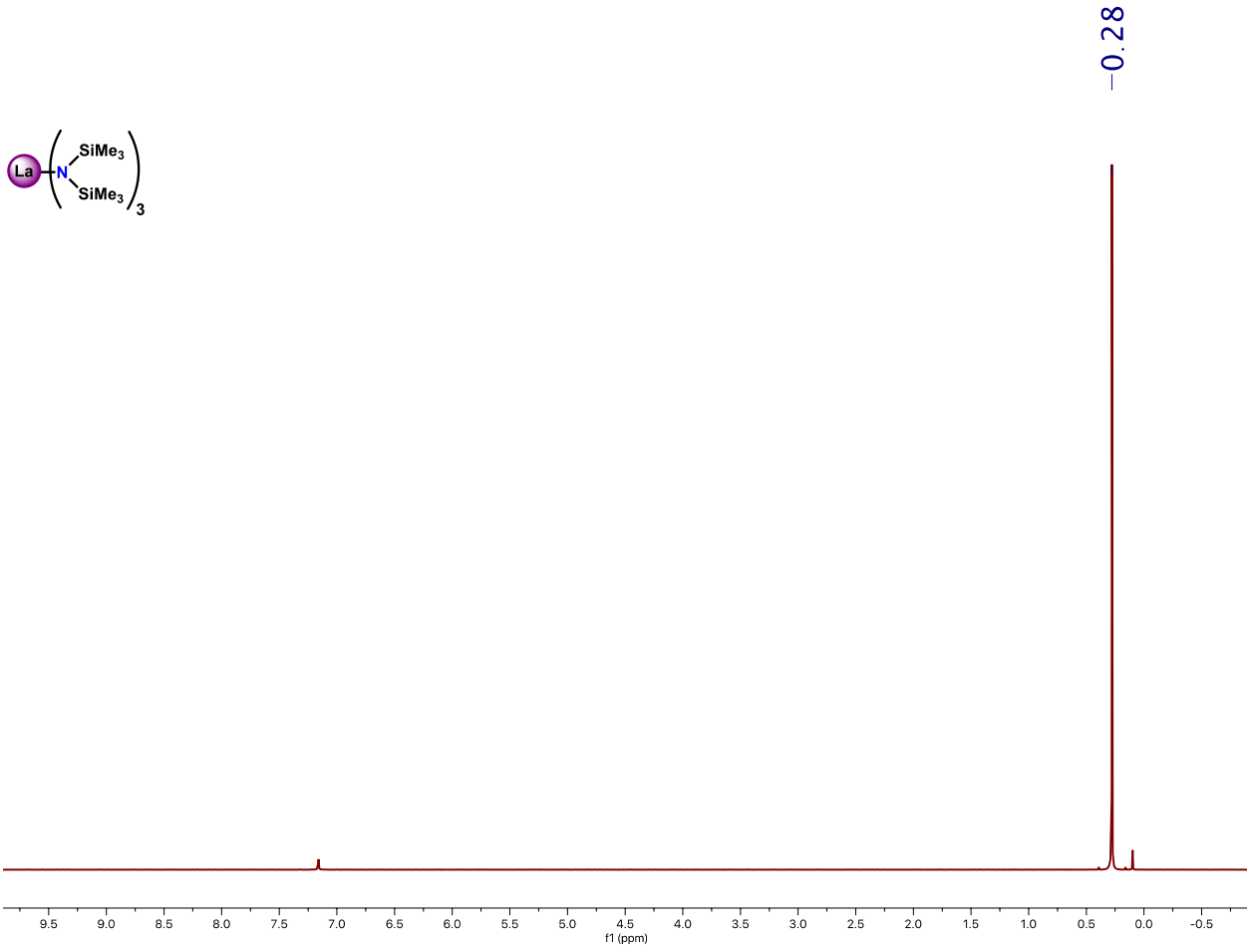

Figure 3.29. ^{1}H-NMR (500 MHz) spectrum of the La^{NTMS} precatalyst in benzene-d_6 included for reference.

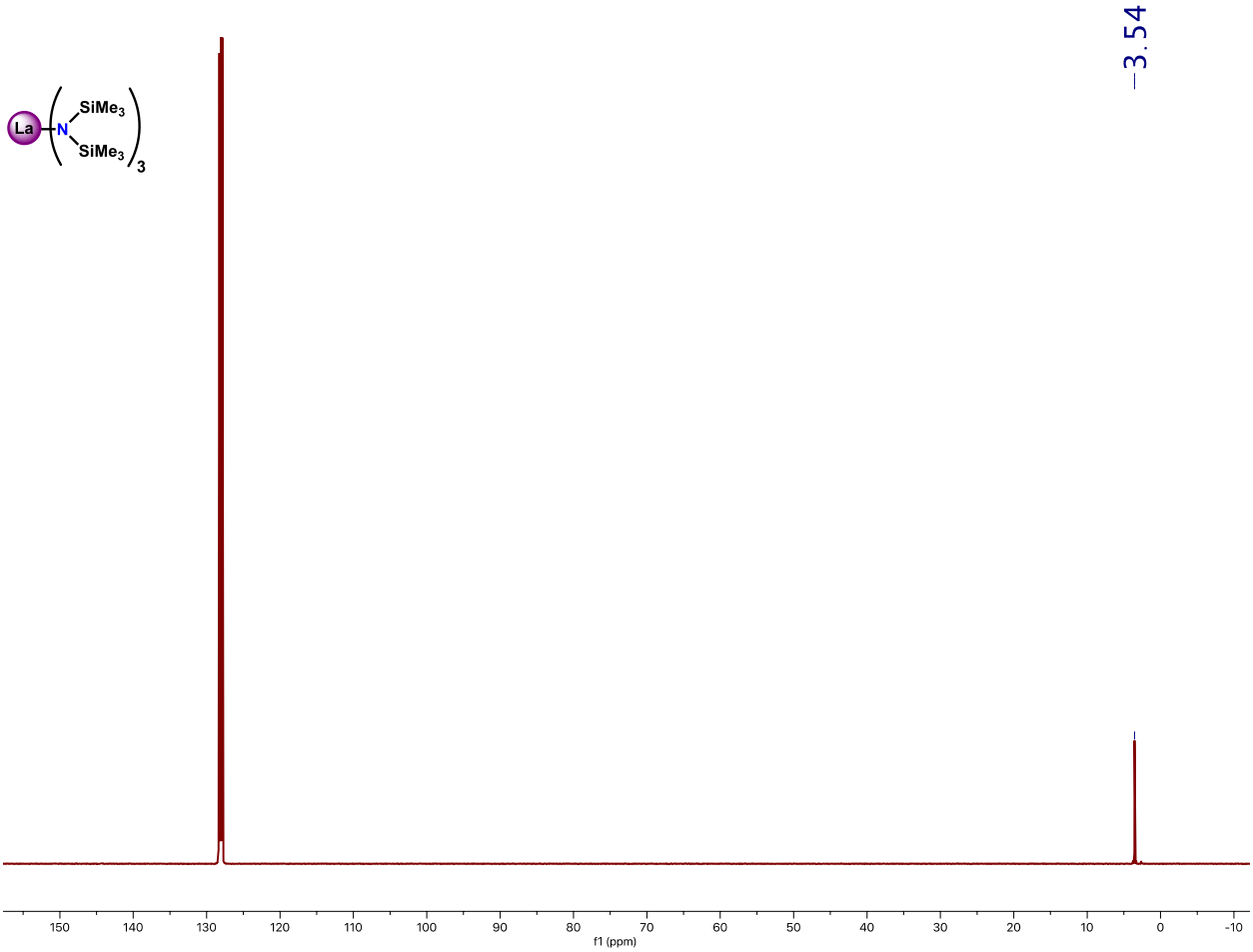

Figure 3.30. ^{13}C-NMR (125 MHz) spectrum of the La^{NTMS} precatalyst in benzene-d_6 included for reference.

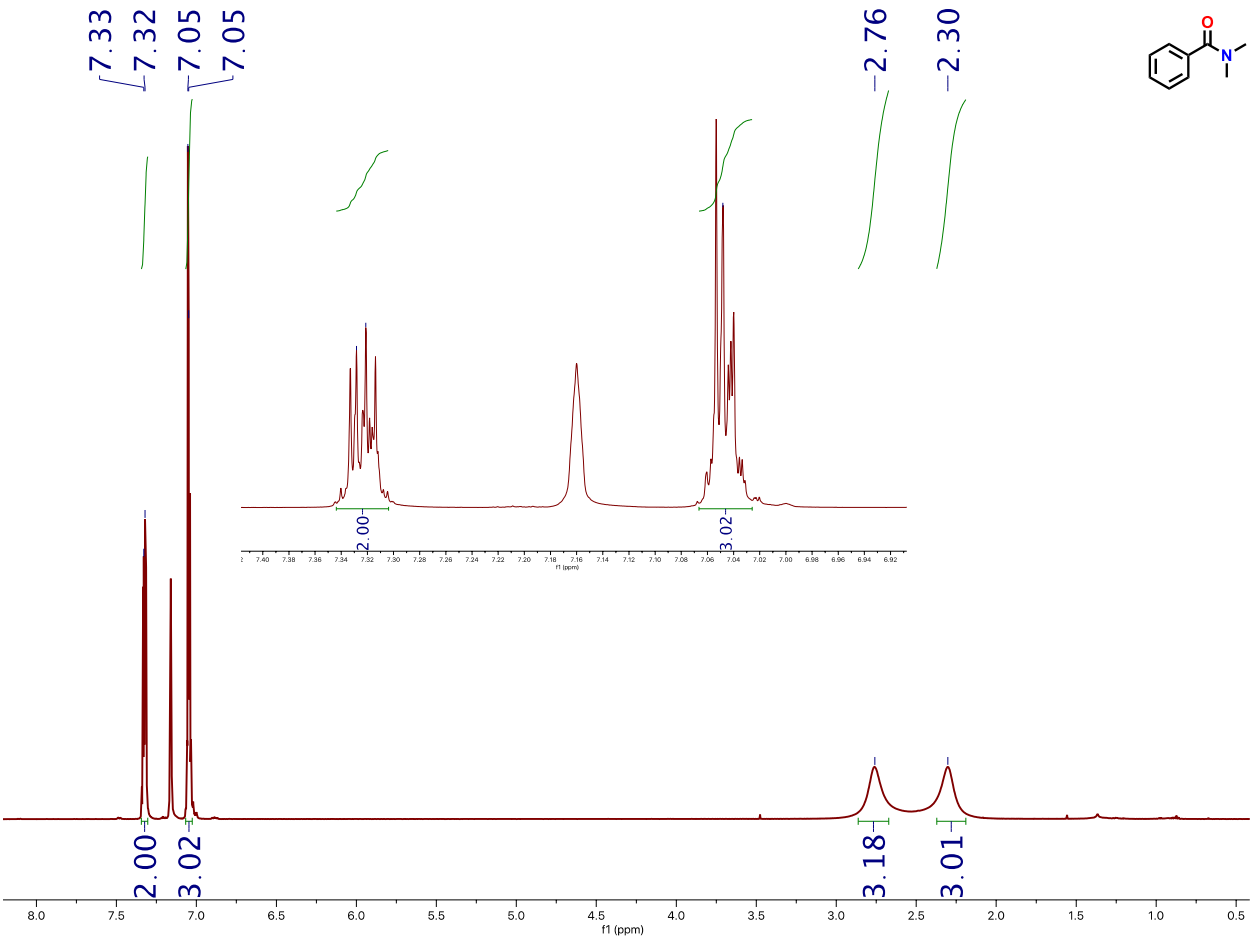

Figure 3.31. ^{1}H-NMR (500 MHz) spectrum of *N*,*N*-dimethylbenzamide in benzene-d_6 included for reference.

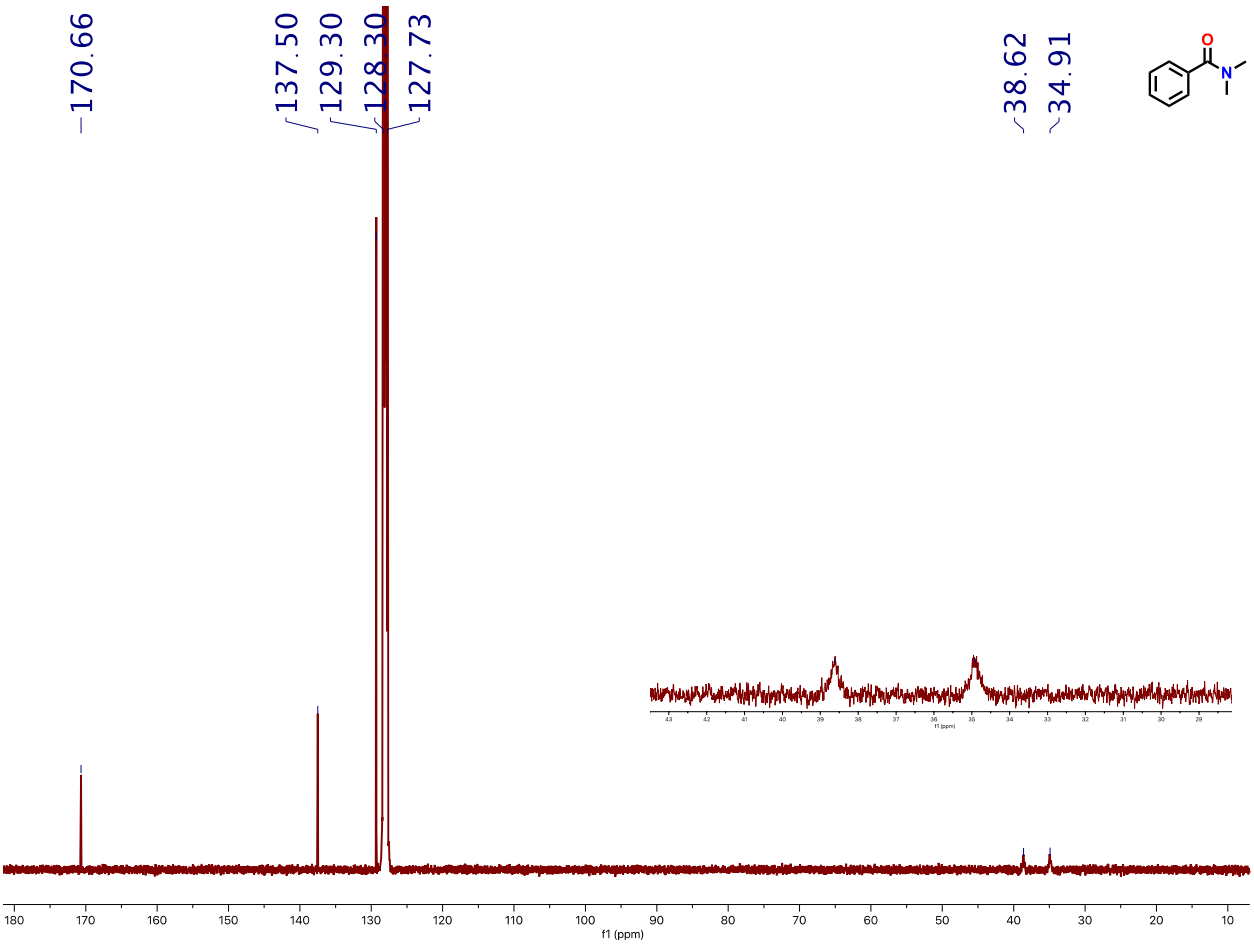

Figure 3.32. ^{13}C-NMR (125 MHz) spectrum of *N*,*N*-dimethylbenzamide in benzene-d_6 included for reference.

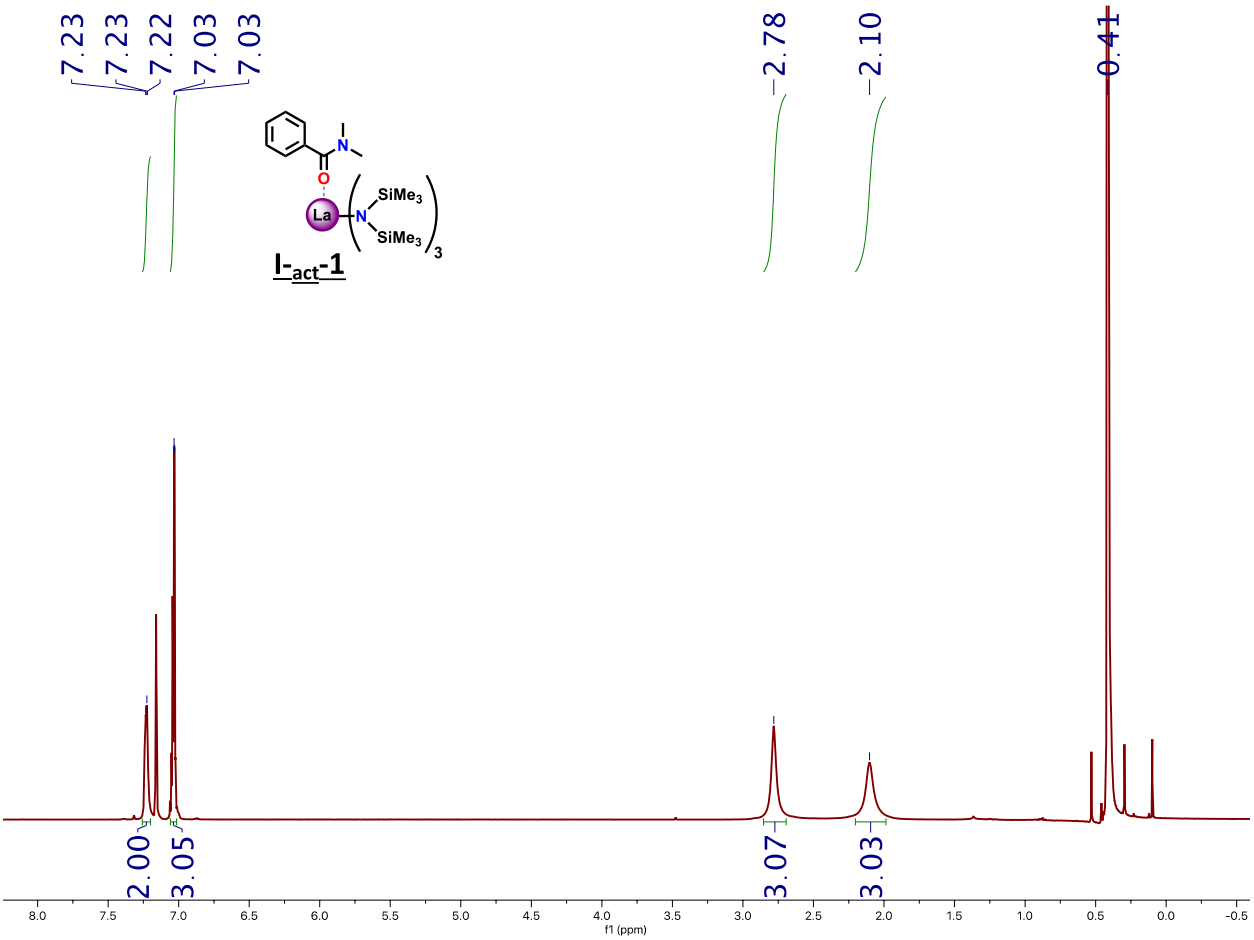

Figure 3.33. ^{1}H-NMR (500 MHz) spectrum of the proposed catalyst activation intermediate **I-act-1** in benzene-d_6.

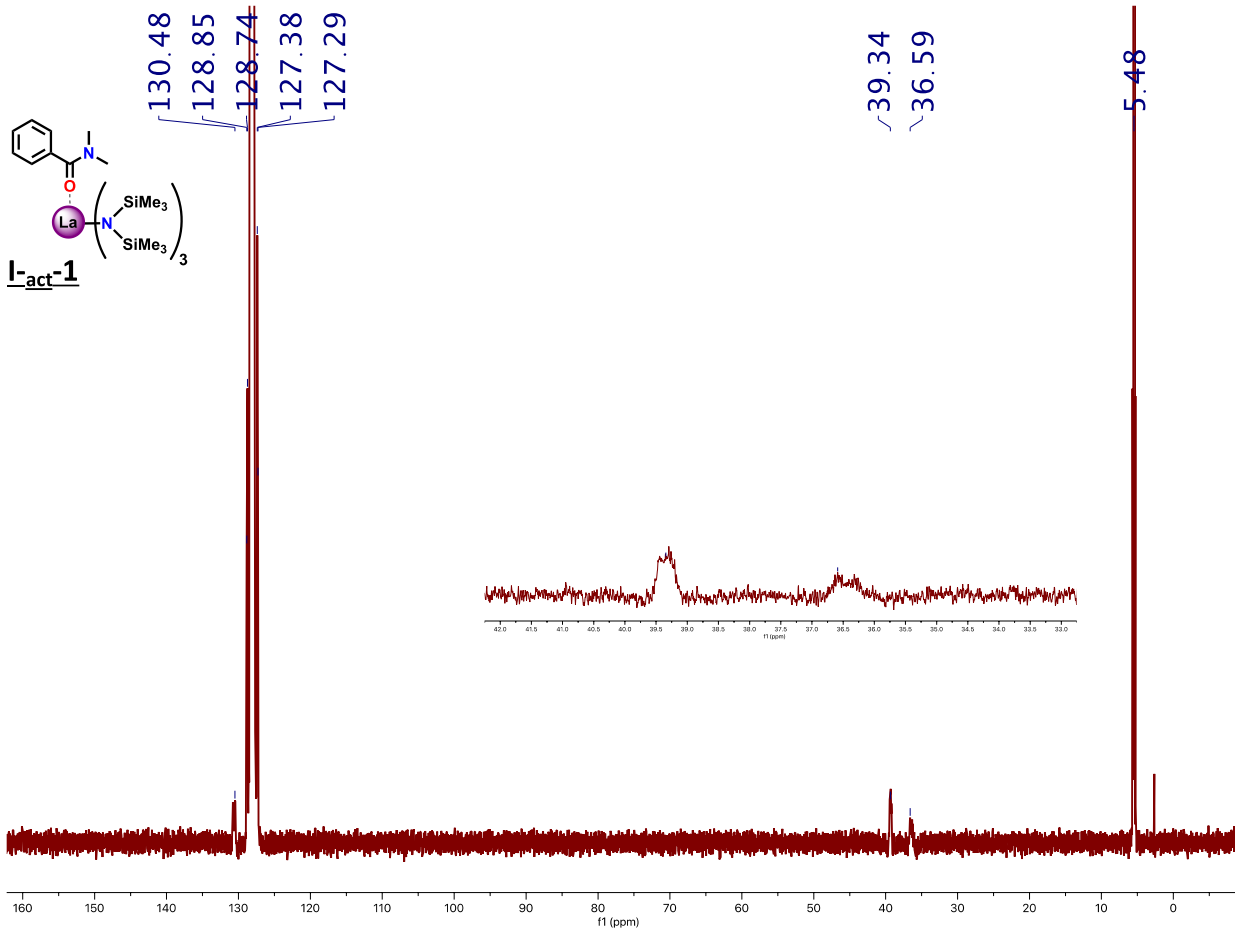

Figure 3.34. ^{13}C-NMR (125 MHz) spectrum of the proposed catalyst activation intermediate **I-act-1** in benzene-d_6.

DFT Examination of Catalyst Decomposition Pathway. DFT calculations were performed to better understand the decomposition path of the La^{NTMS} precatalyst induced by HBpin (Figure 3.35). The decomposition path involves four main steps. The coordination of the first HBpin leads to the formation of the pinBH-$N(SiMe_3)_2^-$ borate species (**I_{deact}-1**, -7.0 kcal/mol). The second step is promoted by the approach of a second HBpin leading to hydride transfer from the pinBH-$N(SiMe_3)_2^-$ species to the coordinated HBpin, producing a new H_2Bpin^- species and releasing pinB-$N(SiMe_3)_2$. This intermediate is stabilized by the coordination of a third HBpin (**I_{deact}-2,** -28.5 kcal/mol). The third step is analogous to the first one involving the formation of a new pinBH-$N(SiMe_3)_2^-$ borate species (**I_{deact}-3,** -29.4 kcal/mol). The last step involves the ring-opening of the H_2Bpin^- species and the subsequent hydride transfer from pinBH-$N(SiMe_3)_2^-$ to the opened H_2Bpin^-, leading to the final product. A second pinB-$N(SiMe_3)_2$ molecule is released and a new HBpin coordinates and stabilizes the final product (-34.5 kcal/mol). This last step is the rate determining step with a Gibbs free energy barrier of 14.9 kcal/mol.

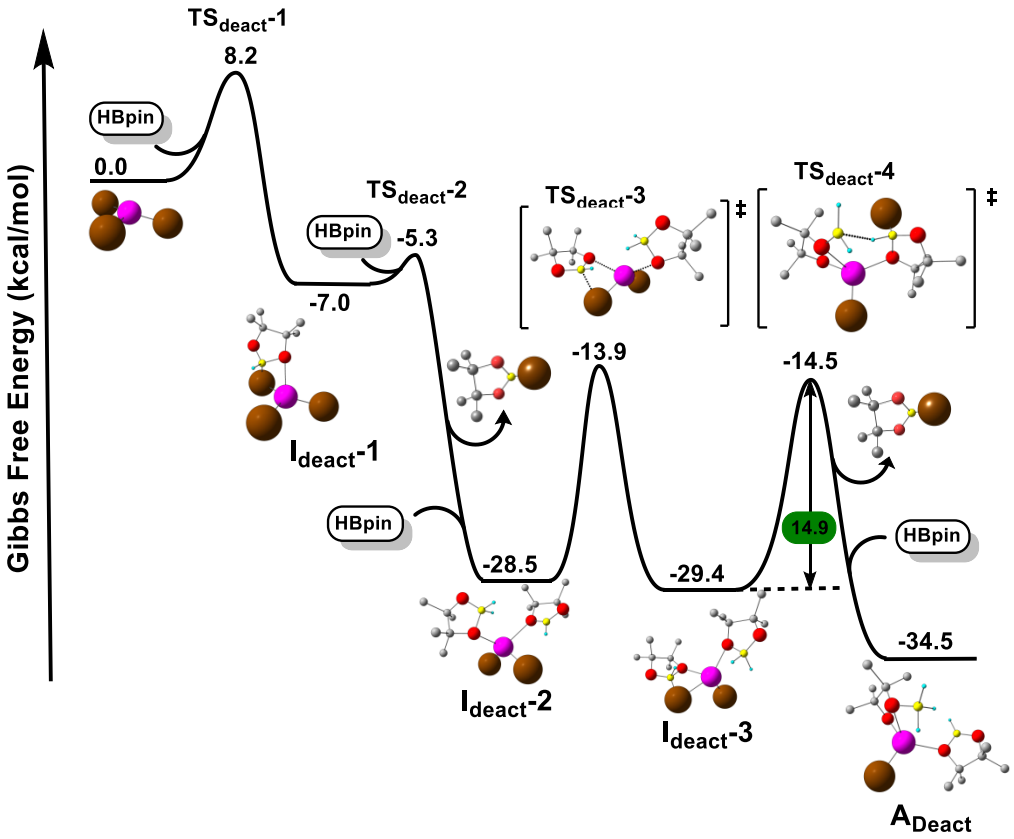

Figure 3.35. Energy profile associated with the decomposition pathway of La^{NTMS} precatalyst induced by HBpin.

Evaluation of the Effect of Different Basis Sets on the Accuracy of the Theoretical Model. It is well known that while 4f electrons must be considered when spectroscopic properties are being studied, it has been shown that the atomic 4f shells of the lanthanides are strongly stabilized and do not contribute significantly to the chemical bonding or reactivity.[94] For this reason, it is expected that adding a polarization function (*f* function) to the basis set used on the lanthanum atom should not have a significant effect on the calculated energetic profile corresponding to the catalytic cycle discussed in this work. Nevertheless, in order to investigate the effects of different basis sets a series of calculations on the key steps of the catalytic cycle were performed. In particular, to evaluate the first hydrogen exchange step we have applied alternative basis sets to the formation of complex **C** and **TS1**. Similarly, to evaluate the second hydrogen exchange step we have applied alternative basis sets to the formation of complex **E** and **TS2**. The data reported in **Table 3.2** show the stabilization energy for the formation of complex **C**, **TS1**, complex **E** and **TS2** computed at the SCF level of theory (at zero kelvin, without considering temperature and pressure) using different basis sets.

Table 3.2. Stabilization energy (kcal/mol) obtained using different basis sets computed at the SCF level of theory.

	LANL2DZ[a]	LANL2DZ + pol[b]	Def2-SVP[c]
C	–32.2	–32.0	–32.7
TS1	–11.0	–11.0	–13.6
E	–72.4	–72.4	–73.9
TS2	–61.1	–62.2	–62.6

[a]ECP and basis set applied to the lanthanum atom in the present work. [b]Geometry optimization using a polarization function (*f* function) added only to the basis set of the lanthanum atom.[95] [c]Geometry optimization using the Def2-SVP basis set reported by Ahlrich and coworkers on all atoms.[96]

It is evident that adding the polarization function to the LANL2DZ basis set (see **Table 3.2**, LANL2DZ + pol) produces negligible changes in the stabilization energies of complex **C**, **TS1** as well as complex **E**. Only **TS2** becomes slightly more stabilized, experiencing a decrease in energy by approximately 1 kcal/mol. Additionally, upon using a full electron basis set plus polarization for all atoms (see **Table 3.2**, Def2-SVP) we obtain a slightly greater stabilization for all intermediates and transition states shown above. Ultimately, these additional calculations suggest that adding the polarization function to the lanthanum atom does not significantly modify the stabilization energies along the catalytic cycle and it does not produce any significant improvement in the accuracy of the calculations.

Characterization of Amide Hydroboration/Reduction Products. Characterization data for the products of amide reduction are given below. Products were converted to amine•HCls (unless otherwise noted) and characterized by ^{1}H and $^{13}C\{^{1}H\}$ NMR. Previously unreported products were compared to amine•HCls synthesized from commercially available amines.

1. 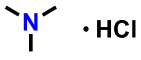 (white powder in 50% yield – low yield due to volatility of amine)

NMR spectra are identical to those reported in the literature.[97]

^{1}H-NMR (D_2O, 500 MHz): 2.93 (9 H) **$^{13}C\{^{1}H\}$-NMR (D_2O, 125 MHz):** 44.76

2. 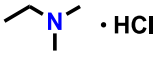 (white powder in 56% yield)

NMR spectra are identical to those reported in the literature. [97]

^{1}H-NMR (D_2O, 500 MHz): 1.32 (t, 3H, $^{3}J_{HH}$=7.3 Hz, N-CH_2CH_3), 2.87 (s, 6H, N-CH_3), 3.20 (q, 2H, $^{3}J_{HH}$=7.2 Hz, N-CH_2CH_3). **^{13}C{^{1}H}-NMR (D_2O, 125 MHz):** 9.02 (N-CH_2CH_3), 42.01 (N-CH_3), 53.01 (N-CH_2CH_3)

3. 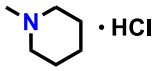 (white powder in 88% yield)

NMR spectra are identical to samples prepared from commercially available amine.

^{1}H-NMR (D_2O, 500 MHz): 1.40-1.54 (m, 1H, N-C_5H_{10}), 1.65-1.88 (m, 3H, N-C_5H_{10}), 1.89-2.02 (m, 2H, N-C_5H_{10}), 2.84 (s, 3H, Me), 2.95 (t, 2H, $^{3}J_{HH}$=12.5 Hz, N-C_5H_{10}), 3.48 (d, 2H, $^{3}J_{HH}$=12.7 Hz, N-C_5H_{10}).**^{13}C{^{1}H}-NMR (D_2O, 125 MHz):** 20.61 (N-C_5H_{10}), 22.98 (N-C_5H_{10}), 43.19 (N-*Me*), 54.92 (N-C_5H_{10}).

4. 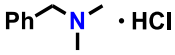 (white powder in 79% yield)

NMR spectra are identical to those reported in the literature. [97]

^{1}H-NMR (D_2O, 500 MHz): 2.87 (s, 6H, N-CH_3), 4.33 (s, 2H, N-CH_2Ph), 7.49-7.58 (m, 5H, N-CH_2*Ph*). **^{13}C{^{1}H}-NMR (D_2O, 125 MHz):** 42.07 (N-CH_3), 61.12 (N-CH_2Ph), 129.30 (N-CH_2*Ph*), 130.15 (N-CH_2*Ph*), 130.77 (N-CH_2*Ph*)

5. 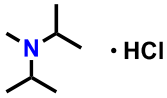 (white powder in 92% yield)

NMR spectra are identical to samples prepared from commercially available amine.

^{1}H-NMR (D_2O, 500 MHz): 1.33 (dd, 12H, $^{3}J_{HH}$=6.7 Hz, $^{4}J_{HH}$=19.2 Hz, N-$(CH(CH_3)_2)_2$), 2.70 (s, 3H, N-CH_3), 3.70 (septet, 2H, $^{3}J_{HH}$=6.7 Hz, N-$(CH(CH_3)_2)_2$). **^{13}C{^{1}H}-NMR (D_2O, 125 MHz):** 15.57 (N-$CH(CH_3)_2$), 18.06 (N-$CH(CH_3)_2$), 30.68 (N-*Me*), 54.92 (N-$CH(CH_3)_2$),

6. 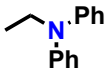

NMR spectra are in accordance with those in the literature.[98]

^{1}H-NMR (C_6D_6, 500 MHz): 0.97 (t, 3H, $^{3}J_{HH}$=7.0 Hz, NCH_2CH_3), 3.47 (q, 2H, $^{3}J_{HH}$=7.0 Hz, NCH_2CH_3), 6.81-6.86 (m, 2H, N-*Ph*), 6.89-6.93 (m, 4H, N-*Ph*), 7.08-7.13 (m, 4H, N-*Ph*)

^{13}C{^{1}H}-NMR (C_6D_6, 125 MHz): 12.77 ($N-CH_2CH_3$), 46.51 ($N-CH_2CH_3$), 121.38 (N-*Ph*), 121.46 (N-*Ph*), 129.58 (N-*Ph*), 148.28 (N-*Ph*)

7. 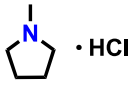 (oily solid in 91% yield)

NMR spectra are identical to samples prepared from commercially available amine.

^{1}H-NMR (D_2O, 500 MHz): 1.98-2.08 (m, 2H, $N-C_4H_8$), 2.13-2.22 (m, 2H, $N-C_4H_8$), 2.93 (s, 3H, N-*Me*), 3.03-3.11 (m, 2H, $N-C_4H_8$), 3.62-3.69 (m, 2H, $N-C_4H_8$). **^{13}C{^{1}H}-NMR (D_2O, 125 MHz):** 22.83 (N-*Me*), 40.56 ($N-C_4H_8$), 55.76 ($N-C_4H_8$)

8. 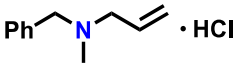 (white powder in 93% yield)

NMR spectra are in accordance with those in the literature. [99]

^{1}H-NMR ($CDCl_3$, 500 MHz): 2.63 (d, 3H, N-C*H*$_3$ coupling to N-*H*), 3.77-3.40 (m, 2H, PhCH_2), 4.20-4.00 (m, 2H, N-CH_2), 5.49 (d, 1H, $^{3}J_{HH}$ = 17.2 Hz, $NCH_2CH=CH_2$), 5.59 (d, 1H, $^{3}J_{HH}$ = 10.1 Hz, $NCH_2CH=CH_2$), 6.29-6.17 (m, 1H, $NCH_2CH=CH_2$), 7.48-7.42 (m, 3H, *Ph*), 7.65-7.59 (m, 2H, *Ph*). **^{13}C{^{1}H}-NMR ($CDCl_3$, 125 MHz):** 131.30, 130.34, 129.60, 128.50, 126.65, 126.09, 59.01, 57.77, 38.89.

9.  (white powder in 66% yield)

NMR spectra are identical to samples prepared from commercially available amine.

^{1}H-NMR (D_2O, 500 MHz): 1.28 (t, 3H, $^{3}J_{HH}$=7.5 Hz, N-CH_2CH_3), 2.70 (s, 3H, N-CH_3), 3.09 (q, 2H, $^{3}J_{HH}$=7.5 Hz, N-CH_2CH_3). **^{13}C{^{1}H}-NMR (D_2O, 125 MHz):** 10.33 (N-CH_2CH_3), 32.12 (N-CH_3), 44.23 (N-CH_2CH_3)

10. 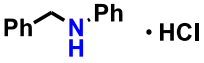 (gray powder in 75% yield)

NMR spectra are identical to samples prepared from commercially available amine.

^{1}H-NMR ($CDCl_3$, 500 MHz): 4.36 (s, 2H, PhCH_2-N), 7.20-7.28 (m, 3H, *Ph*), 7.29-7.40 (m, 7H, *Ph*). **^{13}C{^{1}H}-NMR ($CDCl_3$, 125 MHz):** 56.09 (PhCH_2-N), 124.00 (Ph), 128.84 (Ph), 129.29 (Ph), 129.55 (Ph), 129.82 (Ph), 131.17 (Ph), 134.45 (Ph), 133.93 (Ph)

11. 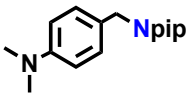

NMR spectra are in accordance with those in the literature. [100]

^{1}H-NMR (C_6D_6, 500 MHz): 1.29-1.39 (m, 2H, *pip*), 1.56 (p, 4H, $^{3}J_{HH}$=5.9 Hz, *pip*), 2.31 (br s, 4H, *pip*), 2.48 (s, 6H, PhNMe_2), 3.45 (br s, 2H, PhCH_2Npip), 6.46 (d, 2H, $^{3}J_{HH}$=8.1 Hz, *Ph*), 7.54 (d, 2H, $^{3}J_{HH}$=8.1 Hz, *Ph*). **^{13}C{^{1}H}-NMR (C_6D_6, 125 MHz):** 17.02 (N-*pip*), 23.25 (N-*pip*), 48.72 (PhNMe_2), 55.58 (N-*pip*), 62.96 (PhCH_2-Npip), 121.25 (*Ph*), 131.86 (*Ph*), 134.86 (*Ph*), 136.24 (*Ph*).

12. 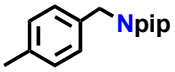

NMR spectra are in accordance with those in the literature. [101]

^{1}H-NMR (C_6D_6, 500 MHz): 1.28-1.39 (m, 2H, *pip*), 1.54 (p, 4H, $^{3}J_{HH}$=5.9 Hz, *pip*), 2.15 (s, 3H, Ph*CH*$_3$), 2.29 (br s, 4H, *pip*), 3.35 (br s, 2H, PhC*H*$_2$Npip), 7.02 (d, 2H, $^{3}J_{HH}$=8.1 Hz, *Ph*), 7.28 (d, 2H, $^{3}J_{HH}$=8.1 Hz, *Ph*). **^{13}C{^{1}H}-NMR (C_6D_6, 125 MHz):** 16.94 (N-*pip*), 21.15 (*Me*Ph), 26.55 (N-*pip*), 54.85 (N-*pip*), 63.97 (Ph*C*H$_2$-Npip), 129.26 (*Ph*), 131.76 (*Ph*), 136.32 (*Ph*), 136.81 (*Ph*).

13. 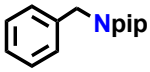

NMR spectra are in accordance with those in the literature. [102]

^{1}H-NMR (C_6D_6, 500 MHz): 1.25-1.35 (m, 2H, *pip*), 1.47 (p, 4H, $^{3}J_{HH}$=5.6 Hz, *pip*), 2.26 (br s, 4H, *pip*), 3.33 (s, 2H, PhC*H*$_2$Npip), 7.07-7.12 (m, 1H, *Ph*), 7.15-7.22 (m, 2H, *Ph*), 7.33-7.38 (m, 2H, *Ph*). **^{13}C{^{1}H}-NMR (C_6D_6, 125 MHz):** 16.94 (N-*pip*), 26.52 (N-*pip*), 54.86 (N-*pip*), 64.17 (Ph*C*H$_2$-Npip), 127.10 (*Ph*), 129.21 (*Ph*), 131.76 (*Ph*), 139.86 (*Ph*).

14. 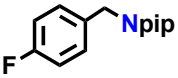

NMR spectra are in accordance with those in the literature.[103]

^{1}H-NMR (C_6D_6, 500 MHz): 1.24-1.32 (m, 2H, *pip*), 1.45 (p, 4H, $^{3}J_{HH}$=5.4 Hz, *pip*), 2.20 (br s, 4H, *pip*), 3.19 (s, 2H, PhC*H*$_2$Npip), 6.80-6.87 (m, 2H, *Ph*), 7.08-7.20 (m, 2H, *Ph*). **^{13}C{^{1}H}-NMR (C_6D_6, 125 MHz):** 16.94 (N-*pip*), 26.48 (N-*pip*), 54.71 (N-*pip*), 63.17 (Ph*C*H$_2$-Npip), 115.07 (*Ph*), 115.24 (*Ph*), 130.62 (*Ph*), 131.76 (*Ph*).

15. 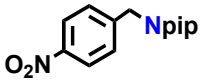

NMR spectra are in accordance with those in the literature.[100]

^{1}H-NMR (C_6D_6, 500 MHz): 1.19-1.23 (m, 2H, *pip*), 1.43 (p, 4H, $^{3}J_{HH}$=5.4 Hz, *pip*), 2.10 (br s, 4H, *pip*), 3.05 (s, 2H, PhC*H*$_2$Npip), 7.01 (d, 2H, $^{3}J_{HH}$=7.9 Hz, *Ph*), 7.88 (d, 2H, $^{3}J_{HH}$=7.9 Hz, *Ph*).

^{13}C{^{1}H}-NMR (C_6D_6, 125 MHz): 22.22 (N-*pip*), 23.92 (N-*pip*), 52.28 (N-*pip*), 60.45 (Ph*C*H$_2$-Npip), 121.04 (*Ph*), 126.75 (*Ph*), 144.58 (*Ph*), 145.02 (*Ph*).

REFERENCES

Chapter 1

1. Smith, M. *March's Advanced Organic Chemistry: Reactions, Mechanisms, and Structure*. Wiley: Hoboken, 2006; pp 1703-1869.

2. Riant, O.; Mostefaï, N.; Courmarcel, J. *Synthesis* **2004,** *2004*, 2943-2958.

3. Yamamoto, K.; Hayashi, T. In *Transition Metals for Organic Synthesis*, Wiley-VCH Verlag GmbH: 2008; pp 167-191.

4. Addis, D.; Das, S.; Junge, K.; Beller, M. Selective reduction of carboxylic acid derivatives by catalytic hydrosilylation. *Angew. Chem., Int. Ed.* **2011,** *50*, 6004-6011.

5. Brunner, H. N., Hisao; Itoh, K. In *Catalytic Asymmetric Synthesis*, Ojima, I., Ed. VCH Publishers, Inc.: New York, N.Y., 1993; pp 303-322.

6. Chong, C. C.; Kinjo, R. Catalytic Hydroboration of Carbonyl Derivatives, Imines, and Carbon Dioxide. *ACS Catal.* **2015**, 3238-3259.

7. Arrowsmith, M.; Hadlington, T. J.; Hill, M. S.; Kociok-Kohn, G. Magnesium-catalysed hydroboration of aldehydes and ketones. *Chem. Comm.* **2012,** *48*, 4567-4569.

8. Manna, K.; Ji, P.; Greene, F. X.; Lin, W. Metal–Organic Framework Nodes Support Single-Site Magnesium–Alkyl Catalysts for Hydroboration and Hydroamination Reactions. *J. Am. Chem. Soc.* **2016**, *138*, 7488-91.

9. Mukherjee, D.; Shirase, S.; Spaniol, T. P.; Mashima, K.; Okuda, J., Magnesium hydridotriphenylborate [Mg(thf)6][HBPh3]2: a versatile hydroboration catalyst. *Chem. Comm.* **2016**, *52*, 13155-13158.

10. Oluyadi, A. A.; Ma, S.; Muhoro, C. N. Titanocene(II)-Catalyzed Hydroboration of Carbonyl Compounds. *Organometallics* **2013,** *32*, 70-78.

11. Eedugurala, N.; Wang, Z. R.; Chaudhary, U.; Nelson, N.; Kandel, K.; Kobayashi, T.; Slowing, I. I.; Pruski, M.; Sadow, A. D. Mesoporous Silica-Supported Amidozirconium-Catalyzed Carbonyl Hydroboration. *ACS Catal.* **2015,** *5*, 7399-7414.

12. Koren-Selfridge, L.; Londino, H. N.; Vellucci, J. K.; Simmons, B. J.; Casey, C. P.; Clark, T. B. Synthesis of Ruthenium Boryl Analogues of the Shvo Metal–Ligand Bifunctional Catalyst. *Organometallics* **2009,** *28*, 2085-2090.

13. Kaithal, A.; Chatterjee, B.; Gunanathan, C. Ruthenium Catalyzed Selective Hydroboration of Carbonyl Compounds. *Org. Lett.* **2015,** *17*, 4790-4793.

14. Guo, J.; Chen, J.; Lu, Z. Cobalt-catalyzed asymmetric hydroboration of aryl ketones with pinacolborane. *Chem. Comm.* **2015,** *51*, 5725-5727.

15. Bagherzadeh, S.; Mankad, N. P. Extremely efficient hydroboration of ketones and aldehydes by copper carbene catalysis. *Chem. Comm.* **2016,** *52*, 3844-3846.

16. Zhang, G.; Zeng, H.; Wu, J.; Yin, Z.; Zheng, S.; Fettinger, J. C. Highly Selective Hydroboration of Alkenes, Ketones and Aldehydes Catalyzed by a Well-Defined Manganese Complex. *Angew. Chem., Int. Ed.* **2016**, *55*, 14369-14372.

17. Drover, M. W.; Schafer, L. L.; Love, J. A. Capturing HBCy2: Using N,O-Chelated Complexes of Rhodium(I) and Iridium(I) for Chemoselective Hydroboration. *Angew. Chem., Int. Ed.* **2016**, *55*, 3181-3186.

18. Hadlington, T. J.; Hermann, M.; Frenking, G.; Jones, C. Low Coordinate Germanium(II) and Tin(II) Hydride Complexes: Efficient Catalysts for the Hydroboration of Carbonyl Compounds. *J. Am. Chem. Soc.* **2014,** *136*, 3028-3031.

19. Chong, C. C.; Hirao, H.; Kinjo, R. Metal-free σ-bond metathesis in 1,3,2-diazaphospholene-catalyzed hydroboration of carbonyl compounds. *Angew. Chem., Int. Ed.* **2015,** *54*, 190-194.

20. Query, I. P.; Squier, P. A.; Larson, E. M.; Isley, N. A.; Clark, T. B. Alkoxide-Catalyzed Reduction of Ketones with Pinacolborane. *J. Org. Chem.* **2011,** *76*, 6452-6456.

21. Mukherjee, D.; Osseili, H.; Spaniol, T. P.; Okuda, J. Alkali Metal Hydridotriphenylborates [(L)M][HBPh3] (M = Li, Na, K): Chemoselective Catalysts for Carbonyl and CO2 Hydroboration. *J. Am. Chem. Soc.* **2016,** *138*, 10790-3.

22. Jakhar, V. K.; Barman, M. K.; Nembenna, S. Aluminum Monohydride Catalyzed Selective Hydroboration of Carbonyl Compounds. *Org. Lett.* **2016,** *18*, 4710-3.

23. Stubbert, B.D.; Marks, T.J., Mechanistic Investigation of Intramolecular Aminoalkene and Aminoalkyne Hydroamination/Cyclization Catalyzed by Highly Electrophilic, Tetravalent

Constrained Geometry 4d and 5f Complexes. Evidence for an M−N σ-Bonded Insertive Pathway. *J. Am. Chem. Soc.*, **2007**, *129*, 6149-6167.

24. Horino, Y.; Livinghouse, T. Alkene and Diene Hydrosilylations Catalyzed by Lanthanum Tris[bis(trimethylsilyl)amide]. *Organometallics* **2004,** *23*, 12-14.

25. Horino, Y.; Livinghouse, T.; Stan, M. Alkene-Pinacolborane Hydroborations Catalyzed by Lanthanum Tris[bis(trimethylsilyl)amide]. *Synlett* **2004,** *2004*, 2639-2641.

26. Weiss, C.J.; Marks, T.J. Organo-f-element catalysts for efficient and highly selective hydroalkoxylation and hydrothiolation. *Dalton Trans. Perspective*, **2010**, *39*, 6576-6588.

27. Yu, X.; Seo, S.; Marks, T. J. Effective, Selective Hydroalkoxylation/Cyclization of Alkynyl and Allenyl Alcohols Mediated by Lanthanide Catalysts. *J. Am. Chem. Soc.* **2007,** *129*, 7244-7245.

28. Seo, S.; Yu, X.; Marks, T. J. Intramolecular Hydroalkoxylation/Cyclization of Alkynyl Alcohols Mediated by Lanthanide Catalysts. Scope and Reaction Mechanism. *J. Am. Chem. Soc.* **2009,** *131*, 263-276.

29. Kawaoka, A. M.; Douglass, M. R.; Marks, T. J. Homoleptic Lanthanide Alkyl and Amide Precatalysts Efficiently Mediate Intramolecular Hydrophosphination/Cyclization. Observations on Scope and Mechanism. *Organometallics* **2003,** *22*, 4630-4632.

30. Dudnik, A. S.; Weidner, V. L.; Motta, A.; Delferro, M.; Marks, T. J. Atom-efficient regioselective 1,2-dearomatization of functionalized pyridines by an earth-abundant organolanthanide catalyst. *Nat. Chem.* **2014,** *6*, 1100-7.

31. Seo, S.; Marks, T. J. Mild Amidation of Aldehydes with Amines Mediated by Lanthanide Catalysts. *Org. Lett.* **2008,** *10*, 317-319.

32. Berberich, H.; Roesky, P. W. Homoleptic Lanthanide Amides as Homogeneous Catalysts for the Tishchenko Reaction. *Angew. Chem., Int. Ed.* **1998,** *37*, 1569-1571.

33. Bürgstein, M. R.; Berberich, H.; Roesky, P. W. Homoleptic Lanthanide Amides as Homogeneous Catalysts for Alkyne Hydroamination and the Tishchenko Reaction. *Chem. – Eur. J.* **2001,** *7*, 3078-3085.

34. Weidner, V.L; Barger, C.J; Lohr, T.L.; Marks, T.J., 2016, unpublished results.

35. Jaffe, H. H., A Reexamination of the Hammett Equation. *Chem. Rev.* **1953**, *53*, 191-261.

36. Li, Z.; Assary, R. S.; Atesin, A. C.; Curtiss, L. A.; Marks, T. J. Rapid Ether and Alcohol C–O Bond Hydrogenolysis Catalyzed by Tandem High-Valent Metal Triflate + Supported Pd Catalysts. *J. Am. Chem. Soc.* **2014,** *136*, 104-107.

37. Eedugurala, N.; Wang, Z.; Chaudhary, U.; Nelson, N.; Kandel, K.; Kobayashi, T.; Slowing, I. I.; Pruski, M; Sadow, A. D. Mesoporous Silica-Supported Amidozirconium-Catalyzed Carbonyl Hydroboration. *ACS Catal* **2015**, 5, 7399-7414.

38. Oluyadi, A. A.; Ma, S.; Muhoro, C. N. Titanocene(II)-Catalyzed Hydroboration of Carbonyl Compounds. *Organometallics* **2013**, 32, 70-78.

39. Chong, C. C.; Hirao, H.; Kinjo, R. Metal-free σ-bond metathesis in 1,3,2-diazaphospholene-catalyzed hydroboration of carbonyl compounds. *Angew Chem Int Ed* **2015**, 54, 190-194.

40. Yang, Z.; Zhong, M.; Ma, X.; De, S.; Anusha, C.; Parameswaran, P.; Roesky, H. W. An Aluminum Hydride That Functions like a Transition-Metal Catalyst. *Angew Chem Int Ed* **2015**, 54, 10225-10229.

41. Arrowsmith, M.; Hadlington, T. J.; Hill, M. S.; Kociok-Koehn, G. Magnesium-catalysed hydroboration of aldehydes and ketones. *Chem Commun* **2012**, 48, 4567-4569.

Chapter 2

1. (a) Cornils, B.; Hermann, W. A.; Beller, M.; Paciello, R., *Applied Homogeneous Catalysis with Organometallic Compounds: A Comprehensive Handbook in Four Volumes, Volume 4*. Wiley-VCH Verlag GmbH & Co: Weinheim, Germany, 2017; (b) Andersson, P. G.; Munslo, I. J., In *Modern Reduction Methods*, Wiley: New York, 2008; (c) Roberts, S. M.; Whittall, J., *Regio- and Stereo-Controlled Oxidations and Reductions*. John Wiley & Sons: West Sussex, England, 2007; Vol. 5; (d) Otera, J., *Modern Carbonyl Chemistry*. Wiley-VCH: Weinheim, Germany, 2000.

2. Magano, J.; Dunetz, J. R. Large-Scale Carbonyl Reductions in the Pharmaceutical Industry. *Org. Proc. Res. Dev.* **2012,** *16*, 1156-1184.

3. (a) Lohr, T. L.; Li, Z.; Marks, T. J. Thermodynamic Strategies for C–O Bond Formation and Cleavage via Tandem Catalysis. *Acc. Chem. Res.* **2016,** *49*, 824-834; (b) Wu, L.; Moteki, T.; Gokhale, A. A.; Flaherty, D. W.; Toste, F. D. Production of Fuels and Chemicals from Biomass: Condensation Reactions and Beyond. *Chem* **2016,** *1*, 32-58; (c) Hu, C.; Creaser, D.; Siahrostami, S.; Grönbeck, H.; Ojagh, H.; Skoglundh, M. Catalytic hydrogenation of C=C and C=O in unsaturated fatty acid methyl esters. *Catal. Sci. Tech.* **2014,** *4*, 2427-2444; (d) Turek, T.; Trimm, D. L. The Catalytic Hydrogenolysis of Esters to Alcohols. *Cat. Rev. - Sci. Eng.* **1994,** *36*, 645-683.

4. (a) Smith, M., *March's Advanced Organic Chemistry: Reactions, Mechanisms, and Structure*. Wiley: Hoboken, 2013; (b) Seyden-Penne, J., *Reductions by the Alumino- and Borohydrides in Organic Synthesis*. 2nd ed.; Wiley-VCH: Weinheim, Germany, 1997; (c) Brown, H. C.; Krishnamurthy, S. Forty years of hydride reductions. *Tetrahedron* **1979,** *35*, 567-607; (d) Nystrom, R. F.; Brown, W. G. Reduction of Organic Compounds by Lithium Aluminum Hydride. III. Halides, Quinones, Miscellaneous Nitrogen Compounds1. *J. Am. Chem. Soc.* **1948,** *70*, 3738-3740.

5. (a) Liu, W.; Sahoo, B.; Junge, K.; Beller, M. Cobalt Complexes as an Emerging Class of Catalysts for Homogeneous Hydrogenations. *Acc. Chem. Res.* **2018,** *51*, 1858-1869; (b) Pritchard, J.; Filonenko, G. A.; van Putten, R.; Hensen, E. J. M.; Pidko, E. A. Heterogeneous and homogeneous catalysis for the hydrogenation of carboxylic acid derivatives: history, advances and future directions. *Chem. Soc. Rev.* **2015,** *44*, 3808-3833; (c) Chakraborty, S.; Bhattacharya, P.; Dai, H.; Guan, H. Nickel and Iron Pincer Complexes as Catalysts for the Reduction of Carbonyl Compounds. *Acc. Chem. Res.* **2015,** *48*, 1995-2003; (d) Werkmeister, S.; Junge, K.; Beller, M. Catalytic Hydrogenation of Carboxylic Acid Esters, Amides, and Nitriles with Homogeneous Catalysts. *Org. Proc. Res. Dev.* **2014,** *18*, 289-302; (e) Saudan, L. A., Hydrogenation of Esters. In *Sustainable Catalysis*, Dunn, P. J.; Hii, K. K.; Krische, M. J.; Williams, M. T., Eds. 2013; (f) Clarke, M. L. Recent developments in the homogeneous hydrogenation of carboxylic acid esters. *Catal. Sci. Tech.* **2012,** *2*, 2418-2423; (g) Dub, P. A.; Ikariya, T. Catalytic Reductive Transformations of Carboxylic and Carbonic Acid Derivatives Using Molecular Hydrogen. *ACS Catal.* **2012,** *2*, 1718-1741.

6. (a) Andrews, R. J.; Chitnis, S. S.; Stephan, D. W. Carbonyl and olefin hydrosilylation mediated by an air-stable phosphorus(iii) dication under mild conditions. *Chem. Commun.* **2019,** *55*, 5599-5602; (b) Gebbink, R. J. M. K.; Moret, M.-E., *Non-Noble Metal Catalysis: Molecular Approaches and Reactions*. Wiley-VCH: Weinheim, Germany, 2019; (c) Raya-Barón, Á.; Oña-Burgos, P.; Fernández, I. Iron-Catalyzed Homogeneous Hydrosilylation of Ketones and Aldehydes: Advances and Mechanistic Perspective. *ACS Catal.* **2019**, *9*, 5400-5417; (d) Ritter, F.; Mukherjee, D.; Spaniol, T. P.; Hoffmann, A.; Okuda, J. A Masked Cuprous Hydride as a Catalyst for Carbonyl Hydrosilylation in Aqueous Solutions. *Angew. Chem. Int. Ed.* **2019,** *58*, 1818-1822; (e) Zhou, Y.; Khan, R.; Fan, B.; Xu, L. Ruthenium-Catalyzed Selective Reduction of Carboxylic Esters and Carboxamides. *Synthesis* **2019,** *51*, 2491-2505; (f) Rock, C. L.; Groy, T. L.; Trovitch, R. J. Carbonyl and ester C–O bond hydrosilylation using κ^4-diimine nickel catalysts. *Dalton Trans.* **2018,** *47*, 8807-8816; (g) Kelly, C. M.; McDonald, R.; Sydora, O. L.; Stradiotto, M.; Turculet, L. A Manganese Pre-Catalyst: Mild Reduction of Amides, Ketones, Aldehydes, and Esters. *Angew. Chem. Int. Ed.* **2017,** *56*, 15901-15904; (h) Trovitch, R. J. The Emergence of Manganese-Based Carbonyl Hydrosilylation Catalysts. *Acc. Chem. Res.* **2017,** *50*, 2842-2852; (i) Süsse, L.; Hermeke, J.; Oestreich, M. The Asymmetric Piers Hydrosilylation. *J. Am. Chem. Soc.* **2016,** *138*, 6940-6943; (j) Lampland, N. L.; Pindwal, A.; Neal, S. R.; Schlauderaff, S.; Ellern, A.; Sadow, A. D. Magnesium-catalyzed hydrosilylation of α,β-unsaturated esters. *Chem. Sci.* **2015,** *6*, 6901-6907; (k) Trovitch, R. J. Comparing Well-Defined Manganese, Iron, Cobalt, and Nickel Ketone Hydrosilylation Catalysts. *Synlett* **2014,** *25*, 1638-1642; (l) Addis, D.; Das, S.; Junge, K.; Beller, M. Selective Reduction of Carboxylic Acid Derivatives by Catalytic Hydrosilylation. *Angew. Chem. Int. Ed.* **2011,** *50*, 6004-6011; (m) Zhang, M.; Zhang, A. Iron-catalyzed hydrosilylation reactions. *Appl. Organomet. Chem.* **2010,** *24*, 751-757; (n) Yang, J.; Tilley, T. D. Efficient Hydrosilylation of Carbonyl Compounds with the Simple Amide Catalyst $[Fe\{N(SiMe_3)_2\}_2]$. *Angew. Chem. Int. Ed.* **2010,** *49*, 10186-10188; (o) Marciniec, B., *Hydrosilylation: A Comprehensive Review on Recent Advances*. Springer: Berlin, 2009; (p) Díez-González, S.; Nolan, S. P. Transition Metal-Catalyzed Hydrosilylation of Carbonyl Compounds and Imines. A Review. *Org. Prep. Proced. Int.* **2007,** *39*, 523-559; (q) Roy, A. K., A Review of Recent Progress in Catalyzed Homogeneous Hydrosilation (Hydrosilylation). In *Adv. Organomet. Chem.*, West, R.; Hill, A. F.; Fink, M. J., Eds. Academic Press: 2007; Vol. 55, pp 1-59.

7. (a) Patnaik, S.; Sadow, A. D. Interconverting Lanthanum Hydride and Borohydride Catalysts for C=O Reduction and C−O Bond Cleavage. *Angew. Chem. Int. Ed.* **2019,** *58,* 2505-2509; (b) Barman, M. K.; Baishya, A.; Nembenna, S. Magnesium amide catalyzed selective hydroboration of esters. *Dalton Trans.* **2017,** *46*, 4152-4156; (c) Mukherjee, D.; Shirase, S.; Spaniol, T. P.; Mashima, K.; Okuda, J. Magnesium hydridotriphenylborate $[Mg(thf)_6][HBPh_3]_2$: a versatile hydroboration catalyst. *Chem. Commun.* **2016,** *52*, 13155-13158; (d) Mukherjee, D.; Ellern, A.; Sadow, A. D. Magnesium-catalyzed hydroboration of esters: evidence for a new zwitterionic mechanism. *Chem. Sci.* **2014,** *5*, 959-964; (e) Khalimon, A. Y.; Farha, P.; Kuzmina, L. G.; Nikonov, G. I. Catalytic hydroboration by an imido-hydrido complex of Mo(IV). *Chem. Commun.* **2012,** *48*, 455-457; (f) Arrowsmith, M.; Hill, M. S.; Hadlington, T.; Kociok-Köhn, G.; Weetman, C. Magnesium-Catalyzed Hydroboration of Pyridines. *Organometallics* **2011,** *30*, 5556-5559.

8. Obligacion, J. V.; Chirik, P. J. Earth-abundant transition metal catalysts for alkene hydrosilylation and hydroboration. *Nature Reviews Chemistry* **2018,** *2*, 15-34.

9. *For a review, see:* (a) Chong, C. C.; Kinjo, R. Catalytic Hydroboration of Carbonyl Derivatives, Imines, and Carbon Dioxide. *ACS Catal.* **2015,** *5*, 3238-3259; *For selected, recent examples, see:* (b) Dasgupta, R.; Das, S.; Hiwase, S.; Pati, S. K.; Khan, S. N-Heterocyclic Germylene and Stannylene Catalyzed Cyanosilylation and Hydroboration of Aldehydes. *Organometallics* **2019,** *38*, 1429-1435; (c) Kuciński, K.; Hreczycho, G. Lithium triethylborohydride as catalyst for solvent-free hydroboration of aldehydes and ketones. *Green Chemistry* **2019,** *21*, 1912-1915; (d) Woodside, A. J.; Smith, M. A.; Herb, T. M.; Manor, B. C.; Carroll, P. J.; Rablen, P. R.; Graves, C. R. Synthesis and Characterization of a Tripodal Tris(nitroxide) Aluminum Complex and Its Catalytic Activity toward Carbonyl Hydroboration. *Organometallics* **2019,** *38*, 1017-1020; (e) Baishya, A.; Baruah, S.; Geetharani, K. Efficient hydroboration of carbonyls by an iron(ii) amide catalyst. *Dalton Trans.* **2018,** *47*, 9231-9236; (f) Das, U. K.; Higman, C. S.; Gabidullin, B.; Hein, J. E.; Baker, R. T. Efficient and Selective Iron-Complex-Catalyzed Hydroboration of Aldehydes. *ACS Catal.* **2018,** *8*, 1076-1081; (g) Ghatak, T.; Makarov, K.; Fridman, N.; Eisen, M. S. Catalytic regeneration of a Th–H bond from a Th–O bond through a mild and chemoselective carbonyl hydroboration. *Chem. Commun.* **2018,** *54*, 11001-11004; (h) Chen, S.; Yan, D.; Xue, M.; Hong, Y.; Yao, Y.; Shen, Q. Tris(cyclopentadienyl)lanthanide Complexes as Catalysts for Hydroboration Reaction toward Aldehydes and Ketones. *Org. Lett.* **2017,** *19*, 3382-3385; (i) Huang, Z.; Liu, D.; Camacho-Bunquin, J.; Zhang, G.; Yang, D.; López-Encarnación, J. M.; Xu, Y.; Ferrandon, M. S.; Niklas, J.; Poluektov, O. G.; Jellinek, J.; Lei, A.; Bunel, E. E.; Delferro, M. Supported Single-Site Ti(IV) on a Metal–Organic Framework for the Hydroboration of Carbonyl Compounds. *Organometallics* **2017,** *36*, 3921-3930; (j) Schneider, J.; Sindlinger, C. P.; Freitag, S. M.; Schubert, H.; Wesemann, L. Diverse Activation Modes in the Hydroboration of Aldehydes and Ketones with Germanium, Tin, and Lead Lewis Pairs. *Angew. Chem. Int. Ed.* **2017,** *56*, 333-337; (k) Vasilenko, V.; Blasius, C. K.; Wadepohl, H.; Gade, L. H. Mechanism-Based Enantiodivergence in Manganese Reduction Catalysis: A Chiral Pincer Complex for the Highly Enantioselective Hydroboration of Ketones. *Angew. Chem. Int. Ed.* **2017,** *56*, 8393-8397; (l) Weidner, V. L.; Barger, C. J.; Delferro, M.; Lohr, T. L.; Marks, T. J. Rapid, Mild, and Selective Ketone and Aldehyde Hydroboration/Reduction Mediated by a Simple Lanthanide Catalyst. *ACS Catal.* **2017,** *7*, 1244-1247; (m) Wu, D.; Wang, R.; Li, Y.; Ganguly, R.; Hirao, H.; Kinjo, R. Electrostatic Catalyst Generated from Diazadiborinine for Carbonyl Reduction. *Chem* **2017,** *3*, 134-151; (n) Manna, K.; Ji, P.; Greene, F. X.; Lin, W. Metal–Organic Framework Nodes Support Single-Site Magnesium–Alkyl Catalysts for Hydroboration and Hydroamination Reactions. *J. Am. Chem. Soc.* **2016,** *138*, 7488-7491.

10. (a) Lohr, T. L.; Li, Z.; Assary, R. S.; Curtiss, L. A.; Marks, T. J. Mono- and tri-ester hydrogenolysis using tandem catalysis. Scope and mechanism. *Energ. Environ. Sci.* **2016,** *9*, 550-564; (b) Lohr, T. L.; Li, Z.; Assary, R. S.; Curtiss, L. A.; Marks, T. J. Thermodynamically Leveraged Tandem Catalysis for Ester RC(O)O–R′ Bond Hydrogenolysis. Scope and Mechanism. *ACS Catal.* **2015,** *5*, 3675-3679; (c) Lohr, T. L.; Li, Z.; Marks, T. J. Selective

Ether/Ester C–O Cleavage of an Acetylated Lignin Model via Tandem Catalysis. *ACS Catal.* **2015,** *5*, 7004-7007.

11. (a) Schuetz, S. A.; Day, V. W.; Sommer, R. D.; Rheingold, A. L.; Belot, J. A. Anhydrous Lanthanide Schiff Base Complexes and Their Preparation Using Lanthanide Triflate Derived Amides. *Inorg. Chem.* **2001,** *40*, 5292-5295; (b) Bradley, D. C.; Ghotra, J. S.; Hart, F. A. Three-co-ordination in lanthanide chemistry: tris[bis(trimethylsilyl)amido]lanthanide(III) compounds. *J. Chem. Soc., Chem. Commun.* **1972**, 349-350; (c) Alyea, E. C.; Bradley, D. C.; Copperthwaite, R. G. Three-co-ordinated transition metal compounds. Part I. The preparation and characterization of tris(bistrimethylsilylamido)-derivatives of scandium, titanium, vanadium, chromium, and iron. *J. Chem. Soc., Dalton Trans.* **1972**, 1580-1584.

12. (a) Edelmann, F. T. Lanthanides and actinides: Annual survey of their organometallic chemistry covering the year 2017. *Coord. Chem. Rev.* **2018,** *370*, 129-223; (b) Qian, Q.; Zhu, W.; Lu, C.; Zhao, B.; Yao, Y. Asymmetric Michael addition of malonates to unsaturated ketones catalyzed by rare earth metal complexes bearing phenoxy functionalized chiral diphenylprolinolate ligands. *Tetrahedron: Asymmetry* **2016,** *27*, 911-917; (c) Wang, C.; Huang, L.; Lu, M.; Zhao, B.; Wang, Y.; Zhang, Y.; Shen, Q.; Yao, Y. Anionic phenoxy-amido rare-earth complexes as efficient catalysts for amidation of aldehydes with amines. *RSC Advances* **2015,** *5*, 94768-94775; (d) Cotton, S. A., Lanthanide Amides. In *Encyclopedia of Inorganic and Bioinorganic Chemistry*, John Wiley & Sons, Ltd: 2011; (e) Vitanova, D. V.; Hampel, F.; Hultzsch, K. C. Linked bis(β-diketiminato) yttrium and lanthanum complexes as catalysts in asymmetric hydroamination/cyclization of aminoalkenes (AHA). *J. Organomet. Chem.* **2011,** *696*, 321-330; (f) Döring, C.; Kempe, R. Synthesis and Structure of Aminopyridinato-Stabilized Yttrium and Lanthanum Amides and Their Reactivity towards Alkylaluminium Compounds. *Eur. J. Inorg. Chem.* **2009,** *2009*, 412-418; (g) Korobkov, I.; Gambarotta, S. Aluminate Samarium(II) and Samarium(III) Aryloxides. Isolation of a Single-Component Ethylene Polymerization Catalyst. *Organometallics* **2009,** *28*, 4009-4019; (h) Hong, S.; Tian, S.; Metz, M. V.; Marks, T. J. C2-Symmetric Bis(oxazolinato)lanthanide Catalysts for Enantioselective Intramolecular Hydroamination/Cyclization. *J. Am. Chem. Soc.* **2003,** *125*, 14768-14783; (i) Dash, A. K.; Razavi, A.; Mortreux, A.; Lehmann, C. W.; Carpentier, J.-F. Amine Elimination Reactions between Homoleptic Silylamide Lanthanide Complexes and an Isopropylidene-Bridged Cyclopentadiene−Fluorene System. *Organometallics* **2002,** *21*, 3238-3249; (j) Belot, J. A.; Wang, A.; McNeely, R. J.; Liable-Sands, L.; Rheingold, A. L.; Marks, T. J. Highly Volatile, Low Melting, Fluorine-Free Precursors for Metal-Organic Chemical Vapor Deposition of Lanthanide Oxide-Containing Thin Films. *Chem. Vap. Deposition* **1999,** *5*, 65-69; (k) Tian, S.; Arredondo, V. M.; Stern, C. L.; Marks, T. J. Constrained Geometry Organolanthanide Catalysts. Synthesis, Structural Characterization, and Enhanced Aminoalkene Hydroamination/Cyclization Activity. *Organometallics* **1999,** *18*, 2568-2570.

13. (a) Roesky, P., *Molecular Catalysis of Rare-Earth Elements*. Springer-Verlag Berlin Heidelberg: 2010; Vol. 137; (b) Müller, T. E.; Hultzsch, K. C.; Yus, M.; Foubelo, F.; Tada, M. Hydroamination: Direct Addition of Amines to Alkenes and Alkynes. *Chem. Rev.* **2008,** *108*, 3795-3892; (c) Hong, S.; Marks, T. J. Organolanthanide-Catalyzed Hydroamination. *Acc.*

Chem. Res. **2004,** *37*, 673-686; (d) Anwander, R., Lanthanide amides. In *Organolanthoid Chemistry: Synthesis, Structure, Catalysis*, Springer Berlin Heidelberg: Berlin, Heidelberg, 1996; pp 33-112; (e) Weiss, C. J.; Marks, T. J. Organo-f-element catalysts for efficient and highly selective hydroalkoxylation and hydrothiolation. *Dalton Trans.* **2010,** *39*, 6576-6588; (f) Seo, S.; Marks, T. J. Lanthanide-Catalyst-Mediated Tandem Double Intramolecular Hydroalkoxylation/Cyclization of Dialkynyl Dialcohols: Scope and Mechanism. *Chem. - Eur. J.* **2010,** *16*, 5148-5162; (g) Seo, S.; Yu, X.; Marks, T. J. Intramolecular Hydroalkoxylation/Cyclization of Alkynyl Alcohols Mediated by Lanthanide Catalysts. Scope and Reaction Mechanism. *J. Am. Chem. Soc.* **2009,** *131*, 263-276; (h) Yu, X.; Seo, S.; Marks, T. J. Effective, Selective Hydroalkoxylation/Cyclization of Alkynyl and Allenyl Alcohols Mediated by Lanthanide Catalysts. *J. Am. Chem. Soc.* **2007,** *129*, 7244-7245; (i) Horino, Y.; Livinghouse, T. Alkene and Diene Hydrosilylations Catalyzed by Lanthanum Tris[bis(trimethylsilyl)amide]†. *Organometallics* **2004,** *23*, 12-14; (j) Kawaoka, A. M.; Douglass, M. R.; Marks, T. J. Homoleptic Lanthanide Alkyl and Amide Precatalysts Efficiently Mediate Intramolecular Hydrophosphination/Cyclization. Observations on Scope and Mechanism. *Organometallics* **2003,** *22*, 4630-4632; (k) Horino, Y.; Livinghouse, T.; Stan, M. Alkene-pinacolborane hydroborations catalyzed by lanthanum tris[bis(trimethylsilyl)amide]. *Synlett* **2004**, 2639-2641; (l) Hong, S.; Kawaoka, A. M.; Marks, T. J. Intramolecular Hydroamination/Cyclization of Conjugated Aminodienes Catalyzed by Organolanthanide Complexes. Scope, Diastereo- and Enantioselectivity, and Reaction Mechanism. *J. Am. Chem. Soc.* **2003,** *125*, 15878-15892; (m) Bürgstein, M. R.; Berberich, H.; Roesky, P. W. Homoleptic Lanthanide Amides as Homogeneous Catalysts for Alkyne Hydroamination and the Tishchenko Reaction. *Chem. Eur. J.* **2001,** *7*, 3078-3085.

14. (a) Agarwal, S.; Karl, M.; Dehnicke, K.; Seybert, G.; Massa, W.; Greiner, A. Ring-opening polymerization of ε-caprolactone and δ-valerolactone using new Sm(III) μ-halo-bis(trimethylsilyl)amido complexes. *J. Appl. Polym. Sci.* **1999,** *73*, 1669-1674; (b) Hultzsch, K. C.; Spaniol, T. P.; Okuda, J. Chiral Lanthanocene Derivatives Containing Two Linked Amido−Cyclopentadienyl Ligands: Heterobimetallic Structure and Lactone Polymerization Activity. *Organometallics* **1997,** *16*, 4845-4856.

15. (a) Crozier, A. R.; Törnroos, K. W.; Maichle-Mössmer, C.; Anwander, R. Trivalent cerium and praseodymium aromatic Ketone adducts. *Eur. J. Inorg. Chem.* **2013**, 409-414; (b) Allen, M.; Aspinall, H. C.; Moore, S. R.; Hursthouse, M. B.; Karvalov, A. I. Benzophenone complexes of the lanthanides: Synthesis of $[Ln\{N(SiMe_3)_2\}_3(Ph2CO)]$ (L = La, Eu, Tb, Yb or Y) and X-ray crystal structure of the terbium complex. *Polyhedron* **1992,** *11*, 409-413.

16. Ohki, Y.; Takikawa, Y.; Hatanaka, T.; Tatsumi, K. Reductive N−N Bond Cleavage of Diphenylhydrazine and Azobenzene Induced by Coordinatively Unsaturated $Cp^*Fe\{N(SiMe_3)_2\}$. *Organometallics* **2006,** *25*, 3111-3113.

17. Dudnik, A. S.; Weidner, V. L.; Motta, A.; Delferro, M.; Marks, T. J. Atom-efficient regioselective 1,2-dearomatization of functionalized pyridines by an earth-abundant organolanthanide catalyst. *Nat. Chem.* **2014,** *6*, 1100-1107.

18. (a) Bakewell, C.; White, A. J. P.; Long, N. J.; Williams, C. K. Metal-Size Influence in Iso-Selective Lactide Polymerization. *Angew. Chem. Int. Ed.* **2014,** *53*, 9226-9230; (b) Evans, W. J.; Sollberger, M. S.; Hanusa, T. P. Synthesis and structure of the polymetallic yttrium alkoxide complex $Y_3(\mu\text{-}OCMe_3)(\mu_3\text{-}Cl)(\mu\text{-}OCMe_3)_3(OCMe_3)_4(THF)_2$ and related complexes: $Ln_3(\mu_3\text{-}OR)(\mu_3\text{-}X)(\mu\text{-}OR)_3$ building blocks in yttrium and lanthanide alkoxide chemistry. *J. Am. Chem. Soc.* **1988,** *110*, 1841-1850.

19. (a) Horino, Y.; Livinghouse, T. Alkene and Diene Hydrosilylations Catalyzed by Lanthanum Tris[bis(trimethylsilyl)amide]. *Organometallics* **2004,** *23*, 12-14; (b) Fegler, W.; Venugopal, A.; Kramer, M.; Okuda, J. Molecular Rare-Earth-Metal Hydrides in Non-Cyclopentadienyl Environments. *Angew. Chem. Int. Ed.* **2015,** *54*, 1724-1736; (c) Nishiura, M.; Guo, F.; Hou, Z. Half-Sandwich Rare-Earth-Catalyzed Olefin Polymerization, Carbometalation, and Hydroarylation. *Acc. Chem. Res.* **2015,** *48*, 2209-2220; (d) Konkol, M.; Okuda, J. Non-metallocene hydride complexes of the rare-earth metals. *Coord. Chem. Rev.* **2008,** *252*, 1577-1591; (e) Harrison, K. N.; Marks, T. J. Organolanthanide-catalyzed hydroboration of olefins. *J. Am. Chem. Soc.* **1992,** *114*, 9220-9221; (f) Watson, P. L. Facile C-H activation by lutetium-methyl and lutetium-hydride complexes. *J. Chem. Soc., Chem. Commun.* **1983**, 276-277.

20. Laidler, K. J., *Chemical Kinetics*. Pearson Education: 1987.

21. Midland, M. M.; Zderic, S. A. Kinetics of reductions of substituted benzaldehydes with B-alkyl-9-borabicyclo[3.3.1]nonane (9-BBN). *J. Am. Chem. Soc.* **1982,** *104*, 525-528.

22. Kozuch, S.; Shaik, S. How to Conceptualize Catalytic Cycles? The Energetic Span Model. *Acc. Chem. Res.* **2011,** *44*, 101-110.

23. Jaffé, H. H. A Reëxamination of the Hammett Equation. *Chem. Rev.* **1953,** *53*, 191-261.

24. (a) Liu, H.; Khononov, M.; Eisen, M. S. Catalytic 1,2-Regioselective Dearomatization of N-Heteroaromatics via a Hydroboration. *ACS Catal.* **2018,** *8*, 3673-3677; (b) Zhang, F.; Song, H.; Zhuang, X.; Tung, C.-H.; Wang, W. Iron-Catalyzed 1,2-Selective Hydroboration of N-Heteroarenes. *J. Am. Chem. Soc.* **2017,** *139*, 17775-17778.

25. Chong, C. C.; Hirao, H.; Kinjo, R. Metal-Free σ-Bond Metathesis in 1,3,2-Diazaphospholene-Catalyzed Hydroboration of Carbonyl Compounds. *Angew. Chem., Int. Ed.* **2015,** *54*, 190-194.

26. Weetman, C.; Anker, M. D.; Arrowsmith, M.; Hill, M. S.; Kociok-Kohn, G.; Liptrot, D. J.; Mahon, M. F. Magnesium-catalysed nitrile hydroboration. *Chem. Sci.* **2016,** *7*, 628-641.

27. Hartwig, J. F.; Bhandari, S.; Rablen, P. R. Addition of Catecholborane to a Ruthenium-Alkyl: Evidence for .sigma.-Bond Metathesis with a Low-Valent, Late Transition Metal. *J. Am. Chem. Soc.* **1994,** *116*, 1839-1844.

28. Berberich, H.; Roesky, P. W. Homoleptic Lanthanide Amides as Homogeneous Catalysts for the Tishchenko Reaction. *Angew. Chem. Int. Ed.* **1998,** *37*, 1569-1571.

29. Tucker, C. E.; Davidson, J.; Knochel, P. Mild and stereoselective hydroborations of functionalized alkynes and alkenes using pinacolborane. *J. Org. Chem.* **1992,** *57*, 3482-3485.

30. (a) Yang, S. H.; Huh, J.; Jo, W. H. Density Functional Study on the Regioselectivity of Styrene Polymerization with an ansa-Metallocene Catalyst. *Organometallics* **2006,** *25*, 1144-1150; (b) Yang, S. H.; Huh, J.; Yang, J. S.; Jo, W. H. A Density Functional Study on the Stereoselectivity of Styrene Polymerization with ansa-Metallocene Catalyst. *Macromolecules* **2004,** *37*, 5741-5751.

31. Rassolov, V. A.; Pople, J. A.; Ratner, M. A.; Windus, T. L. 6-31G* basis set for atoms K through Zn. *The Journal of Chemical Physics* **1998,** *109*, 1223-1229.

32. Yu, Y. B.; Privalov, P. L.; Hodges, R. S. Contribution of translational and rotational motions to molecular association in aqueous solution. *Biophys. J.* **2001,** *81*, 1632-1642.

33. Gaussian 16, R. B., Frisch, M.J. *et al*. Gaussian, Inc., Wallingford CT, **2016**.

34. Pilling, M. J.; Seakins, P. W., *Reaction Kinetics*. Oxford University Press: New York, 1995.

35. Hansch, C.; Leo, A.; Taft, R. W. A survey of Hammett substituent constants and resonance and field parameters. *Chem. Rev.* **1991,** *91*, 165-195.

36. Lachaize, S.; Essalah, K.; Montiel-Palma, V.; Vendier, L.; Chaudret, B.; Barthelat, J.-C.; Sabo-Etienne, S. Coordination Modes of Boranes in Polyhydride Ruthenium Complexes: σ-Borane versus Dihydridoborate. *Organometallics* **2005,** *24*, 2935-2943.

37. Romero, E. A.; Peltier, J. L.; Jazzar, R.; Bertrand, G. Catalyst-free dehydrocoupling of amines, alcohols, and thiols with pinacol borane and 9-borabicyclononane (9-BBN). *Chem. Commun.* **2016,** *52*, 10563-10565.

38. Monguchi, Y.; Wakayama, F.; Takada, H.; Sawama, Y.; Sajiki, H. Osmium on Chelate Resin: Nonvolatile Catalyst for the Synthesis of Diols from Alkenes. *Synlett* **2015,** *26*, 700-704.

39. Arrowsmith, M.; Hadlington, T. J.; Hill, M. S.; Kociok-Koehn, G. Magnesium-catalyzed hydroboration of aldehydes and ketones. *Chem. Commun. (Cambridge, U. K.)* **2012,** *48*, 4567-4569.

40. Wu, Y.; Shan, C.; Sun, Y.; Chen, P.; Ying, J.; Zhu, J.; Liu, L.; Zhao, Y. Main group metal-ligand cooperation of N-heterocyclic germylene: an efficient catalyst for hydroboration of carbonyl compounds. *Chem. Commun.* **2016,** *52*, 13799-13802.

41. Espinosa-Jalapa, N. A.; Nerush, A.; Shimon, L. J. W.; Leitus, G.; Avram, L.; Ben-David, Y.; Milstein, D. Manganese-Catalyzed Hydrogenation of Esters to Alcohols. *Chem. Eur. J.* **2017,** *23*, 5934-5938.

42. Smith, K. T.; Berritt, S.; González-Moreiras, M.; Ahn, S.; Smith, M. R.; Baik, M.-H.; Mindiola, D. J. Catalytic borylation of methane. *Science* **2016,** *351*, 1424-1427.

43. Jakhar, V. K.; Barman, M. K.; Nembenna, S. Aluminum Monohydride Catalyzed Selective Hydroboration of Carbonyl Compounds. *Org. Lett.* **2016,** *18*, 4710-4713.

Chapter 3

1. Magano, J.; Dunetz, J. R. Large-Scale Carbonyl Reductions in the Pharmaceutical Industry. *Org. Process Res. Dev.* **2012**, *16* (6), 1156– 1184, DOI: 10.1021/op2003826

2. Cornils, B.; Hermann, W. A.; Beller, M.; Paciello, R. *Applied Homogeneous Catalysis with Organometallic Compounds: A Comprehensive Handbook in Four Volumes*, Vol. 4; Wiley-VCH Verlag GmbH & Co.: Weinheim, Germany, 2017.

3. Andersson, P. G.; Munslo, I. J. *Modern Reduction Methods*; Wiley: New York, 2008.

4. Roberts, S. M.; Whittall, J. *Regio- and Stereo-Controlled Oxidations and Reductions*; John Wiley & Sons: West Sussex, England, 2007; Vol. 5.

5. Otera, J. *Modern Carbonyl Chemistry*; Wiley-VCH: Weinheim, Germany, 2000.

6. Werkmeister, S.; Junge, K.; Beller, M. Catalytic Hydrogenation of Carboxylic Acid Esters, Amides, and Nitriles with Homogeneous Catalysts. *Org. Process Res. Dev.* **2014**, *18* (2), 289– 302, DOI: 10.1021/op4003278

7. Smith, M. *March's Advanced Organic Chemistry: Reactions, Mechanisms, and Structure*; Wiley: Hoboken, NJ, 2013.

8. Seyden-Penne, J. *Reductions by the Alumino- and Borohydrides in Organic Synthesis*, 2nd ed.; Wiley-VCH: Weinheim, Germany, 1997.

9. Smith, A. M.; Whyman, R. Review of Methods for the Catalytic Hydrogenation of Carboxamides. *Chem. Rev.* **2014**, *114* (10), 5477– 5510, DOI: 10.1021/cr400609m

10. Constable, D. J. C.; Dunn, P. J.; Hayler, J. D.; Humphrey, G. R.; Leazer, J. L., Jr.; Linderman, R. J.; Lorenz, K.; Manley, J.; Pearlman, B. A.; Wells, A.; Zaks, A.; Zhang, T. Y. Key green chemistry research areas—a perspective from pharmaceutical manufacturers. *Green Chem.* **2007**, *9* (5), 411– 420, DOI: 10.1039/B703488C

11. Marciniec, B. *Hydrosilylation: A Comprehensive Review on Recent Advances*; Springer: The Netherlands, 2009.

12. Roy, A. K. A Review of Recent Progress in Catalyzed Homogeneous Hydrosilation (Hydrosilylation). In *Advances in Organometallic Chemistry*; West, R., Hill, A. F., Fink, M. J., Eds.; Academic Press: 2007; Vol. 55, pp 1– 59.

13. Volkov, A.; Tinnis, F.; Slagbrand, T.; Trillo, P.; Adolfsson, H. Chemoselective reduction of carboxamides. *Chem. Soc. Rev.* **2016**, *45* (24), 6685– 6697, DOI: 10.1039/C6CS00244G

14. Mukherjee, D.; Shirase, S.; Spaniol, T. P.; Mashima, K.; Okuda, J. Magnesium hydridotriphenylborate $[Mg(thf)_6][HBPh_3]_2$: a versatile hydroboration catalyst. *Chem. Commun.* **2016**, *52* (89), 13155– 13158, DOI: 10.1039/C6CC06805G

15. Lampland, N. L.; Hovey, M.; Mukherjee, D.; Sadow, A. D. Magnesium-Catalyzed Mild Reduction of Tertiary and Secondary Amides to Amines. *ACS Catal.* **2015**, *5* (7), 4219– 4226, DOI: 10.1021/acscatal.5b01038

16. Ye, P.; Shao, Y.; Ye, X.; Zhang, F.; Li, R.; Sun, J.; Xu, B.; Chen, J. Homoleptic Bis(trimethylsilyl)amides of Yttrium Complexes Catalyzed Hydroboration Reduction of Amides to Amines. *Org. Lett.* **2020**, *22* (4), 1306– 1310, DOI: 10.1021/acs.orglett.9b04606

17. Das, S.; Karmakar, H.; Bhattacharjee, J.; Panda, T. K. Aluminium complex as an efficient catalyst for the chemo-selective reduction of amides to amines. *Dalton Trans.* **2019**, *48* (31), 11978– 11984, DOI: 10.1039/C9DT01806A

18. Chong, C. C.; Kinjo, R. Catalytic Hydroboration of Carbonyl Derivatives, Imines, and Carbon Dioxide. *ACS Catal.* **2015**, *5* (6), 3238– 3259, DOI: 10.1021/acscatal.5b00428

19. Das, U. K.; Higman, C. S.; Gabidullin, B.; Hein, J. E.; Baker, R. T. Efficient and Selective Iron-Complex-Catalyzed Hydroboration of Aldehydes. *ACS Catal.* **2018**, *8* (2), 1076– 1081, DOI: 10.1021/acscatal.7b03785

20. Schneider, J.; Sindlinger, C. P.; Freitag, S. M.; Schubert, H.; Wesemann, L. Diverse Activation Modes in the Hydroboration of Aldehydes and Ketones with Germanium, Tin, and Lead Lewis Pairs. *Angew. Chem., Int. Ed.* **2017**, *56* (1), 333– 337, DOI: 10.1002/anie.201609155

21. Huang, Z.; Liu, D.; Camacho-Bunquin, J.; Zhang, G.; Yang, D.; López-Encarnación, J. M.; Xu, Y.; Ferrandon, M. S.; Niklas, J.; Poluektov, O. G.; Jellinek, J.; Lei, A.; Bunel, E. E.; Delferro, M. Supported Single-Site Ti(IV) on a Metal–Organic Framework for the Hydroboration of Carbonyl Compounds. *Organometallics* **2017**, *36* (20), 3921– 3930, DOI: 10.1021/acs.organomet.7b00544

22. Vasilenko, V.; Blasius, C. K.; Wadepohl, H.; Gade, L. H. Mechanism-Based Enantiodivergence in Manganese Reduction Catalysis: A Chiral Pincer Complex for the Highly Enantioselective Hydroboration of Ketones. *Angew. Chem., Int. Ed.* **2017**, *56* (29), 8393– 8397, DOI: 10.1002/anie.201704184

23. Wu, D.; Wang, R.; Li, Y.; Ganguly, R.; Hirao, H.; Kinjo, R. Electrostatic Catalyst Generated from Diazadiborinine for Carbonyl Reduction. *Chem.* **2017**, *3* (1), 134– 151, DOI: 10.1016/j.chempr.2017.06.001

24. Manna, K.; Ji, P.; Greene, F. X.; Lin, W. Metal–Organic Framework Nodes Support Single-Site Magnesium–Alkyl Catalysts for Hydroboration and Hydroamination Reactions. *J. Am. Chem. Soc.* **2016**, *138* (24), 7488– 7491, DOI: 10.1021/jacs.6b03689

25. Zhang, G.; Cheng, J.; Davis, K.; Bonifacio, M. G.; Zajaczkowski, C. Practical and selective hydroboration of aldehydes and ketones in air catalysed by an iron(II) coordination polymer. *Green Chem.* **2019**, *21* (5), 1114– 1121, DOI: 10.1039/C9GC00078J

26. Kuciński, K.; Hreczycho, G. Potassium Fluoride-Catalyzed Hydroboration of Aldehydes and Ketones: Facile Reduction to Primary and Secondary Alcohols. *Eur. J. Org. Chem.* **2020**, *2020* (5), 552– 555, DOI: 10.1002/ejoc.201901514

27. Mukherjee, D.; Ellern, A.; Sadow, A. D. Magnesium-catalyzed hydroboration of esters: evidence for a new zwitterionic mechanism. *Chem. Sci.* **2014**, *5* (3), 959– 964, DOI: 10.1039/C3SC52793J

28. Barman, M. K.; Baishya, A.; Nembenna, S. Magnesium amide catalyzed selective hydroboration of esters. *Dalton Trans.* **2017**, *46* (13), 4152– 4156, DOI: 10.1039/C7DT00556C

29. Arrowsmith, M.; Hill, M. S.; Hadlington, T.; Kociok-Köhn, G.; Weetman, C. Magnesium-Catalyzed Hydroboration of Pyridines. *Organometallics* **2011**, *30* (21), 5556– 5559, DOI: 10.1021/om2008138

30. Patnaik, S.; Sadow, A. D. Interconverting Lanthanum Hydride and Borohydride Catalysts for C═O Reduction and C–O Bond Cleavage. *Angew. Chem., Int. Ed.* **2019**, *58* (8), 2505– 2509, DOI: 10.1002/anie.201813305

31. Barger, C. J.; Motta, A.; Weidner, V. L.; Lohr, T. L.; Marks, T. J. La[$N(SiMe_3)_2$]$_3$ – Catalyzed Ester Reductions with Pinacolborane. Scope and Mechanism of Ester Cleavage. *ACS Catal.* **2019**, *9*, 9015– 9024, DOI: 10.1021/acscatal.9b02605

32. Weidner, V. L.; Barger, C. J.; Delferro, M.; Lohr, T. L.; Marks, T. J. Rapid, Mild, and Selective Ketone and Aldehyde Hydroboration/Reduction Mediated by a Simple Lanthanide Catalyst. *ACS Catal.* **2017**, *7* (2), 1244– 1247, DOI: 10.1021/acscatal.6b03332

33. Cotton, S. A. Lanthanide Amides. *Encyclopedia of Inorganic and Bioinorganic Chemistry*; John Wiley & Sons, Ltd.: 2011.

34. Wang, C.; Huang, L.; Lu, M.; Zhao, B.; Wang, Y.; Zhang, Y.; Shen, Q.; Yao, Y. Anionic phenoxy-amido rare-earth complexes as efficient catalysts for amidation of aldehydes with amines. *RSC Adv.* **2015**, *5* (115), 94768– 94775, DOI: 10.1039/C5RA20285J

35. Vitanova, D. V.; Hampel, F.; Hultzsch, K. C. Linked bis(β-diketiminato) yttrium and lanthanum complexes as catalysts in asymmetric hydroamination/cyclization of aminoalkenes (AHA). *J. Organomet. Chem.* **2011**, *696* (1), 321– 330, DOI: 10.1016/j.jorganchem.2010.09.051

36. Dash, A. K.; Razavi, A.; Mortreux, A.; Lehmann, C. W.; Carpentier, J.-F. Amine Elimination Reactions between Homoleptic Silylamide Lanthanide Complexes and an Isopropylidene-

Bridged Cyclopentadiene–Fluorene System. *Organometallics* **2002**, *21* (15), 3238– 3249, DOI: 10.1021/om0200398

37. Edelmann, F. T. Lanthanides and actinides: Annual survey of their organometallic chemistry covering the year 2017. *Coord. Chem. Rev.* **2018**, *370*, 129– 223, DOI: 10.1016/j.ccr.2018.05.013

38. Qian, Q.; Zhu, W.; Lu, C.; Zhao, B.; Yao, Y. Asymmetric Michael addition of malonates to unsaturated ketones catalyzed by rare earth metal complexes bearing phenoxy functionalized chiral diphenylprolinolate ligands. *Tetrahedron: Asymmetry* **2016**, *27* (19), 911– 917, DOI: 10.1016/j.tetasy.2016.07.014

39. Döring, C.; Kempe, R. Synthesis and Structure of Aminopyridinato-Stabilized Yttrium and Lanthanum Amides and Their Reactivity towards Alkylaluminium Compounds. *Eur. J. Inorg. Chem.* **2009**, *2009* (3), 412– 418, DOI: 10.1002/ejic.200800934

40. Korobkov, I.; Gambarotta, S. Aluminate Samarium(II) and Samarium(III) Aryloxides. Isolation of a Single-Component Ethylene Polymerization Catalyst. *Organometallics* **2009**, *28* (14), 4009– 4019, DOI: 10.1021/om900172n

41. Hong, S.; Tian, S.; Metz, M. V.; Marks, T. J. C_2-Symmetric Bis(oxazolinato)lanthanide Catalysts for Enantioselective Intramolecular Hydroamination/Cyclization. *J. Am. Chem. Soc.* **2003**, *125* (48), 14768– 14783, DOI: 10.1021/ja0364672

42. Belot, J. A.; Wang, A.; McNeely, R. J.; Liable-Sands, L.; Rheingold, A. L.; Marks, T. J. Highly Volatile, Low Melting, Fluorine-Free Precursors for Metal-Organic Chemical Vapor Deposition of Lanthanide Oxide-Containing Thin Films. *Chem. Vap. Deposition* **1999**, *5* (2), 65– 69, DOI: 10.1002/(SICI)1521-3862(199903)5:2<65::AID-CVDE65>3.0.CO;2-B

43. Tian, S.; Arredondo, V. M.; Stern, C. L.; Marks, T. J. Constrained Geometry Organolanthanide Catalysts. Synthesis, Structural Characterization, and Enhanced Aminoalkene Hydroamination/Cyclization Activity. *Organometallics* **1999**, *18* (14), 2568– 2570, DOI: 10.1021/om990146a

44. Roesky, P. *Molecular Catalysis of Rare-Earth Elements*; Springer-Verlag: Berlin Heidelberg, 2010; Vol. 137.

45. Müller, T. E.; Hultzsch, K. C.; Yus, M.; Foubelo, F.; Tada, M. Hydroamination: Direct Addition of Amines to Alkenes and Alkynes. *Chem. Rev.* **2008**, *108* (9), 3795– 3892, DOI: 10.1021/cr0306788

46. Hong, S.; Marks, T. J. Organolanthanide-Catalyzed Hydroamination. *Acc. Chem. Res.* **2004**, *37* (9), 673– 686, DOI: 10.1021/ar040051r

47. Anwander, R., Lanthanide amides. *Organolanthoid Chemistry: Synthesis, Structure, Catalysis*; Springer: Berlin, Heidelberg, 1996; pp 33– 112.

48. Weiss, C. J.; Marks, T. J. Organo-f-element catalysts for efficient and highly selective hydroalkoxylation and hydrothiolation. *Dalton Trans.* **2010**, *39* (29), 6576– 6588, DOI: 10.1039/c003089a

49. Seo, S.; Marks, T. J. Lanthanide-Catalyst-Mediated Tandem Double Intramolecular Hydroalkoxylation/Cyclization of Dialkynyl Dialcohols: Scope and Mechanism. *Chem. - Eur. J.* **2010**, *16* (17), 5148– 5162, DOI: 10.1002/chem.200903027

50. Seo, S.; Yu, X.; Marks, T. J. Intramolecular Hydroalkoxylation/Cyclization of Alkynyl Alcohols Mediated by Lanthanide Catalysts. Scope and Reaction Mechanism. *J. Am. Chem. Soc.* **2009**, *131* (1), 263– 276, DOI: 10.1021/ja8072462

51. Yu, X.; Seo, S.; Marks, T. J. Effective, Selective Hydroalkoxylation/Cyclization of Alkynyl and Allenyl Alcohols Mediated by Lanthanide Catalysts. *J. Am. Chem. Soc.* **2007**, *129* (23), 7244– 7245, DOI: 10.1021/ja071707p

52. Horino, Y.; Livinghouse, T. Alkene and Diene Hydrosilylations Catalyzed by Lanthanum Tris[bis(trimethylsilyl)amide]. *Organometallics* **2004**, *23* (1), 12– 14, DOI: 10.1021/om0306168

53. Kawaoka, A. M.; Douglass, M. R.; Marks, T. J. Homoleptic Lanthanide Alkyl and Amide Precatalysts Efficiently Mediate Intramolecular Hydrophosphination/Cyclization. Observations on Scope and Mechanism. *Organometallics* **2003**, *22* (23), 4630– 4632, DOI: 10.1021/om030439a

54. Horino, Y.; Livinghouse, T.; Stan, M. Alkene-pinacolborane hydroborations catalyzed by lanthanum tris[bis(trimethylsilyl)amide]. *Synlett* **2004**, *2004* (14), 2639– 2641, DOI: 10.1055/s-2004-835645

55. Hong, S.; Kawaoka, A. M.; Marks, T. J. Intramolecular Hydroamination/Cyclization of Conjugated Aminodienes Catalyzed by Organolanthanide Complexes. Scope, Diastereo- and Enantioselectivity, and Reaction Mechanism. *J. Am. Chem. Soc.* **2003**, *125* (51), 15878– 15892, DOI: 10.1021/ja036266y

56. Bürgstein, M. R.; Berberich, H.; Roesky, P. W. Homoleptic Lanthanide Amides as Homogeneous Catalysts for Alkyne Hydroamination and the Tishchenko Reaction. *Chem. - Eur. J.* **2001**, *7* (14), 3078– 3085, DOI: 10.1002/1521-3765(20010716)7:14<3078::AID-CHEM3078>3.0.CO;2-E

57. Schuetz, S. A.; Day, V. W.; Sommer, R. D.; Rheingold, A. L.; Belot, J. A. Anhydrous Lanthanide Schiff Base Complexes and Their Preparation Using Lanthanide Triflate Derived Amides. *Inorg. Chem.* **2001**, *40* (20), 5292– 5295, DOI: 10.1021/ic010060l

58. Bradley, D. C.; Ghotra, J. S.; Hart, F. A. Three-co-ordination in lanthanide chemistry: tris[bis(trimethylsilyl)amido]lanthanide(III) compounds. *J. Chem. Soc., Chem. Commun.* **1972**, (6), 349– 350, DOI: 10.1039/c39720000349

59. Alyea, E. C.; Bradley, D. C.; Copperthwaite, R. G. Three-co-ordinated transition metal compounds. Part I. The preparation and characterization of tris(bistrimethylsilylamido)-derivatives of scandium, titanium, vanadium, chromium, and iron. *J. Chem. Soc., Dalton Trans.* **1972**, (14), 1580– 1584, DOI: 10.1039/dt9720001580

60. Seo, S.; Marks, T. J. Mild Amidation of Aldehydes with Amines Mediated by Lanthanide Catalysts. *Org. Lett.* **2008**, *10* (2), 317– 319, DOI: 10.1021/ol702788j

61. Hawkeswood, S.; Stephan, D. W. Syntheses and reactions of the bis-boryloxide $O(Bpin)_2$(pin = $O_2C_2Me_4$). *Dalton Trans.* **2005**, *0* (12), 2182– 7, DOI: 10.1039/b504246a

62. Stanlake, L. J. E.; Beard, J. D.; Schafer, L. L. Rare-Earth Amidate Complexes. Easily Accessed Initiators For ε-Caprolactone Ring-Opening Polymerization. *Inorg. Chem.* **2008**, *47* (18), 8062– 8068, DOI: 10.1021/ic8010635

63. Yin, H.; Carroll, P. J.; Schelter, E. J. Reactions of a cerium(III) amide with heteroallenes: insertion, silyl-migration and de-insertion. *Chem. Commun.* **2016**, *52* (63), 9813– 9816, DOI: 10.1039/C6CC03719D

64. Yang, Y.; Anker, M. D.; Fang, J.; Mahon, M. F.; Maron, L.; Weetman, C.; Hill, M. S. Hydrodeoxygenation of isocyanates: snapshots of a magnesium-mediated C=O bond cleavage. *Chem. Sci.* **2017**, *8* (5), 3529– 3537, DOI: 10.1039/C7SC00117G

65. Punekar, N. S. *ENZYMES: Catalysis, Kinetics and Mechanisms*; Springer Nature: Singapore, 2018.

66. Swiegers, G. F. *Mechanical Catalysis: Methods of Enzymatic, Homogeneous, and Heterogeneous Catalysis*; John Wiley & Sons, Inc.: 2008.

67. Harris, R. J.; Carden, R. G.; Duncan, A. N.; Widenhoefer, R. A. Kinetics and Mechanism of the Gold-Catalyzed Intermolecular Hydroalkoxylation of Allenes with Alcohols. *ACS Catal.* **2018**, *8* (9), 8941– 8952, DOI: 10.1021/acscatal.8b02211

68. Kalow, J. A.; Doyle, A. G. Mechanistic Investigations of Cooperative Catalysis in the Enantioselective Fluorination of Epoxides. *J. Am. Chem. Soc.* **2011**, *133* (40), 16001– 16012, DOI: 10.1021/ja207256s

69. Dunne, J. F.; Fulton, D. B.; Ellern, A.; Sadow, A. D. Concerted C–N and C–H Bond Formation in a Magnesium-Catalyzed Hydroamination. *J. Am. Chem. Soc.* **2010**, *132* (50), 17680– 17683, DOI: 10.1021/ja108881s

70. Di Bella, S.; Lanza, G.; Fragalà, I. L. Equilibrium geometries and harmonic vibrational frequencies of lanthanum trihalides LaX_3 (X = F, Cl). A relativistic effective core potential ab initio MO study. *Chem. Phys. Lett.* **1993**, *214* (6), 598– 602, DOI: 10.1016/0009-2614(93)85689-L

71. Weigend, F.; Ahlrichs, R. Balanced basis sets of split valence, triple zeta valence and quadruple zeta valence quality for H to Rn: Design and assessment of accuracy. *Phys. Chem. Chem. Phys.* **2005**, *7* (18), 3297– 3305, DOI: 10.1039/b508541a

72. Ohki, Y.; Takikawa, Y.; Hatanaka, T.; Tatsumi, K. Reductive N–N Bond Cleavage of Diphenylhydrazine and Azobenzene Induced by Coordinatively Unsaturated $Cp^*Fe\{N(SiMe_3)_2\}$. *Organometallics* **2006**, *25* (13), 3111– 3113, DOI: 10.1021/om0602963

73. Dudnik, A. S.; Weidner, V. L.; Motta, A.; Delferro, M.; Marks, T. J. Atom-efficient regioselective 1,2-dearomatization of functionalized pyridines by an earth-abundant organolanthanide catalyst. *Nat. Chem.* **2014**, *6* (12), 1100– 1107, DOI: 10.1038/nchem.2087

74. Wei, C. S.; Jiménez-Hoyos, C. A.; Videa, M. F.; Hartwig, J. F.; Hall, M. B. Origins of the Selectivity for Borylation of Primary over Secondary C–H Bonds Catalyzed by Cp*-Rhodium Complexes. *J. Am. Chem. Soc.* **2010**, *132* (9), 3078– 3091, DOI: 10.1021/ja909453g

75. Hatanaka, T.; Ohki, Y.; Tatsumi, K. C-H Bond Activation/Borylation of Furans and Thiophenes Catalyzed by a Half-Sandwich Iron *N*-Heterocyclic Carbene Complex. *Chem. - Asian J.* **2010**, *5* (7), 1657– 1666, DOI: 10.1002/asia.201000140

76. Harder, S.; Spielmann, J. Calcium-mediated hydroboration of alkenes: "Trojan horse" or "true" catalysis?. *J. Organomet. Chem.* **2012**, *698*, 7– 14, DOI: 10.1016/j.jorganchem.2011.09.025

77. Macaulay, C. M.; Gustafson, S. J.; Fuller, J. T.; Kwon, D.-H.; Ogawa, T.; Ferguson, M. J.; McDonald, R.; Lumsden, M. D.; Bischof, S. M.; Sydora, O. L.; Ess, D. H.; Stradiotto, M.; Turculet, L. Alkene Isomerization–Hydroboration Catalyzed by First-Row Transition-Metal (Mn, Fe, Co, and Ni) *N*-Phosphinoamidinate Complexes: Origin of Reactivity and Selectivity. *ACS Catal.* **2018**, *8* (11), 9907– 9925, DOI: 10.1021/acscatal.8b01972

78. Laidler, K. J. *Chemical Kinetics*; Pearson Education: 1987.

79. Liu, H.; Khononov, M.; Eisen, M. S. Catalytic 1,2-Regioselective Dearomatization of *N*-Heteroaromatics via a Hydroboration. *ACS Catal.* **2018**, *8* (4), 3673– 3677, DOI: 10.1021/acscatal.8b00074

80. Zhang, F.; Song, H.; Zhuang, X.; Tung, C.-H.; Wang, W. Iron-Catalyzed 1,2-Selective Hydroboration of *N*-Heteroarenes. *J. Am. Chem. Soc.* **2017**, *139* (49), 17775– 17778, DOI: 10.1021/jacs.7b11416

81. Chong, C. C.; Hirao, H.; Kinjo, R. Metal-Free σ-Bond Metathesis in 1,3,2-Diazaphospholene-Catalyzed Hydroboration of Carbonyl Compounds. *Angew. Chem., Int. Ed.* **2015**, *54* (1), 190– 194, DOI: 10.1002/anie.201408760

82. Weetman, C.; Anker, M. D.; Arrowsmith, M.; Hill, M. S.; Kociok-Kohn, G.; Liptrot, D. J.; Mahon, M. F. Magnesium-catalysed nitrile hydroboration. *Chem. Sci.* **2016**, *7* (1), 628– 641, DOI: 10.1039/C5SC03114A

83. Pilling, M. J.; Seakins, P. W.: *Reaction Kinetics*; Oxford University Press: New York, 1995.

84. Dudnik, A. S.; Weidner, V. L.; Motta, A.; Delferro, M.; Marks, T. J. Atom-efficient regioselective 1,2-dearomatization of functionalized pyridines by an earth-abundant organolanthanide catalyst. *Nature Chemistry* **2014**, *6*, 1100-1107.

85. Tucker, C. E.; Davidson, J.; Knochel, P. Mild and stereoselective hydroborations of functionalized alkynes and alkenes using pinacolborane. *The Journal of Organic Chemistry* **1992**, *57*, 3482-3485.

86. Tank, R.; Pathak, U.; Vimal, M.; Bhattacharyya, S.; Pandey, L. K. Hydrogen peroxide mediated efficient amidation and esterification of aldehydes: Scope and selectivity. *Green Chemistry* **2011**, *13*, 3350-3354.

87. Hansch, C.; Leo, A.; Taft, R. W. A survey of Hammett substituent constants and resonance and field parameters. *Chemical Reviews* **1991**, *91*, 165-195.

88. Yang, S. H.; Huh, J.; Yang, J. S.; Jo, W. H. A Density Functional Study on the Stereoselectivity of Styrene Polymerization with ansa-Metallocene Catalyst. *Macromolecules* **2004**, *37*, 5741-5751.

89. Yang, S. H.; Huh, J.; Jo, W. H. Density Functional Study on the Regioselectivity of Styrene Polymerization with an ansa-Metallocene Catalyst. *Organometallics* **2006**, *25*, 1144-1150.

90. Rassolov, V. A.; Pople, J. A.; Ratner, M. A.; Windus, T. L. 6-31G* basis set for atoms K through Zn. *The Journal of Chemical Physics* **1998**, *109*, 1223-1229.

91. Yu, Y. B.; Privalov, P. L.; Hodges, R. S. Contribution of translational and rotational motions to molecular association in aqueous solution. *Biophys J* **2001**, *81*, 1632-1642.

92. Gaussian 16, R. B., Frisch, M.J.; Trucks, G. W.; Schlegel, H. B.; Scuseria, G. E.; Robb, M. A.; Cheeseman, J. R.; Scalmani, G.; Barone, V.; Petersson, G. A.; Nakatsuji, H.; Li, X.; Caricato, M.; Marenich, A. V.; Bloino, J.; Janesko, B. G.; Gomperts, R.; Mennucci, B.; Hratchian, H. P; Ortiz, J. V.; Izmaylov, A. F.; Sonnenberg, J. L.; Williams-Young, D.; Ding, F.; Lipparini, F.; Egidi, F.; Goings, J.; Peng, B.; Petrone, A.; Henderson, T.; Ranasinghe, D.; Zakrzewski, V. G.; Gao, J.; Rega, N.; Zheng, G.; Liang, W.; Hada, M.; Ehara, M.; Toyota, K.; Fukuda, R.; Hasegawa, J.; Ishida, M.; Nakajima, T.; Honda, Y.; Kitao, O.; Nakai, H.; Vreven, T.; Throssell, K.; Montgomery Jr., J. A.; Peralta, J. E.; Ogliaro, F.; Bearpark, M. J.; Heyd, J. J.; Brothers, E.

N.; Kudin, K. N.; Staroverov, V. N.; Keith, T. A.; Kobayashi, R.; Normand, J.; Raghavachari, K.; Rendell, A. P.; Burant, J. C.; Iyengar, S. S.; Tomasi, J.; Cossi, M.; Millam, J. M.; Klene, M.; Adamo, C.; Cammi, R.; Ochterski, J. W.; Martin, R. L.; Morokuma, K.; Farkas, O.; Foresman, J. B.; Fox, D. J. Gaussian, Inc., Wallingford CT, **2016**.

93. Lachaize, S.; Essalah, K.; Montiel-Palma, V.; Vendier, L.; Chaudret, B.; Barthelat, J.-C.; Sabo-Etienne, S. Coordination Modes of Boranes in Polyhydride Ruthenium Complexes: σ-Borane versus Dihydridoborate. *Organometallics* **2005**, *24*, 2935-2943.

94. Dolg, M.; Stoll, H.: Chapter 152 Electronic structure calculations for molecules containing lanthanide atoms. In *Handbook on the Physics and Chemistry of Rare Earths*; Elsevier, 1996; Vol. 22; pp 607-729.

95. Di Bella, S.; Lanza, G.; Fragalà, I. L. Equilibrium geometries and harmonic vibrational frequencies of lanthanum trihalides LaX_3 (X = F, Cl). A relativistic effective core potential ab initio MO study. *Chemical Physics Letters* **1993**, *214*, 598-602.

96. Weigend, F.; Ahlrichs, R. Balanced basis sets of split valence, triple zeta valence and quadruple zeta valence quality for H to Rn: Design and assessment of accuracy. *Physical Chemistry Chemical Physics* **2005**, *7*, 3297-3305.

97. Lampland, N. L.; Hovey, M.; Mukherjee, D.; Sadow, A. D. Magnesium-Catalyzed Mild Reduction of Tertiary and Secondary Amides to Amines. *ACS Catalysis* **2015**, *5*, 4219-4226.

98. Bhojgude, S. S.; Kaicharla, T.; Biju, A. T. Employing Arynes in Transition-Metal-Free Monoarylation of Aromatic Tertiary Amines. *Organic Letters* **2013**, *15*, 5452-5455.

99. Sitte, N. A.; Bursch, M.; Grimme, S.; Paradies, J. Frustrated Lewis Pair Catalyzed Hydrogenation of Amides: Halides as Active Lewis Base in the Metal-Free Hydrogen Activation. *Journal of the American Chemical Society* **2019**, *141*, 159-162.

100. Molander, G. A.; Sandrock, D. L. Aminomethylations via Cross-Coupling of Potassium Organotrifluoroborates with Aryl Bromides. *Organic Letters* **2007**, *9*, 1597-1600.

101. Drinkel, E. E.; Campedelli, R. R.; Manfredi, A. M.; Fiedler, H. D.; Nome, F. Zwitterionic-Surfactant-Stabilized Palladium Nanoparticles as Catalysts in the Hydrogen Transfer Reductive Amination of Benzaldehydes. *The Journal of Organic Chemistry* **2014**, *79*, 2574-2579.

102. Peruzzi, M. T.; Mei, Q. Q.; Lee, S. J.; Gagné, M. R. Chemoselective amide reductions by heteroleptic fluoroaryl boron Lewis acids. *Chemical Communications* **2018**, *54*, 5855-5858.

103. Taylor, N. J.; Emer, E.; Preshlock, S.; Schedler, M.; Tredwell, M.; Verhoog, S.; Mercier, J.; Genicot, C.; Gouverneur, V. Derisking the Cu-Mediated 18F-Fluorination of Heterocyclic

Positron Emission Tomography Radioligands. *Journal of the American Chemical Society* **2017**, *139*, 8267-8276.

Original Research Proposal: CO_2 Fixation by Frustrated Lewis Pair-Functionalized Metal Organic Frameworks

Christopher J Barger

Abstract

Rising atmospheric CO_2 levels are a key contributor to global warming, and drastic steps need to be taken to ensure the continued functioning of the planetary ecosystem. While reducing CO_2 emissions by transitioning to renewable energy sources is the primary component of most strategies aimed at addressing climate change, most experts believe "net-negative" CO_2 emissions are likely to be necessary to successfully limit global warming. Such technologies enabling CO_2 capture, sequestration, and functionalization are relatively nascent in their development, and significant advancements will need to be made to contribute meaningfully to CO_2 reduction.

Both metal-organic frameworks (MOFs) and frustrated Lewis pairs (FLPs) have been studied to address these issues, the former by capturing CO_2 from the atmosphere in its pores, and the latter by functionalizing captured CO_2 into value-added carbon feedstocks. While both approaches show promise, they suffer from drawbacks that would limit their applicability in wide-scale use. The work herein proposes to address these shortcomings by combining both motifs into one hybrid material, harnessing the high porosity and CO_2-selective adsorption of MOFs with the CO_2-activiting capabilities of FLPs. By doing so, a new class of materials (FLP@MOFs) capable of selectively and sustainably adsorbing and functionalizing CO_2 may be realized, reducing our reliance on non-renewable carbon feedstocks and reducing atmospheric CO_2 levels.

Introduction

Rising atmospheric carbon dioxide (CO_2) concentration poses an existential threat to Earth's environment. A multi-faceted approach is likely needed to curb further increases in atmospheric CO_2 levels and prevent catastrophic and irreversible damage to Earth's climate.[1] In addition to a shift to renewable energy sources, removal of CO_2 from the atmosphere (CO_2 sequestration) and a transition to net-negative CO_2 emissions will likely play a major role in meeting the necessarily ambitious goals laid out in the Paris Climate Accord (Figure A.1).[2-4] Given potential limitations and drawbacks associated with conventional geophysical CO_2 sequestration/mineralization (e.g. leakage over time, geological disruptions), novel methods for CO_2 sequestration are currently of great interest.[5] Two promising approaches are CO_2 sequestration in metal-organic frameworks (MOFs) and CO_2 fixation/functionalization with frustrated Lewis pairs (FLPs).

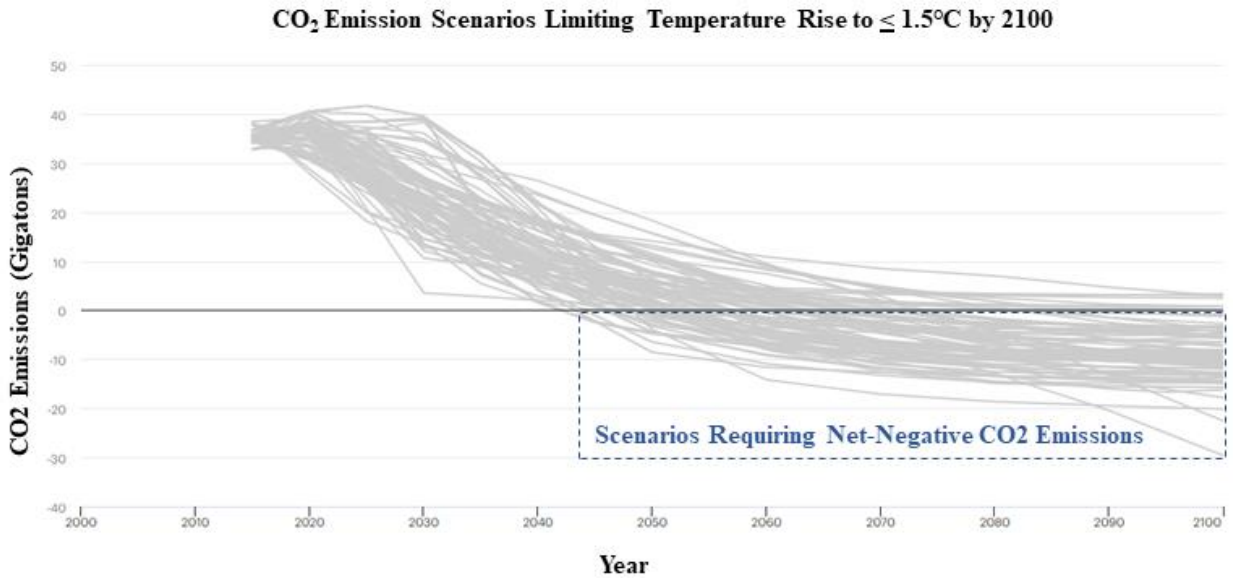

Figure A.1. Analysis of CO_2 emission scenarios that have a $\geq$66% likelihood of successfully limiting global temperature rise to <1.5°C by 2100. Even with aggressive mitigation through reduction in fossil fuel utilization, most scenarios require net-negative emissions through atmospheric CO_2 capture. (Adapted from IEA IPCC Report).[4]

MOFs are a class of highly crystalline, 3-dimensional materials consisting of metal ions (or clusters thereof) connected by bridging organic ligands (Figure A.2).[6] They exhibit exceptionally high surface areas and unparalleled structural tunability. As such, MOFs show great promise for CO_2 sequestration (i.e. the process of removing CO_2 from the atmosphere and storing it underground).[7, 8] CO_2 uptake as high as 37.8 wt. % has been reported for the Mg-MOF-74, all the while maintaining remarkable uptake selectivity over non-polar gases such as methane.[7] This high performance is attributed to the nature of the metal nodes, which are highly Lewis acidic and coordinatively unsaturated.[7, 9, 10] However, sequestration presents a major drawback – while theoretically effective at reducing atmospheric CO_2 levels, the captured CO_2 must be permanently stored, resulting in logistical hurdles. Additionally, since CO_2 is a valuable and essentially unlimited carbon feedstock, a valuable potential source of renewable fuels and chemical feedstocks is wasted.

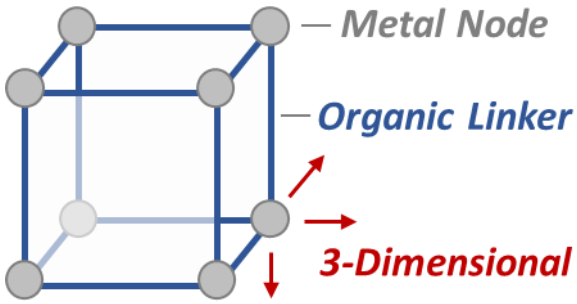

Figure A.2. Representative schematic of Metal-Organic Frameworks (MOFs)

CO_2 fixation and functionalization, on the other hand, converts CO_2 to useful carbon feedstocks like CO, methyl formate, and methanol, not only eliminating CO_2 from the atmosphere, but also lessening our dependence on fossil fuels for commodity chemicals.[11] Frustrated Lewis Pairs (FLPs) offer an exciting approach to catalytic CO_2 fixation that has been extensively studied in laboratory models. An FLP consists of a Lewis acid and a Lewis base that are "frustrated," or prevented from forming an inert adduct, typically by separating them with steric bulk or conformational rigidity (Figure A.3). As such, they are highly reactive and have been shown to

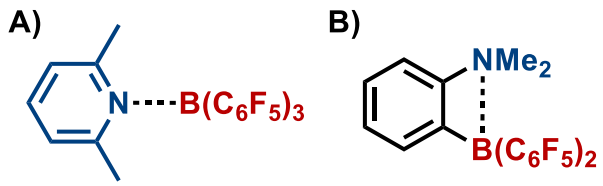

Figure A.3. Representative schematic of sterically frustrated (A) and conformationally frustrated (B) Lewis pairs (FLPs)

efficiently activate a variety of small molecules, including CO_2.[12-17] Most FLPs explored for CO_2 fixation have been studied in homogeneous systems. While this makes them easier to study, heterogeneous systems are more attractive for commercial uses due to their generally improved ease of handling, recyclability, and thermal stability over homogeneous systems.[18] Additionally, advancements in FLP chemistry are limited by strict synthetic requirements: pairs must be sterically encumbered or conformationally constrained to prevent acid/base adduct formation. Novel methods of Lewis acid/base frustration must be explored to fully utilize this unique chemistry.[19]

By integrating FLPs into MOFs, there is the potential for a synergistic relationship. By utilizing the high surface areas and CO_2-selective uptake observed in select MOFs and the high CO_2-fixing activity demonstrated by FLPs, a highly effective and scalable method of converting atmospheric CO_2 to useful products may be realized. Additionally, by appending Lewis basic moieties to MOF linkers and utilizing the inherent Lewis acidity of many MOF metal nodes, an entirely new class of conformationally-constrained FLPs could be discovered. In this work, the current state-of-the-art in the burgeoning field of FLP tethering in MOFs will first be explored before examining potential approaches to synthesizing and characterizing a new class of MOF-tethered FLPs (FLP@MOF).

Scientific Objectives

The objective of this work is to (1) develop a method to synthesize a series of MOFs with Lewis base-appended linkers and Lewis acidic, unsaturated metal nodes (FLP@MOF), and (2) explore their activity and selectivity for the fixation and hydrogenation of CO_2. By integrating CO_2-fixing FLPs onto porous and CO_2-selective MOFs, a new class of CO_2-functionalization catalysts may be realized, offering a novel approach to mitigating the devastating effects of rising atmospheric CO_2 levels.

Previous Work

The heterogenization of FLPs in MOFs is an area of recent, active interest and is a promising approach to overcoming the stability and recyclability shortcomings faced by homogeneous FLP systems. Work in this area to date has focused on tethering one moiety of the Lewis pair onto MOF linkers or nodes, either before or after MOF synthesis, and subsequently introducing the second component of the Lewis pair. This approach was first demonstrated computationally by Ye and Johnson, with UiO-66 serving as the MOF and 1-(difluoroboranyl)-4-methyl-1H-pyrazole, tethered to the aryl linker, serving as the FLP. It was shown in this and subsequent studies that incorporation of various FLPs into the MOF not only lead to retention of the MOF pore structure, but it also afforded clean and selective hydrogenation of CO_2 to formic acid.[20-22] The first experimental confirmation of such a system was in 2018 by Ma and co-workers.[23] In this work, MIL-101(Cr) was synthesized and exposed to a solution of the Lewis base 1,4- diazabicyclo[2.2.2]octane (DABCO), resulting in one of the two Ns in DABCO coordinating to an open metal site in the MOF, with the other protruding into the pore. Lewis acidic $B(C_6F_5)$ was then introduced, forming the FLP *in situ* in the pore of the MOF. The MOF structure was

retained after FLP functionalization, and high activity for the hydrogenation of imines was reported and maintained even after 7 reaction/recovery cycles. Interestingly, the catalyst demonstrated high hydrogenation selectivity for imines with smaller substituents on the imine N, a feature which was not observed in parallel homogeneous FLP hydrogenations, confirming the potential for size-selective catalysis in FLP-decorated MOFs. A subsequent study demonstrated the system's amenability to pore engineering and resulting selectivity for imine hydrogenation in α,β-unsaturated substrates.

An alternative approach to FLP-functionalized MOFs was pursued by Dyson and co-workers, wherein a novel, water stable MOF (SION-105) was synthesized with Eu(III) dimer nodes and tris(p-carboxylic acid)tridurylborane functioning as both the organic linker and as the Lewis acid.[24] A variety of *o*-aryldiamines were then introduced, functioning as both the Lewis basic portion of the FLP and as the substrate in the synthesis of fused benzimidazoles from CO_2 and silane reducing agents. The reaction proceeded cleanly, and no reduction in conversion was observed after 5 recycling experiments. In a subsequent report, the same laboratory achieved direct CO_2 hydrogenation using tetrakis(4-carboxyphenyl)porphyrin-based MOF-545.[24] With the porphyrin linker acting as the Lewis base and tris(pentafluorophenyl)borane as the Lewis acid, CO_2 hydrogenation to give the corresponding methoxyborate was achieved under the relatively mild conditions (100°C, 20 bars of CO_2 and H_2, 20 hours). Notably, while the catalyst is recyclable, hydrolysis of the resulting methoxyborate was necessary to generate free methanol, limiting practical applications.

While the above approaches clearly show great promise for catalytic CO_2 fixation, they suffer a common drawback: by employing pseudo-conventional FLPs that prevent inert adduct

formation through steric bulk or fixed, intramolecular spatial separation, they face the same synthetic constraints for homogeneous FLPs discussed above. Not only do these constraints limit the scope of FLP structures that could be investigated, but it is also likely that this leads to reduced catalytic activity compared to a hypothetical FLP that is sterically unencumbered and conformationally flexible. Additionally, leaving half of the Lewis pair untethered would likely lead to leaching over many catalytic cycles and reduce the long-term recyclability/stability of the catalyst. Finally, the decrease in pore volume that arises from the addition of sterically bulky Lewis basic and Lewis acidic moieties into the MOF significantly reduce the pore volume available for CO_2 adsorption and capture, likely limiting CO_2 uptake and turnover.

Proposed Research

The work proposed herein is hypothesized to circumvent the above-mentioned limitations by tethering a sterically-unencumbered Lewis basic moiety of the FLP to the organic linker of a MOF, with a coordinatively unsaturated metal node acting as the Lewis acidic moiety (Figure A.4). First, by tethering both the Lewis acidic and Lewis basic moieties of the FLP to the framework of the MOF, a new class of FLPs may be realized, relying on the spatial separation afforded by the rigidity of the metal-organic framework to prevent adduct formation rather than steric encumbrance or intramolecular separation. Second, utilizing MOFs with naturally coordinatively-unsaturated, Lewis acidic metal nodes not only simplifies the synthesis of the FLP@MOFs, but it also enhances the atom efficiency of the catalyst, frees up more intra-pore volume for CO_2 adsorption, and avoids the use of costly designer Lewis acids like $B(C_6F_5)_3$. Finally, given the ability of Lewis acidic

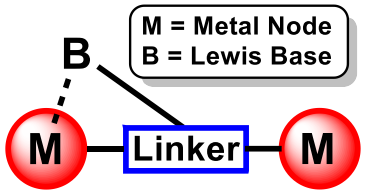

Figure A.4. Representative schematic of FLP@MOFs

MOFs to selectively adsorb CO_2 within their pores, unprecedented selectivities and rates for CO_2 fixation may be realized.

Initial synthetic efforts will be focused on MOFs derived from HKUST-1 (paddlewheel Cu^{2+} dimer nodes with 1,3,5-benzenetricarboxylate linkers) and Mg-MOF-74 (Mg^{2+} ions with 2,5-dihydroxyterephthalate linkers forming cylindrical pores), both of which have unsaturated, Lewis acidic metal sites.[9, 25, 26] While both MOFs have relatively poor water stability that would limit commercial applications, they have been studied and derivatized extensively, making them an ideal proof-of-concept for laboratory-scale investigation. Additionally, favorable CO_2 uptake and selectivity profiles have been described for both MOFs. Initial attempts at linker synthesis will be focused on aryl lithiation of the corresponding benzoic acids for each MOF (trimesic acid for HKUST-1 and 2,5-dihydroxyterephthalic acid for Mg-MOF-74, Scheme A.1).[27, 28] Treatment with excess *s*-BuLi and TMEDA should yielding the corresponding aryl lithiates, which, when exposed to Lewis base-functionalized alkyl chlorides, will form the intended functionalized linkers. An alternative linker syntheses for HKUST-1-based FLP@MOF could also be adapted from that

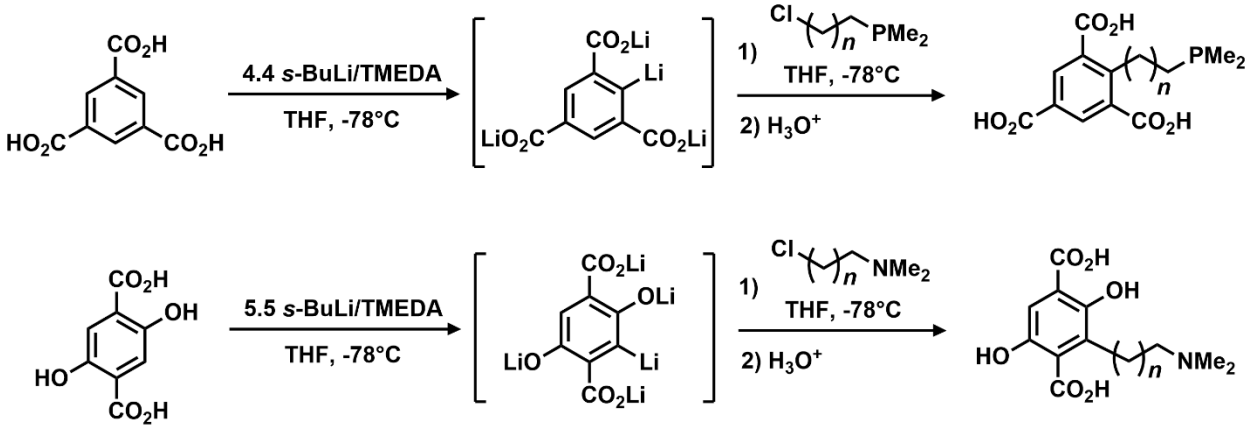

Scheme A.1. Proposed synthetic schemes for the Lewis base-appended linkers to be used in the synthesis of FLP@MOFs

described by Ye and Johnson, wherein 2-bromomesitylene (HKUST-1) or 2-bromo-para-xylene[29] (Mg-MOF-74) is derivatized with a pendant Lewis base through Negishi coupling, followed by oxidation (via the Amoco process or similar oxidative method) to the corresponding benzoic acid used for MOF synthesis.[30, 31] While it is envisioned that a variety of Lewis bases will be explored across multiple MOF architectures, initial efforts will be devoted investigating tertiary phosphines in HKUST-1 and tertiary amines in Mg-MOF-74. Both Lewis bases have been used extensively in FLP research, and the pairing of Cu(II)/P and Mg(II)/N ensures strong FLP activity based on relative acid/base hardness (i.e. Cu(II) and P are soft acids/bases, and Mg(II) and N are hard acids/bases). Since solvothermal synthesis will be used to make the FLP@MOFs, the stability of each tethered Lewis base under these harsh conditions must be considered. Tertiary amines would likely be protonated under these conditions, preventing ligation with the metal node prior to MOF formation and likely helping to maintain the parent structure of Mg-MOF-74. Post-synthetic deprotonation of the amines with a weak base would then activate the FLP. Phosphines, particularly sterically unencumbered alkyl phosphines, would likely be far less stable under solvothermal conditions. Protection of these groups via oxidation to form relatively stable phosphine oxides (prior to MOF synthesis) may be necessary. Post-synthetic silane-mediated reduction of these phosphine oxides would then yield the desired FLP. While this reduction can be forced without a catalyst under harsh conditions, work out of the Beller group demonstrating Cu(II)-catalyzed phosphine oxide reduction with tetramethyldisiloxane suggests the metal node may in fact act as a catalyst.[32]

Solvothermal conditions based on those originally reported for HKUST-1 and Mg-MOF-74 will first be attempted for MOF assembly (**HKUST-1**: 1.8 mM $Cu(NO_3)_2 \cdot 3H_2O$ and 1.0 mM

linker in 1:1 H_2O:EtOH at 180°C for 12 hours in a pressure vessel; **Mg-MOF-74**: 1.85 mM $Mg(NO_3)_2 \cdot 6H_2O$ and 0.559 mM linker in 15:1:1 DMF:EtOH:H_2O at 125°C for 20 hours).[25, 26, 33] It is expected that the FLP@MOFs in this study will retain the structures of their parent MOFs given their ability to maintain structural conformity with other pendant groups.[34, 35] In order to achieve this conformity, Lewis base-functionalized linkers will likely have to be diluted with the standard linkers used in the synthesis of the parent MOFs. Initially, a 1:100 ratio of modified linkers to standard linkers will be tested, with the loading increased systematically to identify the point at which the parent MOF structure is no longer formed. This can be confirmed via powder and/or single crystal x-ray diffraction. N_2 isotherms and BET surface area calculations will determine if the parent MOF pore structure is also maintained upon Lewis base functionalization. Logically, the FLP@MOF's N_2 adsorptive capacity and surface are likely to be reduced in a manner consistent with the loading of the Lewis base-functionalized linkers. However, at sufficiently low modified-linker loadings, the parent adsorption profile should be essentially unperturbed. Measuring adsorption dynamics at progressively higher modified linker ratios will be vital to understanding the ideal loading, maximizing FLP sites while maintaining high surface area and gas flow into and out of the pores. Solid-state ^{31}P and ^{15}N NMR (for diamagnetic Mg-MOF-74) and EXAFS will also be powerful tools for evaluating the coordination environment of the metal nodes and their proximity to the Lewis base moieties, which will help determine whether the Lewis pairs form adducts, are non-interacting, or are truly frustrated.[36, 37]

Disorder in the FLP@MOF crystal structures, due the necessity of a flexible linker for the Lewis base, could preclude structural characterization via single crystal XRD. As such, inferences as to the structure could be made by through a combination of the studies mentioned above and

DFT modeling. DFT could also be very useful for guiding the linker synthesis, particularly with regards to the length of the Lewis base tether. Should the FLP@MOFs not be readily accessible under previously reported conditions, it might be necessary to first synthesize the parent MOFs (Mg-MOF-74 and HKUST-1) then incorporate the Lewis base moiety through post-synthetic linker modification or linker exchange.[38, 39]

Upon successful synthesis and characterization of the FLP@MOFs, CO_2 isotherms will first be collected, and from these, the heats of adsorption for CO_2 will be calculated. A higher heat of adsorption would be expected for the FLP@MOFs than their parent MOFs due to the highly exothermic and irreversible chemisorption of CO_2 to the FLP.[25] In situ diffuse-reflectance UV-Vis and IR spectroscopies (DRUVS and DRIFTS, resp.) will be used to monitor reaction progress and identify intermediates upon exposure of the FLP@MOFs to CO_2 (at various temperatures and pressures). ^{13}C-labeled CO_2 will also be used to facilitate solid state NMR spectroscopic characterization of the intermediates. After CO_2 is confirmed to be fixed in the FLP@MOF via the above methods, hydrogen will be introduced (at various temperatures and pressures) and reaction progress will be monitored by DRUVS, DRIFTS and solid-state NMR. Formation of value-added C1 products (e.g., methanol, formic acid, CO) will be monitored by gas chromatography-mass spectrometry (GC-MS). By conducting initial CO_2 hydrogenation studies in a stepwise fashion, more detailed information can be ascertained about the intermediates formed during the fixation/hydrogenation process. These data will be used to propose a catalytic mechanism for CO_2 hydrogenation with FLP@MOFs, which is expected to resemble mechanisms described for other FLP systems, wherein CO_2 is activated by O coordination to the Lewis acidic metal center, following by nucleophilic attack of the Lewis base, forming a bridging carboxylate.[40] Subsequent

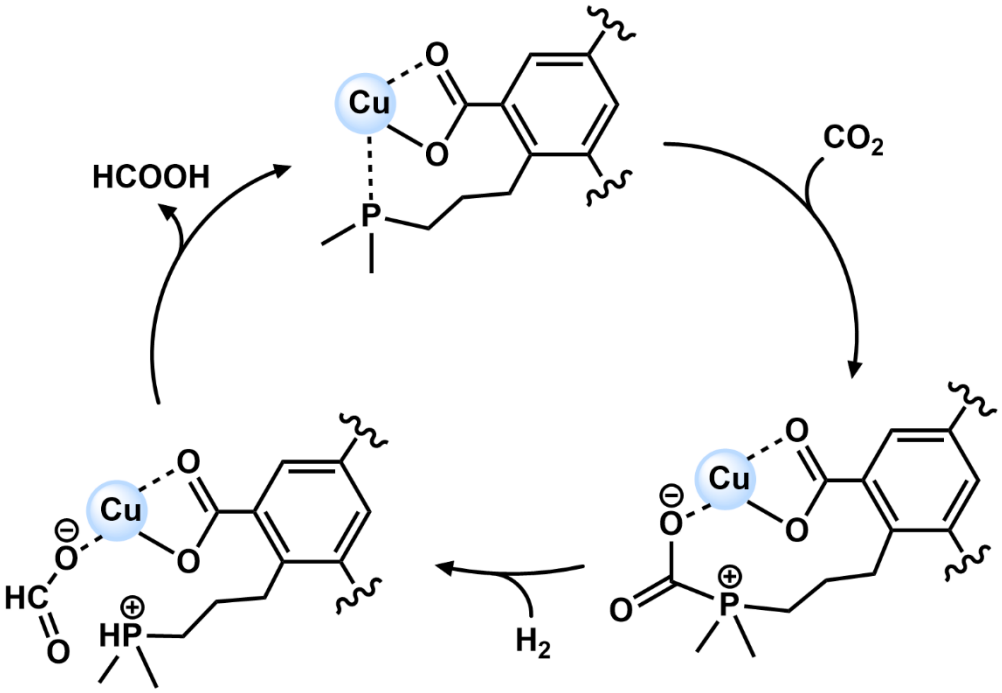

Figure A.5. Proposed catalytic cycle for CO_2 hydrogenation, using phosphine-appended FLP@HKUST-1 as an example catalyst. MOF superstructure omitted for clarity.

hydrogenolysis of the bridging carboxylate to formic acid represents a potential pathway of CO_2 functionalization to value-added C1 product (Figure A.5). After thorough characterization of the catalytic process is achieved through stepwise studies, concerted CO_2 fixation/hydrogenation via a single gas feed will be explored. Batch and plug-flow reactor setups will be screened to determine the optimal reaction conditions. While plug-flow reactors are more scalable, batch reactors allow more flexibility for lab-scale approaches and are easier to manage, making both important to study. The CO_2/H_2 ratio, temperature, pressure and reaction time will be varied to optimize selectivity for reduced C1 products. Reaction progress will be monitored by DRUVS, DRIFTS, and GC-MS, as described above.

Hydrogenation of CO_2, while highly desirable due to its atom-efficiency, is quite challenging, and many FLP systems have proven incapable of reducing CO_2 with hydrogen alone. Hydroboration and hydrosilylation of FLP-fixed CO_2, however, often occurs readily and under mild conditions, and these products can be readily converted to methanol.[19] While not as atom-efficient as direct hydrogenation, these reactions would serve as a proof of concept for this system if hydrogenation fails. It is also possible that, in mixed CO_2/H_2 reactions, the MOF@FLPs could have a higher affinity for activating H_2 than CO_2. It is likely, given previous reports, that CO_2 hydrogenation could still occur (i.e. the FLP is first hydrogenated, then the FLP-hydride facilitates CO_2 fixation/functionalization).[20, 41] However, if H_2 activation by the MOF@FLP does not lead to CO_2 hydrogenation, olefin and imine hydrogenation could be explored. These reactions are less energetically demanding than CO_2 hydrogenation but are still highly useful in academic and industrial synthetic chemistry, and pore constraints from the MOF could give rise to interesting substrate size/shape selectivity.[23, 42]

Summary and Conclusions

The aim of the research proposed herein is to synthesize and characterize a novel class of materials known as FLP@MOFs. By appending Lewis basic moieties to the linkers of MOFs with coordinatively unsaturated, Lewis acidic metal nodes, it is hypothesized that improved activity and stability will be observed over conventional homogeneous FLPs while also harnessing the gas sorption capabilities of MOFs. CO_2 functionalization, a promising approach to reducing the devastating effects of climate change which has been demonstrated in both FLPs and MOFs individually, will then be explored with these hybrid materials.

References

1. Wuebbles, D. J.; Fahey, D. W.; Hibbard, K. A.; DeAngelo, B.; Doherty, S.; Hayhoe, K.; Horton, R.; Kossin, J. P.; Taylor, P. C.; Waple, A. M.; Weaver, C. P., Executive summary. In *Climate Science Special Report: Fourth National Climate Assessment, Volume I*, Wuebbles, D. J.; Fahey, D. W.; Hibbard, K. A.; Dokken, D. J.; Stewart, B. C.; Maycock, T. K., Eds. U.S. Global Change Research Program: Washington, DC, USA, 2017; pp 12-34.

2. Gasser, T.; Guivarch, C.; Tachiiri, K.; Jones, C. D.; Ciais, P., Negative emissions physically needed to keep global warming below 2 °C. *Nature Communications* **2015,** *6* (1), 7958.

3. Sanderson, B. M.; O'Neill, B. C.; Tebaldi, C., What would it take to achieve the Paris temperature targets? *Geophysical Research Letters* **2016,** *43* (13), 7133-7142.

4. IEA, IPCC Pathways with a Less Than 1.5C Temperature Rise in 2100. Paris, 2020.

5. Blondes, M. S.; Merrill, M. D.; Anderson, S. T.; DeVera, C. A. *Carbon dioxide mineralization feasibility in the United States*; 2018-5079; Reston, VA, 2019.

6. James, S. L., Metal-organic frameworks. *Chemical Society Reviews* **2003,** *32* (5), 276-288.

7. Trickett, C. A.; Helal, A.; Al-Maythalony, B. A.; Yamani, Z. H.; Cordova, K. E.; Yaghi, O. M., The chemistry of metal–organic frameworks for CO2 capture, regeneration and conversion. *Nature Reviews Materials* **2017,** *2*, 17045.

8. Li, W.; Wang, H.; Jiang, X.; Zhu, J.; Liu, Z.; Guo, X.; Song, C., A short review of recent advances in CO2 hydrogenation to hydrocarbons over heterogeneous catalysts. *RSC Advances* **2018,** *8* (14), 7651-7669.

9. Bao, Z.; Yu, L.; Ren, Q.; Lu, X.; Deng, S., Adsorption of CO2 and CH4 on a magnesium-based metal organic framework. *Journal of Colloid and Interface Science* **2011,** *353* (2), 549-556.

10. Hu, Z.; Zhao, D., Metal-organic frameworks with Lewis acidity: synthesis, characterization, and catalytic applications. *CrystEngComm* **2017,** *19* (29), 4066-4081.

11. Ganesh, I., Conversion of carbon dioxide into methanol – a potential liquid fuel: Fundamental challenges and opportunities (a review). *Renewable and Sustainable Energy Reviews* **2014,** *31*, 221-257.

12. Courtemanche, M.-A.; Pulis, A. P.; Rochette, E.; Legare, M.-A.; Stephan, D. W.; Fontaine, F.-G., Intramolecular B/N frustrated Lewis pairs and the hydrogenation of carbon dioxide. *Chemical Communications* **2015,** *51* (48), 9797-9800.

13. Stephan, D. W., Frustrated Lewis Pairs: From Concept to Catalysis. *Accounts of Chemical Research* **2015,** *48* (2), 306-316.

14. Stephan, D. W., Frustrated Lewis pairs: a new strategy to small molecule activation and hydrogenation catalysis. *Dalton Transactions* **2009,** (17), 3129-3136.

15. Stephan, D. W.; Erker, G., Frustrated Lewis pair chemistry of carbon, nitrogen and sulfur oxides. *Chemical Science* **2014,** *5* (7), 2625-2641.

16. Courtemanche, M.-A.; Légaré, M.-A.; Maron, L.; Fontaine, F.-G., Reducing CO2 to Methanol Using Frustrated Lewis Pairs: On the Mechanism of Phosphine–Borane-Mediated Hydroboration of CO2. *Journal of the American Chemical Society* **2014,** *136* (30), 10708-10717.

17. Metters, O. J.; Forrest, S. J. K.; Sparkes, H. A.; Manners, I.; Wass, D. F., Small Molecule Activation by Intermolecular Zr(IV)-Phosphine Frustrated Lewis Pairs. *Journal of the American Chemical Society* **2016,** *138* (6), 1994-2003.

18. Rothenberg, G., *Catalysis: Concepts and Green Applications*. Wiley-VCH: 2008.

19. Stephan, D. W., The broadening reach of frustrated Lewis pair chemistry. *Science* **2016,** *354* (6317).

20. Ye, J.; Johnson, J. K., Screening Lewis Pair Moieties for Catalytic Hydrogenation of CO2 in Functionalized UiO-66. *ACS Catalysis* **2015,** *5* (10), 6219-6229.

21. Ye, J.; Johnson, J. K., Catalytic hydrogenation of CO2 to methanol in a Lewis pair functionalized MOF. *Catalysis Science & Technology* **2016,** *6* (24), 8392-8405.

22. Heshmat, M., Alternative Pathway of CO2 Hydrogenation by Lewis-Pair-Functionalized UiO-66 MOF Revealed by Metadynamics Simulations. *The Journal of Physical Chemistry C* **2020,** *124* (20), 10951-10960.

23. Niu, Z.; Bhagya Gunatilleke, W. D. C.; Sun, Q.; Lan, P. C.; Perman, J.; Ma, J.-G.; Cheng, Y.; Aguila, B.; Ma, S., Metal-Organic Framework Anchored with a Lewis Pair as a New Paradigm for Catalysis. *Chem* **2018,** *4* (11), 2587-2599.

24. Shyshkanov, S.; Nguyen, T. N.; Ebrahim, F. M.; Stylianou, K. C.; Dyson, P. J., In Situ Formation of Frustrated Lewis Pairs in a Water-Tolerant Metal-Organic Framework for the Transformation of CO2. **2019,** *58* (16), 5371-5375.

25. Chui, S. S.-Y.; Lo, S. M.-F.; Charmant, J. P. H.; Orpen, A. G.; Williams, I. D., A Chemically Functionalizable Nanoporous Material [Cu₃(TMA)₂(H₂O)₃]_n. *Science* **1999,** *283* (5405), 1148-1150.

26. Rosi, N. L.; Kim, J.; Eddaoudi, M.; Chen, B.; O'Keeffe, M.; Yaghi, O. M., Rod Packings and Metal−Organic Frameworks Constructed from Rod-Shaped Secondary Building Units. *Journal of the American Chemical Society* **2005,** *127* (5), 1504-1518.

27. Bennetau, B.; Mortier, J.; Moyroud, J.; Guesnet, J.-L., Directed lithiation of unprotected benzoic acids. *Journal of the Chemical Society, Perkin Transactions 1* **1995,** (10), 1265-1271.

28. Nguyen, T.-H.; Castanet, A.-S.; Mortier, J., Directed Ortho-Metalation of Unprotected Benzoic Acids. Methodology and Regioselective Synthesis of Useful Contiguously 3- and 6-Substituted 2-Methoxybenzoic Acid Building Blocks. *Organic Letters* **2006,** *8* (4), 765-768.

29. Wu, Y.-Q.; Lu, H.-J.; Zhao, W.-T.; Zhao, H.-Y.; Lin, Z.-Y.; Zhang, D.-F.; Huang, H.-H., A convenient and efficient H2SO4-promoted regioselective monobromination of phenol derivatives using N-bromosuccinimide. *Synthetic Communications* **2020,** *50* (6), 813-822.

30. Li, Y.; Duan, D.; Wu, M.; Li, J.; Yan, Z.; Wang, W.; Zi, G.; Wang, J., One-step synthesis of 2,5-dihydroxyterephthalic acid by the oxidation of p-xylene over M-MCM-41 (M=Fe, Fe/Cu, Cu) catalysts. *Chemical Engineering Journal* **2016,** *306*, 777-783.

31. Ye, J.; Johnson, J. K., Design of Lewis Pair-Functionalized Metal Organic Frameworks for CO2 Hydrogenation. *ACS Catalysis* **2015,** *5* (5), 2921-2928.

32. Li, Y.; Das, S.; Zhou, S.; Junge, K.; Beller, M., General and Selective Copper-Catalyzed Reduction of Tertiary and Secondary Phosphine Oxides: Convenient Synthesis of Phosphines. *Journal of the American Chemical Society* **2012,** *134* (23), 9727-9732.

33. Caskey, S. R.; Wong-Foy, A. G.; Matzger, A. J., Dramatic Tuning of Carbon Dioxide Uptake via Metal Substitution in a Coordination Polymer with Cylindrical Pores. *Journal of the American Chemical Society* **2008,** *130* (33), 10870-10871.

34. Su, X.; Bromberg, L.; Martis, V.; Simeon, F.; Huq, A.; Hatton, T. A., Postsynthetic Functionalization of Mg-MOF-74 with Tetraethylenepentamine: Structural Characterization and Enhanced CO2 Adsorption. *ACS Applied Materials & Interfaces* **2017,** *9* (12), 11299-11306.

35. Cai, Y.; Kulkarni, A. R.; Huang, Y.-G.; Sholl, D. S.; Walton, K. S., Control of Metal–Organic Framework Crystal Topology by Ligand Functionalization: Functionalized HKUST-1 Derivatives. *Crystal Growth & Design* **2014,** *14* (11), 6122-6128.

36. Dawson, D. M.; Jamieson, L. E.; Mohideen, M. I. H.; McKinlay, A. C.; Smellie, I. A.; Cadou, R.; Keddie, N. S.; Morris, R. E.; Ashbrook, S. E., High-resolution solid-state 13C NMR spectroscopy of the paramagnetic metal-organic frameworks, STAM-1 and HKUST-1. *Physical Chemistry Chemical Physics* **2013,** *15* (3), 919-929.

37. Morel, F. L.; Pin, S.; Huthwelker, T.; Ranocchiari, M.; van Bokhoven, J. A., Phosphine and phosphine oxide groups in metal-organic frameworks detected by P K-edge XAS. *Physical Chemistry Chemical Physics* **2015,** *17* (5), 3326-3331.

38. Marshall Ross, J.; Forgan Ross, S., Postsynthetic Modification of Zirconium Metal-Organic Frameworks. *European Journal of Inorganic Chemistry* **2016,** *2016* (27), 4310-4331.

39. Karagiaridi, O.; Bury, W.; Mondloch Joseph, E.; Hupp Joseph, T.; Farha Omar, K., Solvent-Assisted Linker Exchange: An Alternative to the De Novo Synthesis of Unattainable Metal–Organic Frameworks. *Angewandte Chemie International Edition* **2014,** *53* (18), 4530-4540.

40. Ashley, A. E.; O'Hare, D., FLP-Mediated Activations and Reductions of CO2 and CO. In *Frustrated Lewis Pairs II: Expanding the Scope*, Erker, G.; Stephan, D. W., Eds. Springer Berlin Heidelberg: Berlin, Heidelberg, 2013; pp 191-217.

41. Jiang, B.; Zhang, Q.; Dang, L., Theoretical studies on bridged frustrated Lewis pair (FLP) mediated H2 activation and CO2 hydrogenation. *Organic Chemistry Frontiers* **2018,** *5* (12), 1905-1915.

42. Greb, L.; Oña-Burgos, P.; Schirmer, B.; Grimme, S.; Stephan Douglas, W.; Paradies, J., Metal-free Catalytic Olefin Hydrogenation: Low-Temperature H2 Activation by Frustrated Lewis Pairs. *Angewandte Chemie International Edition* **2012,** *51* (40), 10164-10168.